UNITED STATES DEPARTMENT OF THE INTERIOR

GEOLOGICAL SURVEY

STATIC AND CYCLIC STRENGTH PROPERTIES OF MOUNT ST. HELENS DEBRIS AVALANCHE AND ASH CLOUD MATERIALS

by

William J. Winters[1]

and

Robert E. Kayen[2]

Open-File Report

85-518

[1] Woods Hole, Massachusetts 02543

[2] Menlo Park, California 94025

August 1985

TABLE OF CONTENTS

INTRODUCTION:

On May 18, 1980 the northern flank of Mount St. Helens turned into an enormous debris avalanche that traveled up to 23 km in a period of approximately ten minutes and buried an area of about 60 km^2 to an average depth of 45 m (Voight and others, 1983). The mass movement dammed a number of streams, created a blockage in front of Spirit Lake, and deposited approximately 0.4 km^3 of material into Spirit Lake raising the water level 60 m (Glicken and others, in preparation). New impoundments were formed when natural drainage routes were blocked (Fig. 1). South Fork Castle Creek was dammed by the debris avalanche and formed a lake with a volume of approximately 0.02 km^3. That lake level has been presently stabilized by the construction of a spillway. The mass flow consists of poorly sorted mixtures of material ranging from large boulders to clay size with a sand and gravel matrix (Meyer and others, 1985). Layers of volcanic ash cloud deposits are present in many locations, typically near the ground surface.

The physical properties, and static and dynamic strength of material obtained from the Spirit Lake and Castle Creek blockages are presented in this report. Two samples were obtained from each of those blockages (Table 1, Fig. 1). Surface grab samples were seived, reconstituted, and reconsolidated in the laboratory. Also, samples of the ash cloud deposit were obtained near the surface of the Spirit Lake blockage. The samples were subjected to static (in order to assess pre- or post-earthquake stability) and cyclic triaxial tests (to evaluate the effects of cyclic loading on material behavior). Sample consolidation stresses, overconsolidation ratios, dry densities, and grain sizes were varied to determine their effect on sample behavior.

The results of the test program can be used to assess the liquefaction susceptibility of the material. The liquefaction potential can then be determined by comparing the susceptibility of the material to anticipated earthquake loadings at Mount St. Helens.

Liquefaction of a significant amount of the debris flow material could lead to failure or overtopping of the recently formed dams by the impoundments during or immediately after an earthquake. Flooding and mud flows could then threaten both lives and property downstream. Many small and moderate earthquakes have occurred in the Mount St. Helens region both before and after the 1980 eruption (Voight and others, 1983).

SAMPLE PREPARATION AND TESTING METHODOLOGY

Sampling:

In August of 1982 and March of 1983 surface grab samples were collected on the north side of Mount St. Helens at the Spirit Lake (SL) and South Fork Castle Creek (CC) localities (Table 1). The debris flow material was bagged and allowed to dry. Particles greater than 64 mm in diameter were removed from the grab samples. The finer-grained ash cloud deposit (SL1) from Spirit Lake was sampled by vertically pushing a 48 mm inside-diameter thin-walled tube into a horizontal bench cut into the deposit.

Laboratory testing methodology:

Two subsamples were taken from each of the Spirit Lake and South Fork Castle Creek grab samples. The first subsample contained only particles finer than 5.6 mm in diameter, while the second contained particles finer than 3.3 mm in diameter. These grain sizes represent one-sixth and one-tenth of the reconstituted triaxial specimen diameter (36 mm) respectively. The grain size distributions from the grab sample and subsample with particles less than 5.6 mm in diameter were obtained by dry sieving in a mechanical sieve shaker in accordance with the American Society for Testing and Materials (ASTM), Test for Particle-Size Analysis of Soils (D 422) (Fig. 2). Ash cloud material (SL1) was tested intact, without remolding or seiving. Intact samples were trimmed on a standard soil lathe to the appropriate dimensions.

Triaxial samples were prepared within a 0.3 mm thick commercial geotechnical membrane stretched inside a hollow cylindrical mold. Two procedures were employed to reconstitute the material within the confines of the membrane:

1) Material was pluviated through deaired water (i.e., the particles were allowed to fall through approximately 20 mm of standing water) until a 90 mm tall cylindrical sample was formed. The top soil was removed until a 70 mm high specimen remained.

2) Material was pluviated in 10 mm high layers through deaired water and tamped up to 25 times per layer with a 9 mm diameter rod. The initial 90 mm high sample was trimmed to a height of 70 mm.

Tamping was used to densify the material and to remove entrapped air bubbles. Once the sample was prepared, it was placed in a triaxial cell with deaired water as a confining fluid. Water was slowly flushed through the sample to expel interstitial air, until the sample was nearly saturated. The cell and sample water pressure were then raised similtaneously to 345 kPa in order to dissolve any remaining gas bubbles and fully saturate the sample. Skempton's B-coefficient values typically were greater than 0.95, indicating a nearly saturated condition existed (Skempton, 1954).

Upon completion of saturation (typically overnight), the material was consolidated by increasing the cell pressure and allowing pore water to drain. After consolidation was complete, the drainage valve was closed and the sample was tested by increasing the axial load on the cylindrical sample. Static triaxial shear tests were performed on 38 reconstituted samples. The water content and dry density of the sample were determined after each test was finished. Material from sample SL4 had the highest water content and lowest dry densities, followed by material from CC1 and CC2 (Fig. 3).

Fifty cyclic triaxial tests were performed using an electropneumatic cyclic loading system similar to the equipment discussed by Chan (1981). Uniform sinusoidal cyclic deviator stresses with almost full stress reversals were applied at a rate of 0.1 Hz. Pore water pressure, axial deformation and axial load were continually monitored and automatically recorded during the static and cyclic triaxial tests.

RESULTS:

Static triaxial tests:

Samples were isotropically and anisotropically consolidated to either 100 or 300 kPa (representative of field overburden stresses) and subsequently were sheared undrained with pore pressure measurements until 20 percent axial strain was reached. A few specimens were rebounded to a lower consolidation stress prior to shear in order to produce an overconsolidated sample. Failure occurred at the point of maximum shear stress, q, (Table 2).

Peak friction angles, ϕ', were determined at points of maximum obliquity, σ'_1/σ'_3, assuming no cohesion intercept. The peak friction angles ranged from 35.4 to 51.1 degrees for the reconstituted material (Table 2, Figs. 4-6). The intact (non-reconstituted) ash deposit from Spirit Lake (SL1) had the lowest peak friction angle, 34.1 degrees.

A quasi-residual friction angle, ϕ'_r, was determined from each test at the point of lowest obliquity after peak deviator stress was reached. The residual strength of material is typically determined from direct shear tests (Lambe and Whitman, 1969, p. 302; Huang, 1983, p. 31). In addition, residual strength can also be determined from consolidated-undrained triaxial tests (Bowles, 1979, p. 368). However, when the triaxial test is performed to high strain levels, in the order of 20 percent, the sample looses its right circular cylindrical shape, producing a variable cross-sectional area. Therefore, the validity of calculated stresses is lowered. Although many triaxial test stress paths have an approximate straight-line failure envelope, most of the Mt. St. Helens tests produced a backward flip at higher stains (Appendix A) and in this region the residual friction angle was often determined. The validity of comparing the calculated quasi-residual friction angles to residual friction angles determined from direct shear tests or consolidated-drained triaxial tests is questionable.

Results from four static triaxial tests are plotted on Figs. 7-9 showing the effect of dry density on the stress path, stress-strain, and pore-water pressure-strain response of the samples. Individual test results, including stress paths, shear stress versus strain, and pore-water pressure response versus strain, are plotted in Appendix A.

Cyclic triaxial tests:

Isotropically consolidated undrained cyclic triaxial tests were performed on reconstituted material from samples CC1, CC2, and SL4 (Table 3). The ash cloud deposit from sample SL1 was trimmed intact from material extruded from the sampling tube.

The cyclic stress ratio, τ/σ'_c, where τ is the maximum average peak cyclic shear stress and σ'_c is the consolidation stress, is plotted versus the number of cycles to reach two percent single-amplitude strain or 80 percent pore pressure equalization (values after which necking of the sample in tension became more common) for various dry densities (determined at the end of the tests) (Figs 10-17). Lines of approximately equal densities have been drawn on the figures. The maximum, minimum, and mid-point stress ratios at

ten loading cycles (approximately equal to a magnitude 6.75 earthquake, Seed and others, 1983) is shown in each figure and in Table 4. A stress ratio for SL1 material was not determined because of a lack of data. Minimum stress ratios are approximately equal for the material from CC1, CC2, and SL4.

Wide scatter exists in the data with respect to dry densities and effect of grain size and consolidation stress. The larger grain size material from CC1 and CC2 appears to be more susceptible to cyclic loading (Figs. 10 and 11), possibly because a looser structure (lower dry density) was formed during reconstitution. Individual test results are shown in Appendix B.

DISCUSSION:

Modeling field behavior in the laboratory with small-scale specimens:

Inherently, problems exist when trying to model the in-situ behavior of extremely coarse-grained material containing gravel and boulders by small-scale laboratory tests. A case can be made that the large-grained material exists within a matrix of finer-grained material and that it is the finer material that determines the overall behavior of the material; the boulders just "float" in the matrix.

The largest grain size tested from Mount St. Helens was 5.6 mm in diameter. That is one-sixth of the triaxial specimen diameter. According to the ASTM Test for Unconsolidated Undrained Compressive Strength of Cohesive Soils in Triaxial Compression (D2850-82), only particles one-tenth of the sample diameter, for specimens less than 71 mm, should be present. However, the larger grain sizes probably do not invalidate the test results; additionally, the larger particles indicate the trend of results as grain sizes increase. That may allow extrapolation of laboratory based results to field conditions.

The use of a maximum cut-off sieve size creates another problem when testing small samples. The gradation of the sample material differs from the parent material (Fig. 2). Alternatively, parallel grading, i.e., selectively removing certain grain sizes from the sieved sample to achieve a sieved grain-size curve that is parallel to the field curve, has been used by Banerjee and others (1979) to model cyclic behavior of coarse-grained material in the laboratory. However, that technique markedly changes the median grain size, D_{50}, of the tested material. Townsend (1978) showed that the technique was not valid for cyclic testing. Also, parallel grading may not be applicable if a large difference exists between field and laboratory grain sizes.

The debris blockages consist of heterogeneous materials. Samples from the surface of the dams may not adequately represent the material at depth.

Static triaxial test results:

Peak friction angles, ϕ', typically increased as the dry density of the tested material increased (Figs. 4-6). The quasi-residual friction angles, ϕ'_r, exhibiting a more random distribution, were affected to a lesser degree by the dry density (Figs. 4-6).

At a dry density of 1.82 g/cm^3, the debris avalanche material (for all test types) from sample CC1 had peak and quasi-residual friction angles of about 43 and 36 degrees, respectively. This is in very close agreement with peak and residual friction angles of 42.5 and 36.5 degrees, respectively, determined from direct shear tests performed on debris avalanche material finer than 2 mm in diameter reported by Youd and others (1981). Voight and others (1983) reported obtaining friction angles from 40 to 44 degrees from direct shear tests performed on material smaller than 4.75 mm. Youd and others (1981) determined a range of dry densities from 1.71 to 1.94 g/cm^3 at eleven locations on the debris avalanche. Peak friction angles were within the typical range of coarse sand to fine gravel (Lambe and Whitman, 1969, p. 149; Bowles, 1979, p. 382). Quasi-residual friction angles were typically within, or somewhat higher than, the range reported for coarse sand to fine gravel reported by Lambe and Whitman (1969, p.149).

The results plotted in Figs. 7-9 show the effect of density on the static behavior of material from sample CC1. At the lowest density the material exhibited, upon shear, a contractive behavior (Fig. 7), low strength (Fig. 8), and positive pore pressure response. As the dry density increased, the material progressively increased in dilative behavior, possessed higher strength, and generated greater negative pore pressure response.

Sample preparation:

The method used to reconstitute the laboratory sample has an important effect on the cyclic behavior of material. Mulilis and others (1977) found that pluviating Monterey No. 0 sand through a water-filled mold and then vibrating the sample to the required density produced the second greatest liquefaction susceptibility out of 11 different compaction procedures. That method is similar to the techniques used in this study, except that rodding of the Mount St. Helens material was performed instead of vibrating the sample. This indicates that the results of this study imply a greater susceptibility to liquefaction than would have been obtained had another preparation method been used.

Anisotropic field stress state and reconstitution method:

Most parts of the Mt. St. Helens debris blockages probably exist with an anisotropic state of stress. Therefore, initial shear stresses are present on horizontal surfaces in the dams. Seed (1979) stated that the presence of initial shear stresses typically reduces the rate of pore pressure generation and that a critical condition exists when no initial shear stresses are present, i.e., under level ground. We have assumed that intial shear stresses on horizontal surfaces were negligible because of the isotropic consolidation condition of the triaxial samples. Therefore, the test results present conservative estimates of shear stress ratios, τ/σ'_c, that would induce liquefaction.

Correction factors applied to cyclic triaxial test results:

1. Membrane compliance:

Ideally, cyclic triaxial tests are performed undrained with constant specimen volume. However, even with all drainage lines closed, a small amount of drainage occurs around the periphery of the sample because penetration of the rubber membrane into the voids between coarse particles decreases with a reduction in the effective confining stress (Raju and Sadasivan, 1974). In contractive soil, as pore pressure increases, the membrane flexes outward, away from the sample, (accompanied by a volume loss within the grain structure) thereby relieving some of the excess pore water pressure (Kiekbusch and Schuppener, 1977). Therefore, pore pressure builds to a lower level than it would in a truly undrained test. Because of the reduction in pressure response, test results are unconservative (i.e., without membrane compliance the sample would fail quicker, either from a lower number of loading cycles or from a lower stress ratio).

Membrane compliance effects are a function of mean particle diameter, void ratio, effective confining stress, the change in pore pressure during shear, and the amount of surface area of the sample (Lade and Hernandez, 1977). As the grain size increases, more initial penetration of the membrane into the voids between grains occurs, thereby causing subsequent compliance errors to increase. A well graded (poorly sorted) soil, like the Mt St. Helens debris avalanche material, is affected less than a poorly graded soil because the void space between surface grains is reduced.

Soils with a mean particle diameter, D_{50}, less than 0.1 mm generate negilgible membrane compliance errors (Lade and Hernandez, 1977; Martin and others, 1978). However, because the material tested from Mt. St. Helens possessed D_{50} values larger than 0.1 mm corrections were applied to account for membrane compliance.

Most of the static triaxial tests generated negative pore pressures during shear. Those tests, therefore, were conservative with respect to membrane penetration. That is, the negative pore pressures would have become even more negative without membrane penetration. Cyclic tests, however, generate positive pore pressures and would, if not corrected for membrane compliance, lead to unconservative results. Ramana and Raju (1981) found little change in ϕ' determined from static triaxial tests even with significant changes in pore pressure response. Therefore, we are correcting cyclic tests for membrane compliance but not static tests.

The profession is not consistent on how to correct tests for membrane penetration. Raju and Sadasivan (1974) improved a technique, first suggested by Roscoe and others (1963), of using brass rods surrounded by sample material to determine effects of membrane compliance. However, Vaid and Negussey (1984) indicated that those techniques were incorrect and proposed alternate methods. Kiekbusch and Schuppener (1977) indicated that undrained tests could not be simply corrected for membrane compliance, the way that drained tests could be. Instead, they suggested using liquid rubber that would harden around the periphery of the sample thereby reducing the amount of change in the membrane penetration as the test progressed.

Seed (1979) determined that a correction factor to the stress ratio of about 25 percent was required to account for membrane compliance of Monterey No. 0 uniform medium sand (D_{50} equals 0.4 mm) (Mulilis and others, 1977) used in simple shear tests. However, Seed (1979) also stated that the need for such correction factors has not been widely recognized.

The Mount St. Helens samples were corrected for membrane compliance using the data of Martin and others (1978). The errors (defined as the percentage of the corrected stress ratio) in the cyclic stress ratios varied with the mean grain size, D_{50}. The mean particle size of material from CC1 passing the 5.6 mm sieve is 0.8 mm, CC2 is 0.4 mm, and SL4 is about 1.0 mm (Fig. 2). According to Martin and others (1978) the error in cyclic stress ratios for 36 mm diameter samples of uniform grading with the mean grain sizes of the Mt. St. Helens samples are approximately 75 percent, 55 percent, and 80 percent respectively. Those values are inexact, however, and in-depth studies on actual Mt. St. Helens samples would be needed to better quantify the effect of system compliance.

The compliance correction values reported by Martin and others (1978) were arbitrarily reduced by 25 percent because the Mount St. Helens samples are well graded. Therefore, the error in stress ratios for the Mt. St. Helens samples were 0.55, 0.40, and 0.60 for CC1, CC2, and SL4, respectively. The corrected stress ratio equals the stress ratio determined from testing minus the estimated error. The error values reported by Martin and others (1978) of 0.55, 0.40, and 0.60 based on final (corrected) stress ratios correspond to membrane compliance coefficients 0.65, 0.71, and 0.63 based on initial test stress ratios. The initial cyclic stress ratios (Table 4) were multiplied by those coefficiants to account for membrane penetration (Table 5).

2. Isotropic consolidation:

One of the largest variations between field and laboratory conditions results from using a coefficient of earth pressure at rest, K_o, equal to 1.0 in the laboratory (i.e., the horizontal and vertical effective stresses are equal prior to cyclic loading). Field conditions, however, typically have values of K_o less than 1.0 for normally consolidated material. Seed (1979) suggested a correction factor of 0.57 for a K_o value of about 0.4. Seed's factor, that is applied to the cyclic stress ratio, corrects isotropically consolidated triaxial test results to agree with anisotropic simple shear behavior that is more representative of field conditions. The factor also accounts for multidirectional earthquake shaking in the field. A factor of about 0.6 was used with coarser-grained material by Banerjee and others (1979). Therefore, the cyclic stress ratios presented in Table 5 were multiplied by 0.57 to correct for field conditions (Table 6).

Test results (Tables 4-6, Figs. 10-17) show that similar results are derived from both failure criteria (2 percent strain or 80 percent pore pressure equalization). Additionally, the minimum stress ratios required to cause failure are very similar between CC1, CC2, and SL4. A greater difference between stress ratios is present for denser states.

Normalized shear stress curves for use with the simplified method to determine liquefaction potential:

The simplified method to determine liquefaction potential (Seed and Idriss, 1971; Seed, 1979; Seed and others, 1983) enables irregular field earthquake loadings to be modeled in the laboratory by uniform sinusoidally loaded cyclic triaxial tests. That method requires the use of a normalized shear stress versus number of cycles to reach failure plot (Fig. 18) in order to determine the cyclic stress ratio necessary to induce liquefaction in the field for different magnitude earthquakes.

The plot used by Seed and others (1983) (Fig. 19) is for sands and is not directly applicable to the Mt. St. Helens area. Therefore, using results from the cyclic triaxial tests, normalized curves were plotted for different materials (Fig. 18). The normalized factor τ/τ_1, where τ_1 is the estimated shear stress required to cause failure (two percent strain) in one cycle, is a representation of the slope of the stress ratio-cycle to failure plots (Figs. 10-13). Because of the lack of data in some areas the extrapolated value of τ_1 is inexact. The family of curves (with the exception of the ash cloud deposit, SL1) shows a tight grouping up to 10 cycles. After 10 cycles, more divergence is apparent.

An average curve for the Mt. St. Helens material is shown in Fig. 19, weighted towards the tests from CC2 and SL4 because more data exists for those locations. The curves were also corrected for membrane compliance and isotropic consolidation as previously discussed, however those corrections were typically normalized out of the plot and had little effect on the curves. Results for the ash cloud deposit, SL1, are located well below the other materials and are more consistent with the data of Seed and others (1983) for sands. However, limited data were used to determine the curve for SL1, and the failure criterion used by Seed and others (1983) (pore water pressure equalization and ±5 percent strain) was different than the criterion used in this report.

The simplified method to determine liquefaction potential for the Mount St. Helens blockages, using the normalized shear stress curve (Fig. 19), is explained in more detail in a different publication (Chen and others, in press).

LIQUEFACTION SUSCEPTIBILITY ASSESSMENT:

The uncorrected midpoint cyclic stress ratios required to cause failure at 10 loading cycles for the Mt. St. Helens samples (Table 4) are approximately equal to or greater than the stress ratios (approximately 0.35) determined for Monterey sands No. 0 and No. 1 at a relative density of 60 percent (prepared by the wet tamping procedure) (Silver and others, 1976). The uncorrected minimum stress ratios (Table 4) for the Mt. St. Helens samples are somewhat lower than for the Monterey sand and the corrected minimum stress ratios (approximately 0.1) are substantially lower (Table 6). The corrected Mt. St. Helens stress ratios are also substantially lower than the stress ratios required to fail northern Bering Sea sediment in 10 loading cycles (Hampton and Winters, 1983).

Qualitatively, the loosest reconstituted Mt. St. Helens samples are defininely susceptible to liquefaction from moderately sized earthquakes. However, field conditions differ markedly from the laboratory setting. The Mt. St. Helens material grain sizes (Fig. 2) are substantially coarser than those reported to be the most easily liquefied (Finn, 1972) (Fig. 20). Townsend (1978) reported that the most liquefaction prone samples possessed a D_{50} of approximately 0.1 mm with susceptibility decreasing as the mean grain size increased or decreased from that value.

With few exceptions, most of the static triaxial tests from CC1 and CC2 produced negative pore pressures upon substantial strain (Appendix A). Therfore, even if movement started to occur due to earthquake induced shaking, the material at those locations in all but the loosest condition would dilate after strain, reduce the excess positive pore pressures, and thereby stabilize itself. Tests performed on SL4 samples showed a greater tendency to produce positive pore pressures.

Drainage of pore water and subsequent reduction of excess pore pressures was not considered in this study. Due to the large grain sizes of the field material, some drainage may occur, thereby reducing the liquefaction potential.

Erosion at some locations will produce an overconsolidated stress history (thereby reducing the liquefaction susceptibility) in the remaining material, however that may be offset by the increased potential for creating an unstable geometry in the blockages. As time passes, the material's strength will probably increase due to aging effects (Mitchell and Solymar, 1984).

CONCLUSIONS:

Corrected results of cyclic triaxial tests performed on loose reconstituted, seived Mt. St. Helens debris avalanche material and on an intact ash cloud deposit indicate that low resistance to cyclic loading is present. However, major reductions in the cyclic strength were due to inexact membrane compliance correction factors that were used from another study. Membrane compliance correction factors for the actual Mt. St. Helens samples may not be as severe.

The laboratory samples possessed grain size distributions significantly different from those of the field material. Increased coarseness of field material will probably reduce the liquefaction susceptibility.

If failure does occur in any of the blockages, dilation of dense material will tend to stabilize the movement. Dilation will not occur in debris material present in a loose condition.

As time passes after the formation of the debris avalanche in 1980, the stability of the blockages will increase due to aging effects. However, that may be locally offset by the undercutting of individual slopes by erosion.

Future laboratory studies should utilize larger sample dimensions in order to better represent field conditions. Larger specimen sizes will also

reduce the effects of membrane penetration. Liquid rubber applied to the test membrane may be used to reduce the effect of membrane compliance.

In-situ density measurements, borings, seismic exploration, standard penetration tests, and cone penetration tests (if possible) would enable additional liquefaction susceptibility analyses to be made.

ACKNOWLEDGEMENTS:

The authors wish to thank the reviewer of this report, H. J. Lee, for his helpful comments. T. L. Youd, A. T. F. Chen, and R. L. Schuster provided suggestions and assistance. D. J. Bright performed much of the laboratory testing.

The cover photograph of Mount St. Helens was taken in April 1981 looking south across Spirit Lake. Lyn Topinka is thanked for giving permission to use the photograph.

REFERENCES

Banerjee, N.G., Seed, H.B., and Chan, C.K., 1979, Cyclic behavior of dense coarse-grained materials in relation to the seismic stability of dams. Earthquake Engineering Research Center Report 79/13, University of California, Berkeley, 252 p.

Bowles, J.E., 1979, Physical and Geotechnical Properties of Soils. New York, McGraw-Hill Book Company, 478 p.

Chan, C.K., 1981, An electropneumatic cyclic loading system. Geotechnical Testing Journal, ASTM, Vol. 4, No. 4, December, p. 183-187.

Chen, A. T. F., Youd, T. L., Winters, W. J., and Bennett, M. J., in preparation, Liquefaction resistance of debris dams. In: Schuster, R. L. and Meyers, W. (eds.), U.S. Geological Survey Professional Paper.

Finn, W.D., 1972, Soil dynamics liquefaction of sands. Proceedings International Conference on Microzonation for Safer Construction Research and Application, Vol. 1, Seattle, p. 87-111.

Glicken, H., Meyer, W., and Sabol, M., in preparation, Geohydrology of Spirit Lake blockage with reference to lake impoundment. U.S. Geological Survey Open-File Report.

Hampton, M.A. and Winters, W.J., 1983, Geotechnical framework study of the northern Bering Sea, Alaska. U.S. Geological Survey Open-File Report 83-404, 382 p.

Huang, Y.H., 1983, Stability Analysis of Earth Slopes. New York, Van Nostrand Reinhold Company, 305 p.

Kishida, H., 1969, A note on the liquefaction of hydraulic fill during the Tokachi-Oki earthquake. Second Seminar on Soil Behavior and Ground Response During Earthquakes, University of California, Berkeley, Aug.

Kiekbusch, Manfred and Schuppener, Bernd, 1977, Membrane penetration and its effect on pore pressures. Journal of the Geotechnical Engineering Division, Vol. 103, No. GT11, Nov., p. 1267-1279.

Lambe, T.W. and Whitman, R.V., 1969, Soil Mechanics. New York, John Wiley & Sons, 553 p.

Lade, P.V. and Hernandez, S.B., 1977, Membrane penetration effects in undrained tests. Journal of the geotechnical Engineering Division, ASCE, Vol.103, No. GT 2, Feb., p. 109-125.

Lee, K.L. and Fitton, J.A., 1969, Factors affecting the cyclic loading strength of soil. In: Vibration Effects of Earthquakes on Soils and Foundations, ASTM Special Technical Publication 450, p. 71-95.

Martin, G.R., Finn, W.D.L., and Seed, H.B., 1978, Effects of system compliance on liquefaction tests. Journal of the Geotechnical Engineering Division, ASCE, Vol. 104, No. GT 4, April, p. 463-479.

Meyer, W., Sabol, M.A., Glicken, H.X., and Voight, B., 1985, The effects of ground water, slope stability and seismic hazard on the stability of the South Fork Castle Creek blockage in the Mount St. Helens area, Washington. U.S. Geological Survey Professional Paper 1345.

Mitchell, J.K. and Solymar, Z.V., 1984, Time-dependent strength gain in freshly deposited or densified sand. Journal of Geotechnical Engineering, ASCE, Vol. 110, No. 11, November, p. 1559-1576.

Mulilis, J.P., Seed, H.B., Chan, C.K., Mitchell, J.K., and Arulanandan, K., 1977, Effects of sample preparation on sand liquefaction. Journal of the Geotechnical Engineering Division, ASCE, Vol. 103, No. GT2, Feb., p. 91-108.

Ramana, K.V. and Raju, V.S., 1981, Constant-volume triaxial tests to study the effects of membrane penetration. Geotechnical Testing Journal, ASTM, Vol. 4, No. 3, Sept., p. 117-122.

Raju, V.S. and Sadasivan, S.K., 1974, Membrane penetration in triaxial tests on sands. Journal of the Geotechnical Engineering Division, ASCE, Vol. 100, No. GT4, April, p. 482-489.

Roscoe, K.H., Schofield, A.N., and Thurairajah, A., 1963, An evaluation of test data for selecting a yield criterion for soils. Laboratory Shear Testing of Soils, ASTM, Special Technical Publication 361, p. 111-128.

Seed, H.B., 1979, Soil liquefaction and cyclic mobility evaluation for level ground during earthquakes. Journal of the Geotechnical Engineering Division, ASCE, Vol. 105, No. GT 2, Feb., p. 201-255.

Seed, H.B. and Idriss, I.M., 1971, Simplified procedure for evaluating soil liquefaction potential. Journal of the Soil Mechanics and Foundations Division, Vol. 97, No. SM9, Sept., p. 1249-1273.

Seed, H.B., Idriss, I.M., and Arango, I., 1983, Evaluation of liquefaction potential using field performance data. Journal of Geotechnical Engineering, ASCE, Vol. 109, No. 3, March, p. 458-482.

Silver, M.L., Chan, C.K., Ladd, R.S., Lee, K.L., Tiedemann, D.A., Townsend, F.C., Valera, J.E., and Wilson, J.H., 1976, Cyclic triaxial strength of standard test sand. Journal of the Geotechnical Engineering Division, ASCE, Vol. 102, No. GT5, May, p. 511-523.

Skempton, A. W., 1954, The pore-pressure coefficient A and B. Geotechnique, Vol. 4, p. 143-147.

Townsend, F.C., 1978, A review of factors affecting cyclic triaxial tests. In: Dynamic Geotechnical Testing, ASTM, Special Technical Publication 654, p. 356-383.

Vaid, Y.P. and Negussey, Dawit, 1984, A critical assessment of membrane penetration in the triaxial test. Geotechnical Testing Journal, ASTM, Vol. 7, No. 2, p. 70-76.

Voight, B., Janda, R.J., Glicken, H. and Douglass, P.M., 1983, Nature and mechanics of the Mount St Helens rockslide-avalanche of 18 May 1980. Geotechnique, Vol. 33, No. 3, Sept., p. 243-273.

Youd, T.L., Wilson, R.C., and Schuster, R.L., 1981, Stability of blockage in North Fork Toutle River. In: Lipman, P.W. and Mullineaux, D.R., (eds.), The 1980 Eruptions of Mount St. Helens, Washington, U.S. Geological Survey Professional Paper 1250, p. 821-828.

NOMENCLATURE AND SYMBOLS:

A Coeff. - Pore pressure parameter at failure (maximum q), equal to the change in pore pressure divided by the deviator stress.

ASTM - American Society for Testing and Materials.

D_{50} - Mean grain size.

DELTA u - The change in excess pore water pressure from the beginning of a shear test.

Dev Stress - The deviator stress or difference between the major and minor principal effective stresses, $(\sigma'_1 - \sigma'_3)$.

K_o - Coefficient of earth pressure at rest, (σ'_h/σ'_v)

OCR - Overconsolidation ratio, $(\sigma'_{vm}/\sigma'_{vo})$.

p' - The normal effective stress acting on a plane inclined at 45 degrees from the horizontal in a triaxial test, $(\sigma'_1 + \sigma'_3)/2$.

q - The shear stress acting on a plane inclined at 45 degrees from the horizontal in a triaxial test, $(\sigma'_1 - \sigma'_3)/2$.

q_{max} - Maximum value of q reached during a static triaxial test, equal to S_u.

SIG 1_c' - The major (or vertical) principal stress applied to a triaxial test sample prior to shear.

SIG 3_c' - The minor (or horizontal) principal stress applied to a triaxial test sample prior to shear.

TE - Prefix for a static triaxial test number.

w - Water content (weight of water/weight of solids).

σ'_1 - The major principal effective stress applied to a triaxial test sample.

σ'_1/σ'_3 - obliquity factor; it is a maximum at the point of the largest friction angle during a triaxial test.

σ'_3 - The minor principal effective stress applied to a triaxial test sample.

σ'_c - The isotropic consolidation stress imposed on a triaxial test sample prior to shear.

$\sigma'_v = \sigma'_{vo}$ - The in-situ vertical effective stress exerted by the weight of overburden.

τ - Shear stress.

τ_1 - Estimated shear stress required to cause failure in one cycle during a cyclic triaxial test.

ϕ' - The peak friction angle expressed in terms of effective stresses.

ϕ'_r - The quasi-residual friction angle expressed in terms of effective stresses.

Table 1. Sample information.

Sample I.D.	Alternate I.D.	Location	Date Obtained	Field Density (g/cm^3)	Grain Specific Gravity (g/cm^3)	Sample Type	Material Type
CC1	-	S.F. Castle Creek	3-8-83	-	2.75	Grab	Debris Avalanche
CC2	JM-82-826-2	S.F. Castle Creek	8-26-82	1.59	2.76	Grab	Debris Avalanche
SL1	-	Spirit Lake	3-8-83	-	-	Tube	Ash Cloud Deposit
SL4	JM-82-825-7	Spirit Lake	8-25-82	1.79	2.65	Grab	Debris Avalanche

Table 2. Static triaxial test results

Sample	Test No.	Passing Sieve Size(mm)	Consol. Stress (kPa)	Water Content After Shear (%)	A Coeff.	Strain at Failure(%)	OCR	q Failure (kPa)	p' Failure (kPa)	ϕ' Peak (deg.)	ϕ' Res. (deg.)	Dry Density (g/cm^3)
CC1	123	3.3	101	18.6	-0.02	16.3	1.0	168	275	38.4	36.6	1.82
	124	3.3	103	17.7	-0.19	7.9	1.0	639	980	45.6	34.7	1.85
	127	3.3	100	21.8	0.41	19.6	1.0	64	110	35.9	35.2	1.72
	128	3.3	100	19.0	-0.16	19.2	1.0	266	452	38.1	35.6	1.81
	130	3.3	99	17.0	-0.18	7.5	1.0	603	914	45.0	37.2	1.87
	131	3.3	99	17.6	-0.15	5.7	1.0	497	740	46.2	36.7	1.85
	132	3.3	98	18.9	-0.24	17.0	1.0	724	1168	43.7	37.7	1.82
	133	3.3	98	17.9	-0.19	7.0	1.0	844	1266	45.4	35.3	1.84
	134	3.3	96	17.7	-0.21	7.0	1.0	669	1045	43.6	34.3	1.85
	136	3.3	204/99	18.6	-0.19	9.4	1.0	451	721	43.9	35.7	1.82
	125	3.3	300	19.8?	0.01	7.7	1.0	465	756	42.0	35.2	1.78?
	126	3.3	300	18.1	-0.05	8.5	1.0	655	1024	42.7	34.7	1.83
	135	3.3	49	18.5	-0.23	9.8	6.1	500	780	44.0	36.3	1.82
	176	5.6	87	19.7	-0.03	6.0	1.0	171	267	40.1	38.3	1.78
	178	5.6	101	15.0	0.13	5.3	1.0	1075	1460	51.1	38.2	1.94
CC2	137	3.3	99	15.9	-0.26	11.8	1.0	551	932	41.7	33.8	1.92
	138	3.3	100	15.0	-0.24	7.8	1.0	663	1078	42.6	33.7	1.95
	139	3.3	98	14.5	-0.20	9.9	1.0	909	1372	44.6	39.0	1.97
	140	3.3	99	14.2	-0.17	8.4	1.0	1185	1697	46.4	40.2	1.98
	143	3.3	100	15.4	-0.20	9.1	1.0	927	1395	45.5	36.9	1.94
	144	3.3	97	16.6	-0.21	6.5	1.0	471	761	42.9	35.2	1.89
	155	3.3	100	17.2	-0.20	8.7	1.0	514	816	42.1	36.6	1.87
	164	3.3	97	16.4	-0.17	8.3	1.0	306	506	40.5	34.5	1.90
	147	3.3	299	14.0	-0.09	5.3	1.0	1250	1762	46.4	35.5	1.99
	148	3.3	295	13.6	-0.12	7.9	1.0	1456	2093	45.3	39.0	2.01
	149	3.3	299	15.3	-0.10	6.2	1.0	1262	1815	45.1	34.3	1.94
	150	3.3	296	15.1	-0.11	7.0	1.0	745	1210	41.8	31.5	1.95
	151	3.3	267/107	14.9	-0.22	6.5	1.0	717	1134	41.9	36.3	1.95
	152	3.3	45	14.7	-0.25	7.2	6.7	645	996	42.5	35.5	1.96
	179	5.6	97	15.7	-0.01	9.3	1.0	146	244	36.9	34.3	1.92
	183	5.6	97	15.9	0.19	7.5	1.0	107	164	41.7	38.5	1.92
SL1	129	-	101	31.4	0.06	13.8	1.0	96	185	34.1	30.2	1.34
SL4	170	3.3	97	24.5	-0.12	14.5	1.0	206	353	39.3	35.0	1.61
	173	3.3	103	22.2	-0.24	11.2	1.0	739	1201	43.4	32.2	1.67
	175	3.3	298	24.1	0.09	12.0	1.0	378	609	39.5	35.4	1.62
	177	3.3	296	23.0	0.34	8.0	1.0	210	364	35.4	29.7	1.65
	184	5.6	96	27.0	1.21	11.3	1.0	163	281	37.3	32.6	1.54
	185	5.6	99	20.7	0.23	10.2	1.0	583	952	42.4	30.9	1.71

Table 3. Cyclic triaxial test results

Sample	Test No.	Passing Sieve Size(mm)	Consolidation Stress (kPa)	Water Content After Shear (%)	OCR	$\frac{\tau}{\sigma'_c}$ (%)	Cycles to 2% Strain	Cycles to Pore Pressure Equalization 70%	80%	90%	Dry Density (g/cm^3)
CC1	130	3.3	100	17.2	1.0	97	7	3	5	-	1.87
	131	3.3	97	20.8	1.0	57	-	2	2	-	1.75
	132	3.3	98	19.0	1.0	33	12	6	8	10	1.80
	133	3.3	100	16.6	1.0	24	121	78	87	95	1.89
	134	3.3	98	16.5	1.0	50	25	6	8	11	1.89
	135	3.3	100	18.9	1.0	48	7	5	6	-	1.81
	136	3.3	98	18.0	1.0	60	2	2	-	-	1.84
	197	5.6	95	19.8	1.0	40	1	2	-	-	1.79
	198	5.6	96	18.1	1.0	27	19	17	18	20	1.84
CC2	137	3.3	100	17.0	1.0	33	18	14	16	18	1.88
	138	3.3	98	14.8	1.0	41	22	15	18	23	1.96
	139	3.3	99	14.7	1.0	31	19	11	12	14	1.96
	140	3.3	98	14.8	1.0	48	6	3	4	5	1.96
	141	3.3	99	13.4	1.0	29	55	40	43	46	2.02
	142	3.3	98	13.8	1.0	48	4	3	3	4	2.00
	143	3.3	99	13.9	1.0	23	344	309	319	327	1.99
	144	3.3	98	14.2	1.0	35	23	12	13	15	1.98
	145	3.3	98	14.4	1.0	51	7	4	5	6	1.97
	161	3.3	94	15.9	1.0	37	14	7	8	11	1.92
	162	3.3	72	17.6	1.0	55	1	-	-	-	1.86
	146	3.3	299	13.9	1.0	33	13	9	11	-	1.99
	147	3.3	297	13.0	1.0	40	8	4	5	7	2.03
	148	3.3	297	13.6	1.0	35	22	12	15	22	2.01
	149	3.3	297	14.5	1.0	45	2	-	-	-	1.97
	179	5.6	96	18.8	1.0	53	1	-	-	-	1.82
	180	5.6	101	16.2	1.0	27	34	31	32	34	1.91
	181	5.6	109	22.4	1.0	36	3	-	-	-	1.71
	182	5.6	94	16.7	1.0	46	2	2	3	4	1.89
	183	5.6	98	17.0	1.0	43	4	3	4	6	1.90
	184	5.6	100	17.3	1.0	22	33	28	30	31	1.89
	195	5.6	96	16.3	1.0	44	3	2	3	-	1.90
	185	5.6	295	16.3	1.0	39	3	4	5	-	1.92
	186	5.6	297	15.8	1.0	31	6	5	6	7	1.92
	187	5.6	293	15.7	1.0	34	5	3	4	5	1.93
	188	5.6	297	14.2	1.0	27	50	38	42	47	1.98
SL1	155	-	99	30.8	1.0	80	1	2	2	2	1.42
	156	-	98	28.0	1.0	48	3	3	3	4	1.56
SL4	163	3.3	93	25.8	1.0	41	7	5	7	8	1.57
	164	3.3	96	26.3	1.0	22	131	114	121	127	1.59
	165	3.3	88	23.8	1.0	29	16	11	14	16	1.62
	166	3.3	87	22.4	1.0	28	103	95	99	102	1.66
	169	3.3	100	24.7	1.0	38	-	8	11	18	1.60
	170	3.3	97	17.3	1.0	50	14	7	9	-	1.82
	189	5.6	97	21.8	1.0	29	49	42	46	50	1.68
	190	5.6	98	20.3	1.0	42	19	14	16	-	1.72
	191	5.6	97	26.4	1.0	32	14	14	17	20	1.56
	192	5.6	99	25.6	1.0	40	9	9	12	-	1.58
	196	5.6	97	14.6	1.0	34	9	6	7	9	1.91
	193	5.6	275	20.1	1.0	48	5	5	-	-	1.75
	194	5.6	275	25.0	1.0	32	6	6	7	-	1.61

Table 4. Cyclic stress ratios, τ/σ'_c, at 10 loading cycles determined from Figs. 10-17.

Sample	τ/σ'_c at 2 % strain			τ/σ'_c at 80 % pore pressure equalization		
	max.	midpoint	min.	max.	midpoint	min.
CC1	0.76	0.50	0.24	0.82	0.55	0.28
CC2	0.48	0.37	0.26	0.46	0.36	0.26
SL1		0.3 - 0.2 (?)			0.3 - 0.1 (?)	
SL4	0.54	0.41	0.28	0.48	0.38	0.28

Table 5. Cyclic stress ratios, τ/σ'_c, at 10 loading cycles determined from Figs. 10-17 corrected for membrane compliance.

Sample	τ/σ'_c at 2 % strain			τ/σ'_c at 80 % pore pressure equalization		
	max.	midpoint	min.	max.	midpoint	min.
CC1	0.49	0.33	0.16	0.53	0.36	0.18
CC2	0.34	0.26	0.19	0.33	0.26	0.19
SL1		0.3 - 0.2 (?)			0.3 - 0.1 (?)	
SL4	0.34	0.26	0.18	0.30	0.24	0.18

Table 6. Cyclic stress ratios, τ/σ'_c, at 10 loading cycles determined from Figs. 10-17 corrected for membrane compliance and multiplied by 0.57 to simulate field conditions.

Sample	τ/σ'_c at 2 % strain			τ/σ'_c at 80 % pore pressure equalization		
	max.	midpoint	min.	max.	midpoint	min.
CC1	0.28	0.19	0.09	0.30	0.21	0.10
CC2	0.19	0.15	0.11	0.19	0.15	0.11
SL1		0.2 - 0.1 (?)			0.2 - 0.05 (?)	
SL4	0.19	0.15	0.10	0.17	0.14	0.10

LIST OF FIGURES

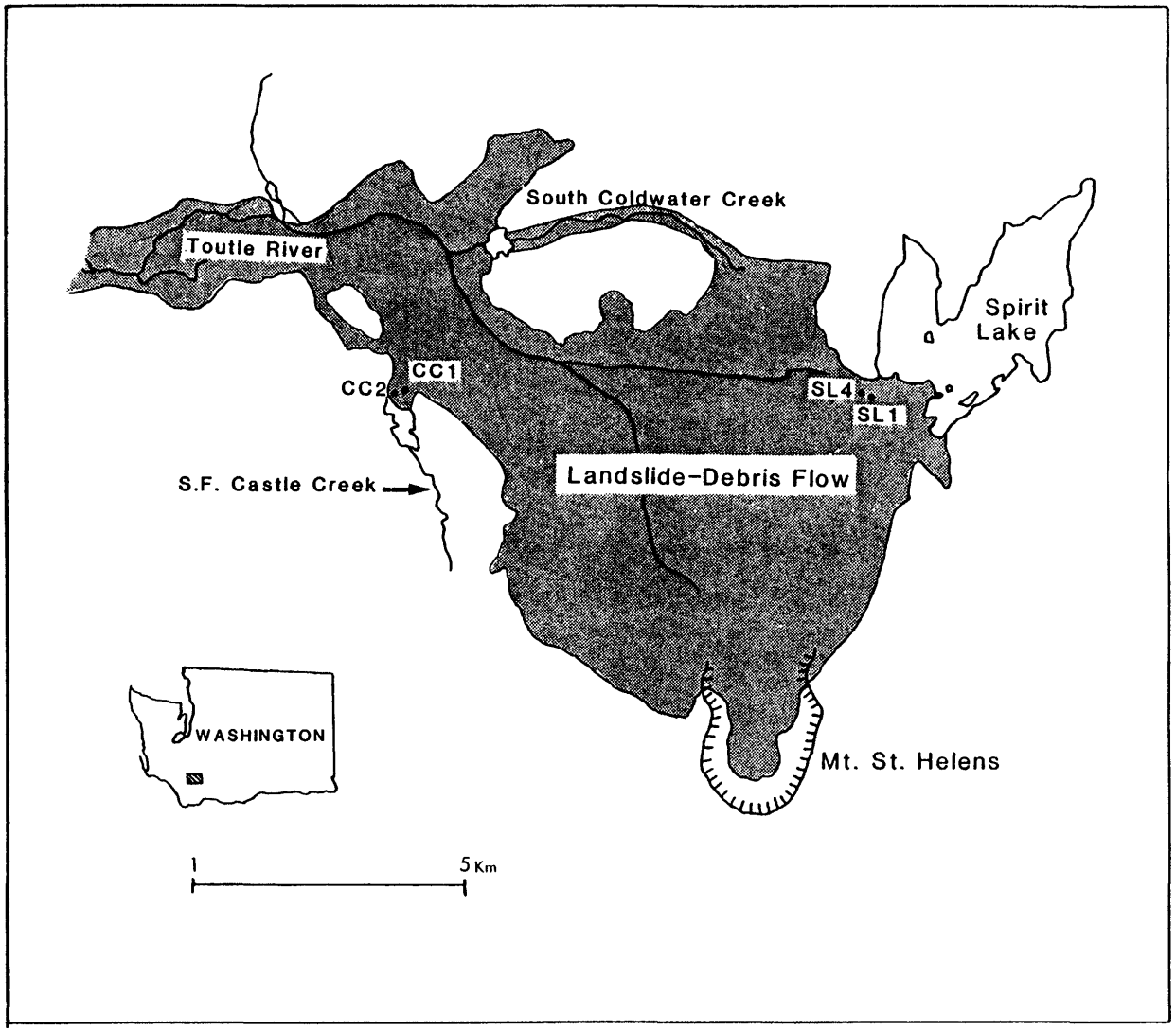

Fig. 1. Sample location map.

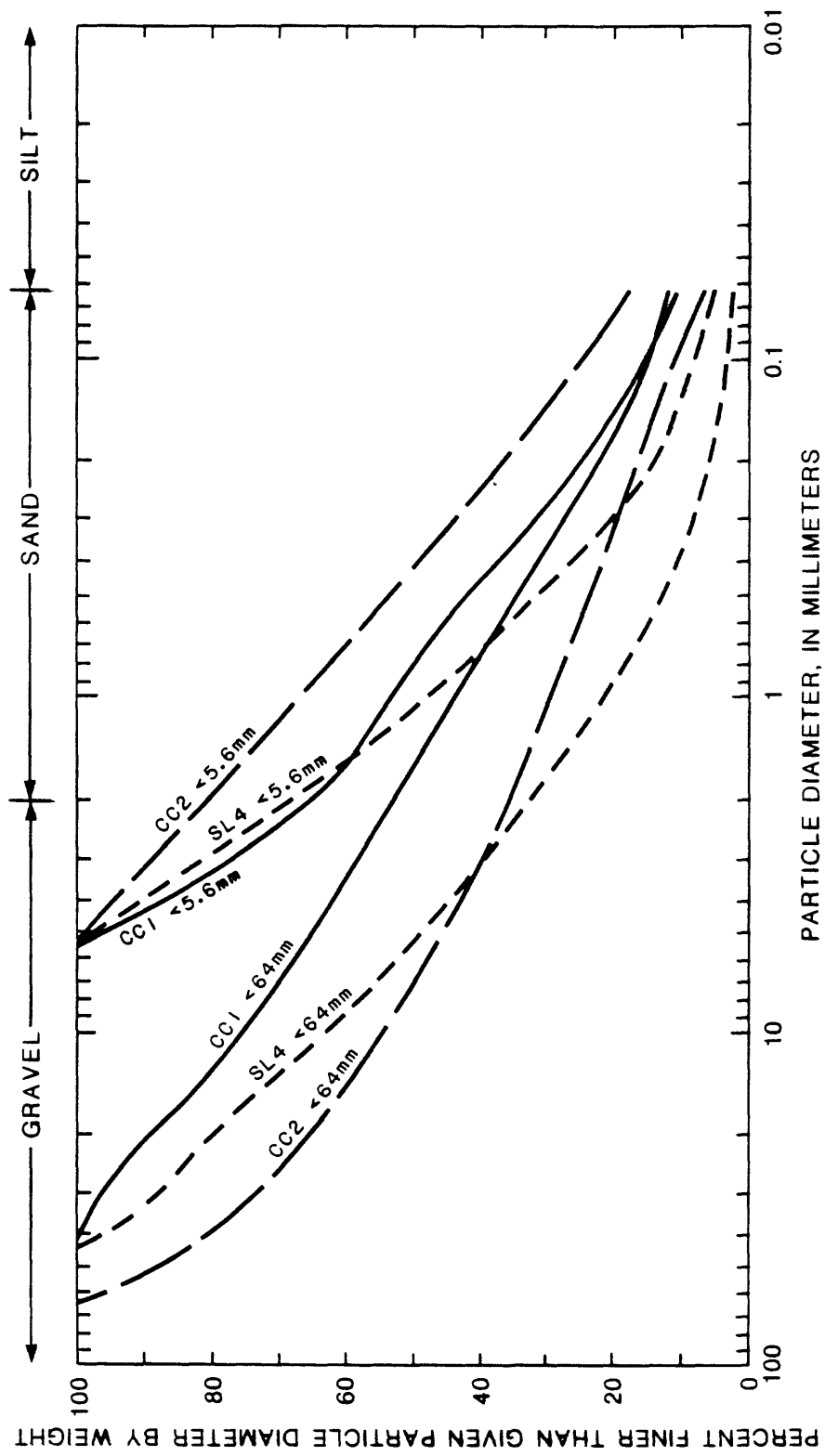

Fig. 2. Grain size distribution curves.

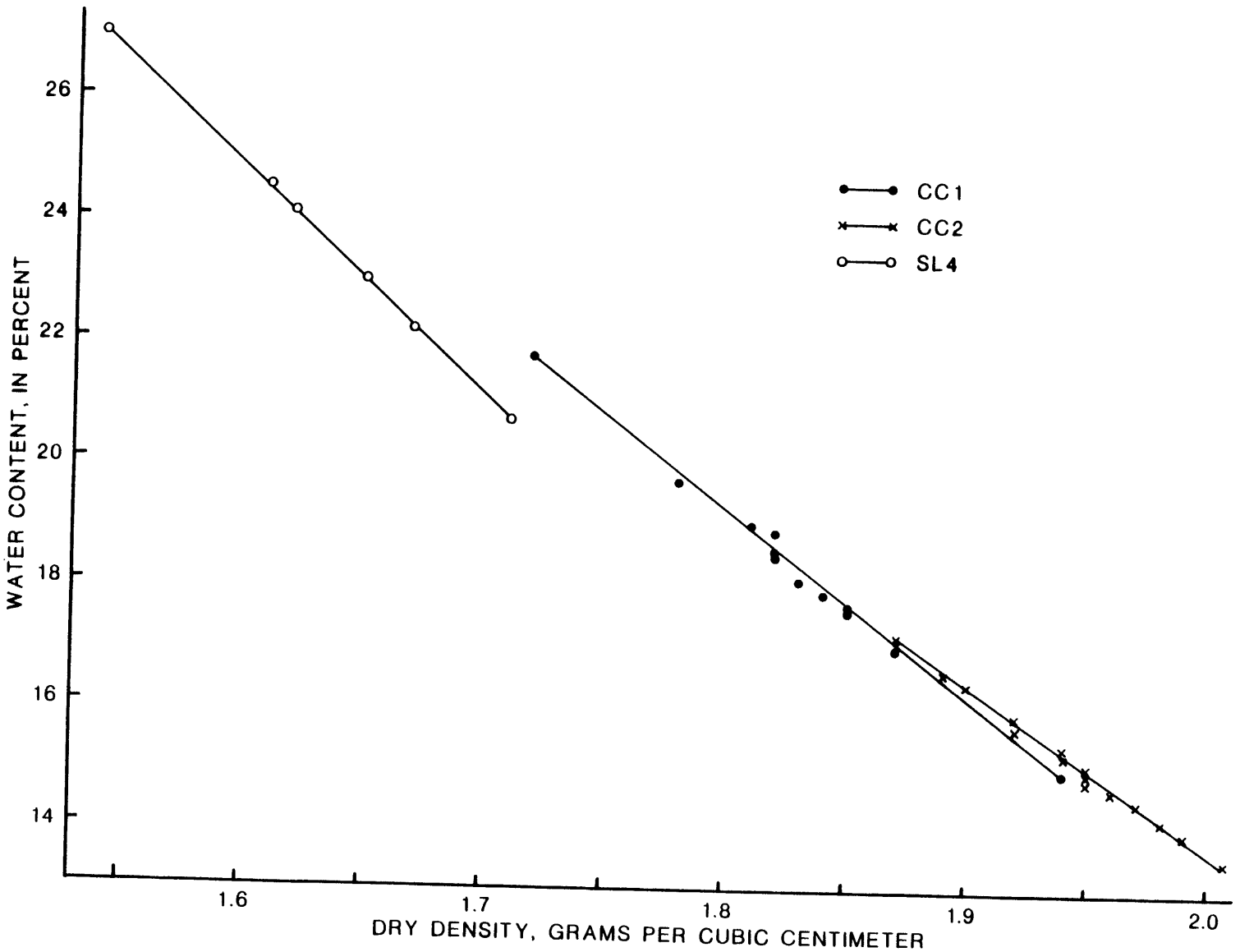

Fig. 3. Water content versus dry density for seived triaxial samples after testing.

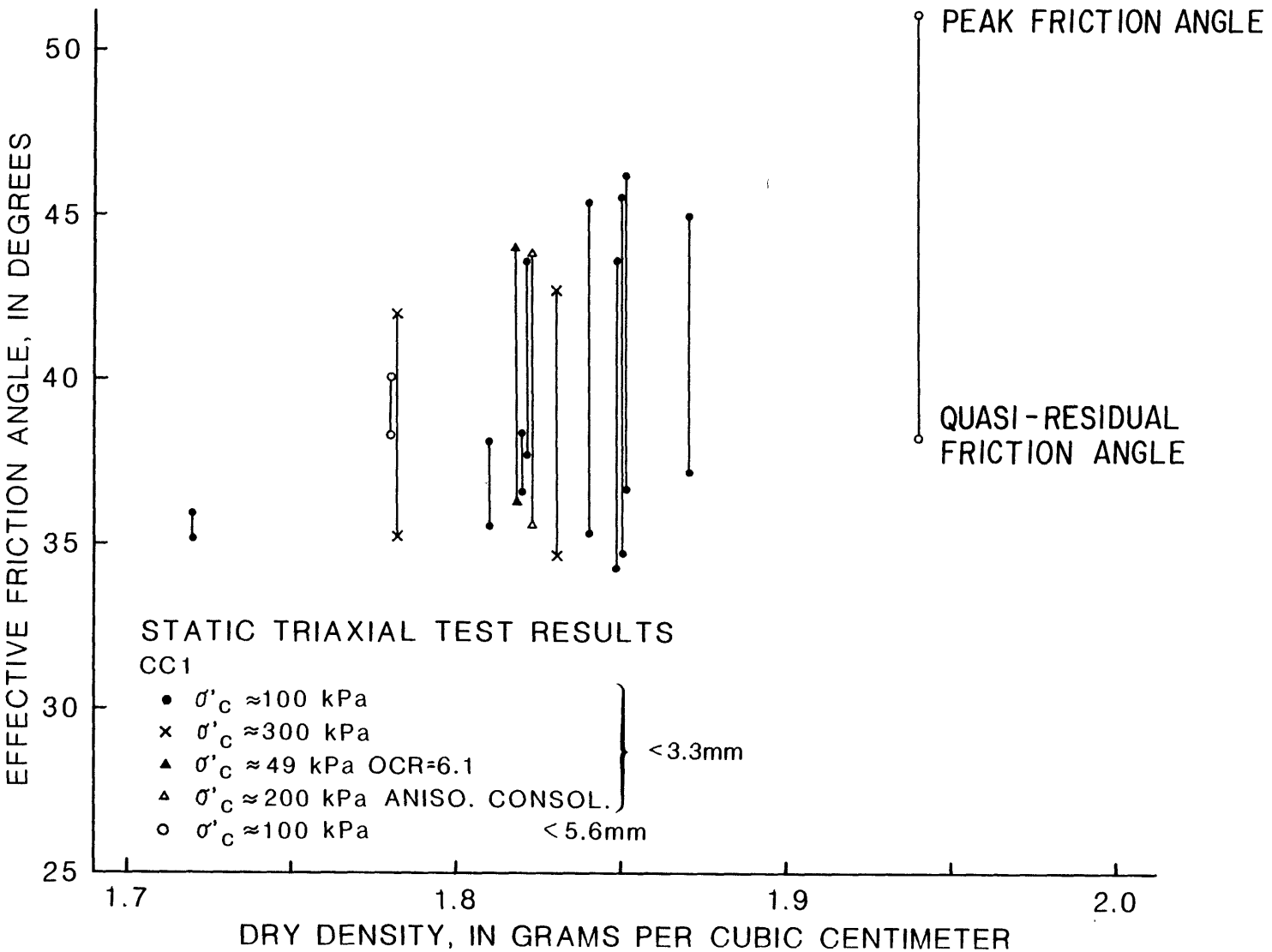

Fig. 4. Static triaxial test results for site CC1.

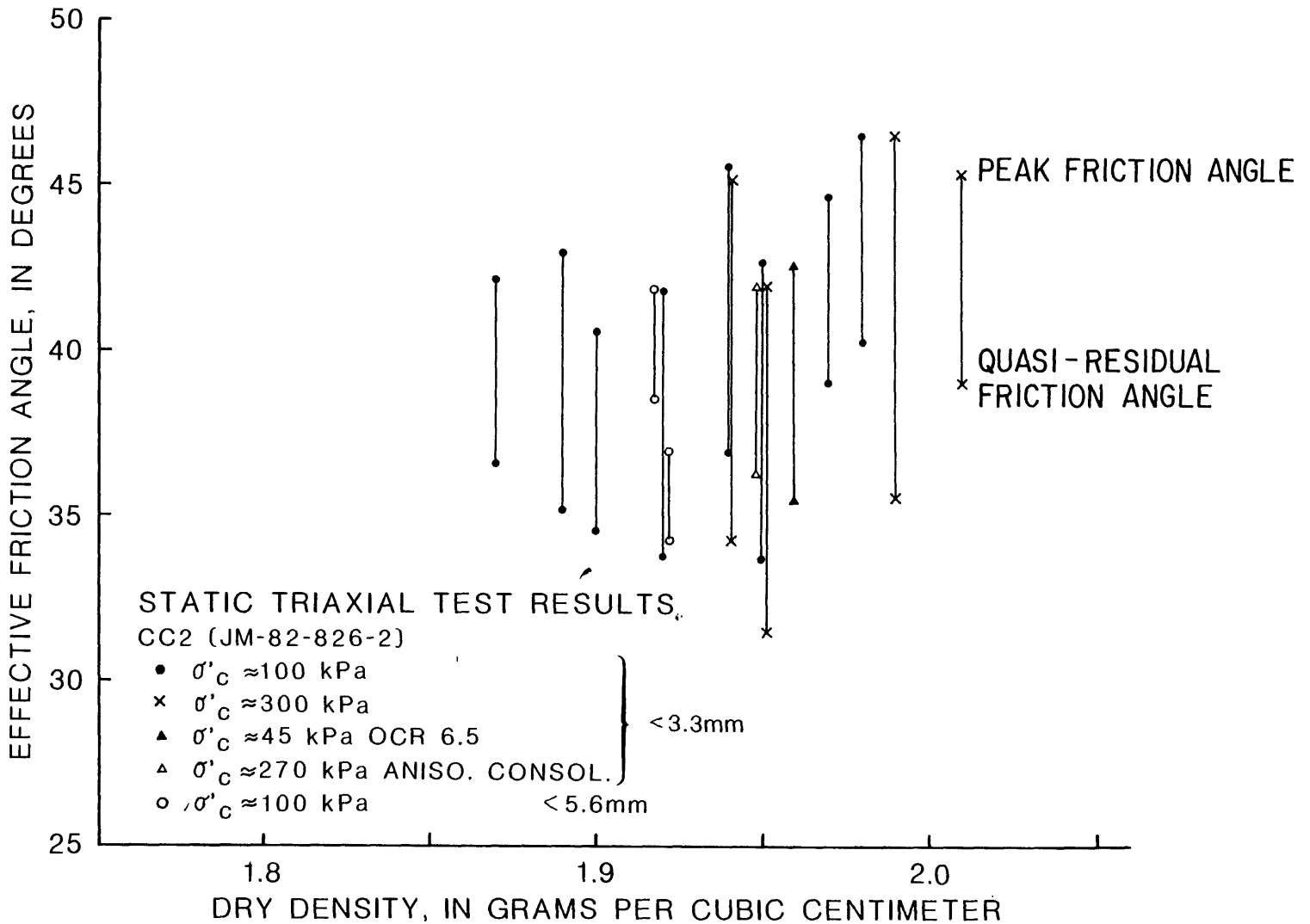

Fig. 5. Static triaxial test results for site CC2.

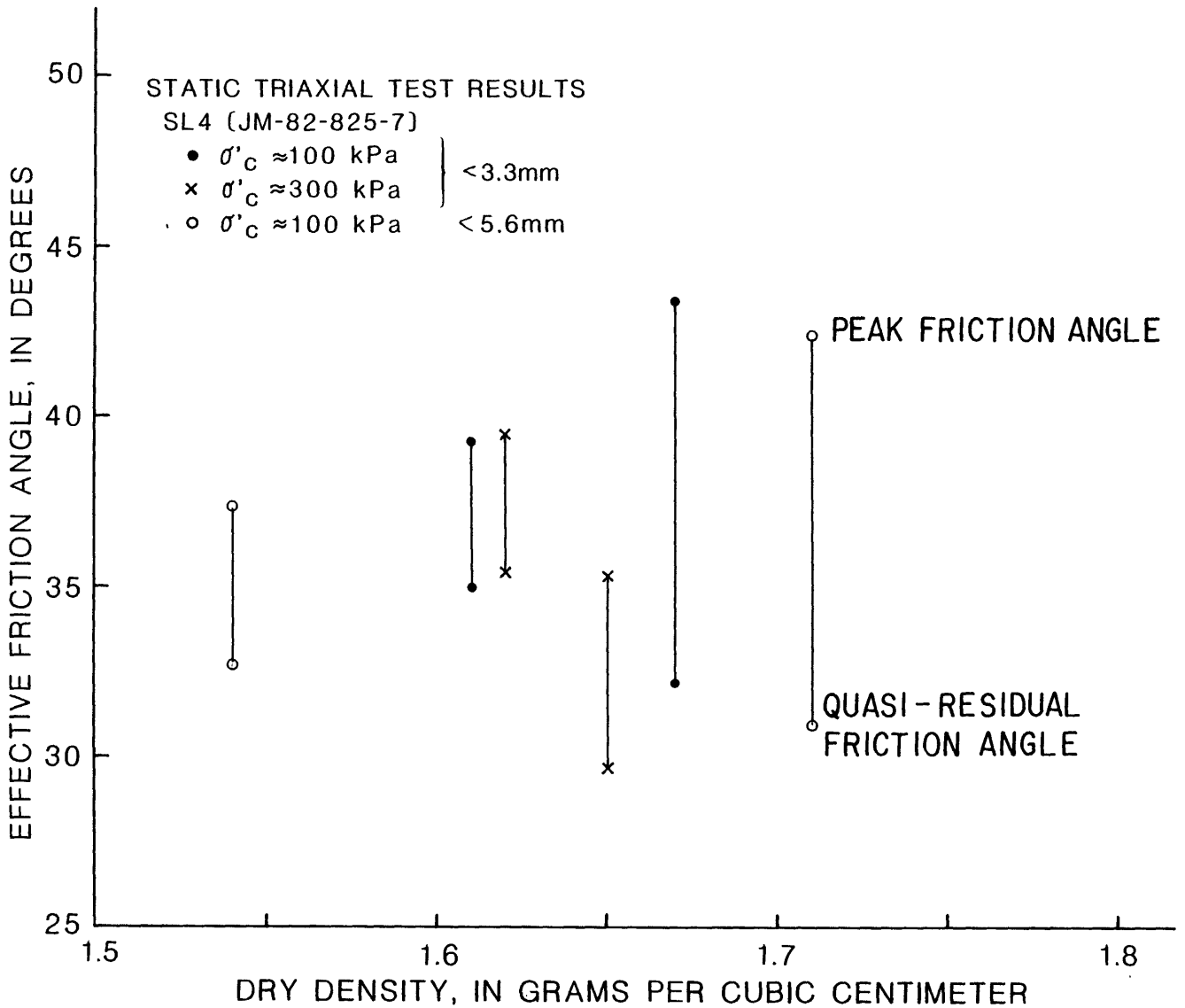

Fig. 6. Static triaxial test results for site SL4.

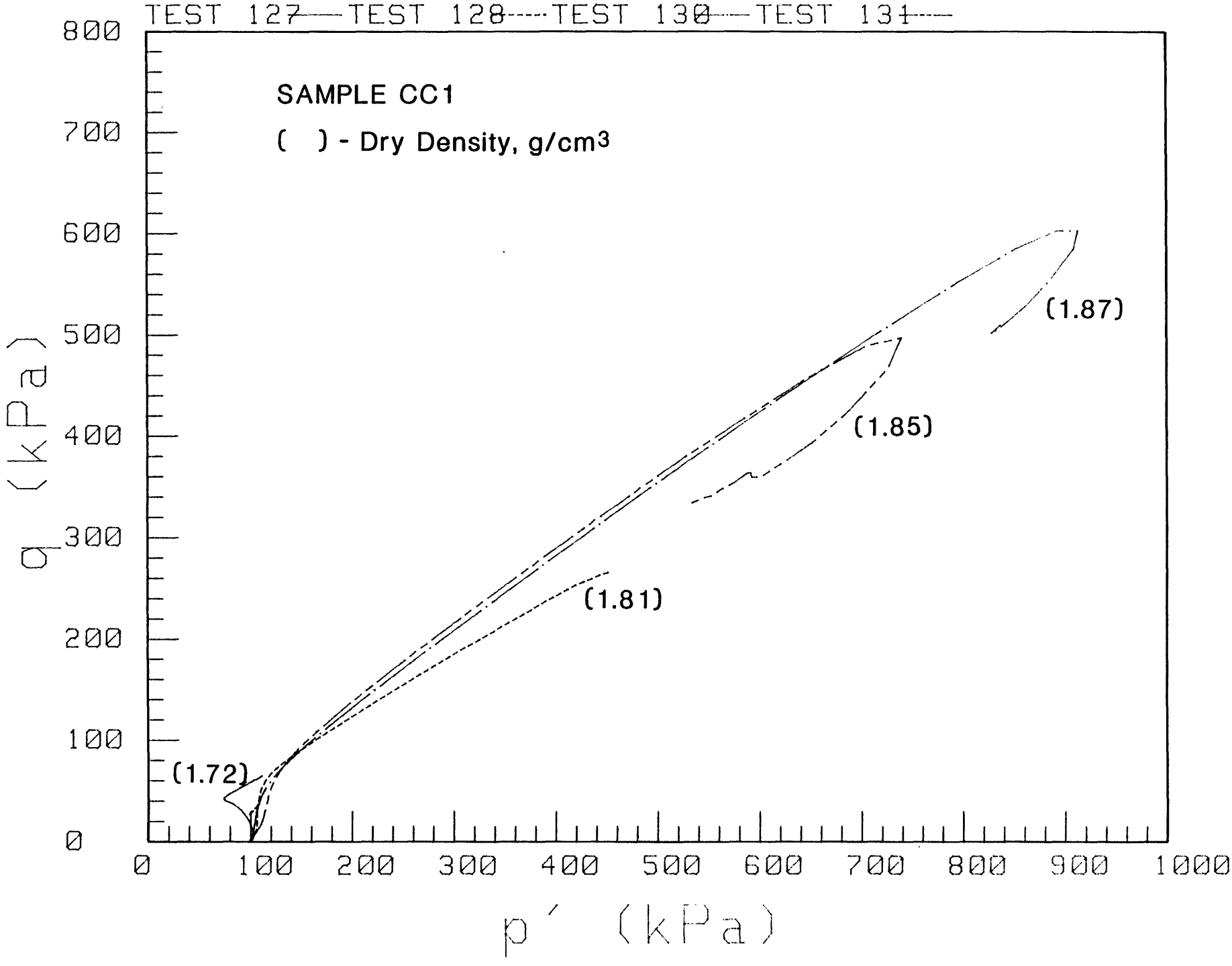

Fig. 7. Stress paths for CC1 material (<3.3 mm) showing effect of dry density on static triaxial test behavior.

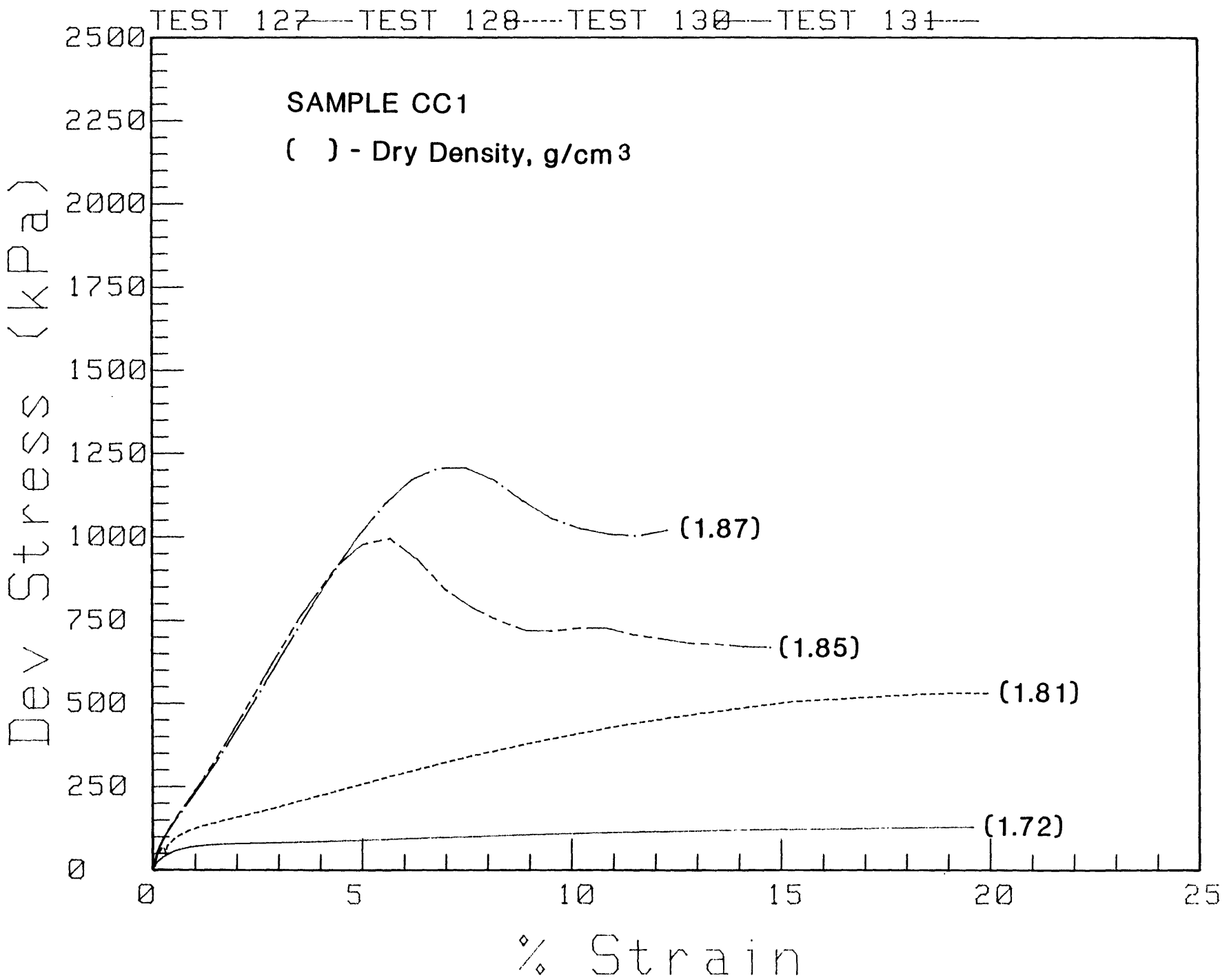

Fig. 8. Deviator stress versus strain for CC1 material (<3.3 mm) showing effect of dry density on static triaxial test behavior.

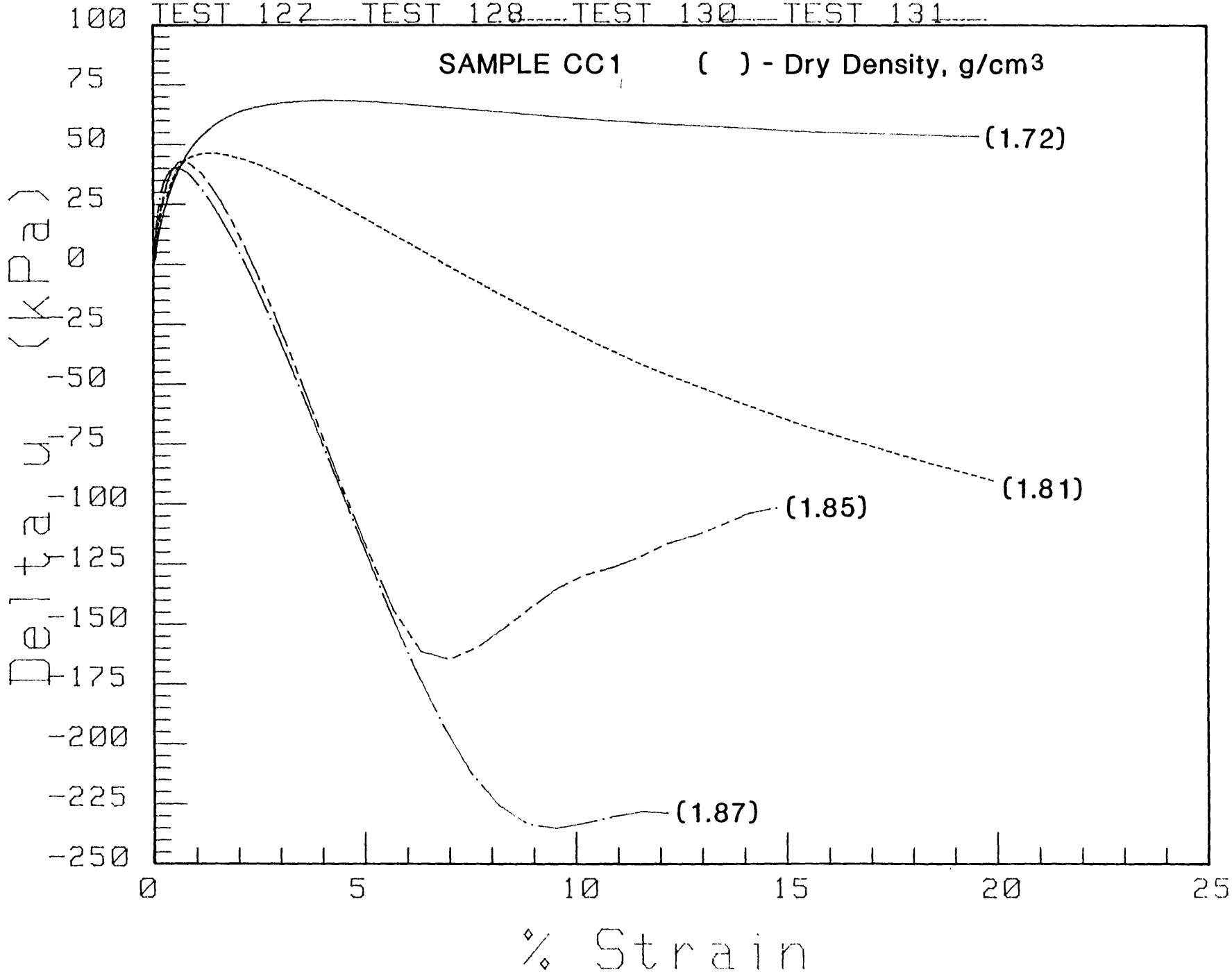

Fig. 9. Change in pore water pressure versus strain for CC1 material (<3.3 mm) showing effect of dry density on static triaxial test behavior.

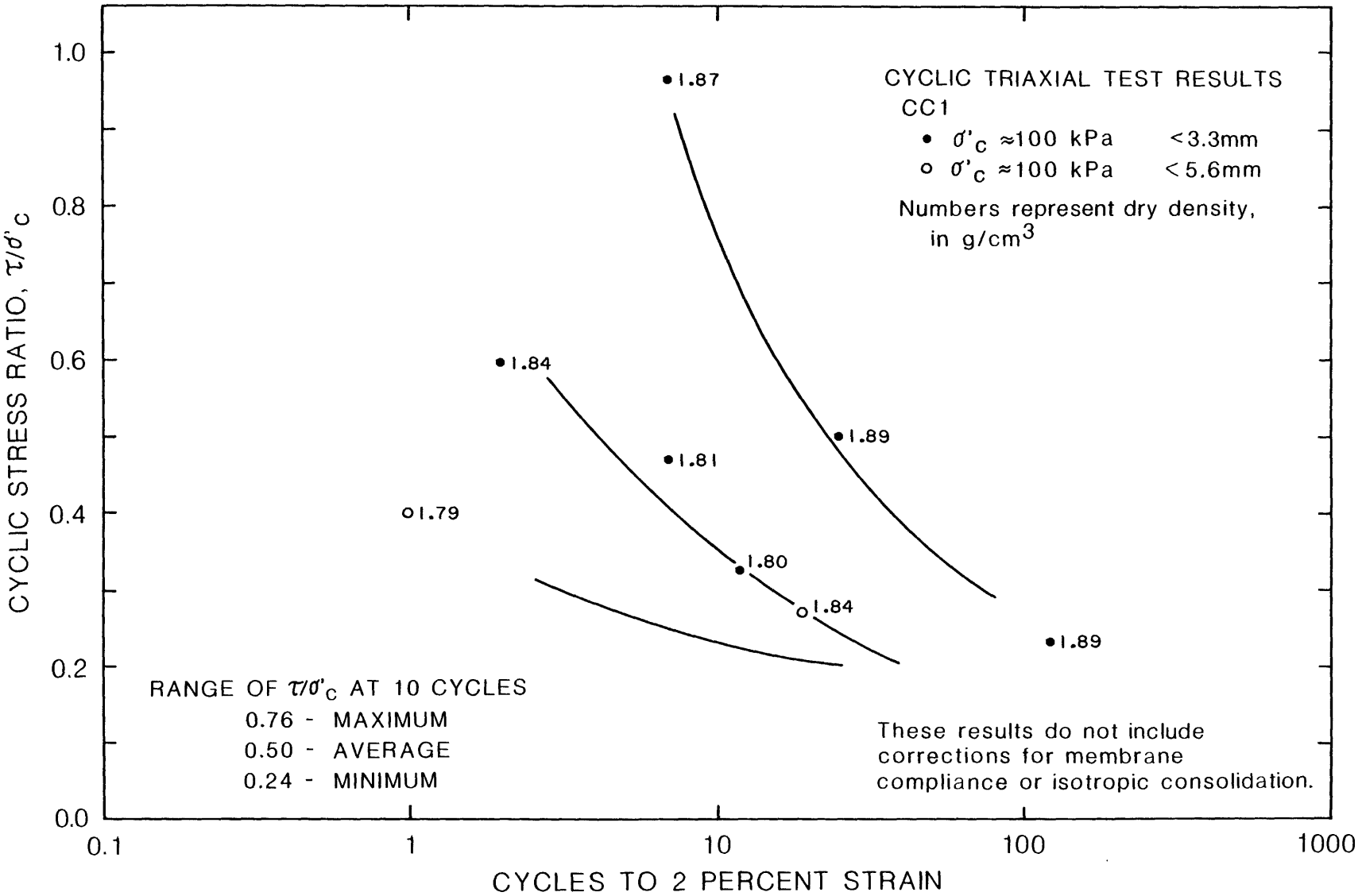

Fig.10. Cyclic stress ratio, τ/σ'_c, versus cycles to 2 percent single-amplitude strain for site CC1.

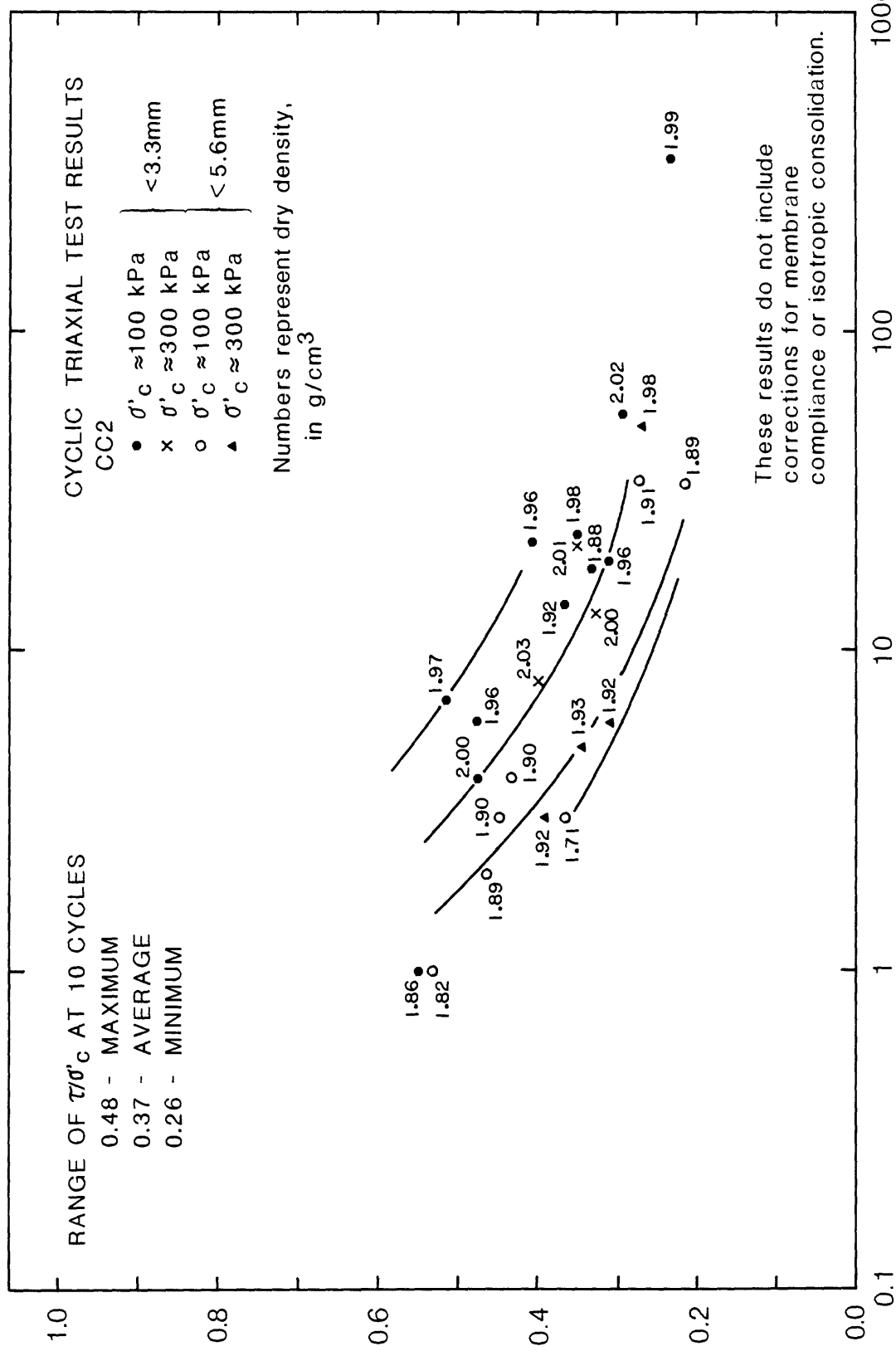

Fig.11. Cyclic stress ratio, τ/σ'_c, versus cycles to 2 percent single-amplitude strain for site CC2.

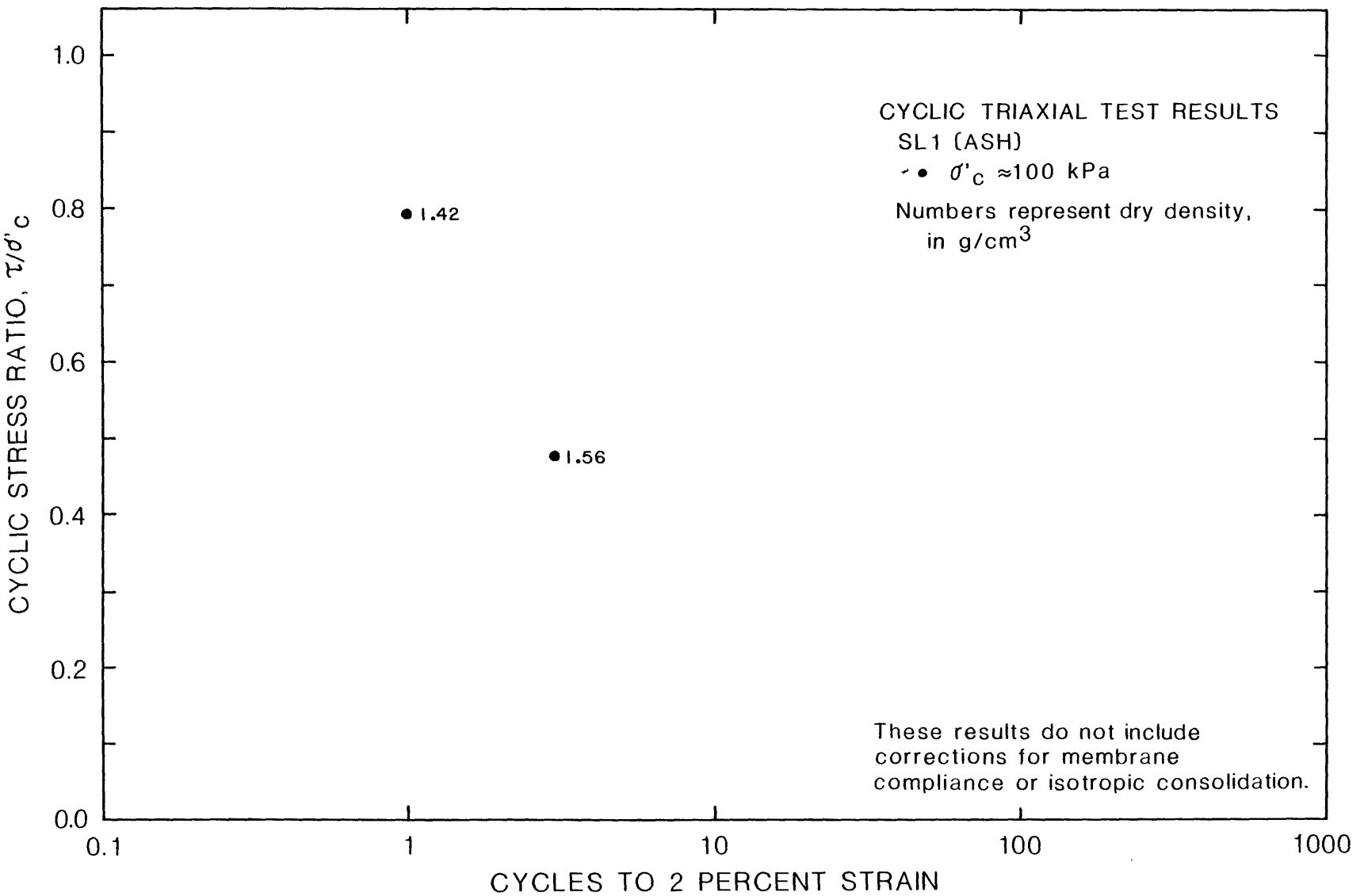

Fig.12. Cyclic stress ratio, τ/σ'_c, versus cycles to 2 percent single-amplitude strain for site SL1.

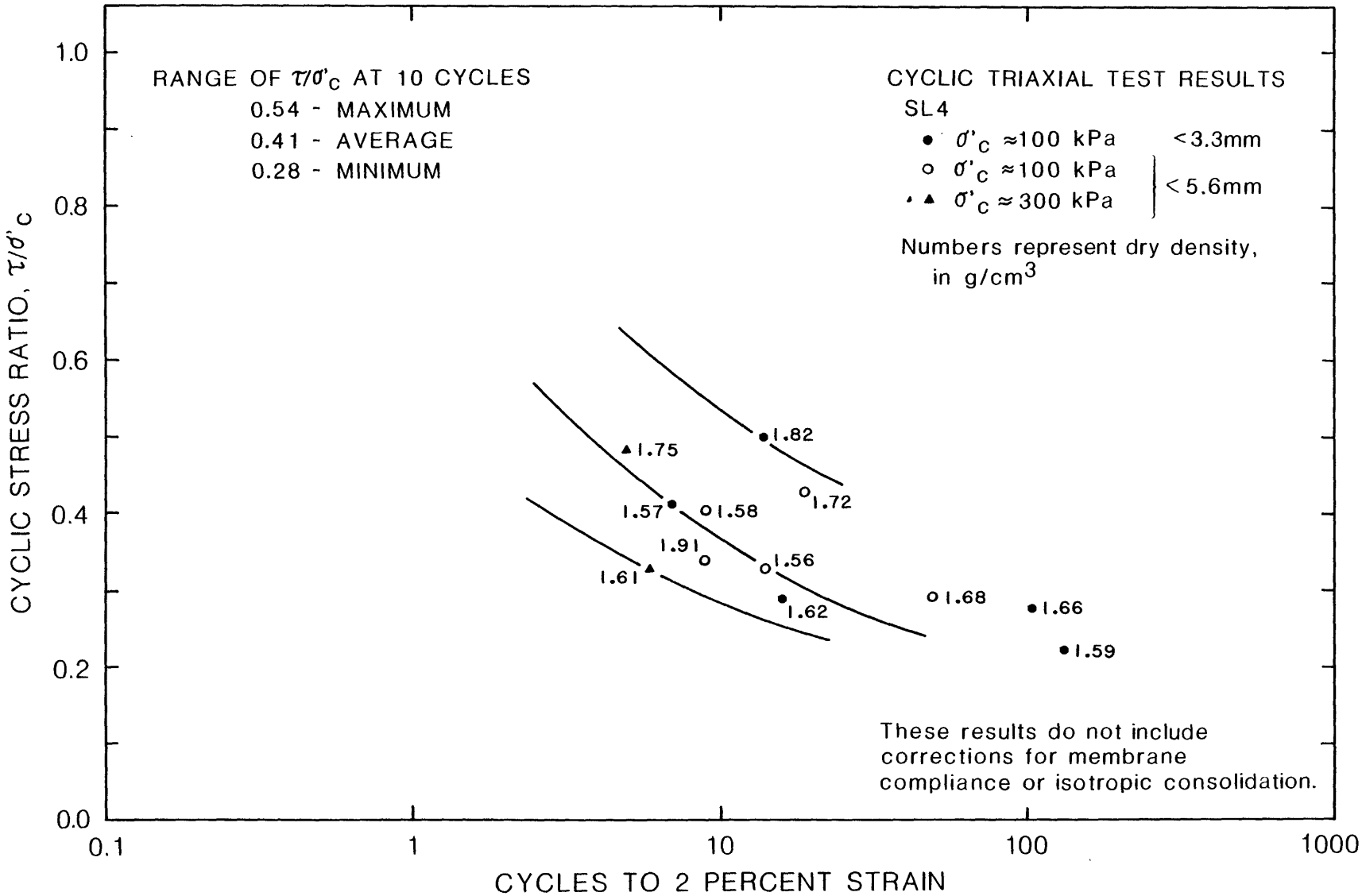

Fig.13. Cyclic stress ratio, τ/σ'_c, versus cycles to 2 percent single-amplitude strain for site SL4.

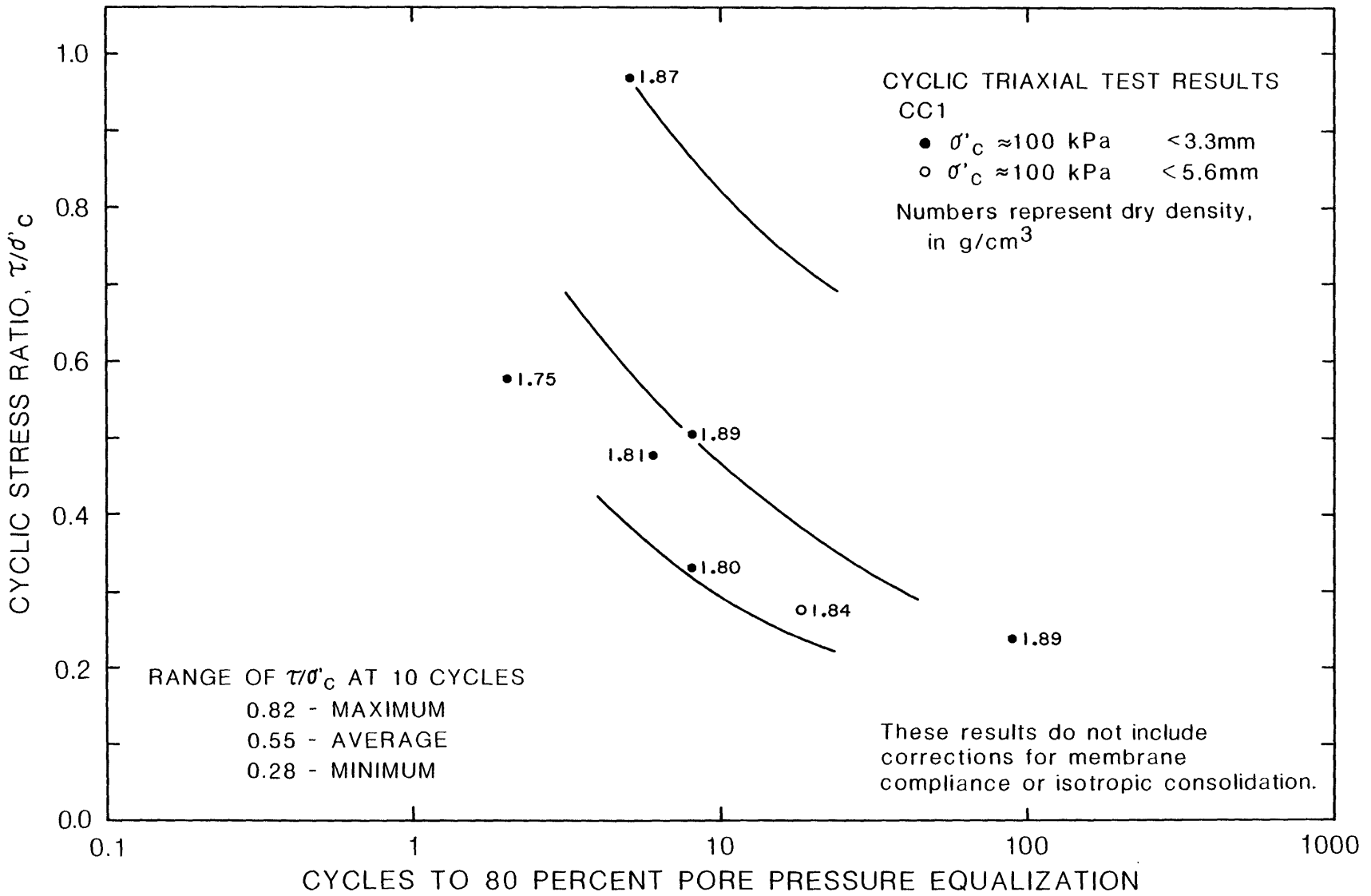

Fig.14. Cyclic stress ratio, τ/σ'_c, versus cycles to 80 percent pore pressure equalization for site CC1.

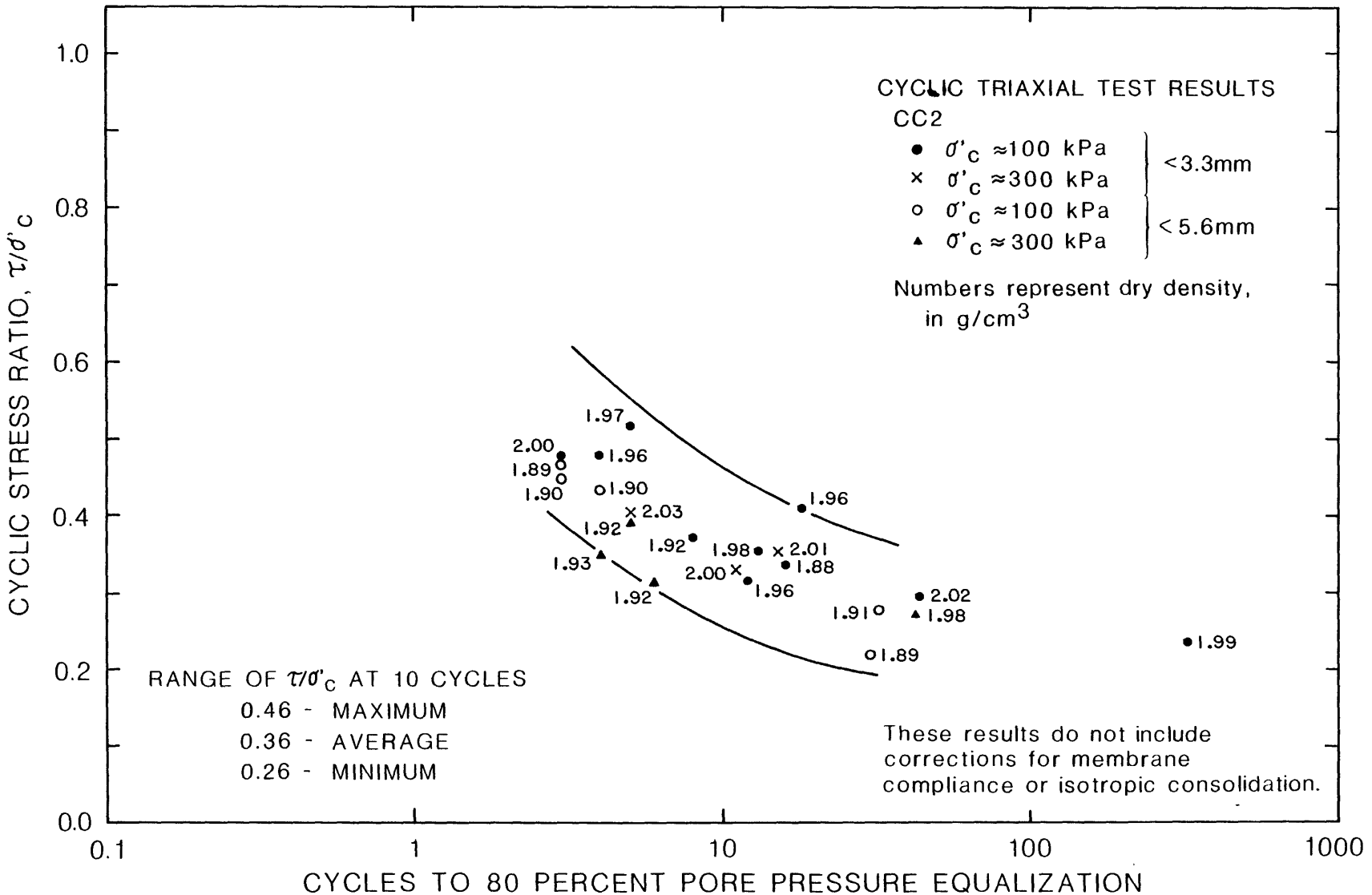

Fig.15. Cyclic stress ratio, τ/σ'_c, versus cycles to 80 percent pore pressure equalization for site CC2.

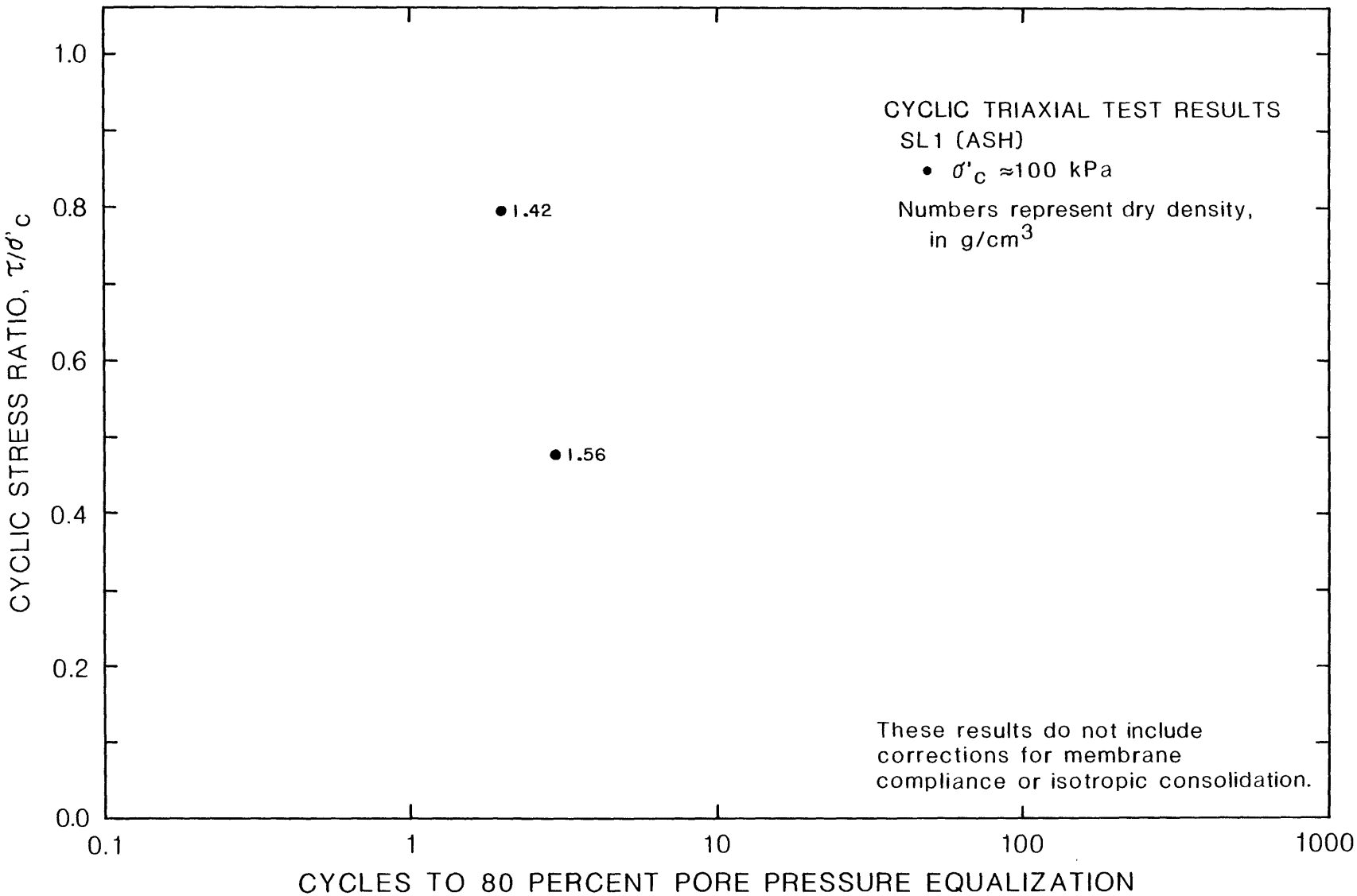

Fig.16. Cyclic stress ratio, τ/σ'_c, versus cycles to 80 percent pore pressure equalization for site SL1.

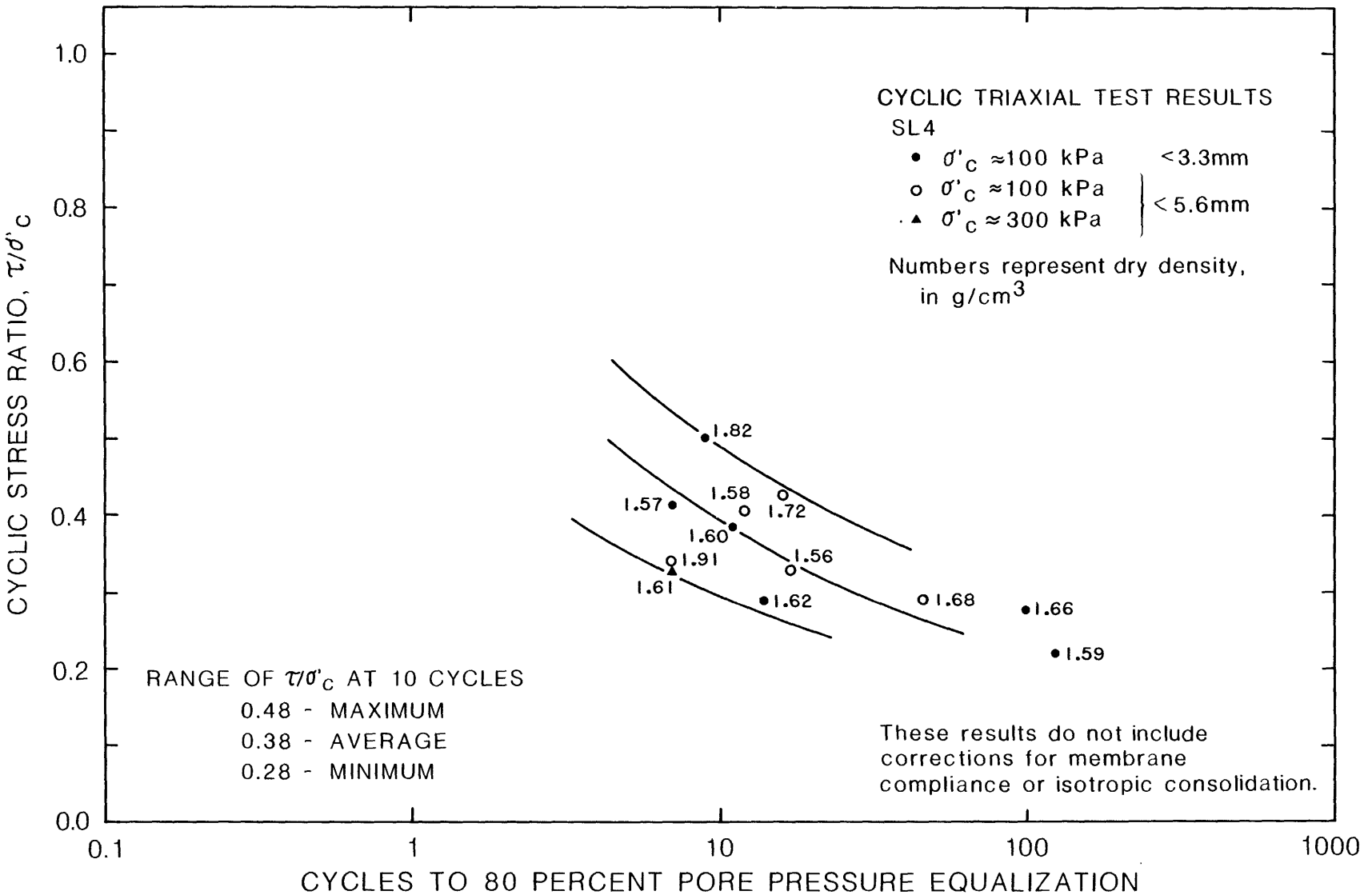

Fig.17. Cyclic stress ratio, τ/σ'_c, versus cycles to 80 percent pore pressure equalization for site SL4.

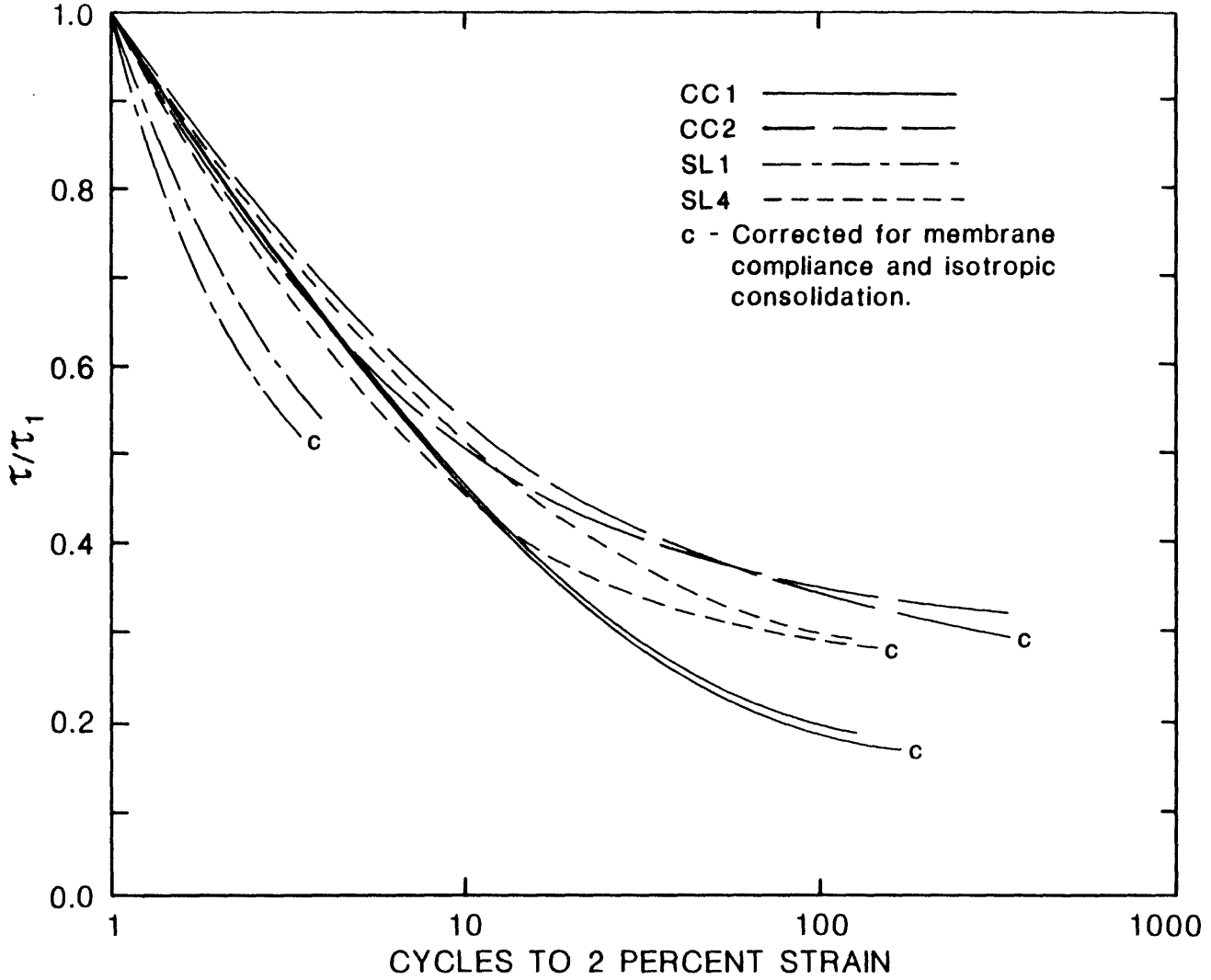

Fig.18. τ/τ_1 versus cycles to 2 percent single amplitude strain for Mt. St. Helens cyclic triaxial test samples.

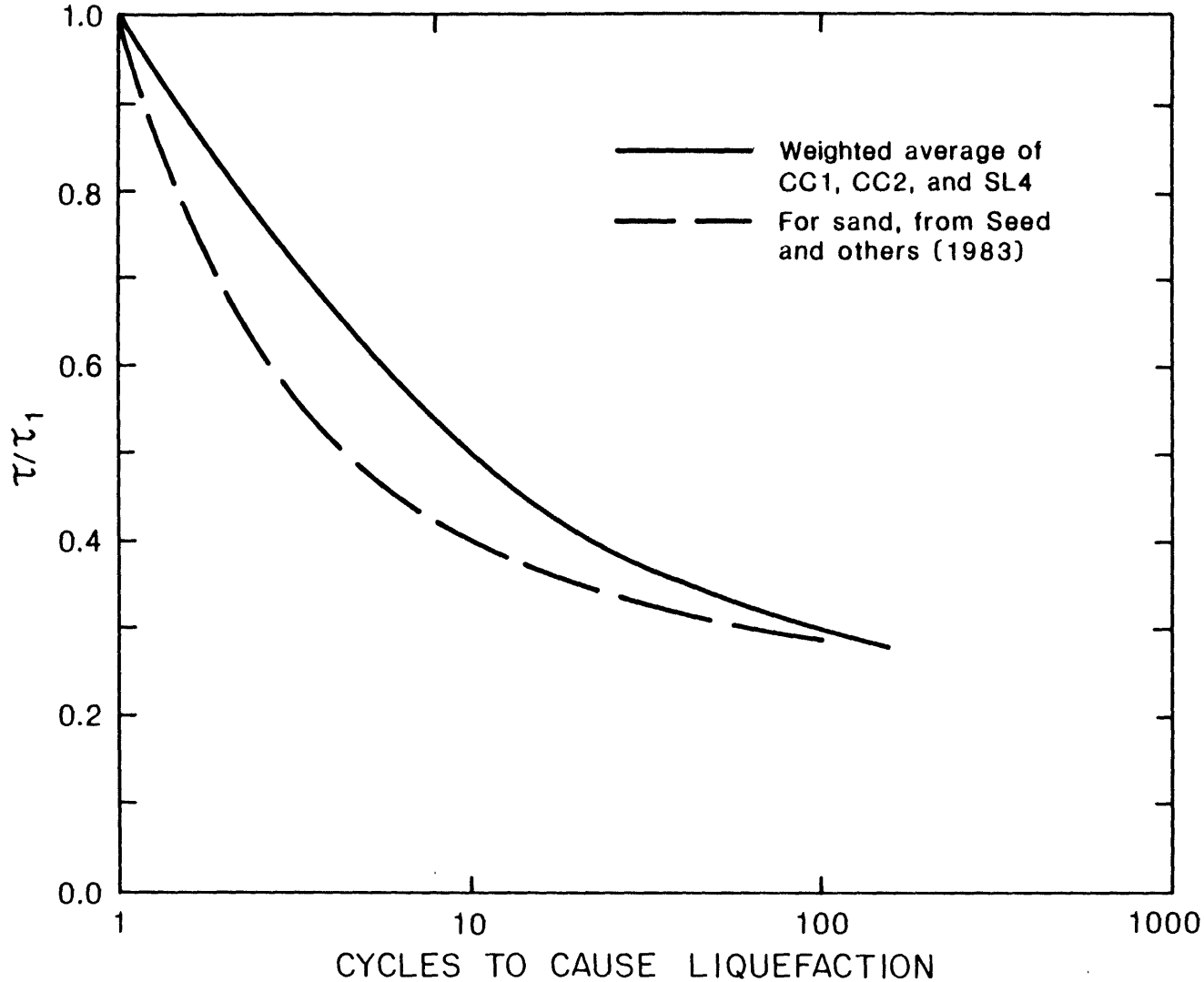

Fig.19. Weighted average τ/τ_1 curve for Mt. St. Helens samples, Seed and others (1983) used a failure criterion of 100 percent pore pressure equalization and ±5 percent strain.

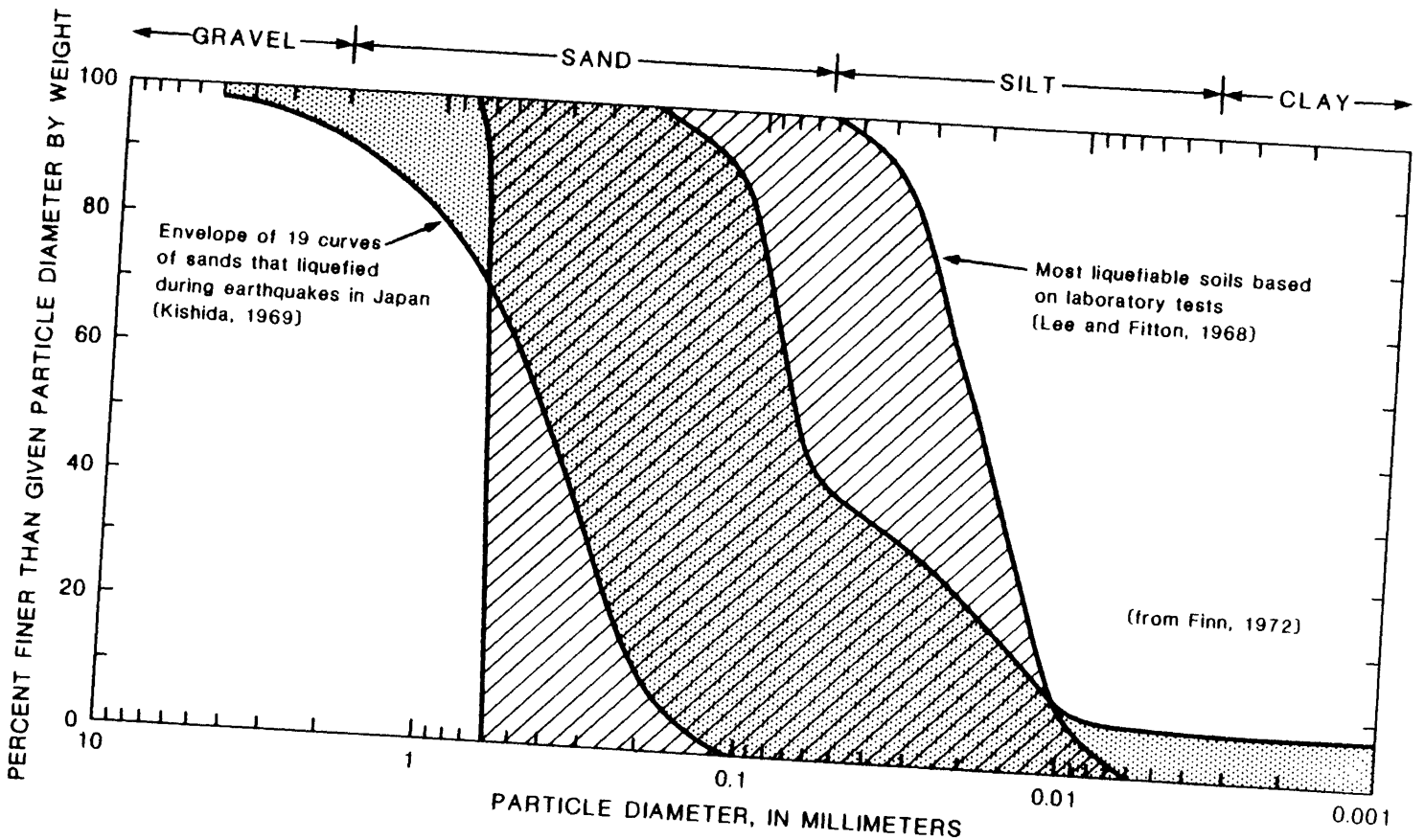

Fig. 20. Zones of grain size distrbution curves of liquefaction prone materials.

APPENDIX A

STATIC TRIAXIAL TEST RESULTS

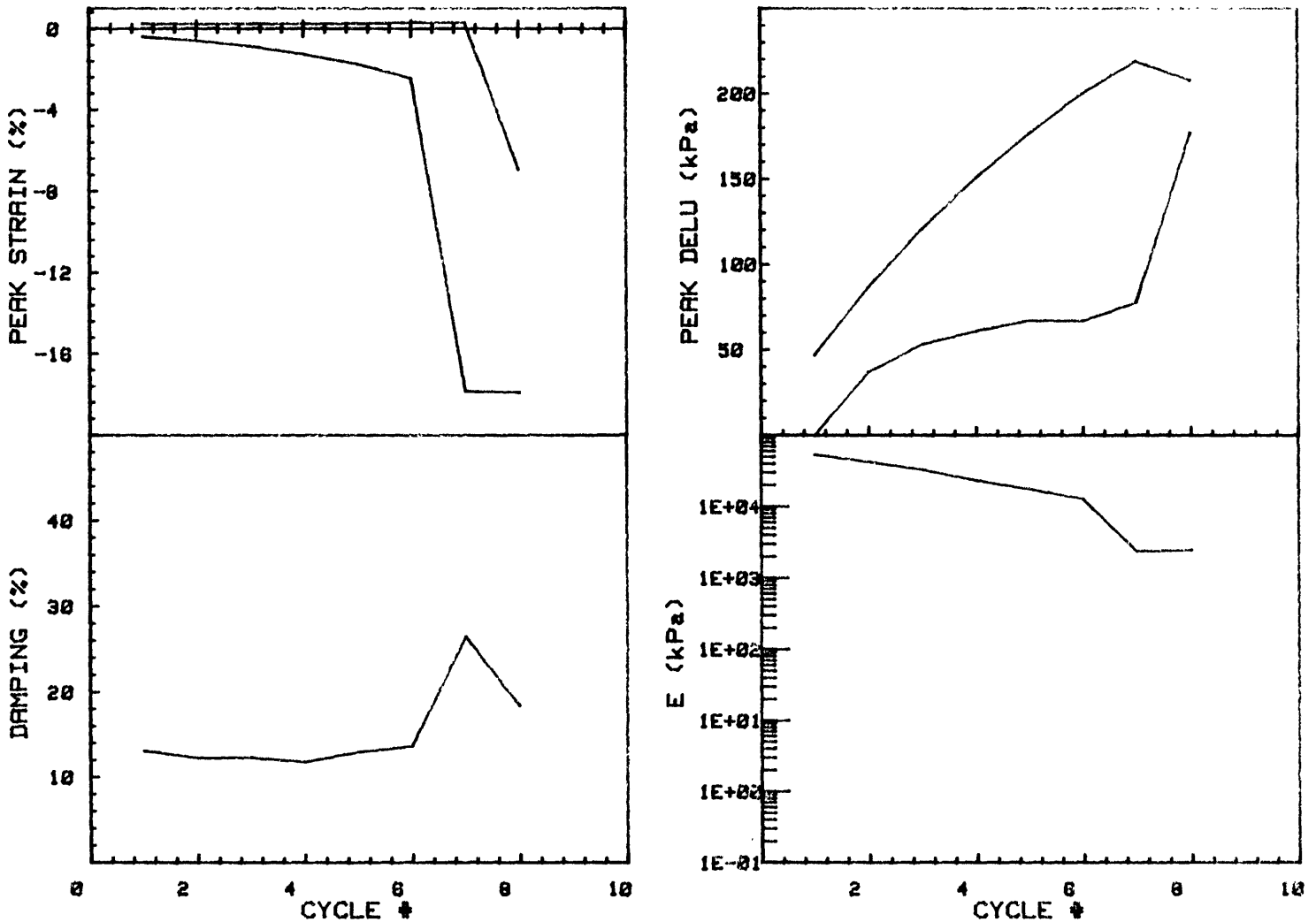

CRUISE ST HELENS		INCREMENT (cm)	REMOLDED SURF
CORE NO.	SL4	TEST NO.	D194
SIG1c'(kPa)	275.2	STATIC qf (kPa)	280.0
SIG3c'(kPa)	275.2	AVG MAX q (kPa)	89.2 (31.9%)
INDUCED OCR	1.0	AVG MIN q (kPa)	-78.1 (27.9%)

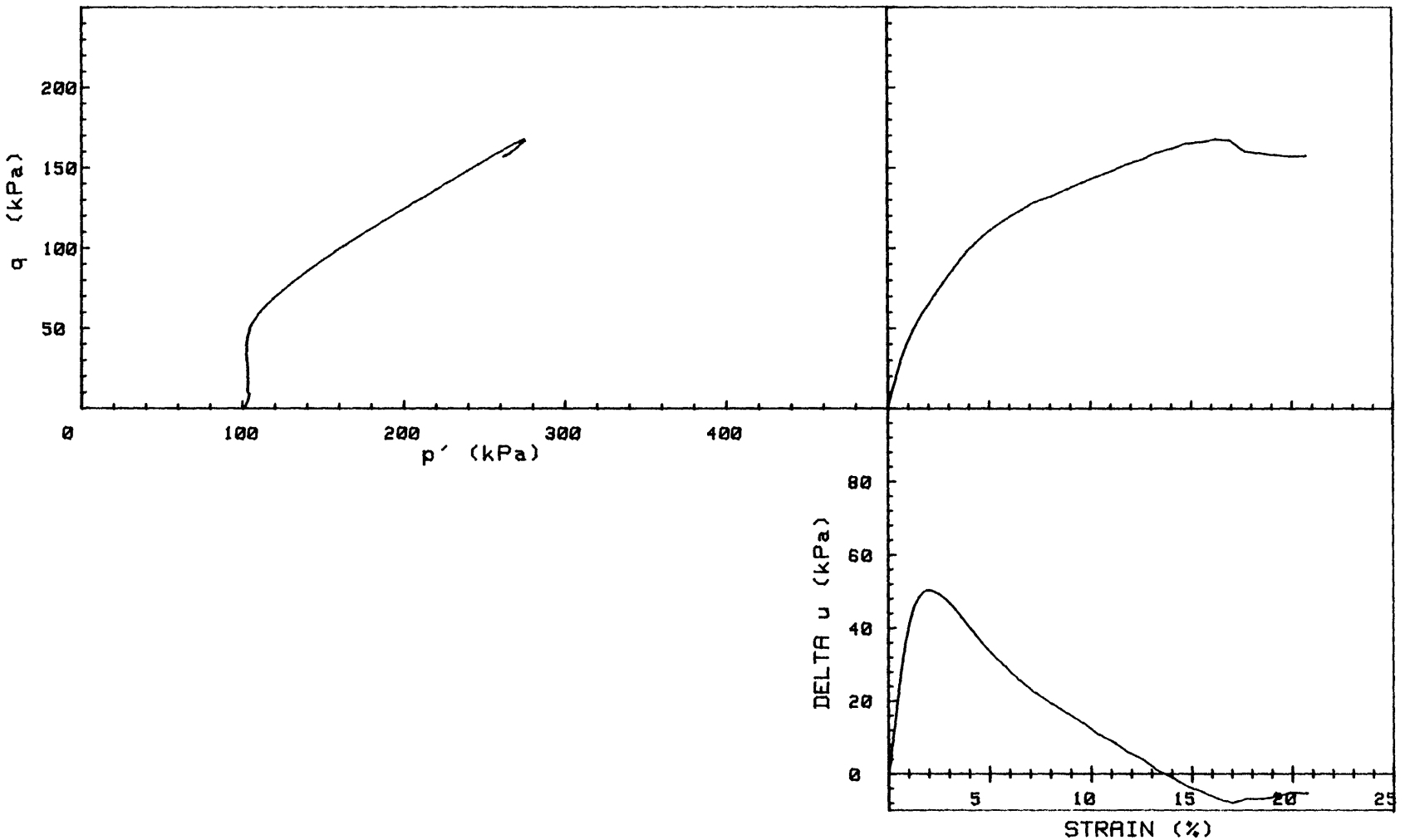

CRUISE ST HELENS		INCREMENT (cm)	REMOLDED-SURF
CORE NO.	CASTLE CR	TEST NO.	TE123

SIG1c'(kPa)	100.8
SIG3c'(kPa)	100.8
INDUCED OCR	1.0

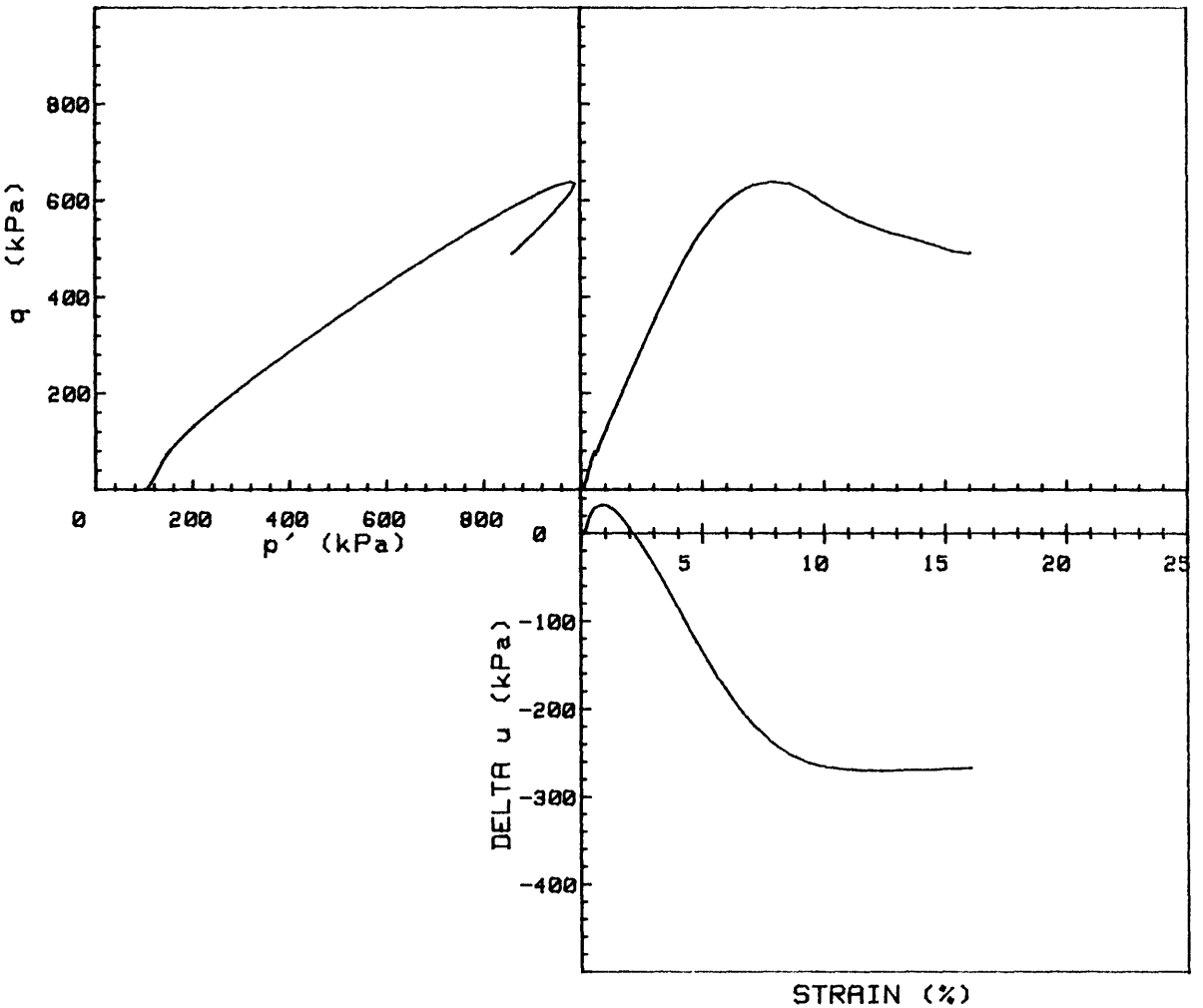

CRUISE ST HELENS		INCREMENT (cm)	REMOLDED-SURF
CORE NO.	CASTLE CR	TEST NO.	TE124

SIG1c'(kPa)	103.1
SIG3c'(kPa)	103.1
INDUCED OCR	1.0

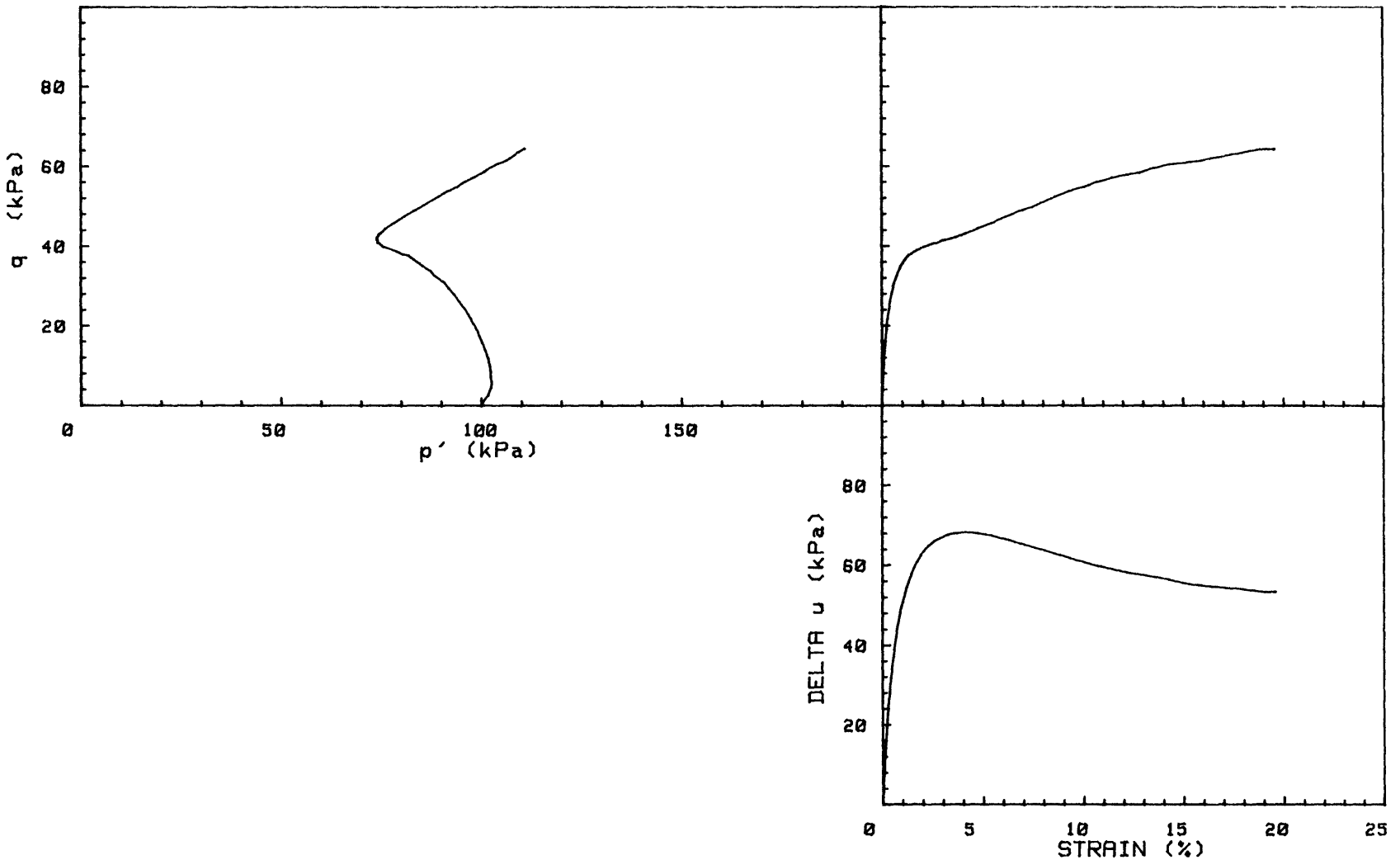

CRUISE ST HELENS		INCREMENT (cm)	REMOLDED-SURF
CORE NO.	CASTLE CR	TEST NO.	TE127

SIG1c'(kPa)	99.9
SIG3c'(kPa)	99.9
INDUCED OCR	1.0

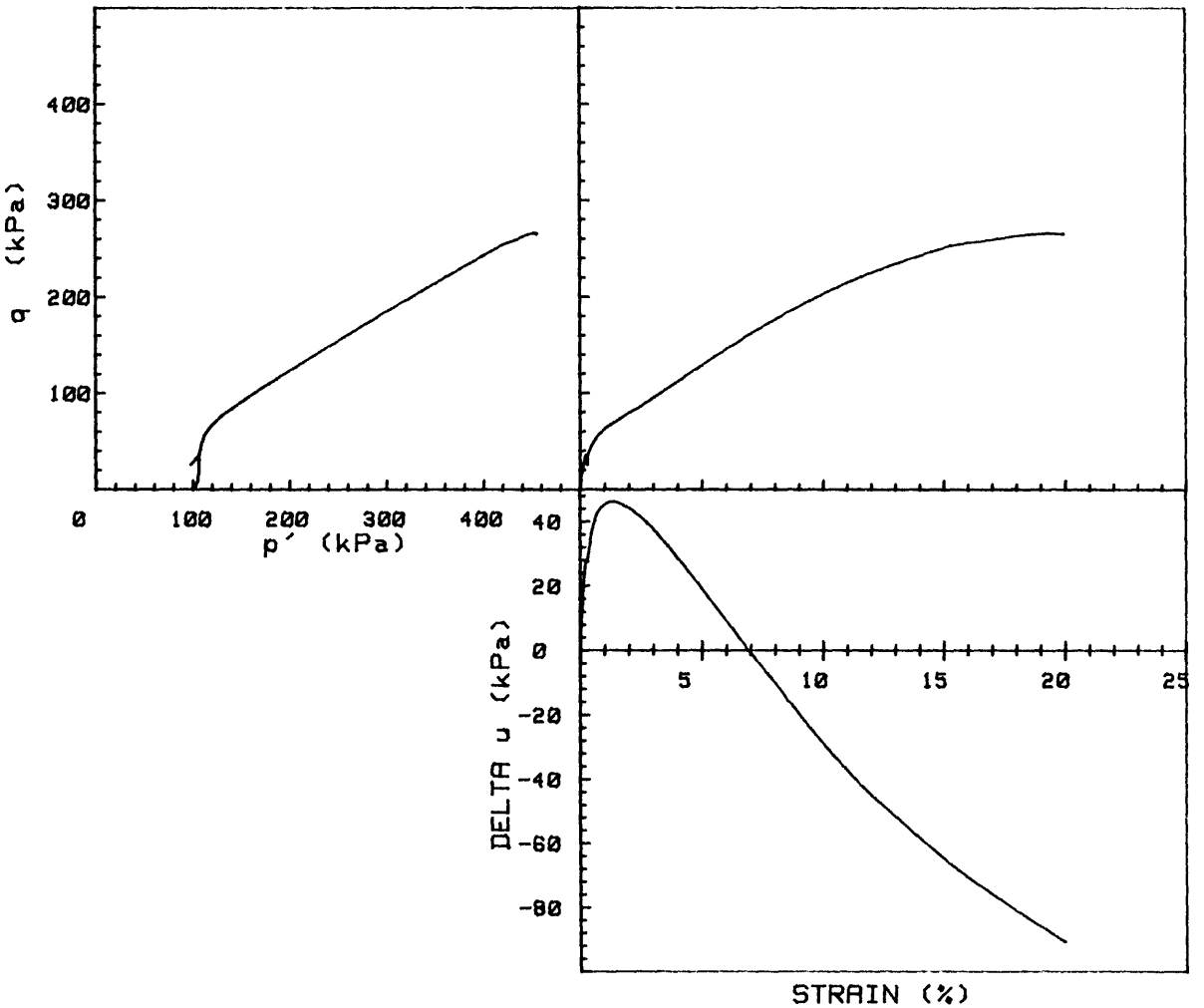

CRUISE ST HELENS		INCREMENT (cm)	REMOLDED-SURF
CORE NO.	CASTLE CR	TEST NO.	TE128

SIG1c´(kPa)	99.8
SIG3c´(kPa)	99.8
INDUCED OCR	1.0

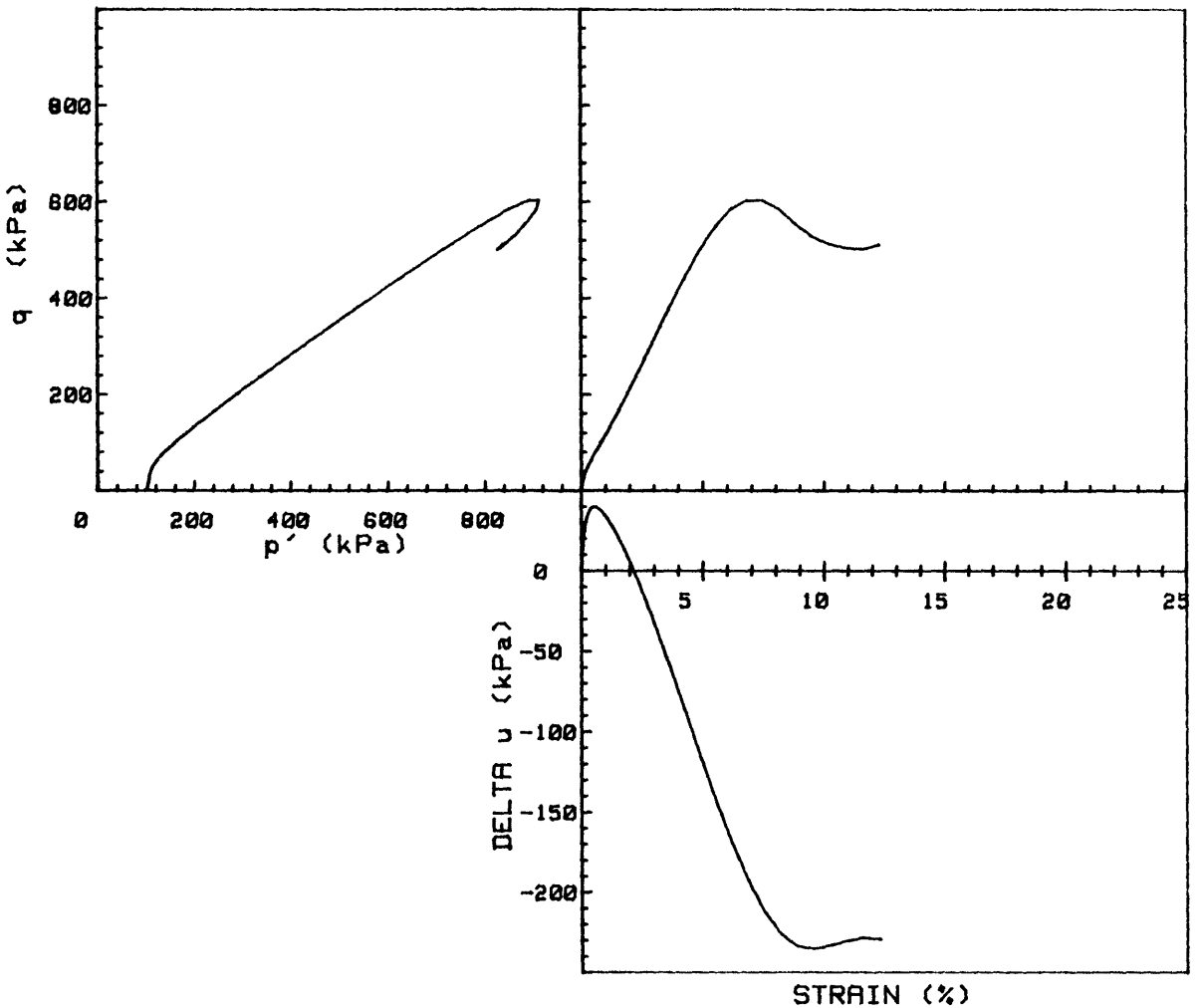

CRUISE ST HELENS		INCREMENT (cm)	REMOLDED-SURF
CORE NO.	CC1	TEST NO.	TE130

SIG1c´(kPa)	98.6
SIG3c´(kPa)	98.6
INDUCED OCR	1.0

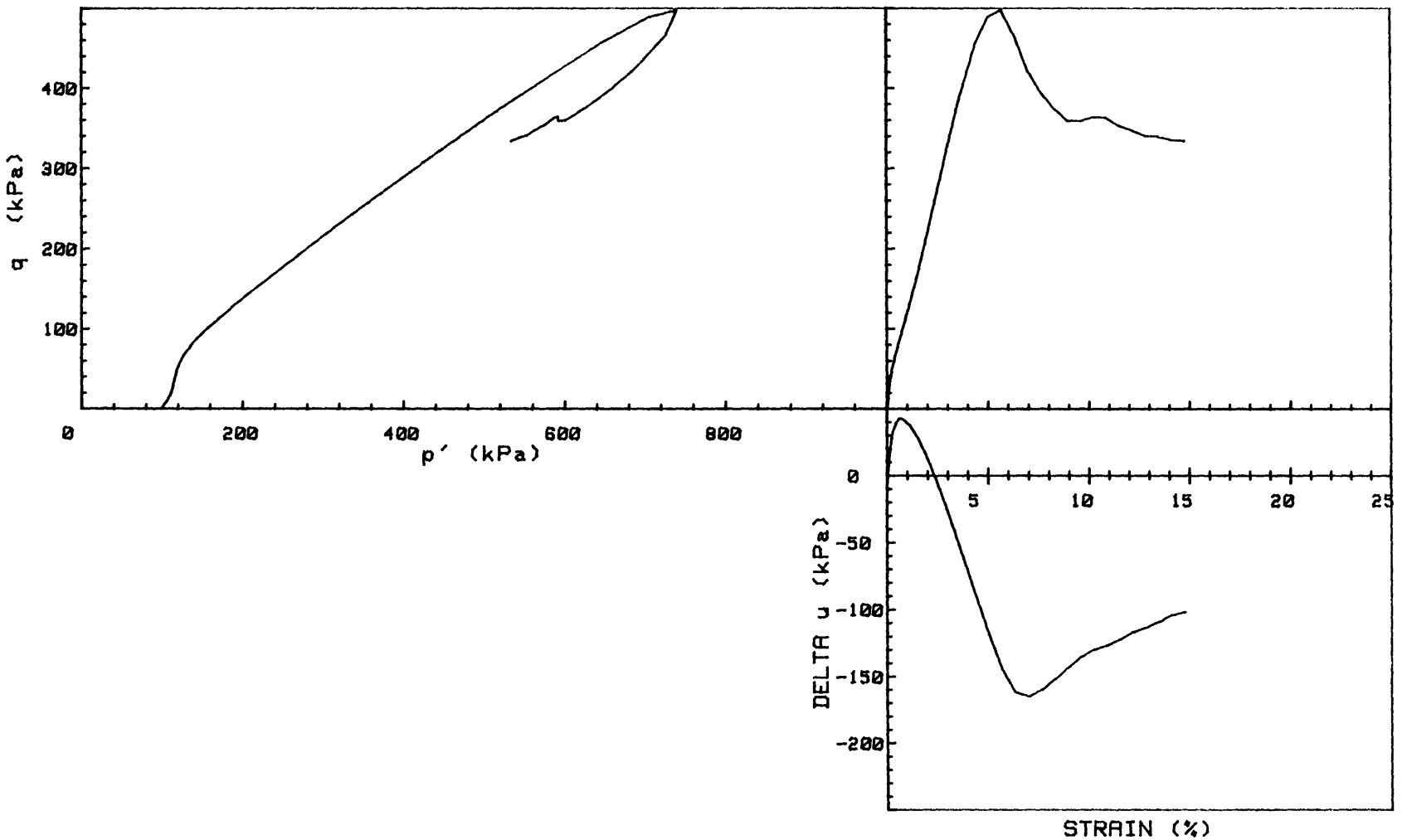

CRUISE ST HELENS	INCREMENT (cm)	REMOLDED-SURF
CORE NO. CC1	TEST NO.	TE131

SIG1c'(kPa)	98.9
SIG3c'(kPa)	98.9
INDUCED OCR	1.0

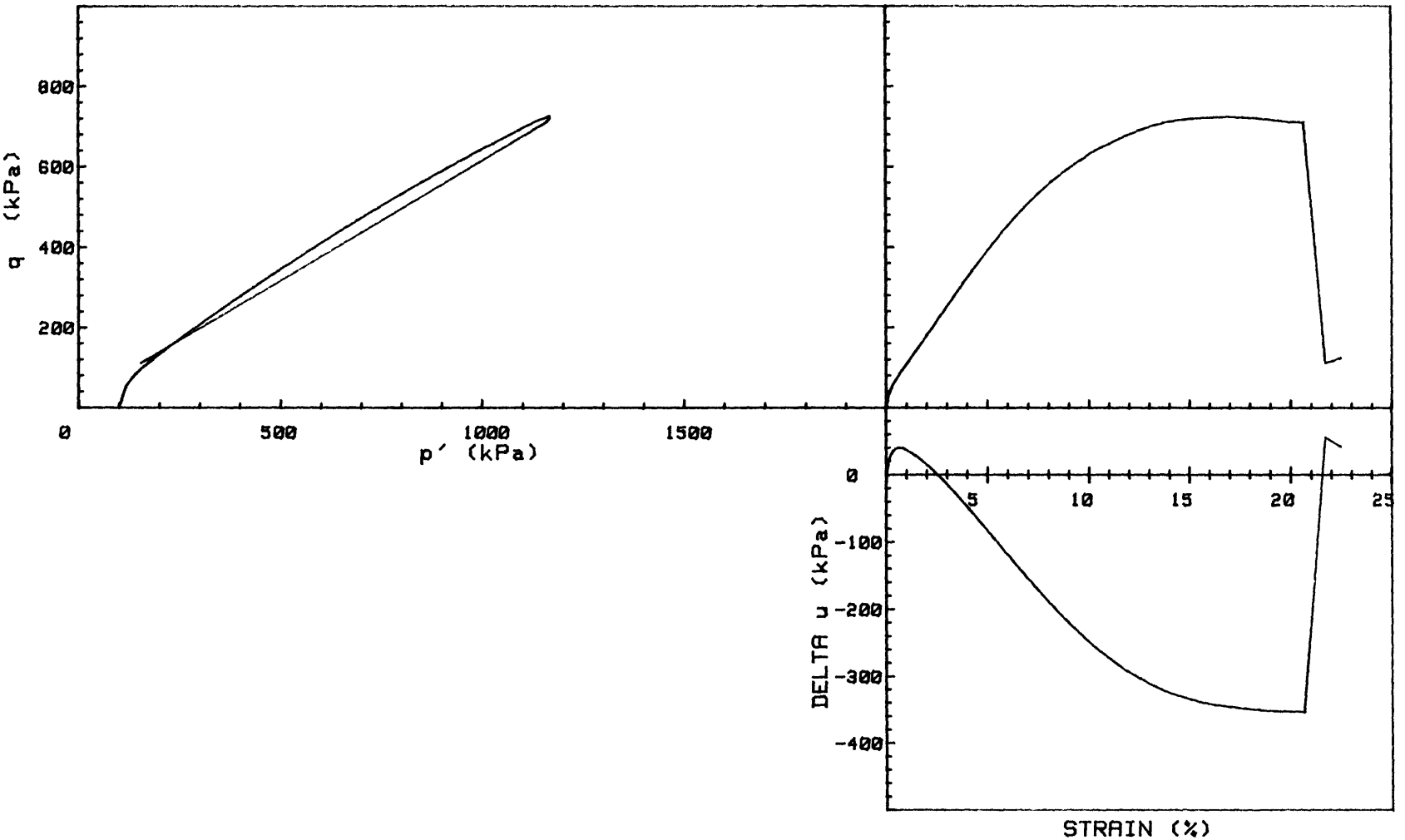

CRUISE ST HELENS		INCREMENT (cm)	REMOLDED-SURF
CORE NO.	CC1	TEST NO.	TE132

SIG1c'(kPa)	98.1
SIG3c'(kPa)	98.1
INDUCED OCR	1.0

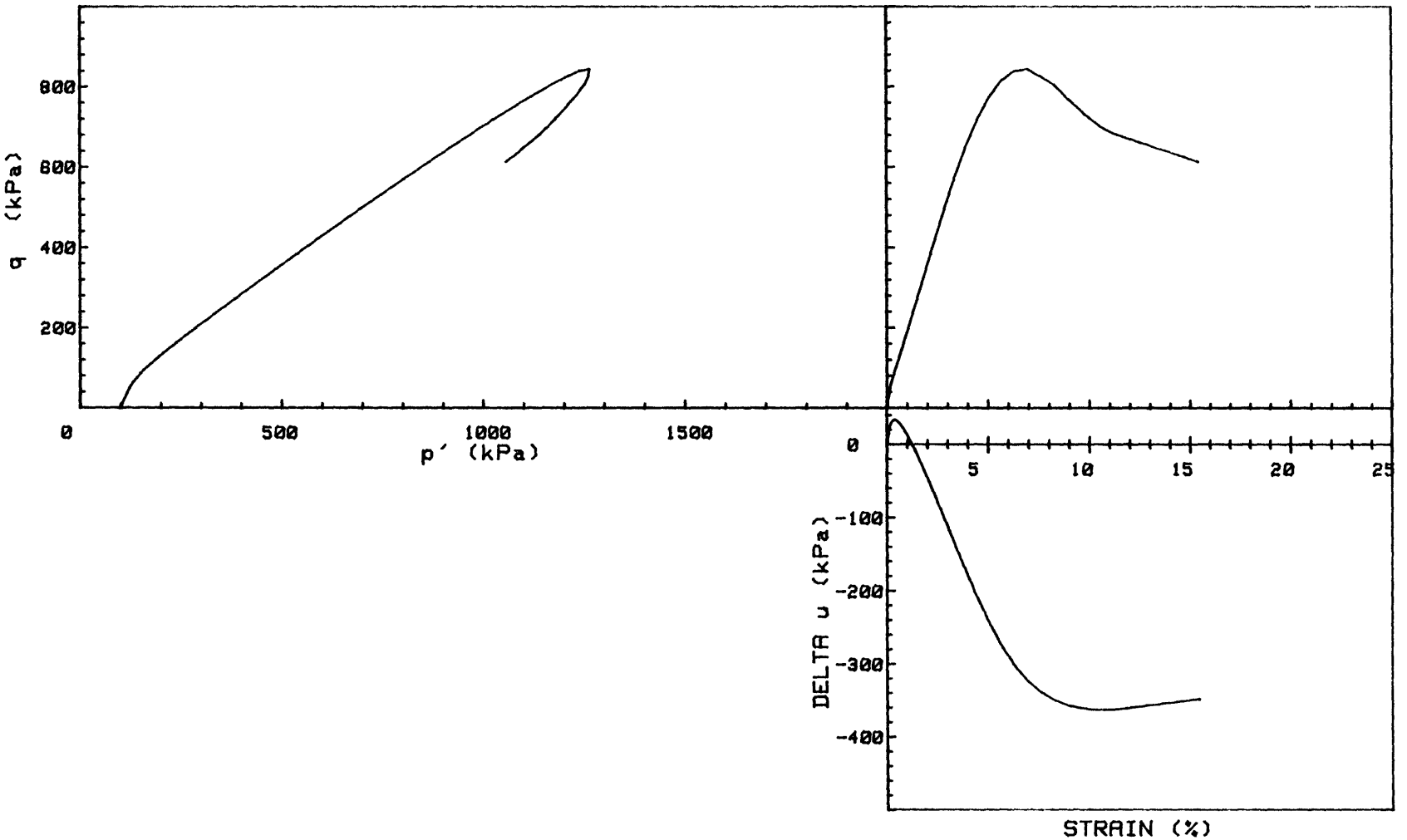

CRUISE ST HELENS		INCREMENT (cm)	REMOLDED-SURF
CORE NO.	CC1	TEST NO.	TE133

SIG1c'(kPa)	98.2
SIG3c'(kPa)	98.2
INDUCED OCR	1.0

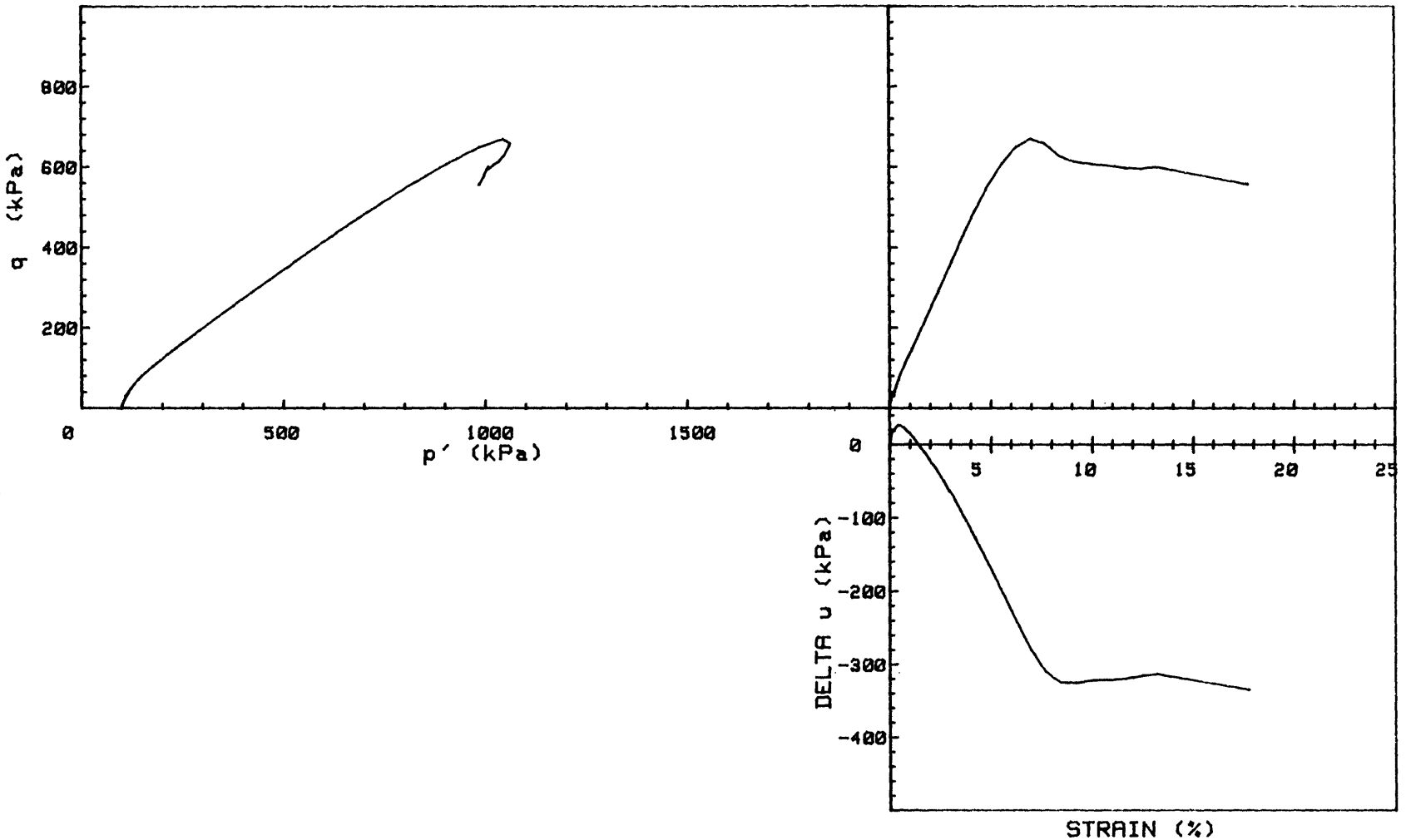

CRUISE ST HELENS		INCREMENT (cm)	REMOLDED-SURF
CORE NO.	CC1	TEST NO.	TE134

SIG1c'(kPa)	96.0
SIG3c'(kPa)	96.0
INDUCED OCR	1.0

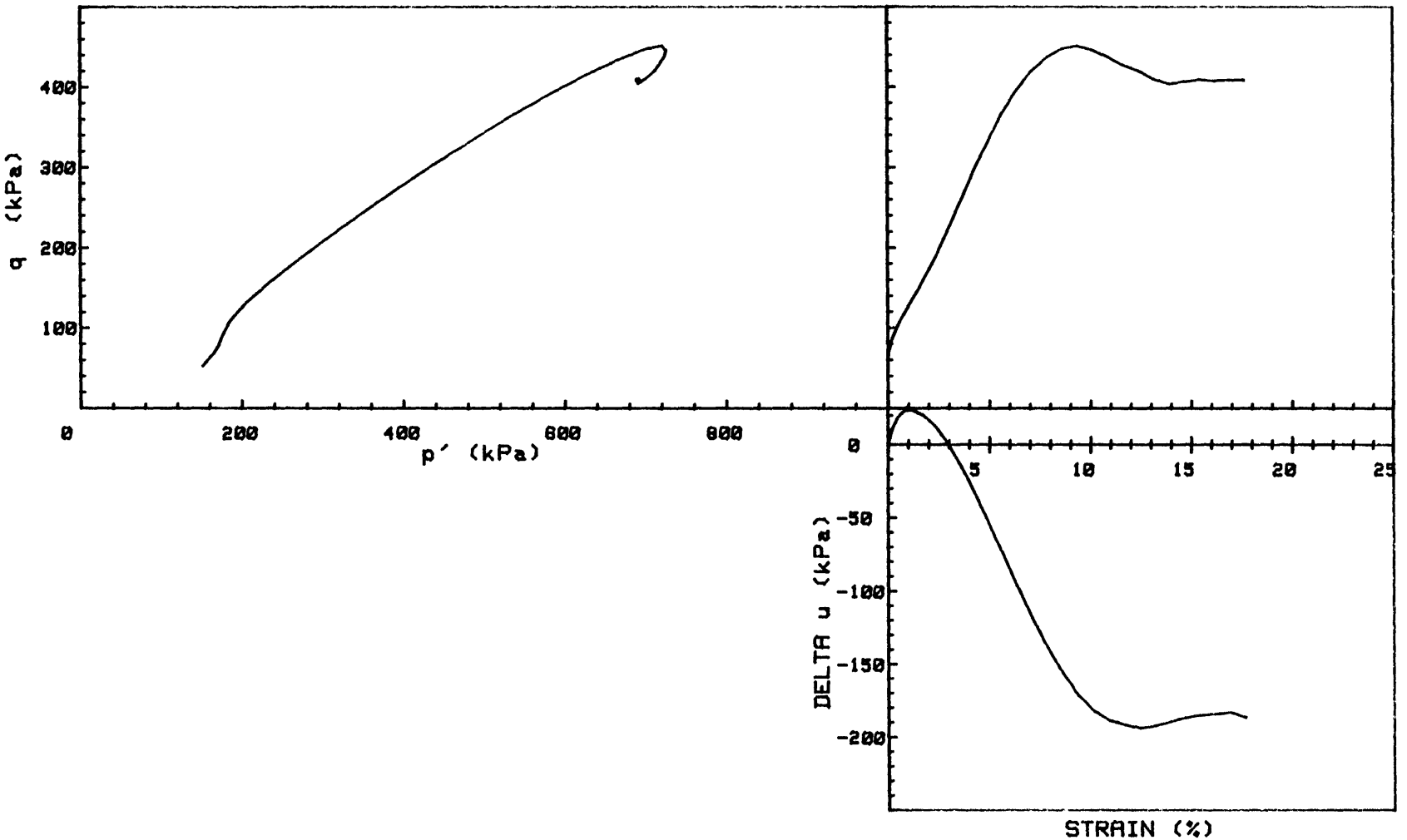

CRUISE ST HELENS		INCREMENT (cm)	REMOLDED-SURF
CORE NO.	CC1	TEST NO.	TE136

SIG1c'(kPa)	204.3
SIG3c'(kPa)	98.9
INDUCED OCR	1.0

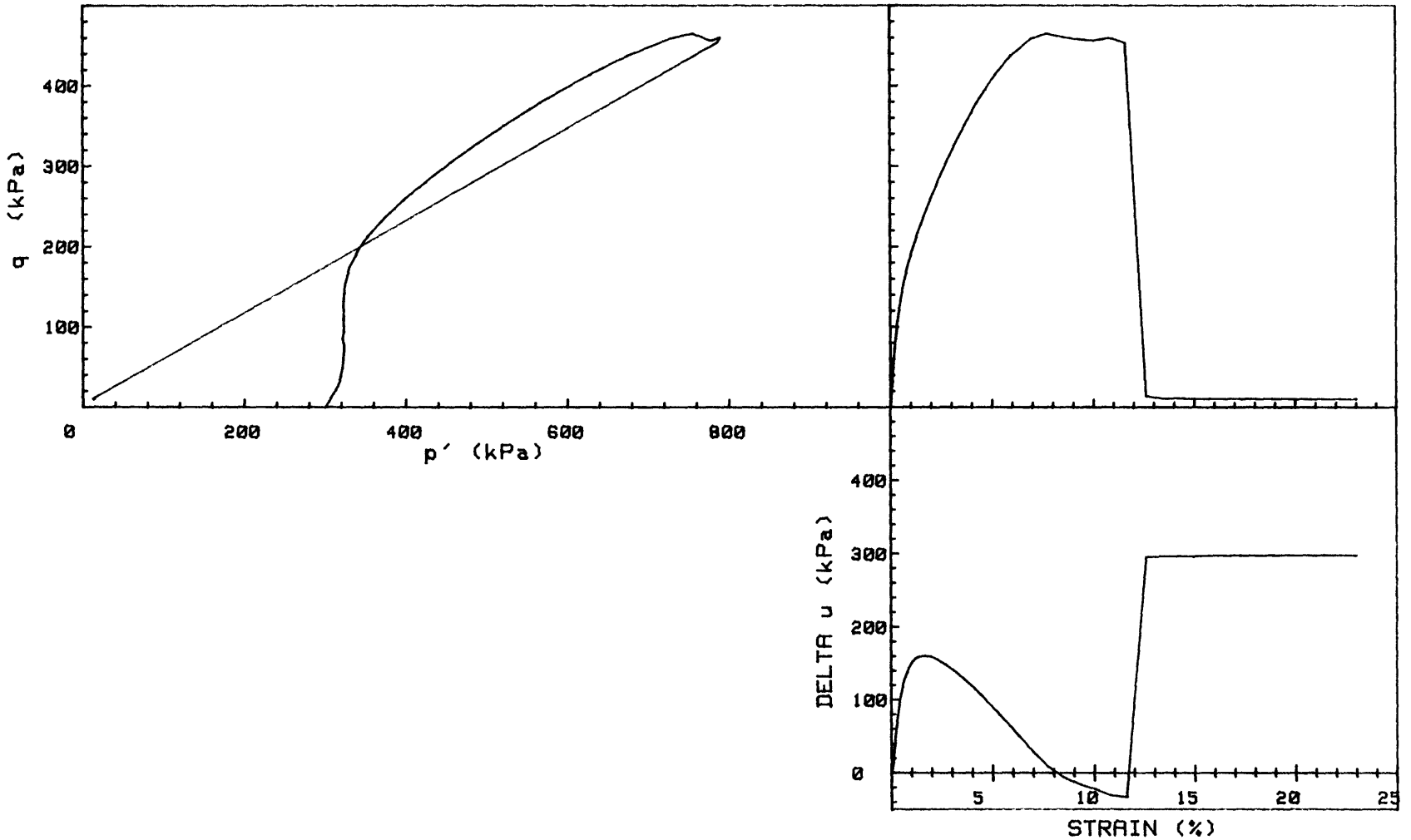

CRUISE ST HELENS		INCREMENT (cm)	REMOLDED-SURF
CORE NO.	CASTLE CR	TEST NO.	TE125

SIG1c'(kPa)	299.9
SIG3c'(kPa)	299.9
INDUCED OCR	1.0

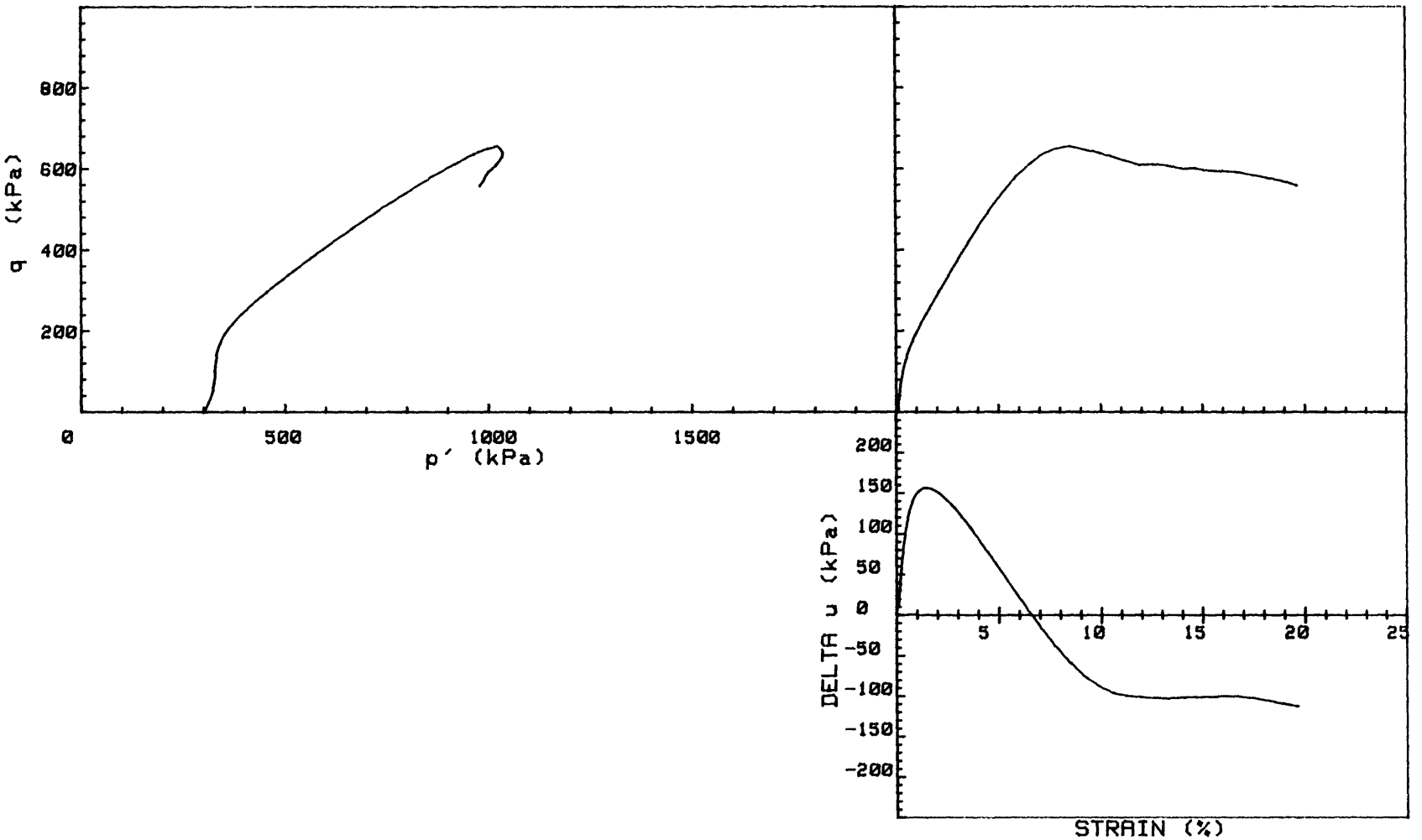

CRUISE ST HELENS		INCREMENT (cm)	REMOLDED-SURF
CORE NO.	CASTLE CR	TEST NO.	TE126

SIG1c'(kPa)	300.0
SIG3c'(kPa)	300.0
INDUCED OCR	1.0

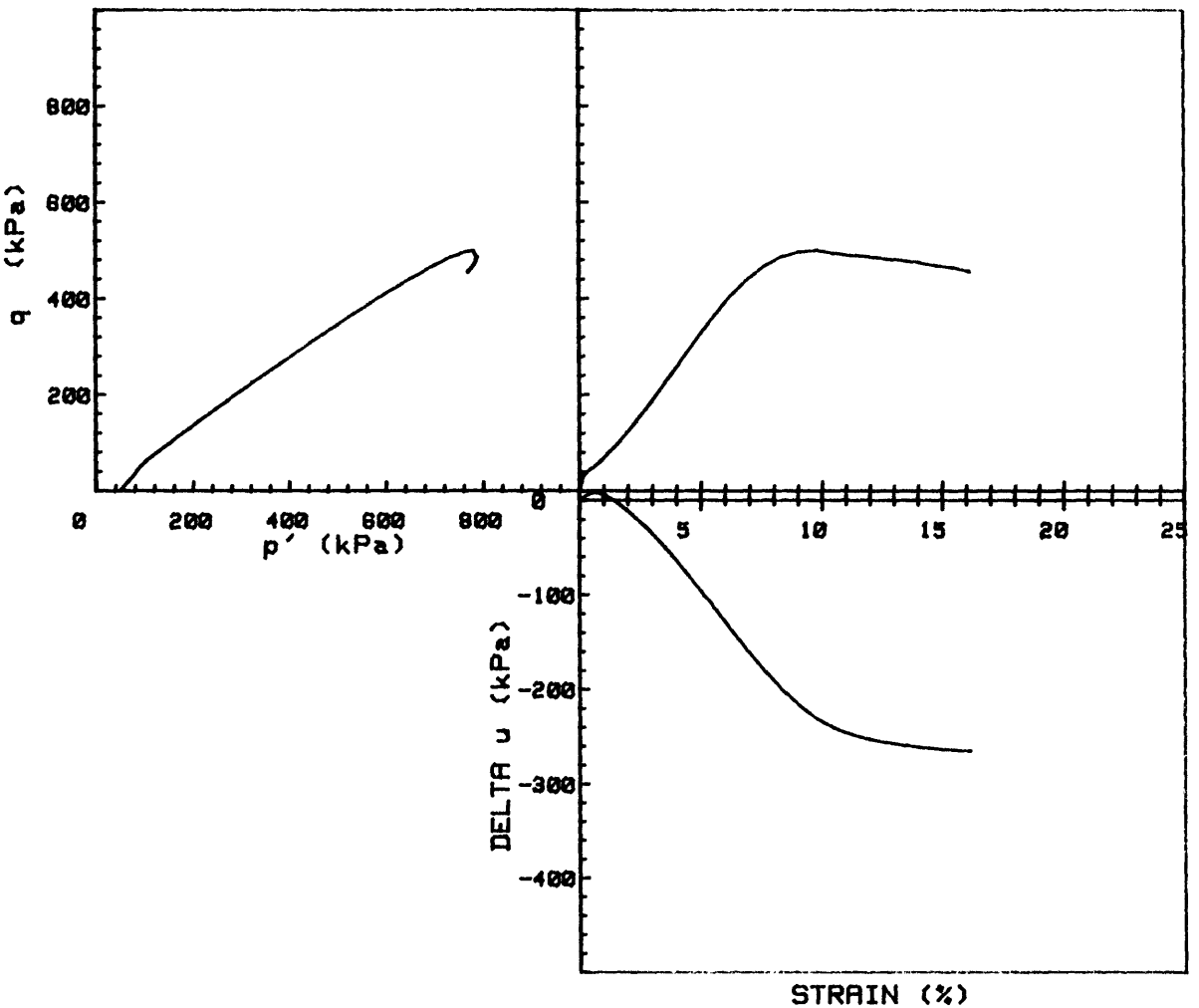

CRUISE ST HELENS		INCREMENT (cm)	REMOLDED-SURF
CORE NO.	CC1	TEST NO.	TE135

SIG1c'(kPa)	48.9
SIG3c'(kPa)	48.9
INDUCED OCR	6.0

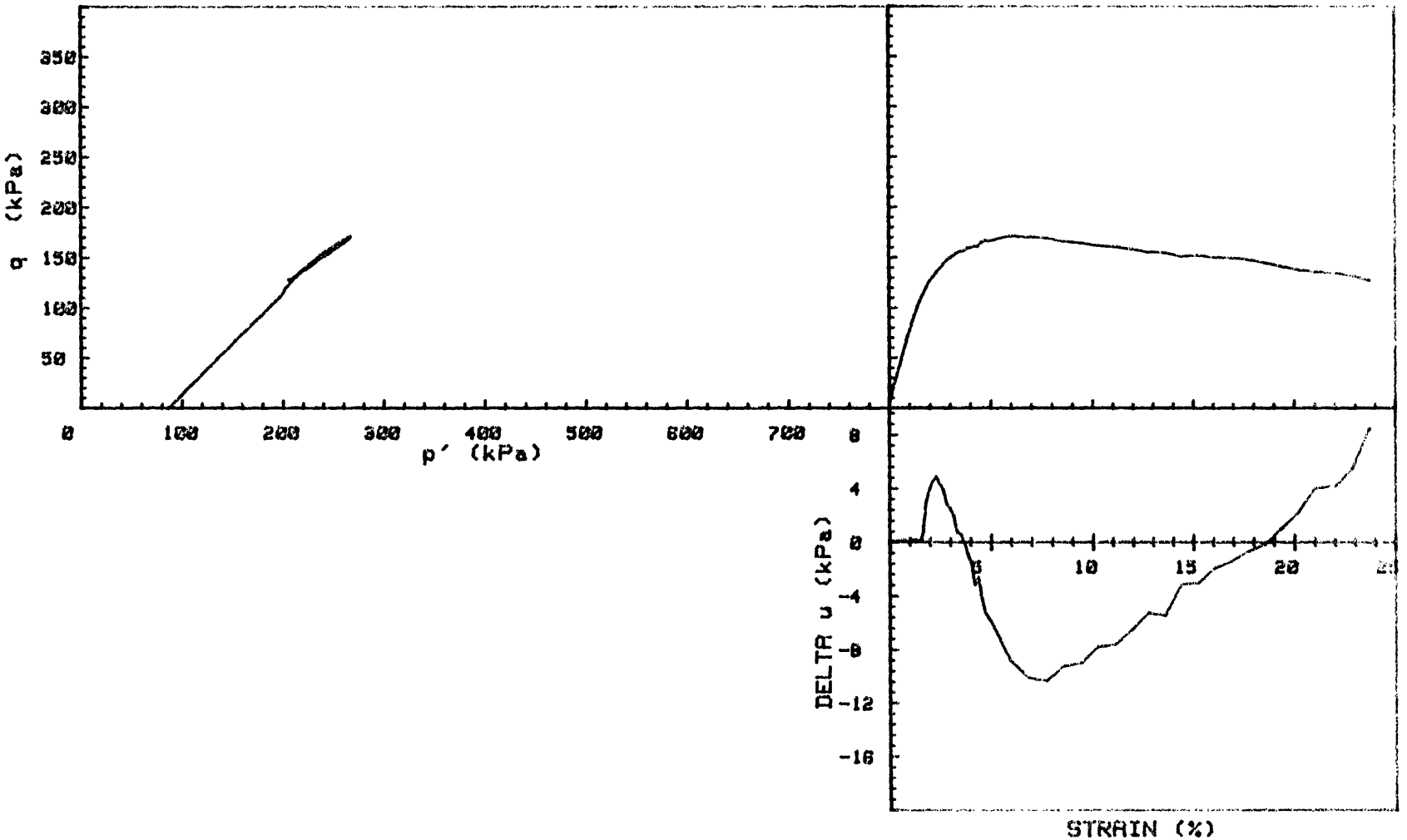

ST HELENS		INCREMENT (cm)	REMOLDED-SURF
CORE NO.	CC1	TEST NO.	TE176

SIG1c'(kPa)	87.0
SIG3c'(kPa)	87.0
INDUCED OCR	N/A

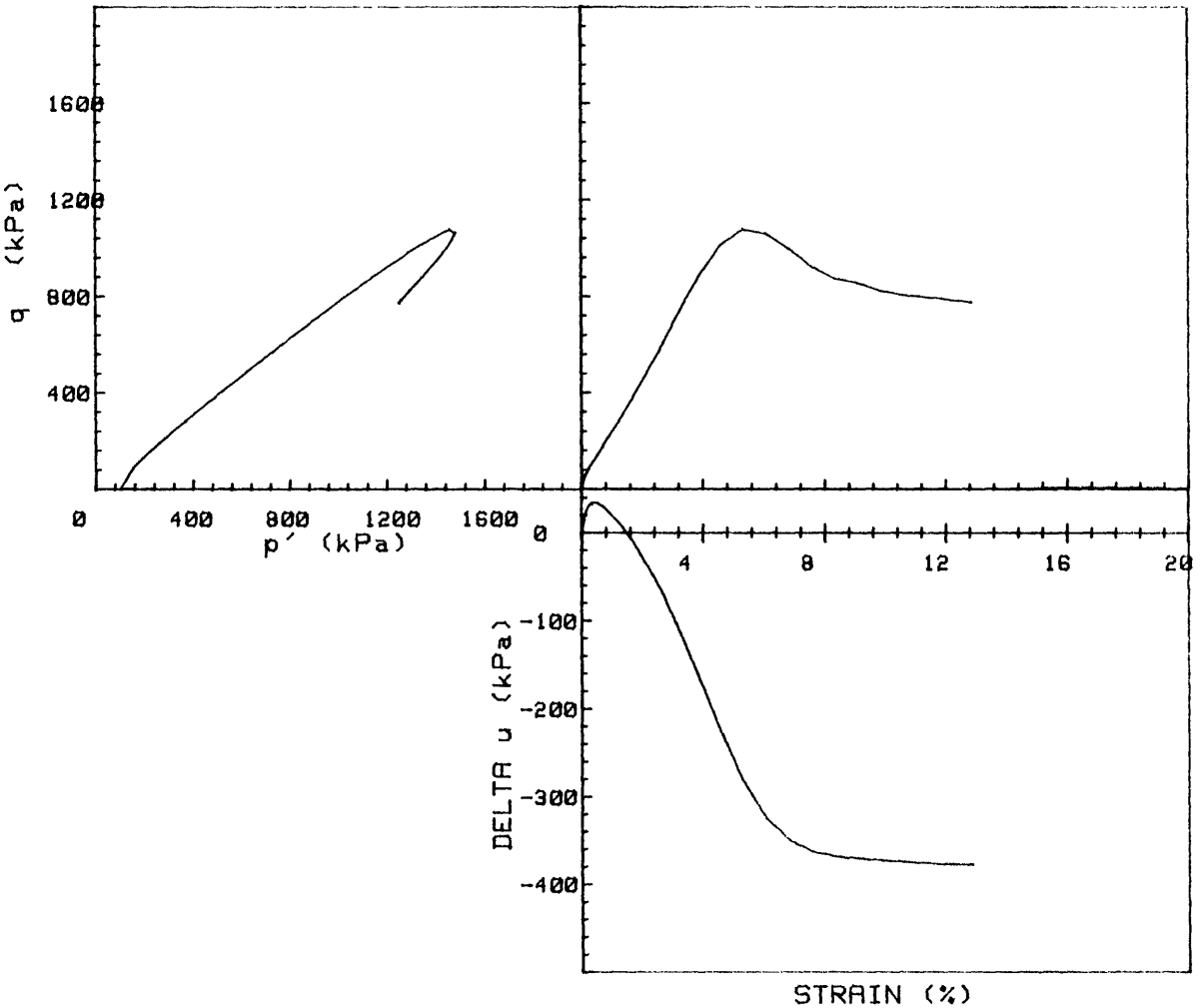

CRUISE ST HELENS	INCREMENT (cm)	REMOLDED SURF
CORE NO. CC1	TEST NO.	TE178
SIG1c´(kPa) 100.7		
SIG3c´(kPa) 100.7		
INDUCED OCR 1.0		

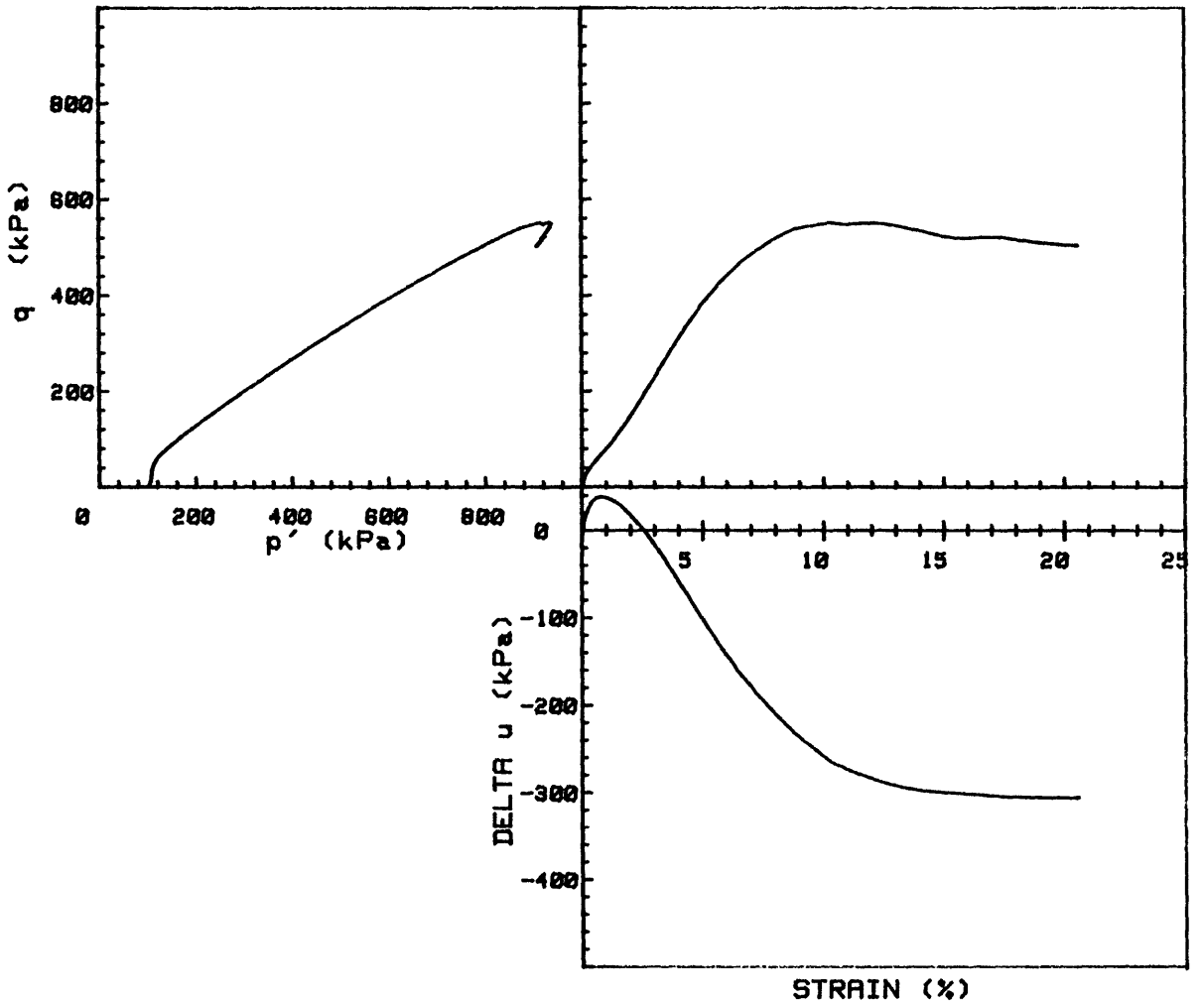

CRUISE ST HELENS		INCREMENT (cm)	REMOLDED-SURF
CORE NO.	CC2	TEST NO.	TE137

SIG1c'(kPa)	98.9
SIG3c'(kPa)	98.9
INDUCED OCR	1.0

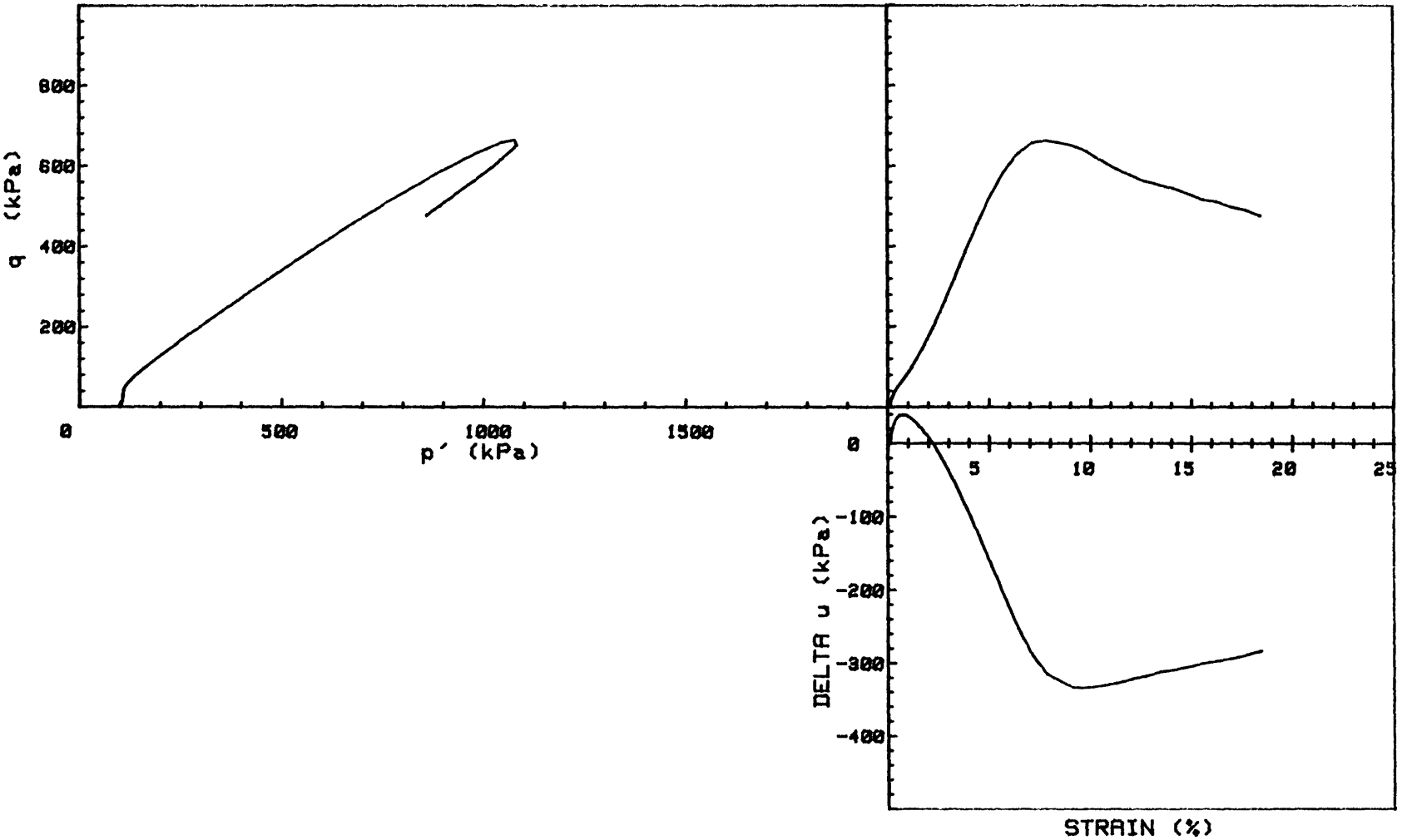

CRUISE ST HELENS	INCREMENT (cm)	REMOLDED-SURF
CORE NO. CC2	TEST NO.	TE138
SIG1c'(kPa) 99.6		
SIG3c'(kPa) 99.6		
INDUCED OCR 1.0		

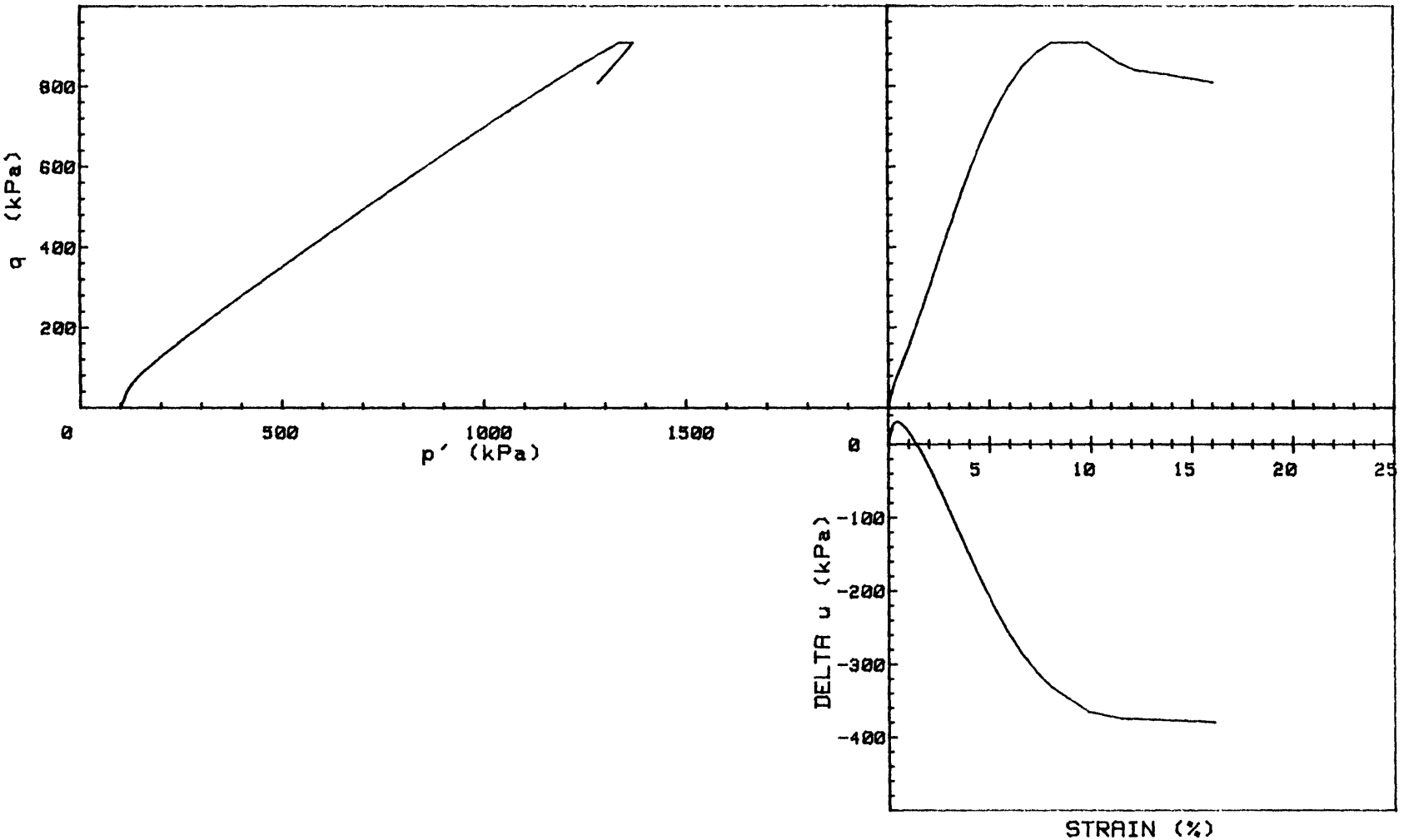

CRUISE ST HELENS		INCREMENT (cm)	REMOLDED-SURF
CORE NO.	CC2	TEST NO.	TE139

SIG1c'(kPa)	97.8
SIG3c'(kPa)	97.8
INDUCED OCR	1.0

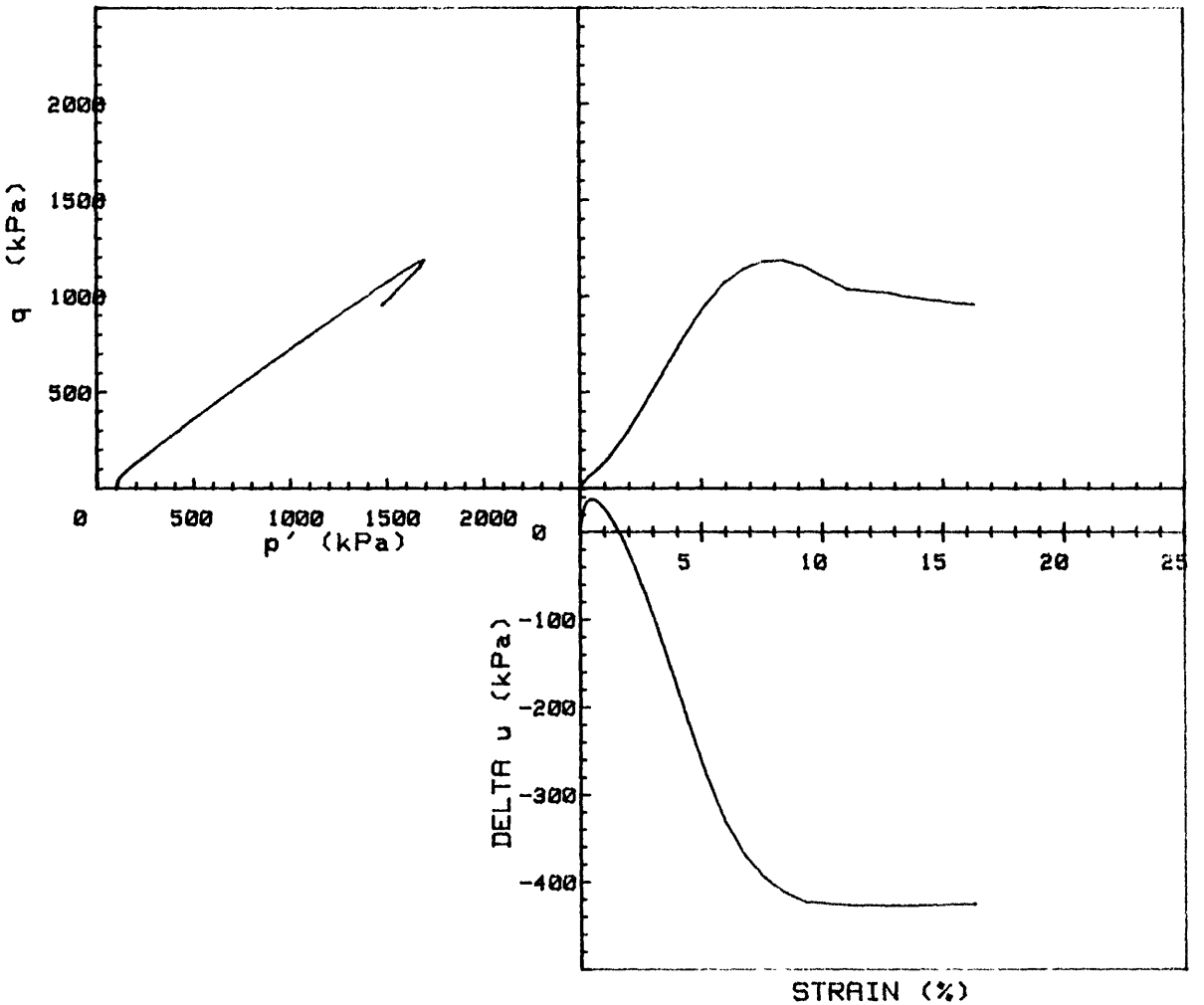

CRUISE ST HELENS		INCREMENT (cm)	REMOLDED-SURF
CORE NO.	CC2	TEST NO.	TE140

SIG1c'(kPa)	98.5
SIG3c'(kPa)	98.5
INDUCED OCR	1.0

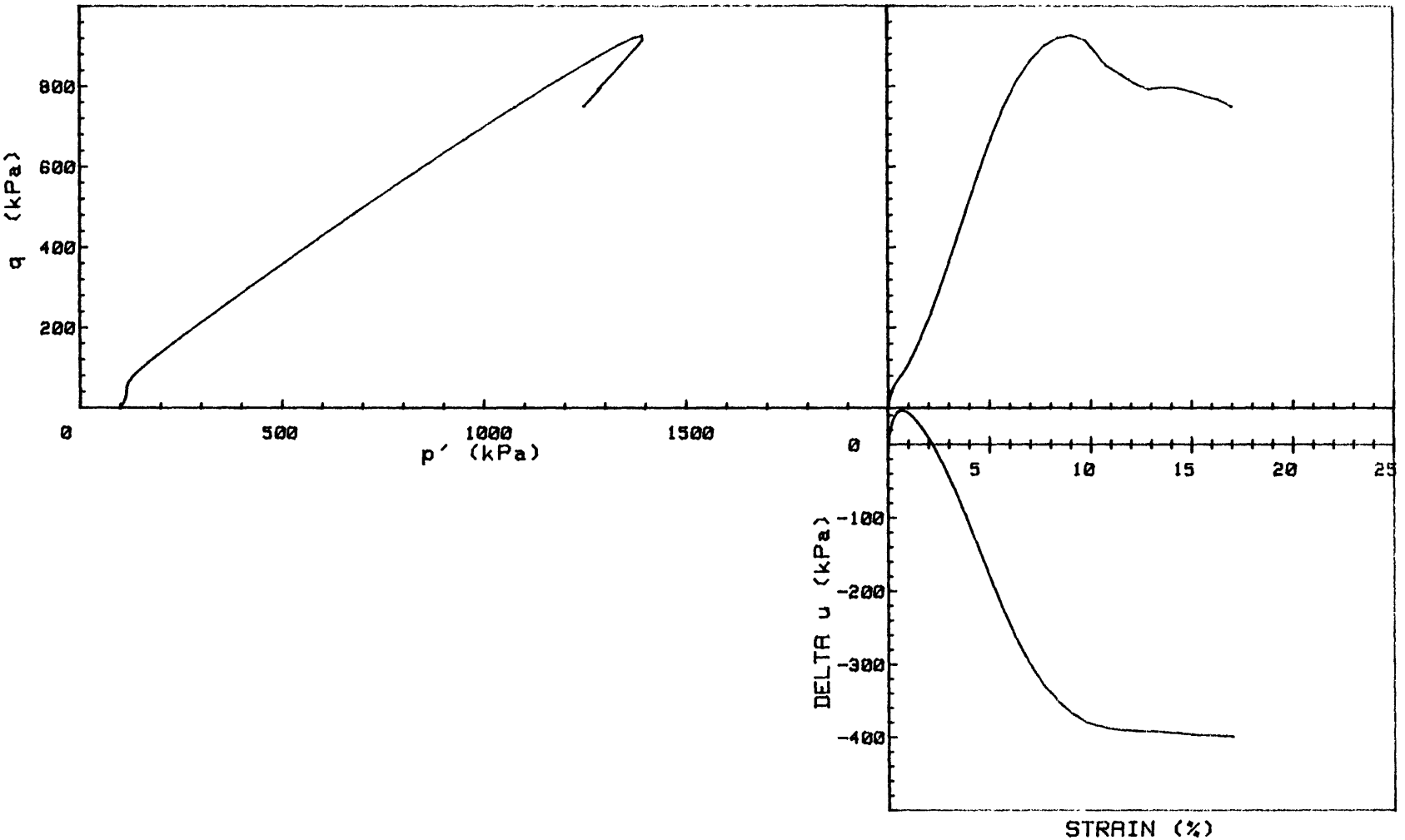

CRUISE ST HELENS	INCREMENT (cm)	REMOLDED-SURF
CORE NO. CC2	TEST NO.	TE143
SIG1c'(kPa) 100.2		
SIG3c'(kPa) 100.2		
INDUCED OCR 1.0		

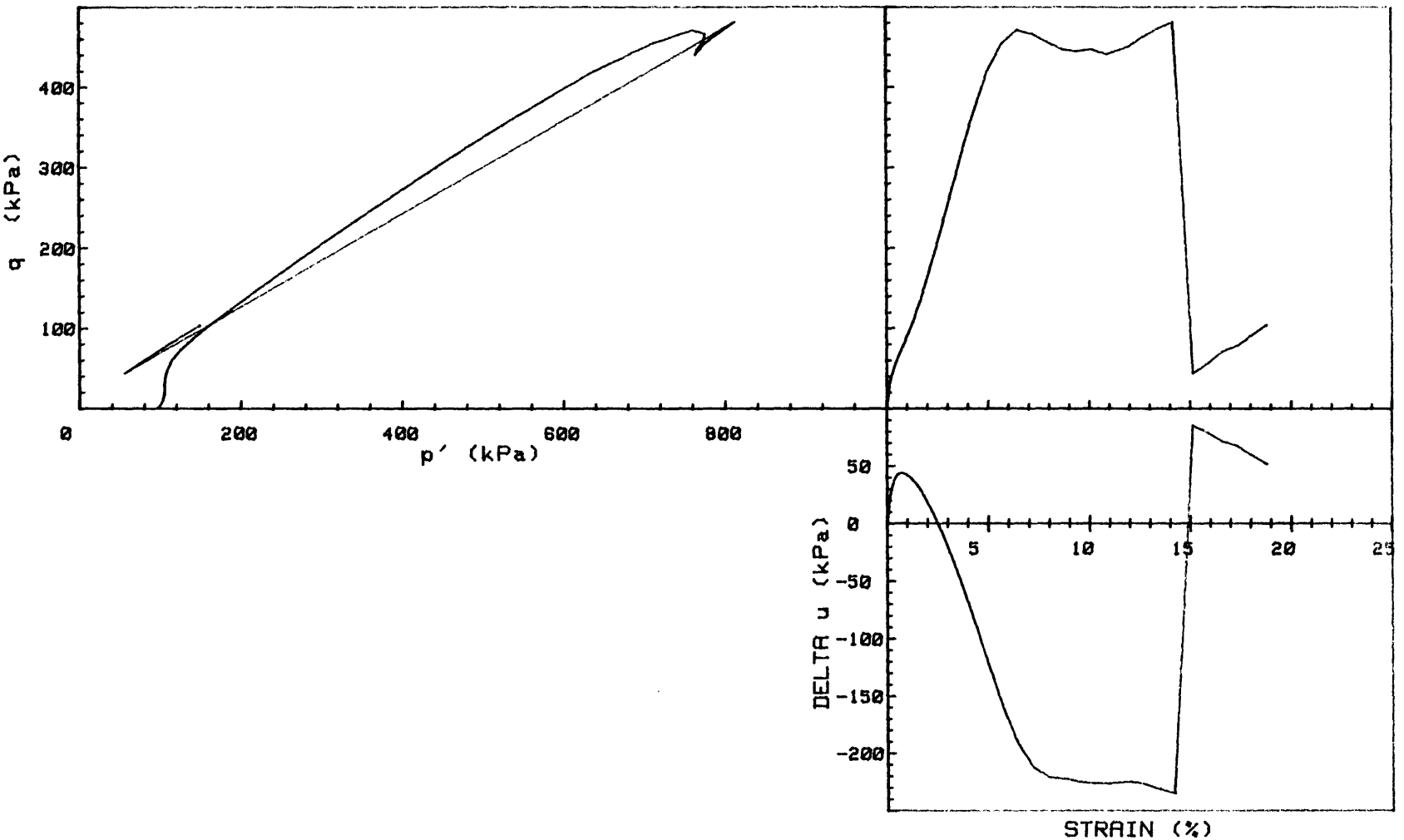

CRUISE ST HELENS	INCREMENT (cm)	REMOLDED-SURF
CORE NO. CC2	TEST NO.	TE144

SIG1c'(kPa)	97.0
SIG3c'(kPa)	97.0
INDUCED OCR	1.0

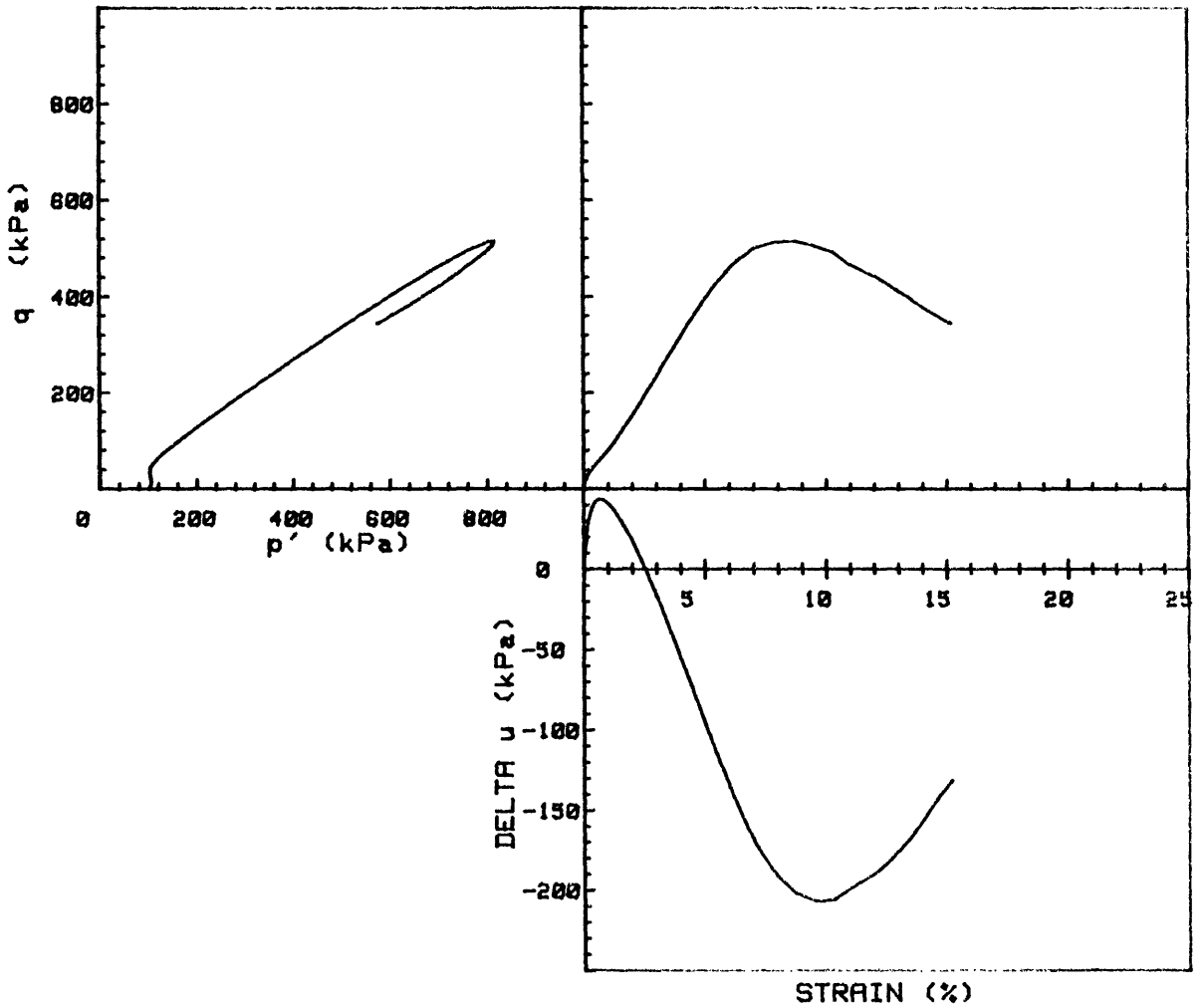

CRUISE ST HELENS		INCREMENT (cm)	REMOLDED-SURF
CORE NO.	CC2	TEST NO.	TE155

SIG1c'(kPa)	100.1
SIG3c'(kPa)	100.1
INDUCED OCR	1.0

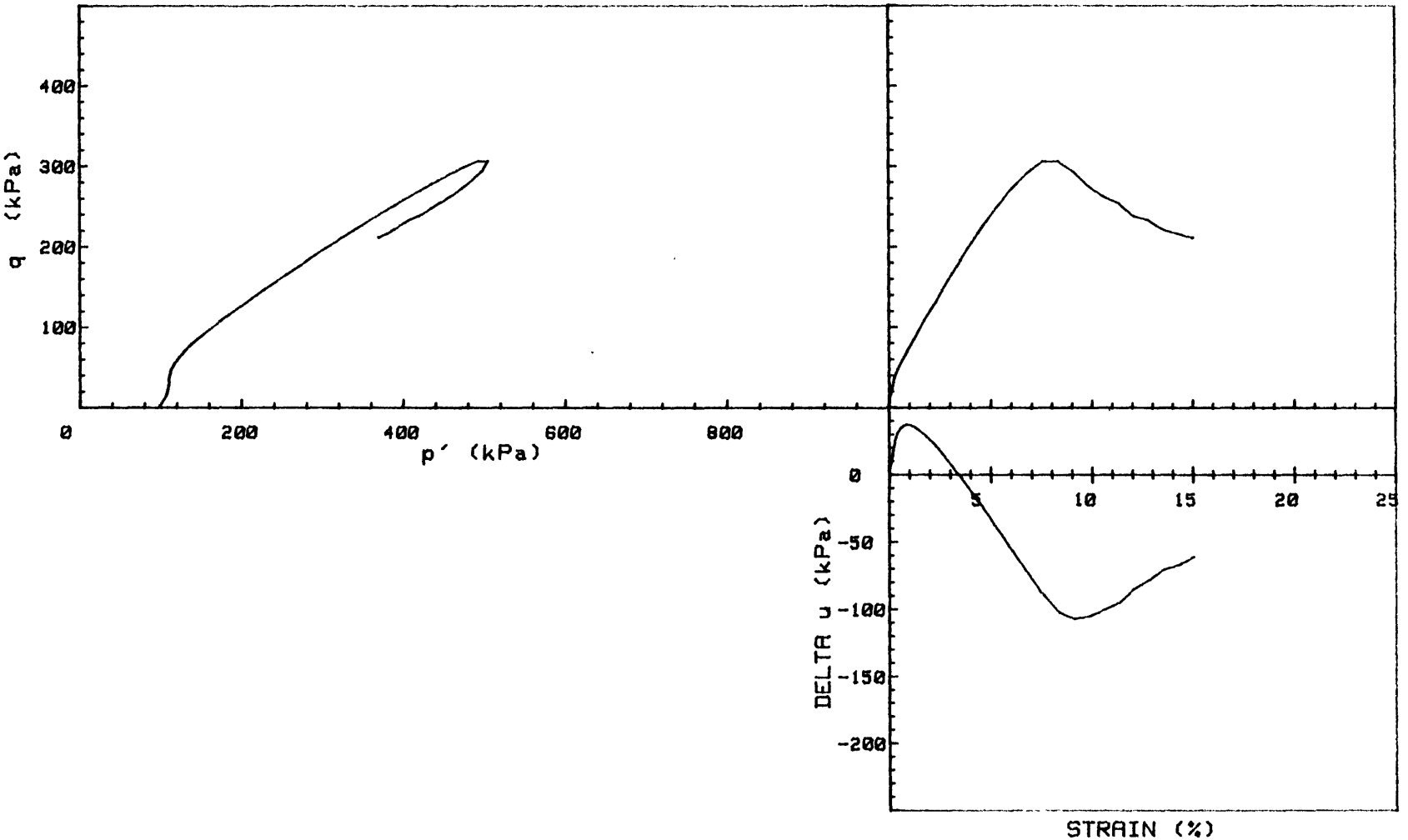

CRUISE ST HELENS	INCREMENT (cm)	REMOLDED-SURF
CORE NO. CC2	TEST NO.	TE164

SIG1c'(kPa)	97.4
SIG3c'(kPa)	97.4
INDUCED OCR	1.0

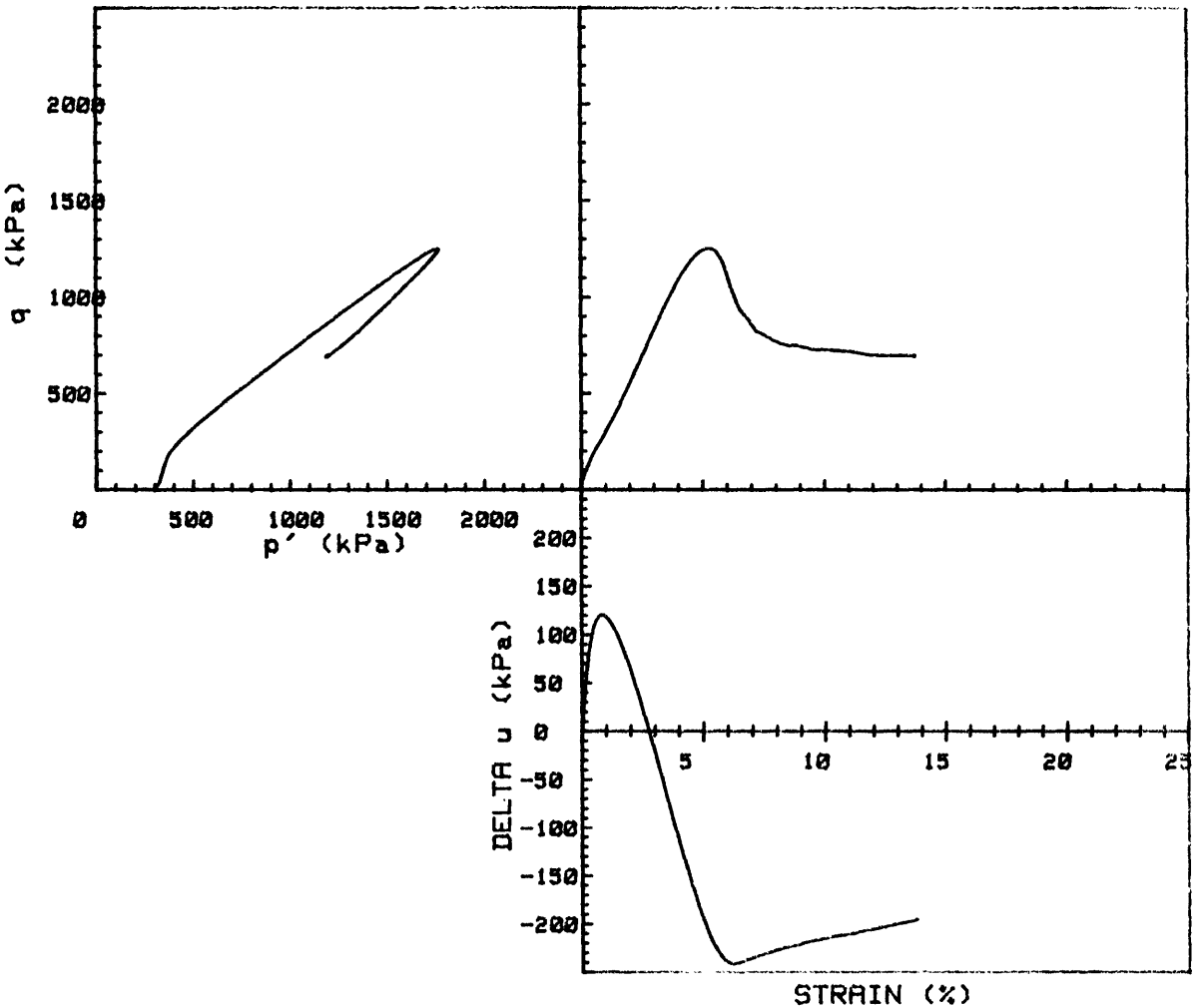

CRUISE ST HELENS	INCREMENT (cm)	REMOLDED-SURF
CORE NO. CC2	TEST NO.	TE147
SIG1c'(kPa) 299.1		
SIG3c'(kPa) 299.1		
INDUCED OCR 1.0		

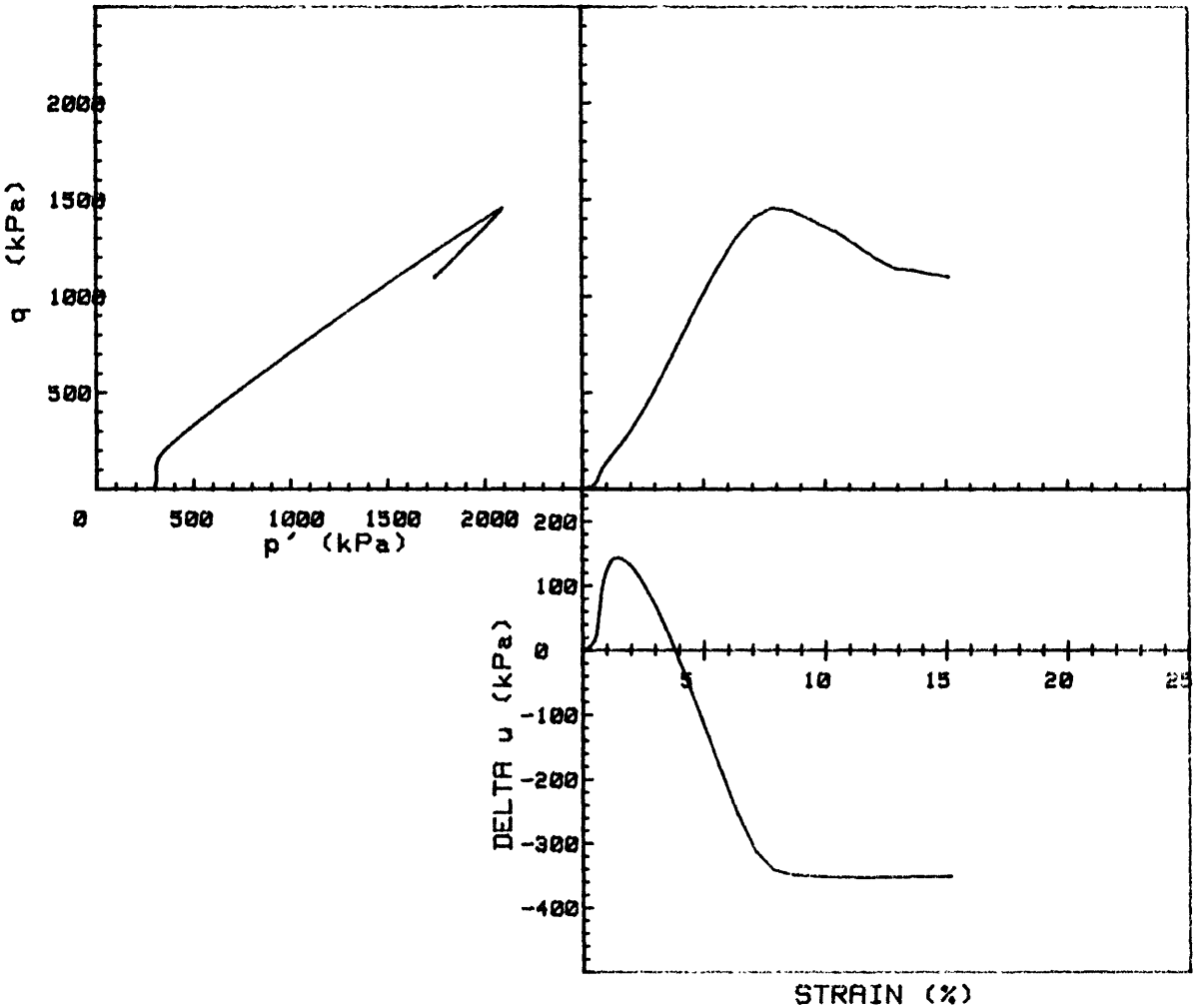

CRUISE ST HELENS		INCREMENT (cm)	REMOLDED-SURF
CORE NO.	CC2	TEST NO.	TE148

SIG1c'(kPa)	294.7
SIG3c'(kPa)	294.7
INDUCED OCR	1.0

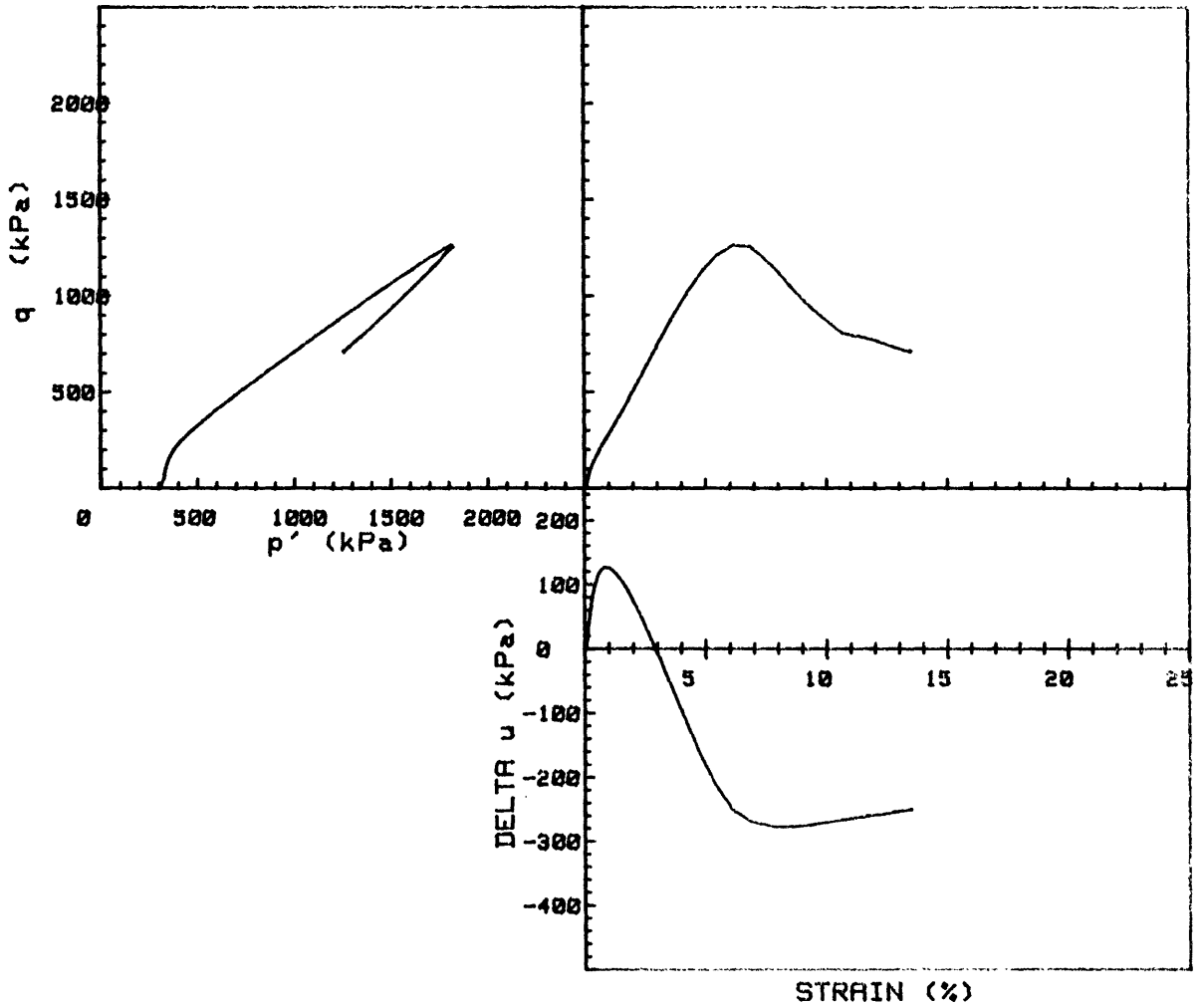

CRUISE ST HELENS		INCREMENT (cm)	REMOLDED-SURF
CORE NO.	CC2	TEST NO.	TE149

SIG1c'(kPa)	299.3
SIG3c'(kPa)	299.3
INDUCED OCR	1.0

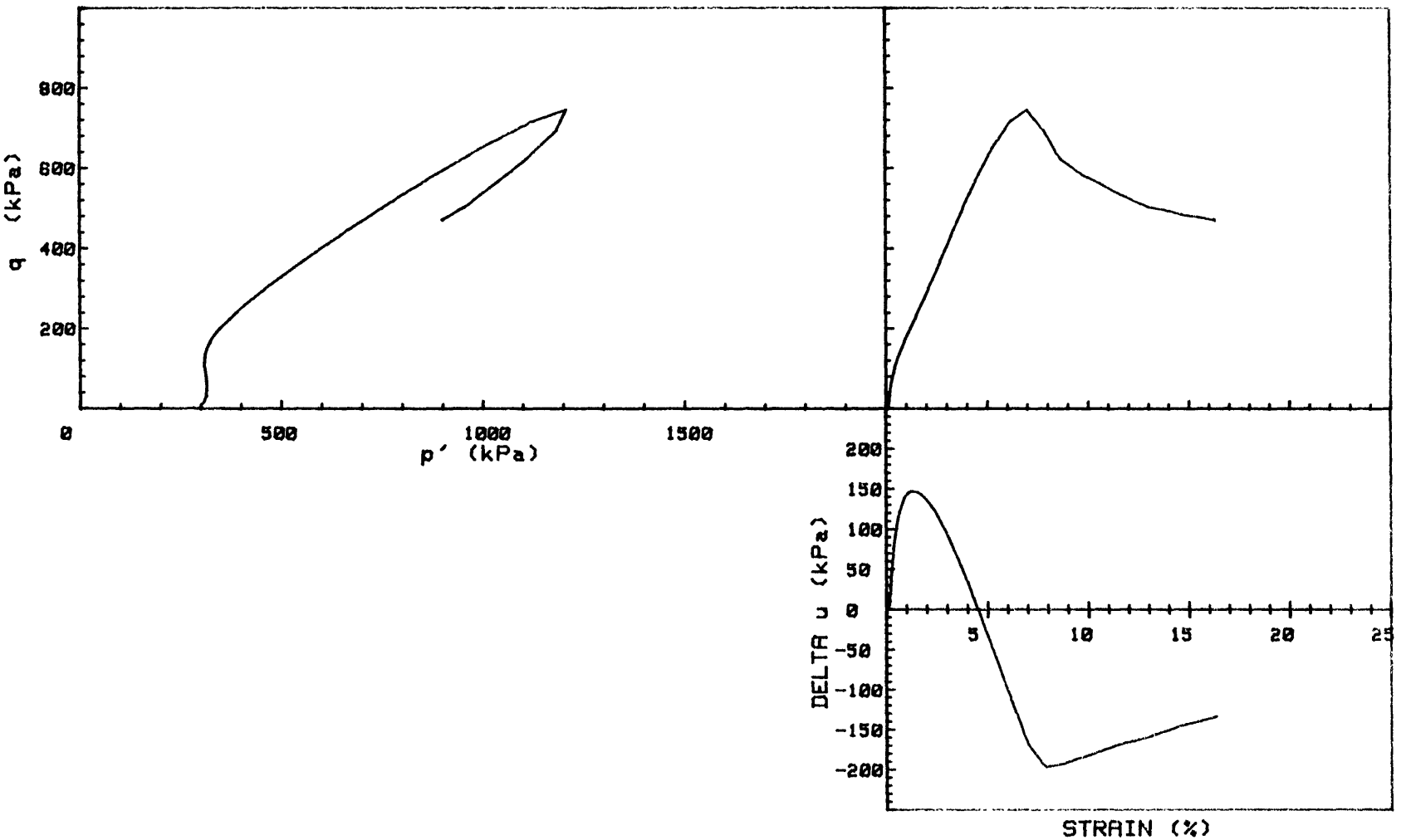

CRUISE ST HELENS	INCREMENT (cm)	REMOLDED-SURF
CORE NO. CC2	TEST NO.	TE150

SIG1c'(kPa)	295.9
SIG3c'(kPa)	295.9
INDUCED OCR	1.0

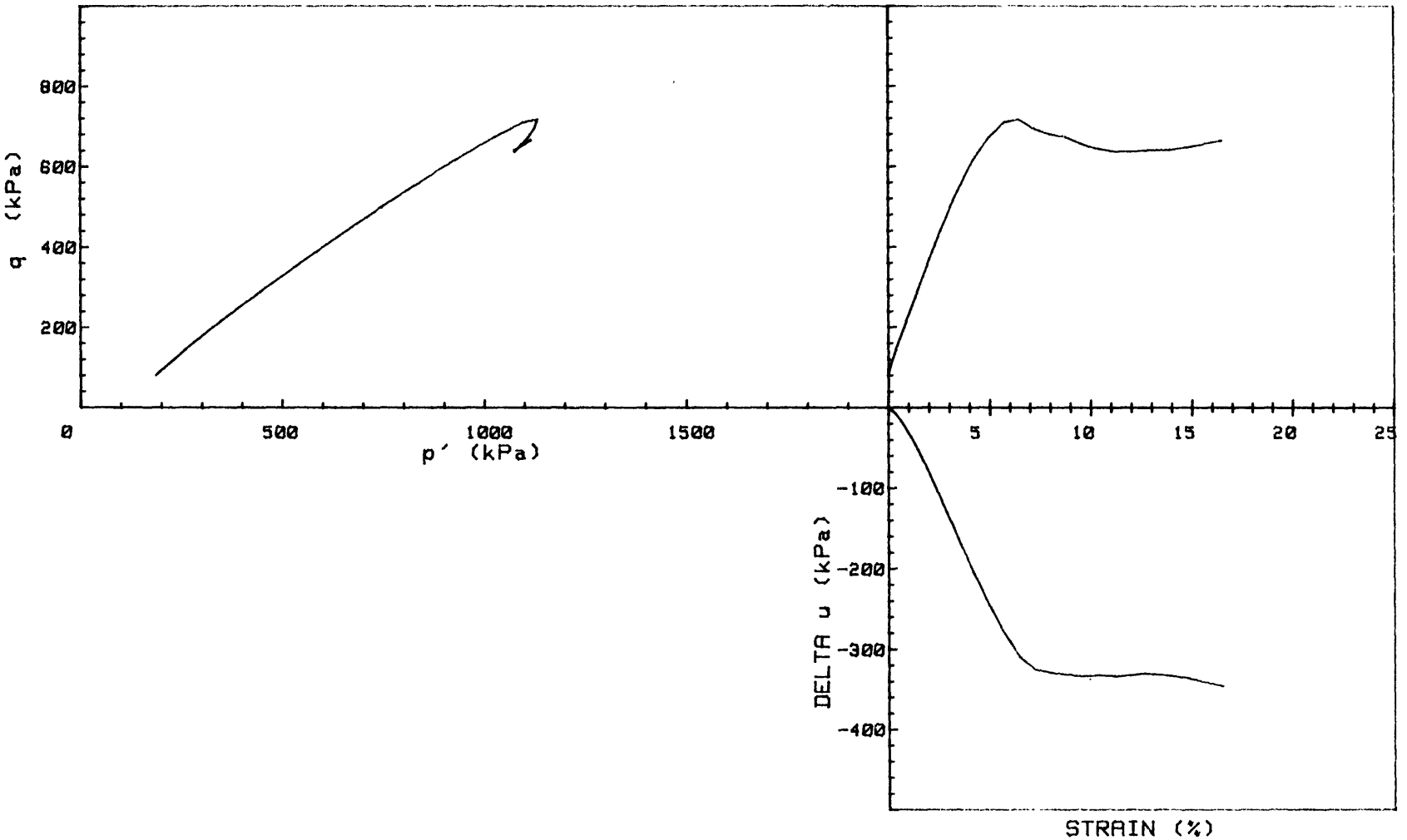

CRUISE ST HELENS		INCREMENT (cm)	REMOLDED-SURF
CORE NO.	CC2	TEST NO.	TE151

SIG1c'(kPa)	267.1
SIG3c'(kPa)	106.8
INDUCED OCR	1.0

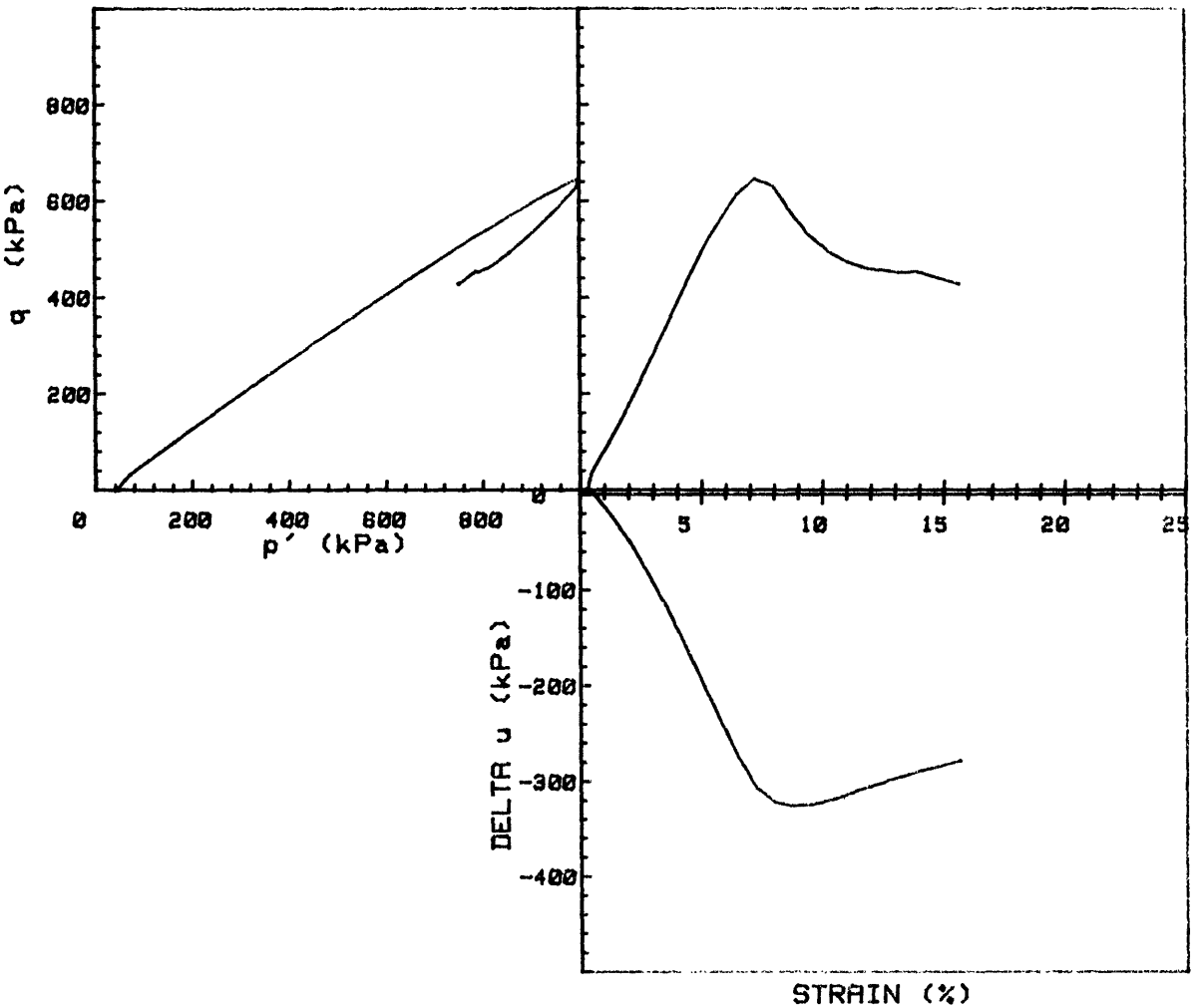

CRUISE ST HELENS		INCREMENT (cm)	REMOLDED-SURF
CORE NO.	CC2	TEST NO.	TE152

SIG1c'(kPa)	44.8
SIG3c'(kPa)	44.8
INDUCED OCR	1.0

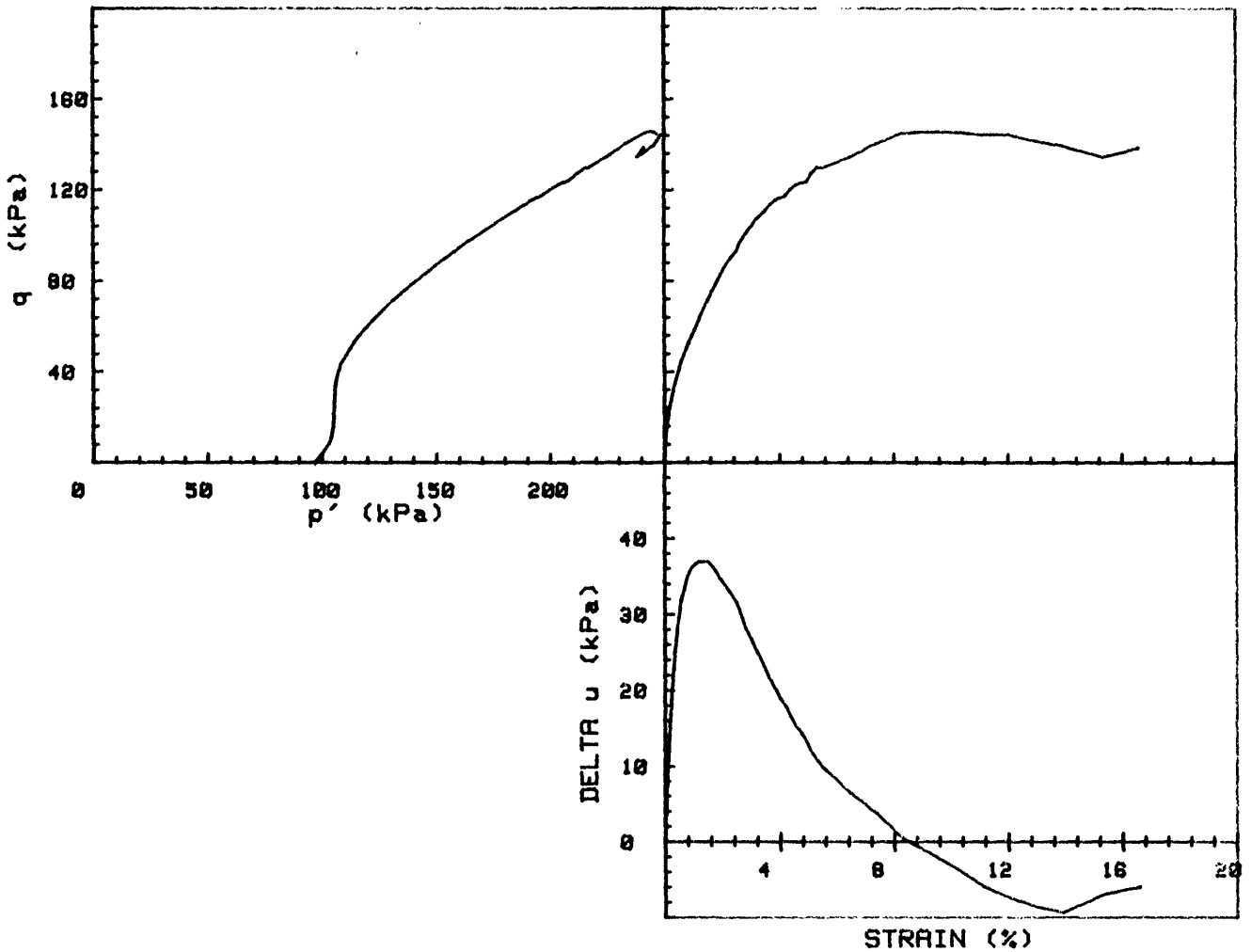

CRUISE ST HELENS	INCREMENT (cm)	REMOLDED SURF
CORE NO. CC2	TEST NO.	TE179

SIG1c'(kPa)	97.0
SIG3c'(kPa)	97.0
INDUCED OCR	1.0

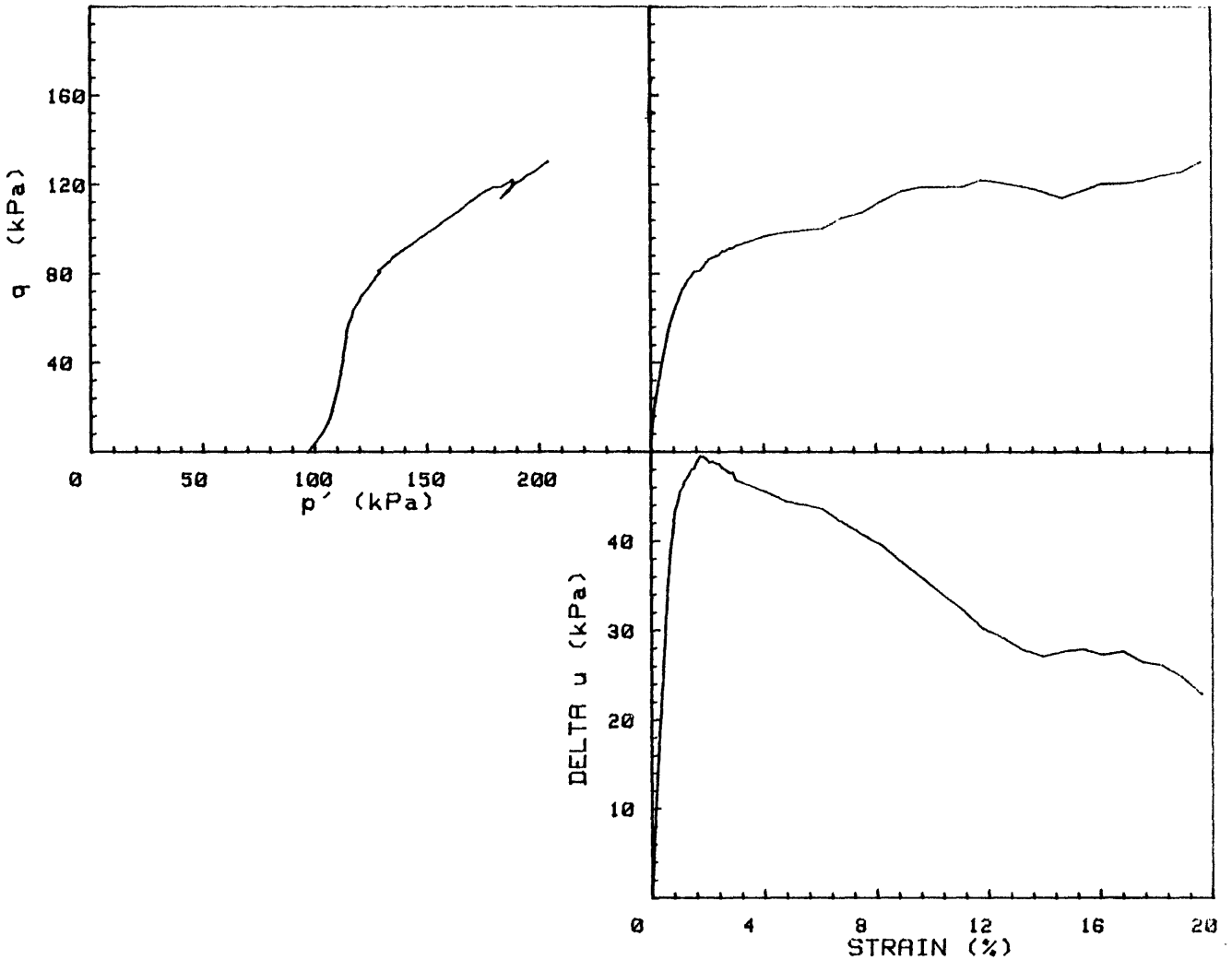

CRUISE ST HELENS	INCREMENT (cm)	REMOLDED SURF
CORE NO. CC2	TEST NO.	TE183

SIG1c'(kPa)	96.8
SIG3c'(kPa)	96.8
INDUCED OCR	1.0

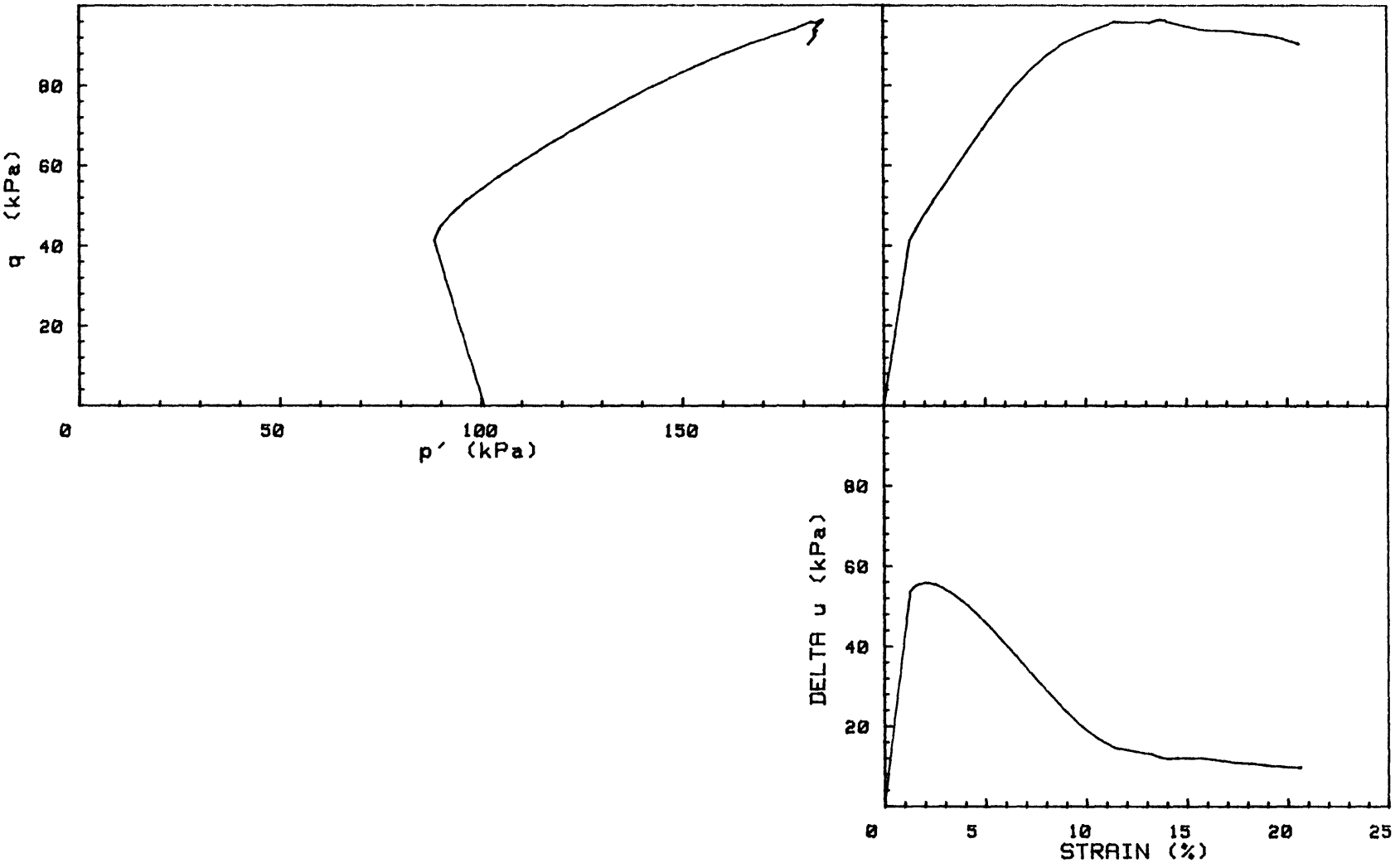

CRUISE ST HELENS		INCREMENT (cm)	ASH (TUBE)
CORE NO.	SL1	TEST NO.	TE129

SIG1c'(kPa)	100.8
SIG3c'(kPa)	100.8
INDUCED OCR	1.0

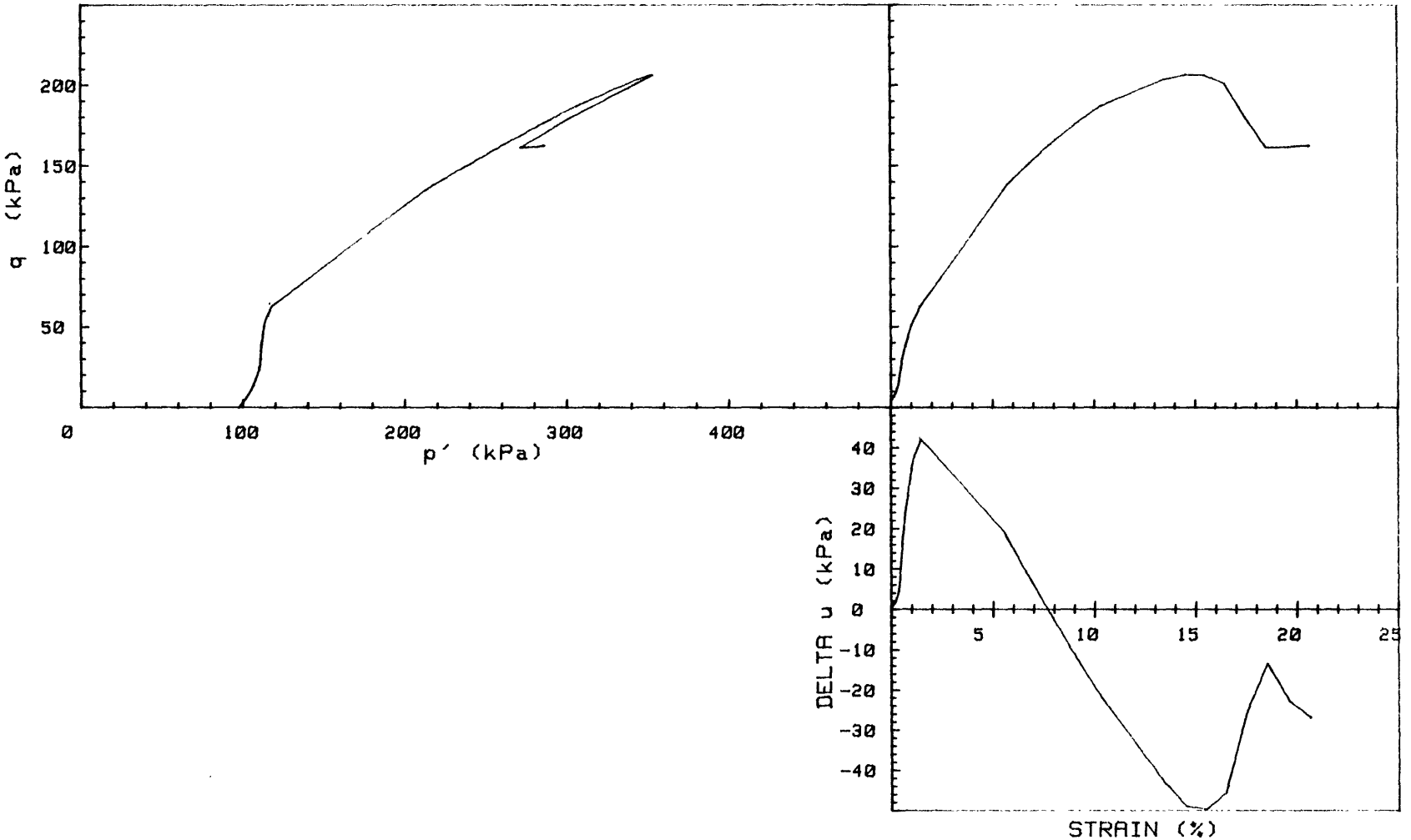

CRUISE ST HELENS		INCREMENT (cm)	REMOLDED-SURF
CORE NO.	SL4	TEST NO.	TE170

SIG1c'(kPa)	97.4
SIG3c'(kPa)	97.4
INDUCED OCR	1.0

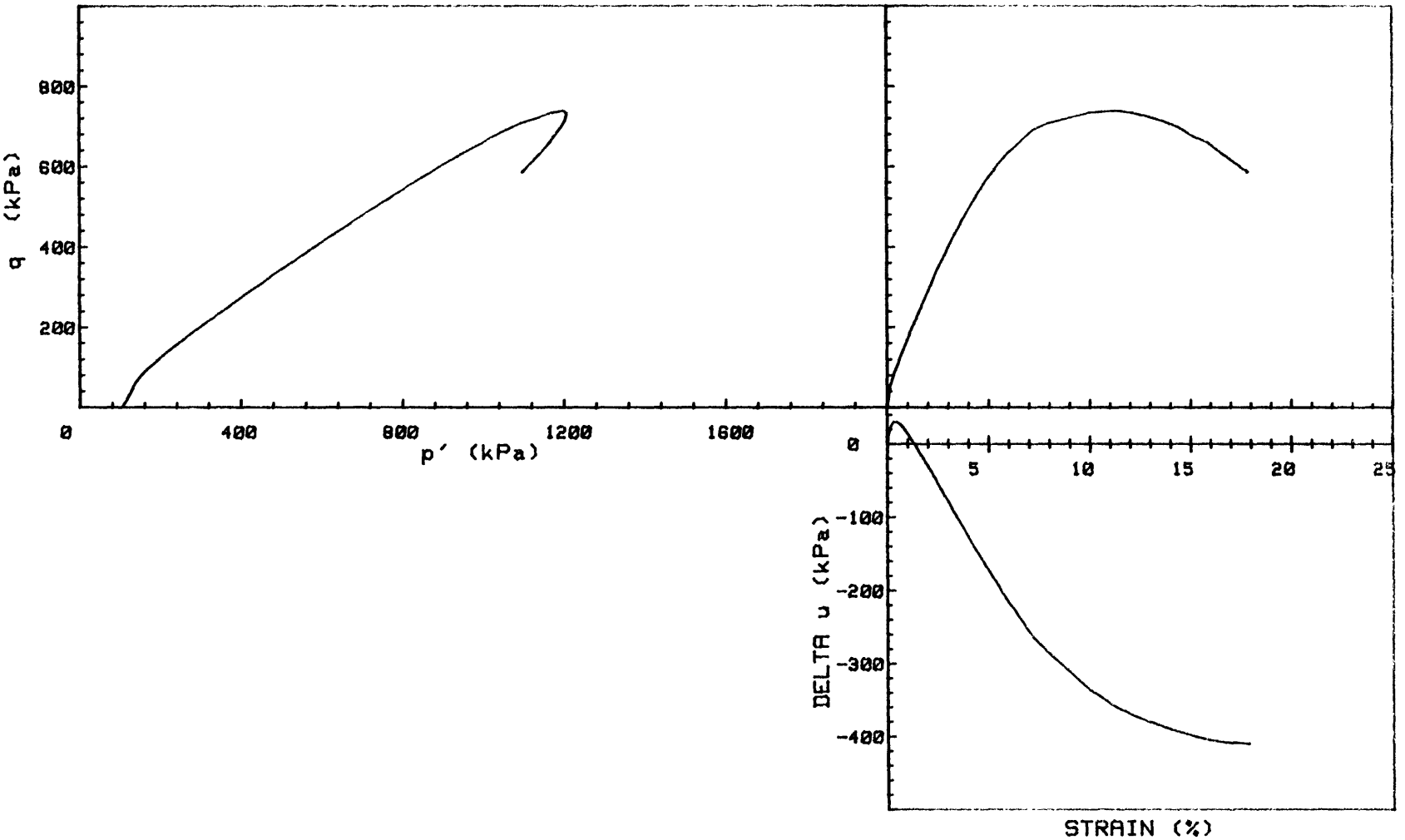

CRUISE ST HELENS		INCREMENT (cm)	REMOLDED SURF
CORE NO.	SL4	TEST NO.	TE173

SIG1c'(kPa)	102.9
SIG3c'(kPa)	102.9
INDUCED OCR	1.0

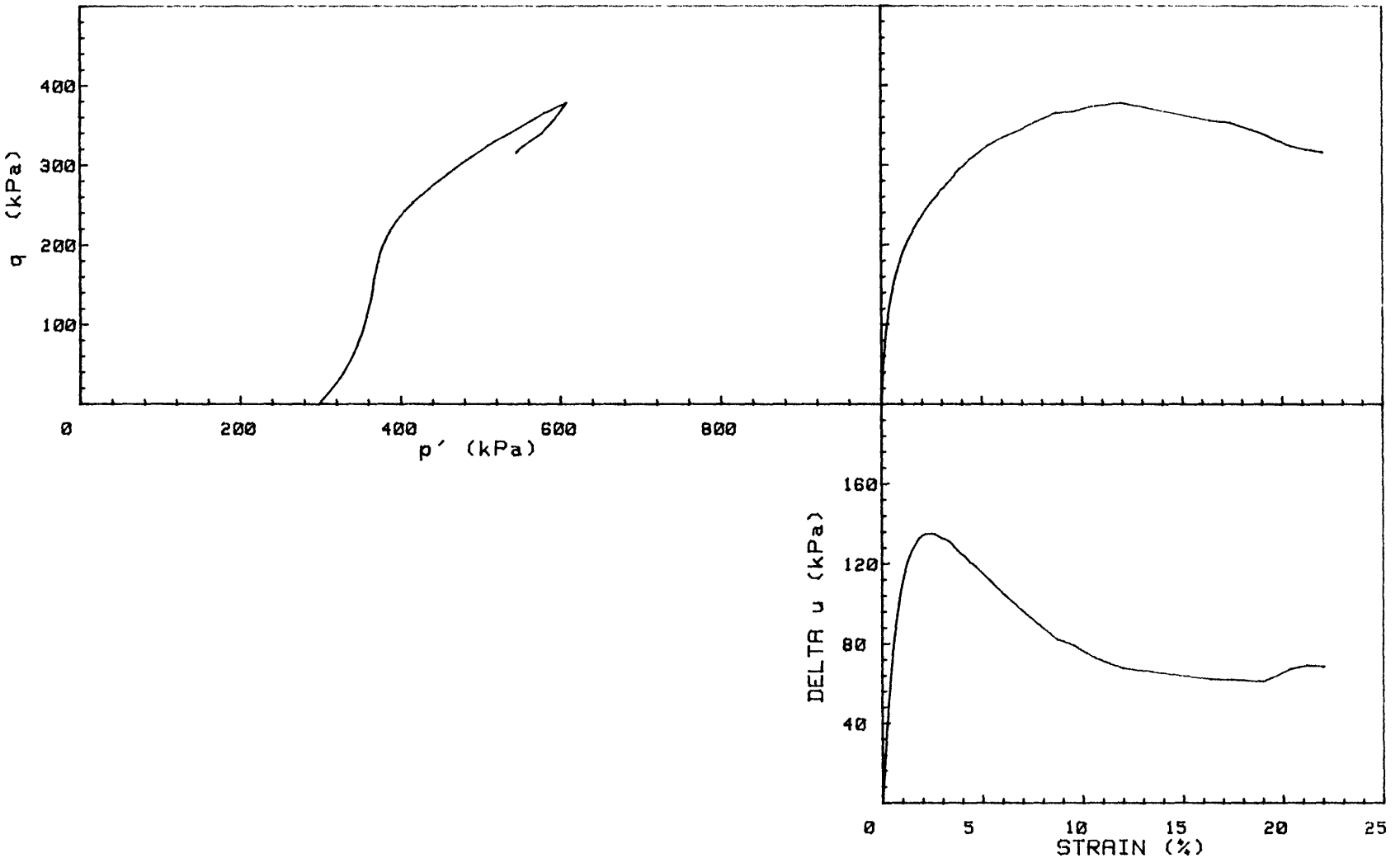

CRUISE ST HELENS	INCREMENT (cm)	REMOLDED SURF
CORE NO. SL4	TEST NO.	TE175

SIG1c'(kPa)	298.3
SIG3c'(kPa)	298.3
INDUCED OCR	1.0

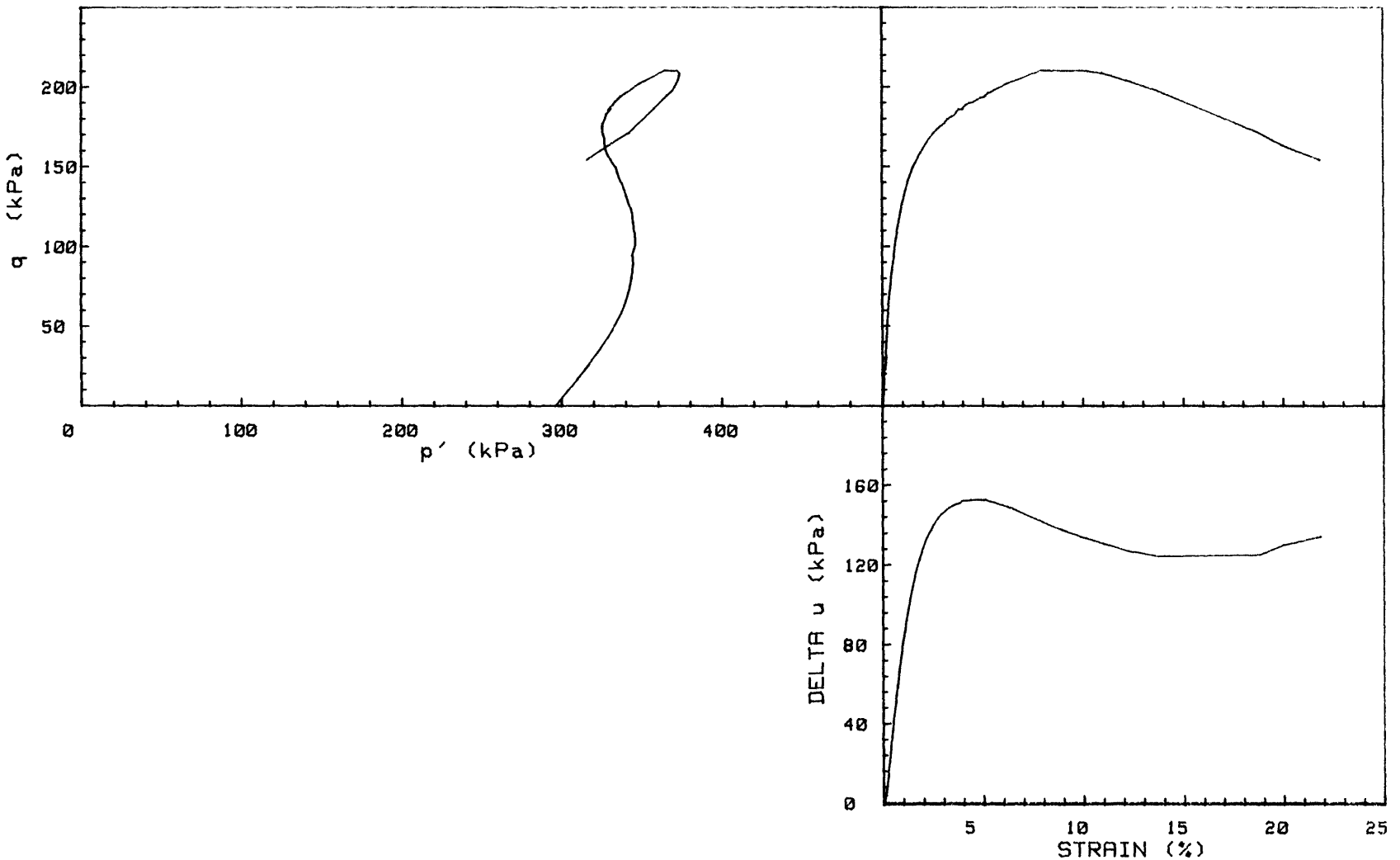

CRUISE ST HELENS		INCREMENT (cm)	REMOLDED SURF
CORE NO.	SL4	TEST NO.	TE177

SIG1c′(kPa)	296.0
SIG3c′(kPa)	296.0
INDUCED OCR	1.0

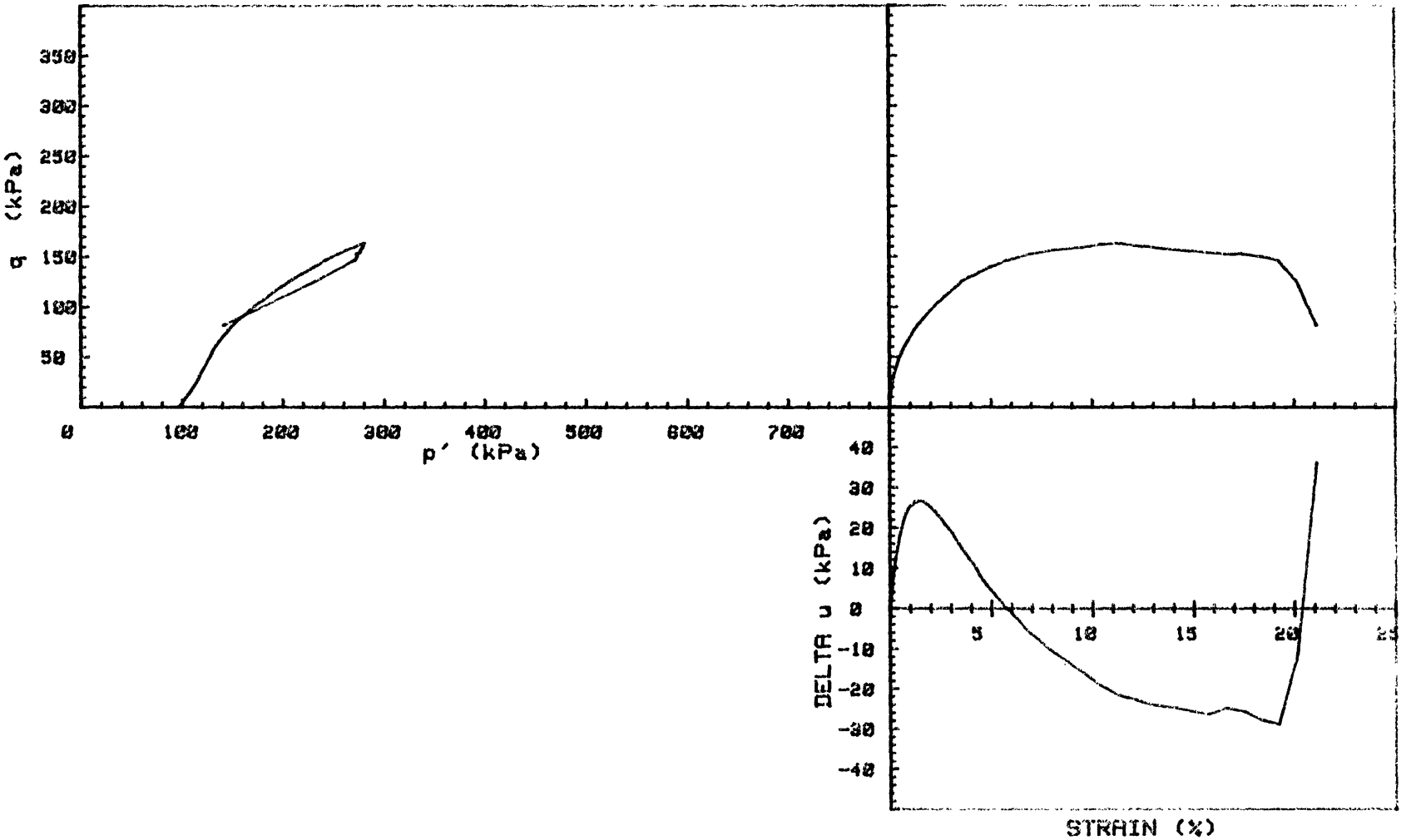

ST HELENS		INCREMENT (cm)	REMOLDED SURF
CORE NO.	SL4	TEST NO.	TE184

SIG1c'(kPa)	96.2
SIG3c'(kPa)	96.2
INDUCED OCR	N/A

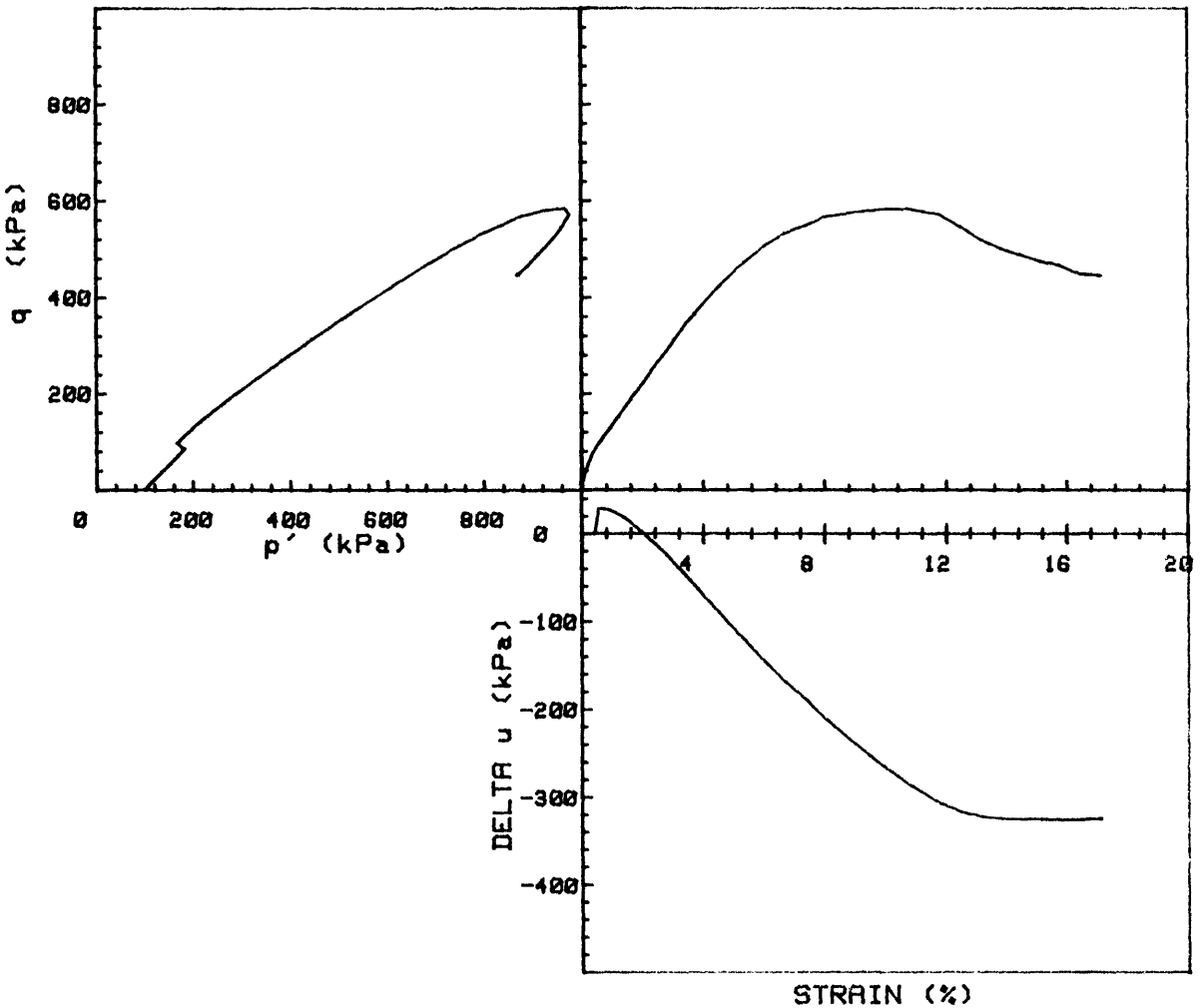

CRUISE ST HELENS		INCREMENT (cm)	REMOLDED-SURF
CORE NO.	SL4	TEST NO.	TE185

SIG1c´(kPa)	98.6
SIG3c´(kPa)	98.6
INDUCED OCR	1.0

APPENDIX B

CYCLIC TRIAXIAL TEST RESULTS

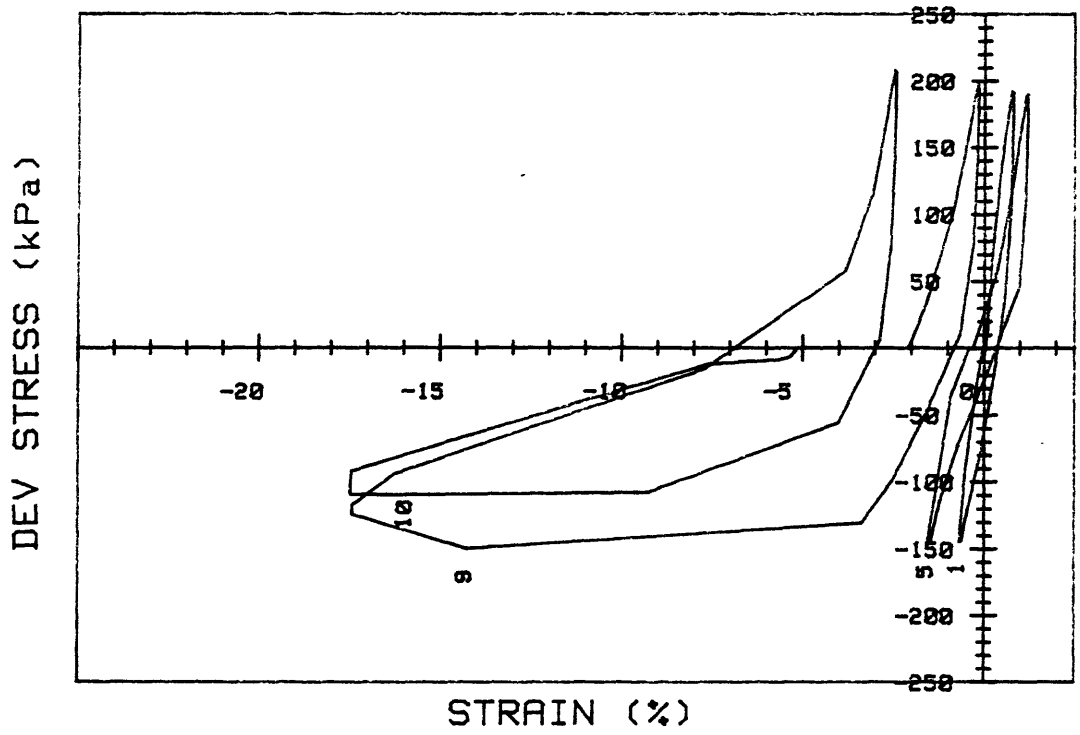

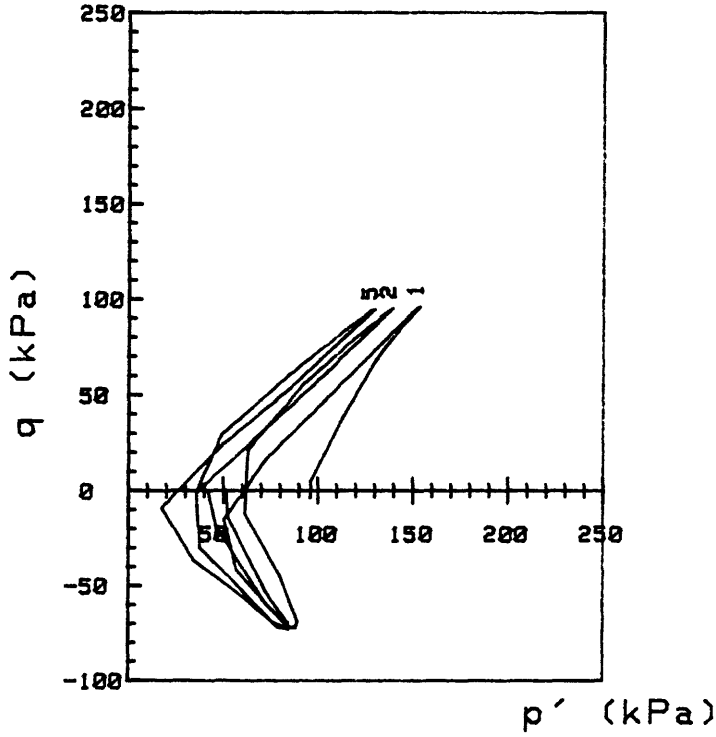

CRUISE ST HELENS		INCREMENT (cm)	REMOLDED-SURF
CORE NO.	CC1	TEST NO.	D130
SIG1c'(kPa)	99.7	STATIC qf (kPa)	100.0
SIG3c'(kPa)	99.7	AVG MAX q (kPa)	96.3 (96.3%)
INDUCED OCR	1.0	AVG MIN q (kPa)	-71.3 (71.3%)

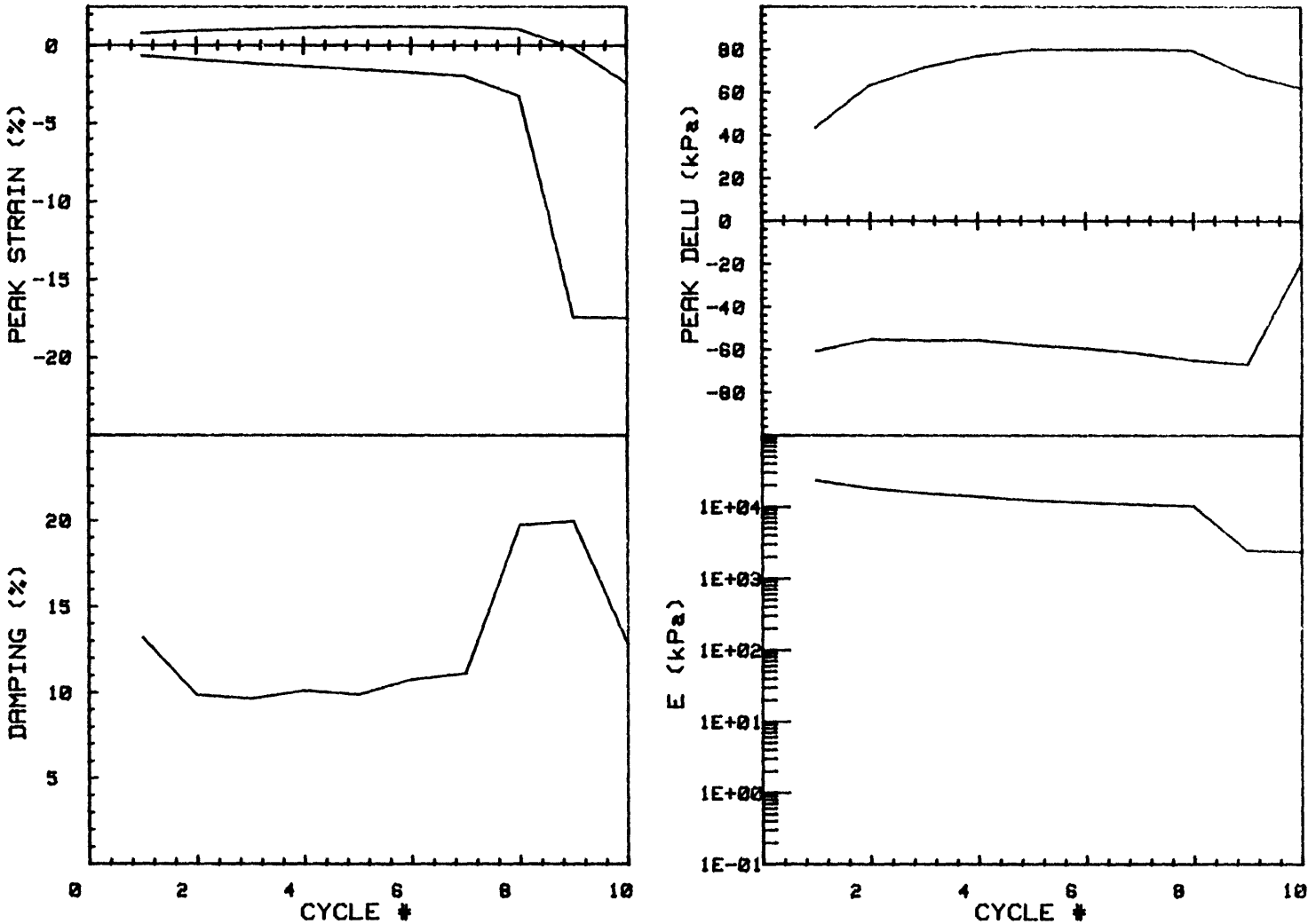

CRUISE ST HELENS		INCREMENT (cm)	REMOLDED-SURF
CORE NO.	CC1	TEST NO.	D130
SIG1c'(kPa)	99.7	STATIC qf (kPa)	100.0
SIG3c'(kPa)	99.7	AVG MAX q (kPa)	96.3 (96.3%)
INDUCED OCR	1.0	AVG MIN q (kPa)	-71.3 (71.3%)

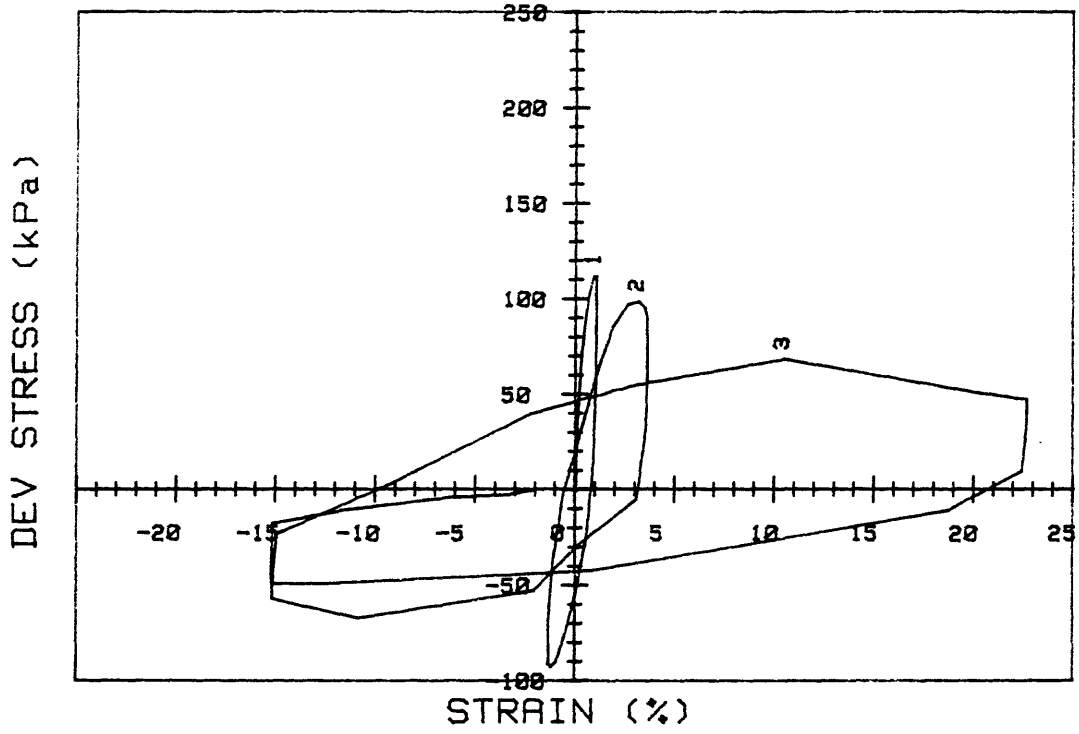

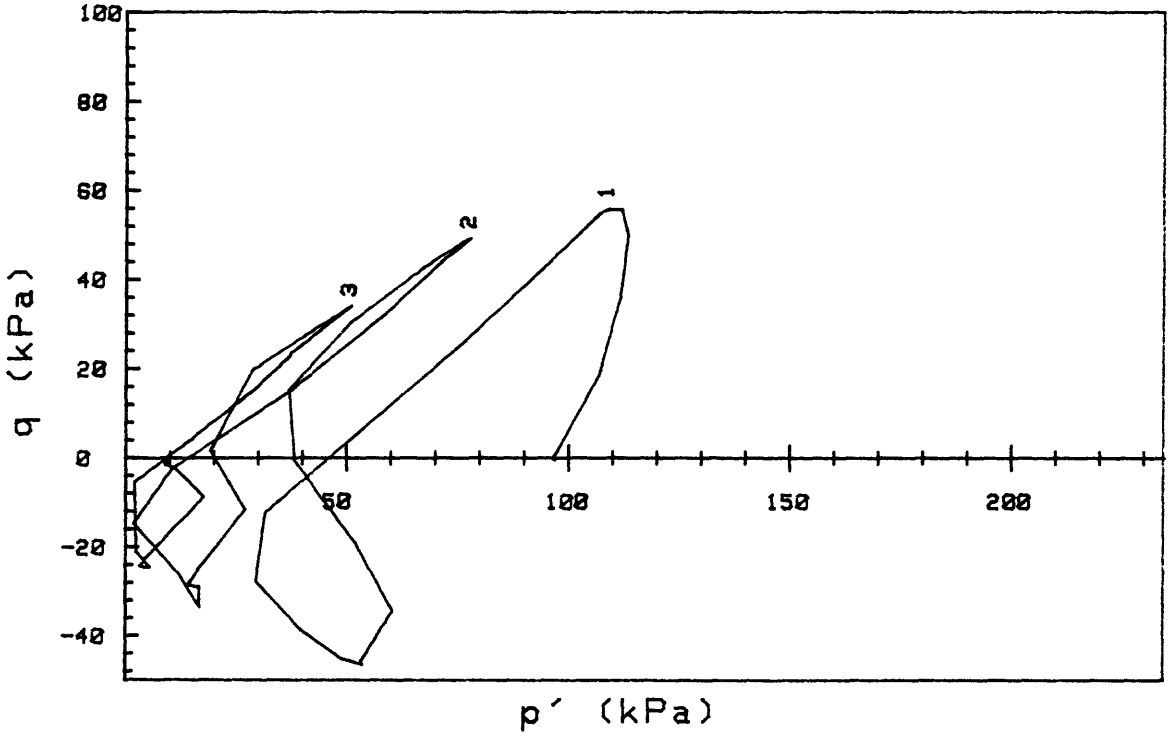

CRUISE ST HELENS		INCREMENT (cm)	REMOLDED-SURF
CORE NO.	CC1	TEST NO.	D131
SIG1c'(kPa)	97.4	STATIC qf (kPa)	100.0
SIG3c'(kPa)	97.4	AVG MAX q (kPa)	46.4 (46.4%)
INDUCED OCR	1.0	AVG MIN q (kPa)	-35.0 (35.0%)

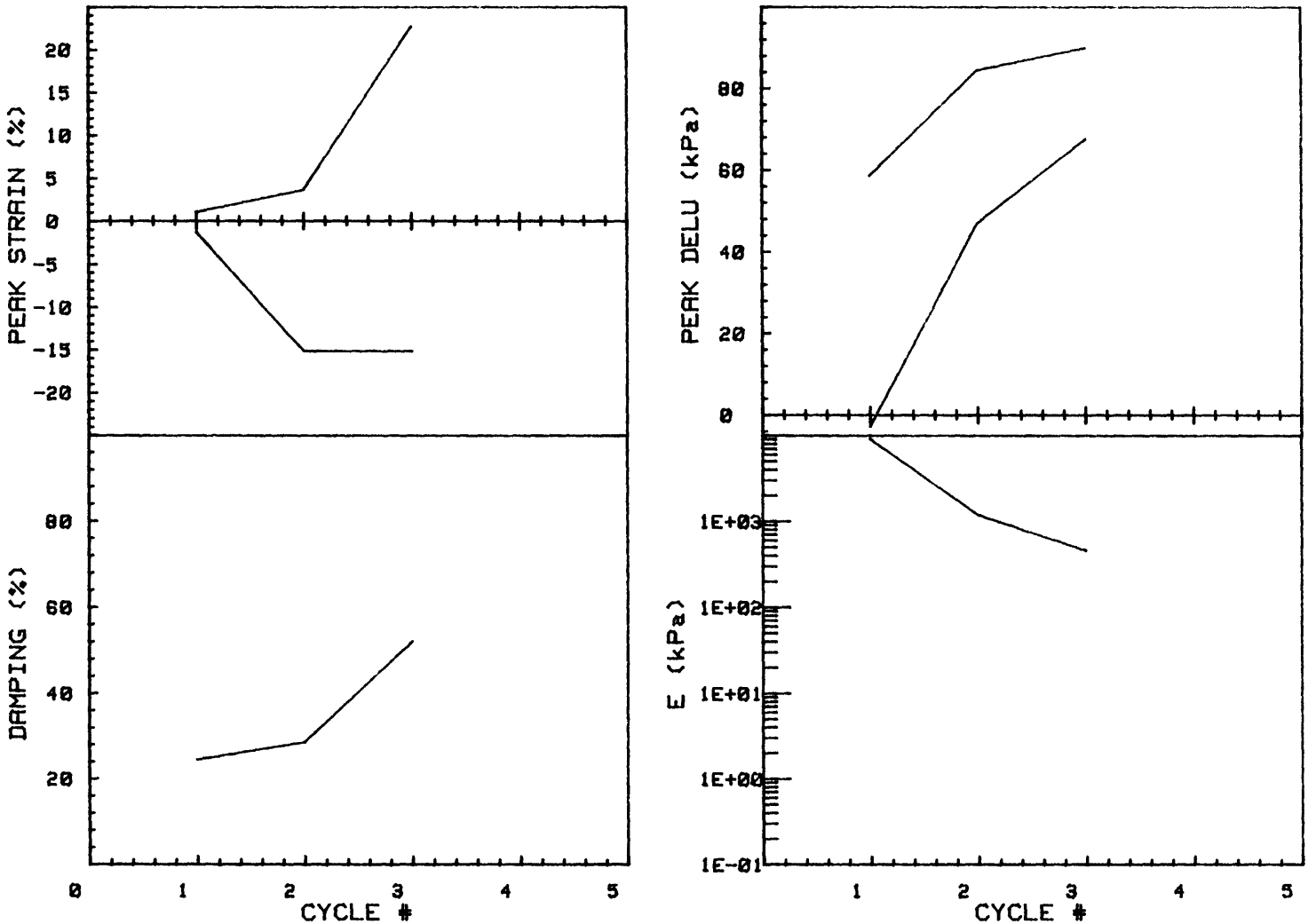

CRUISE ST HELENS		INCREMENT (cm)	REMOLDED-SURF
CORE NO.	CC1	TEST NO.	D131
SIG1c'(kPa)	97.4	STATIC qf (kPa)	100.0
SIG3c'(kPa)	97.4	AVG MAX q (kPa)	46.4 (46.4%)
INDUCED OCR	1.0	AVG MIN q (kPa)	-35.0 (35.0%)

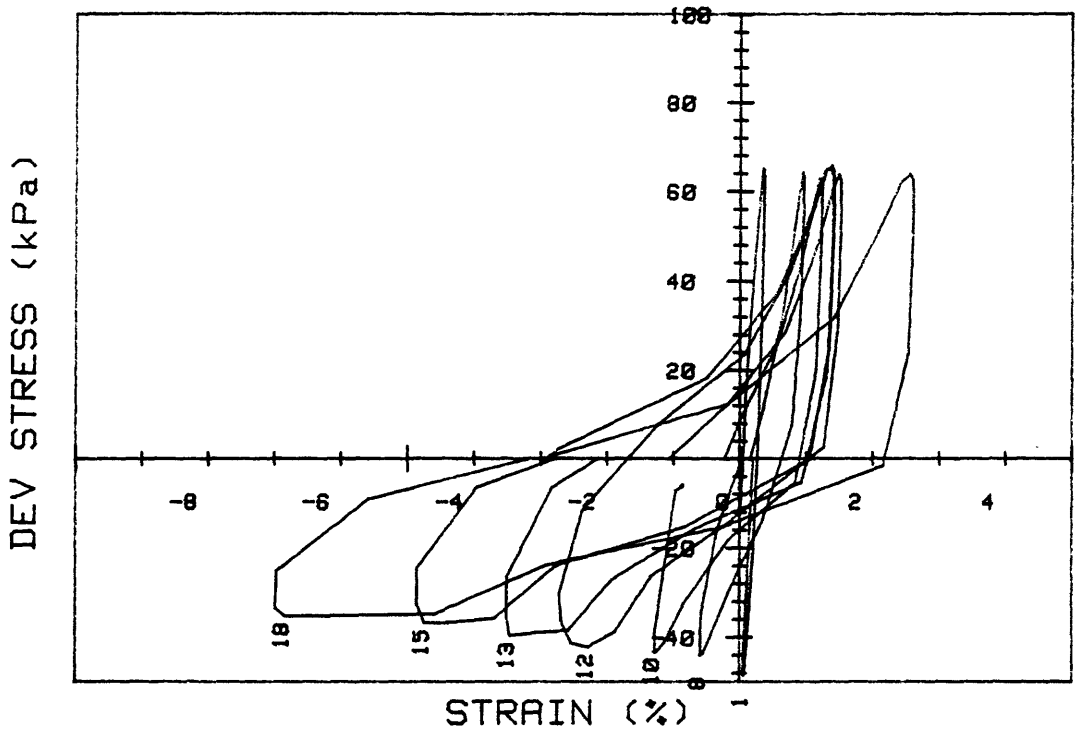

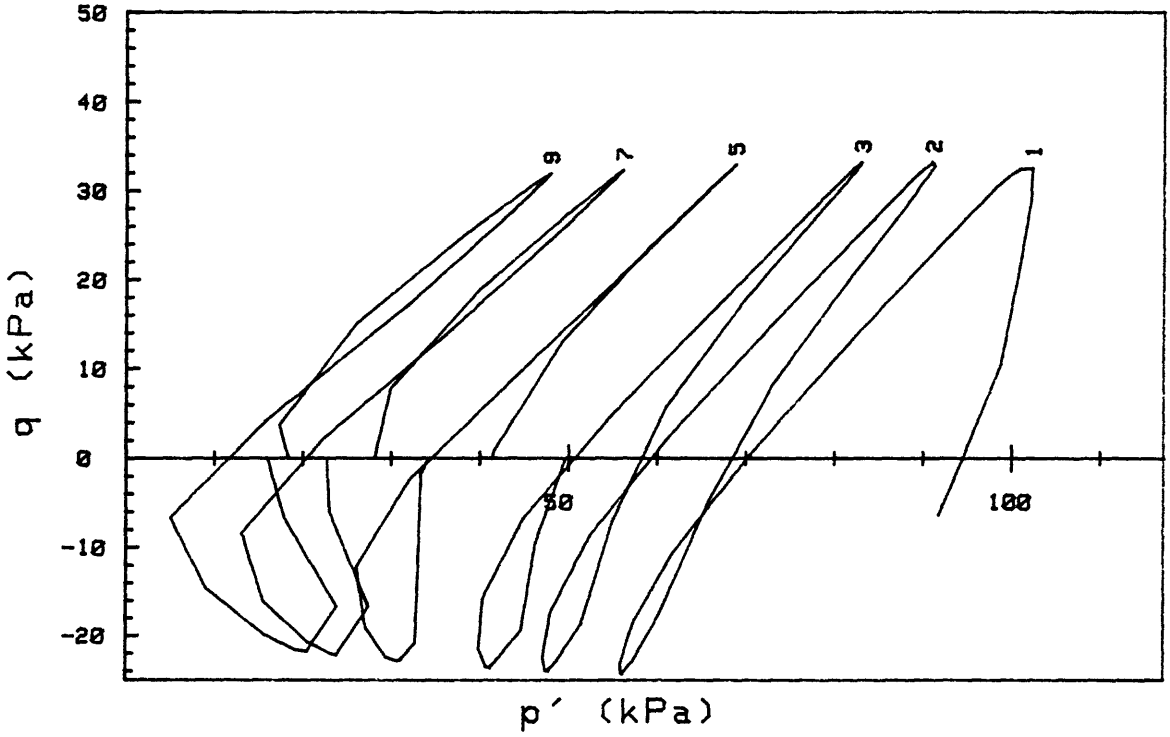

CRUISE ST HELENS		INCREMENT (cm)	REMOLDED-SURF
CORE NO. CC1		TEST NO.	D132
SIG1c´(kPa)	98.2	STATIC qf (kPa)	100.0
SIG3c´(kPa)	98.2	AVG MAX q (kPa)	32.3 (32.3%)
INDUCED OCR	1.0	AVG MIN q (kPa)	-21.1 (21.1%)

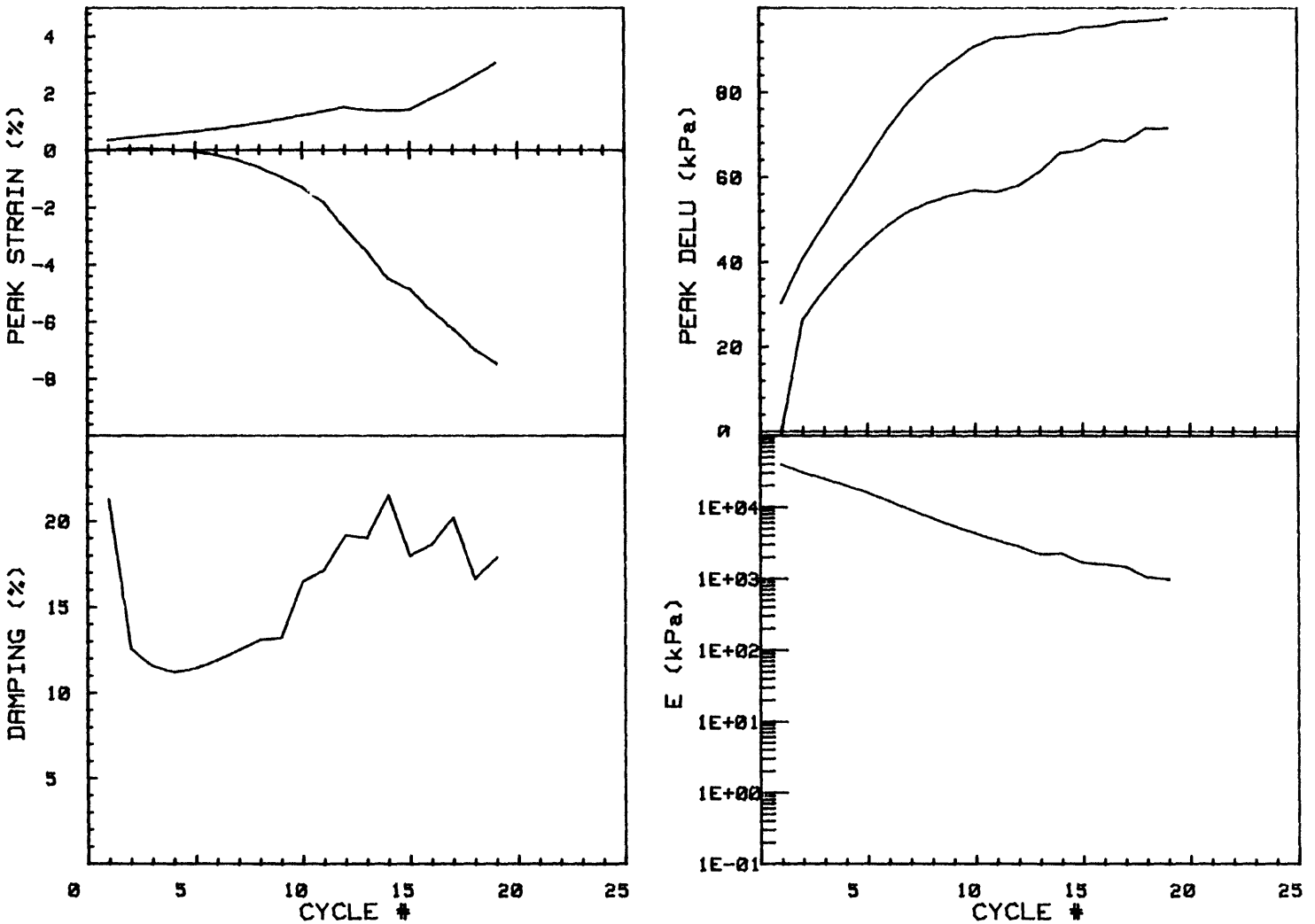

CRUISE ST HELENS		INCREMENT (cm)	REMOLDED-SURF
CORE NO.	CC1	TEST NO.	D132
SIG1c'(kPa)	98.2	STATIC qf (kPa)	100.0
SIG3c'(kPa)	98.2	AVG MAX q (kPa)	32.3 (32.3%)
INDUCED OCR	1.0	AVG MIN q (kPa)	-21.1 (21.1%)

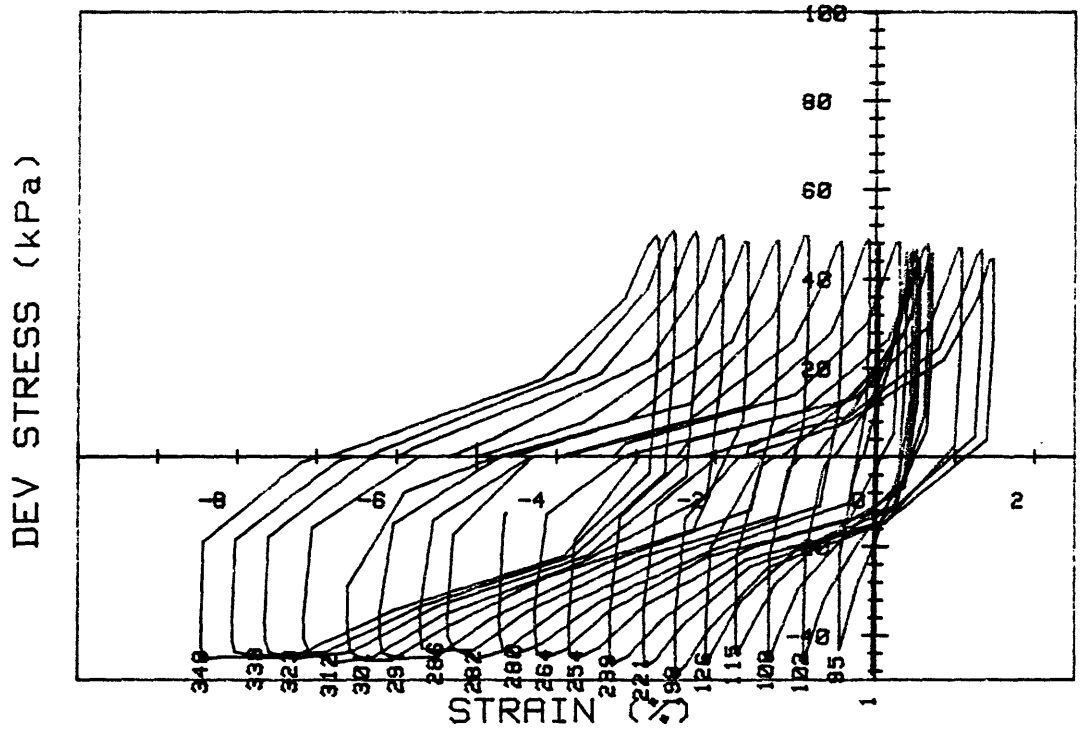

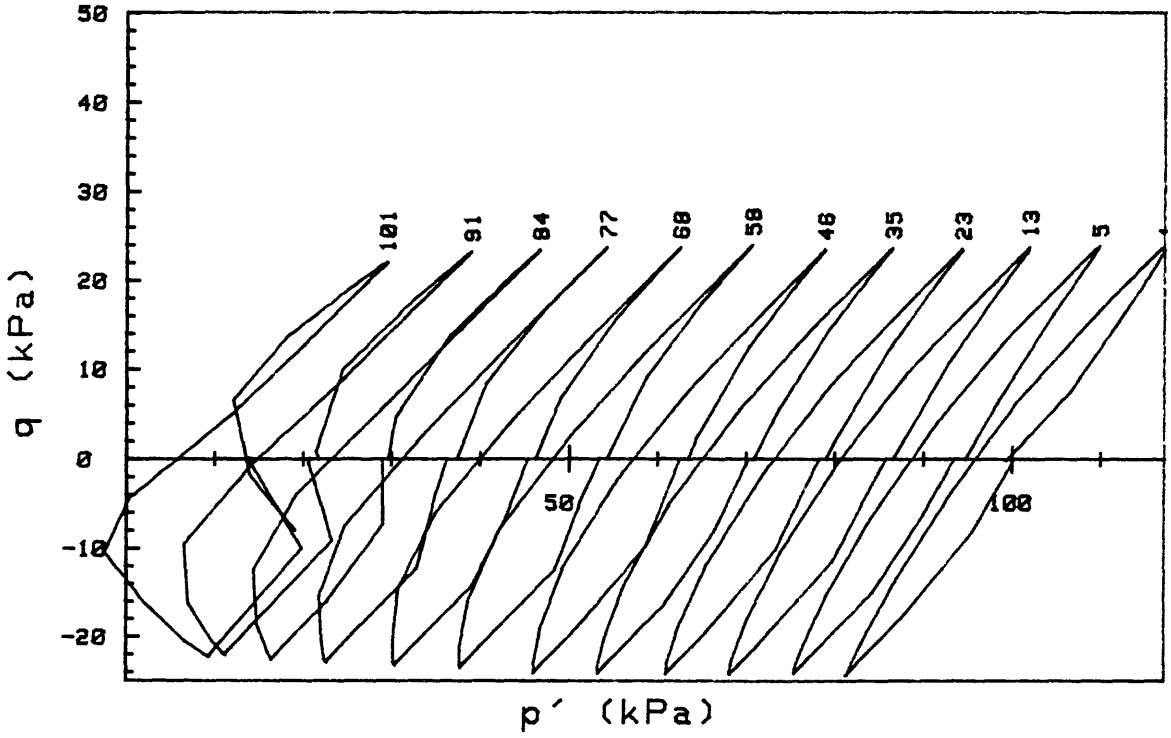

CRUISE ST HELENS		INCREMENT (cm)	REMOLDED-SURF
CORE NO. CC1		TEST NO.	D133
SIG1c´(kPa)	99.5	STATIC qf (kPa)	100.0
SIG3c´(kPa)	99.5	AVG MAX q (kPa)	23.6 (23.6%)
INDUCED OCR	1.0	AVG MIN q (kPa)	-23.1 (23.1%)

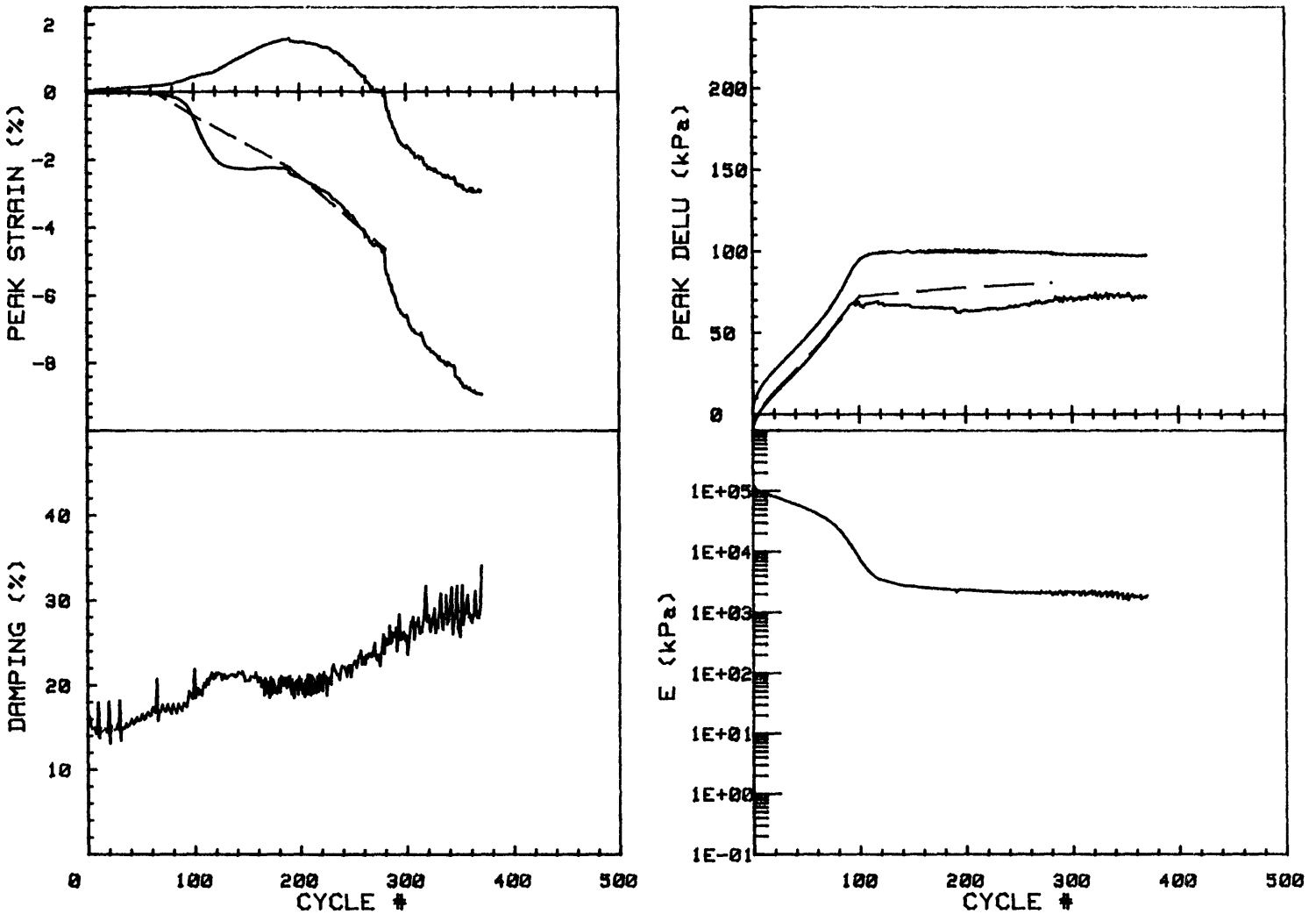

CRUISE ST HELENS		INCREMENT (cm)	REMOLDED-SURF
CORE NO.	CC1	TEST NO.	D133
SIG1c'(kPa)	99.5	STATIC qf (kPa)	100.0
SIG3c'(kPa)	99.5	AVG MAX q (kPa)	23.6 (23.6%)
INDUCED OCR	1.0	AVG MIN q (kPa)	-23.1 (23.1%)

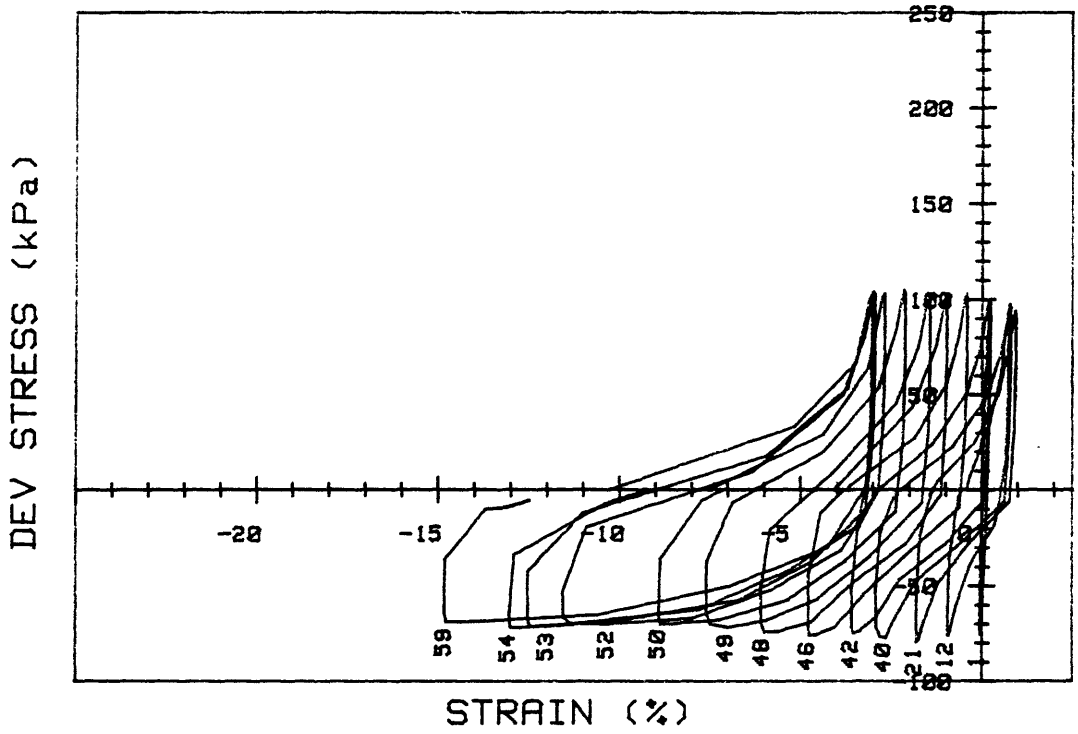

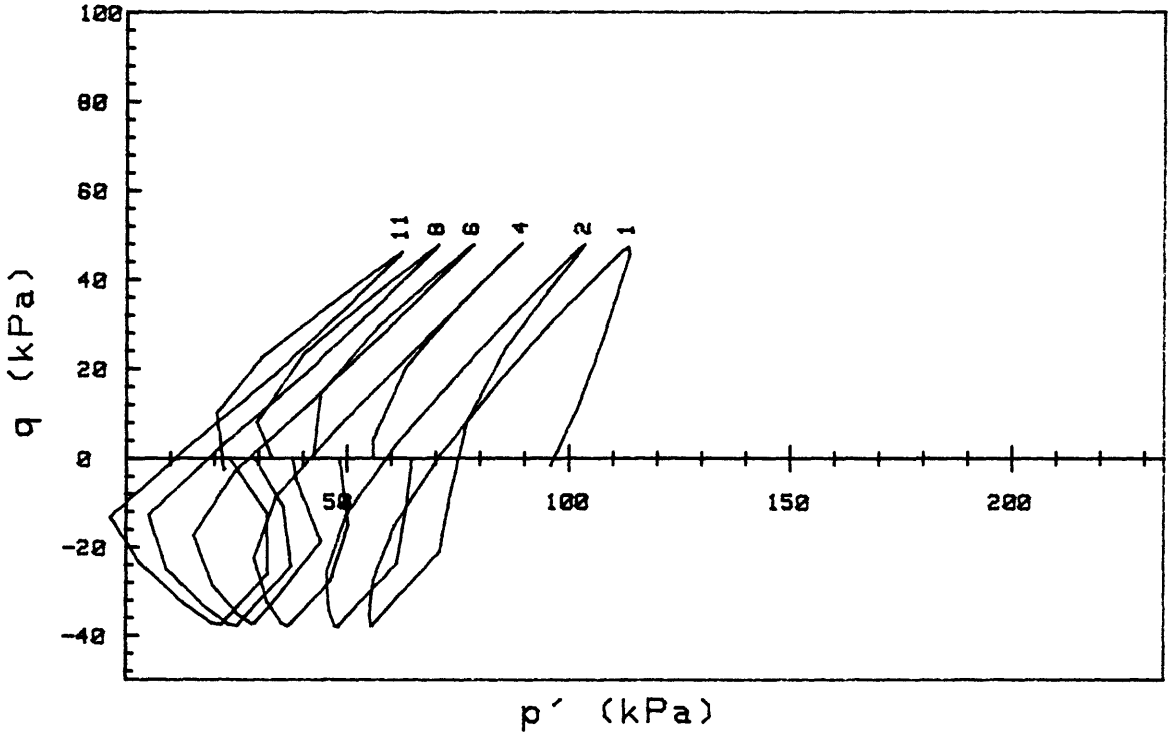

CRUISE ST HELENS		INCREMENT (cm)	REMOLDED-SURF
CORE NO.	CC1	TEST NO.	D134
SIG1c´(kPa)	97.5	STATIC qf (kPa)	100.0
SIG3c´(kPa)	97.5	AVG MAX q (kPa)	48.8 (48.8%)
INDUCED OCR	1.0	AVG MIN q (kPa)	-38.0 (38.0%)

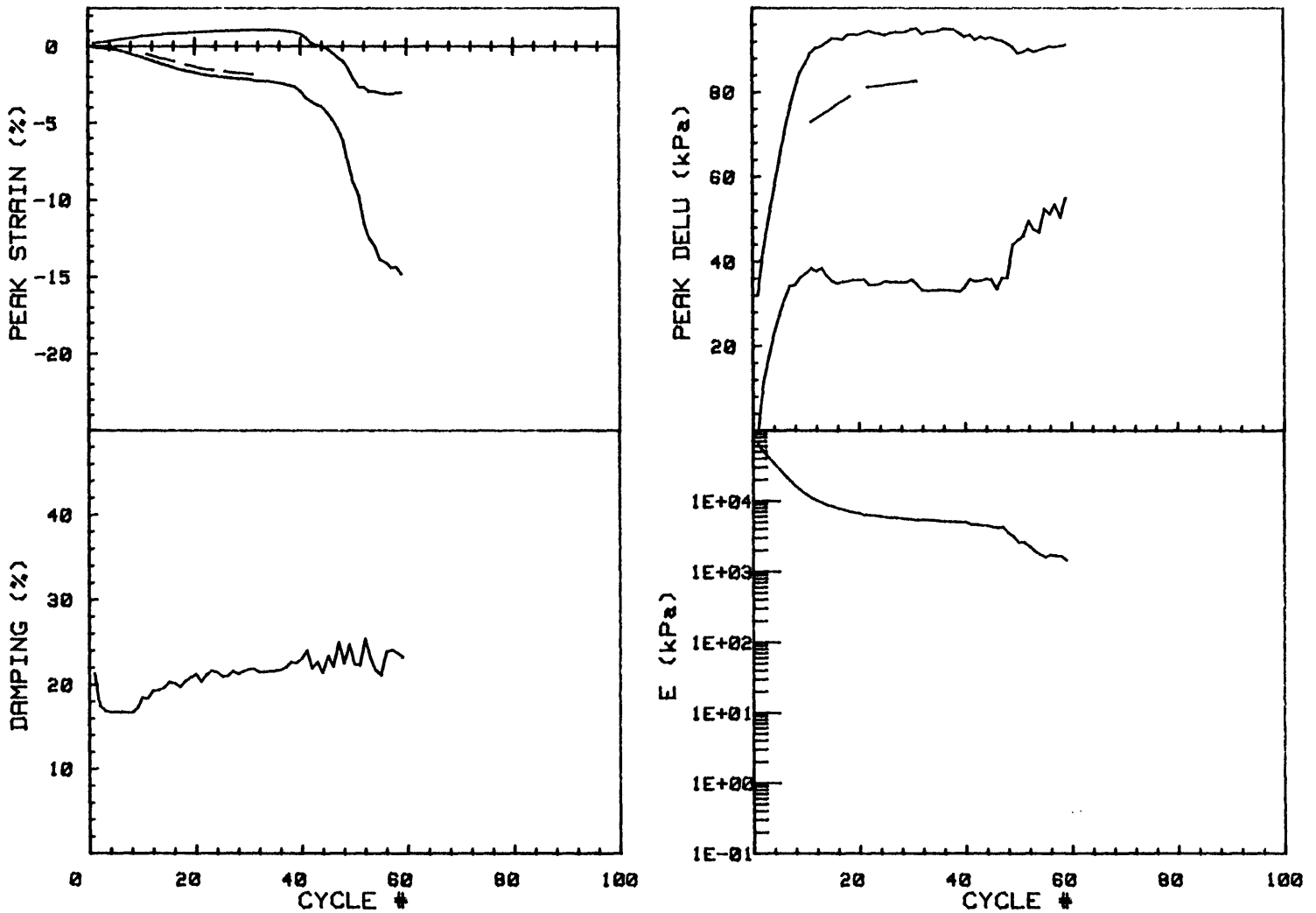

CRUISE ST HELENS		INCREMENT (cm)	REMOLDED-SURF
CORE NO.	CC1	TEST NO.	D134
SIG1c'(kPa)	97.5	STATIC qf (kPa)	100.0
SIG3c'(kPa)	97.5	AVG MAX q (kPa)	48.8 (48.8%)
INDUCED OCR	1.0	AVG MIN q (kPa)	-38.0 (38.0%)

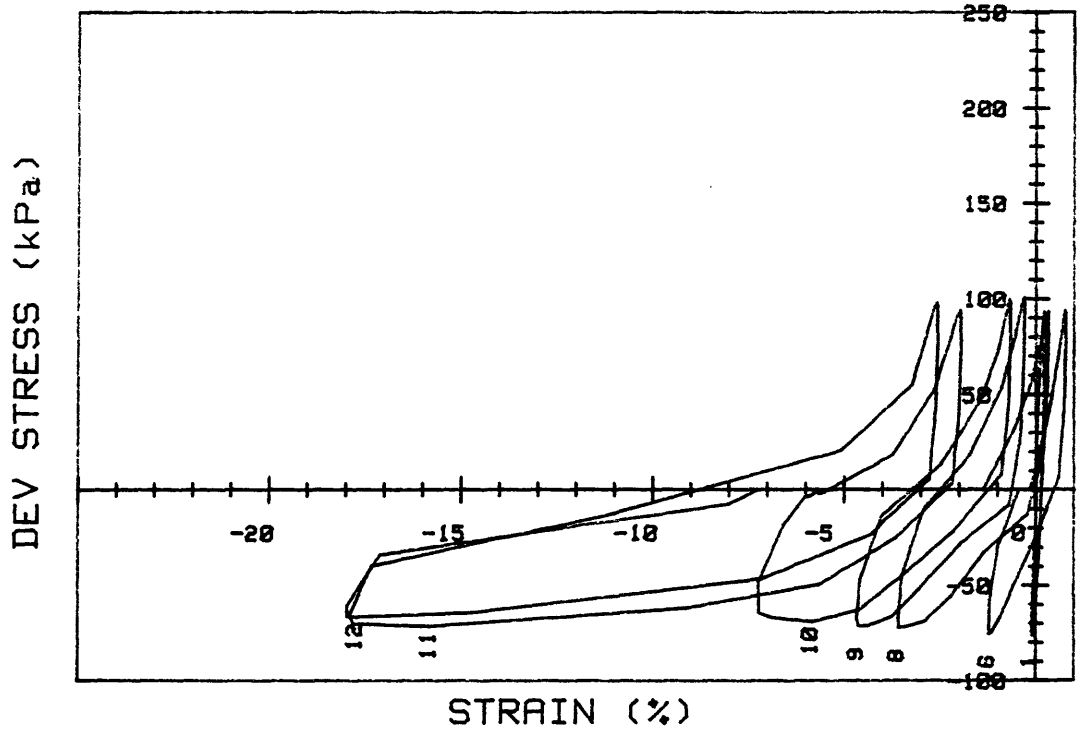

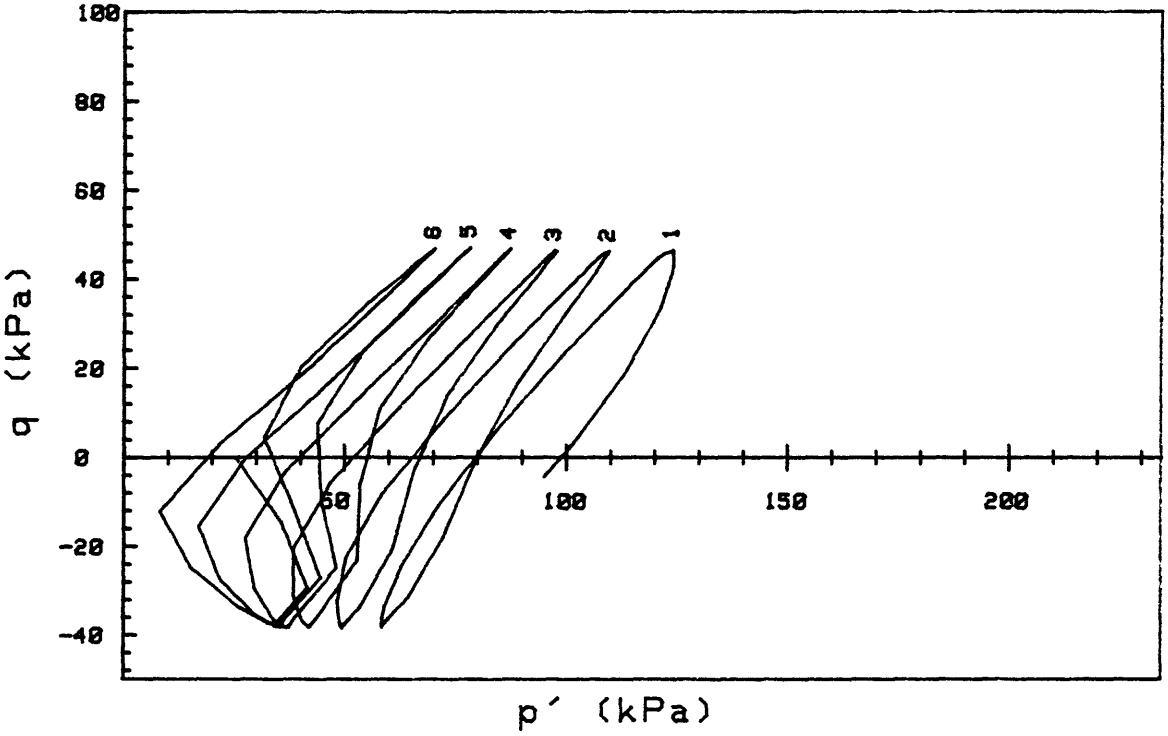

CRUISE ST HELENS		INCREMENT (cm)	REMOLDED-SURF
CORE NO.	CC1	TEST NO.	D135
SIG1c´(kPa)	99.5	STATIC qf (kPa)	100.0
SIG3c´(kPa)	99.5	AVG MAX q (kPa)	47.4 (47.4%)
INDUCED OCR	1.0	AVG MIN q (kPa)	-36.4 (36.4%)

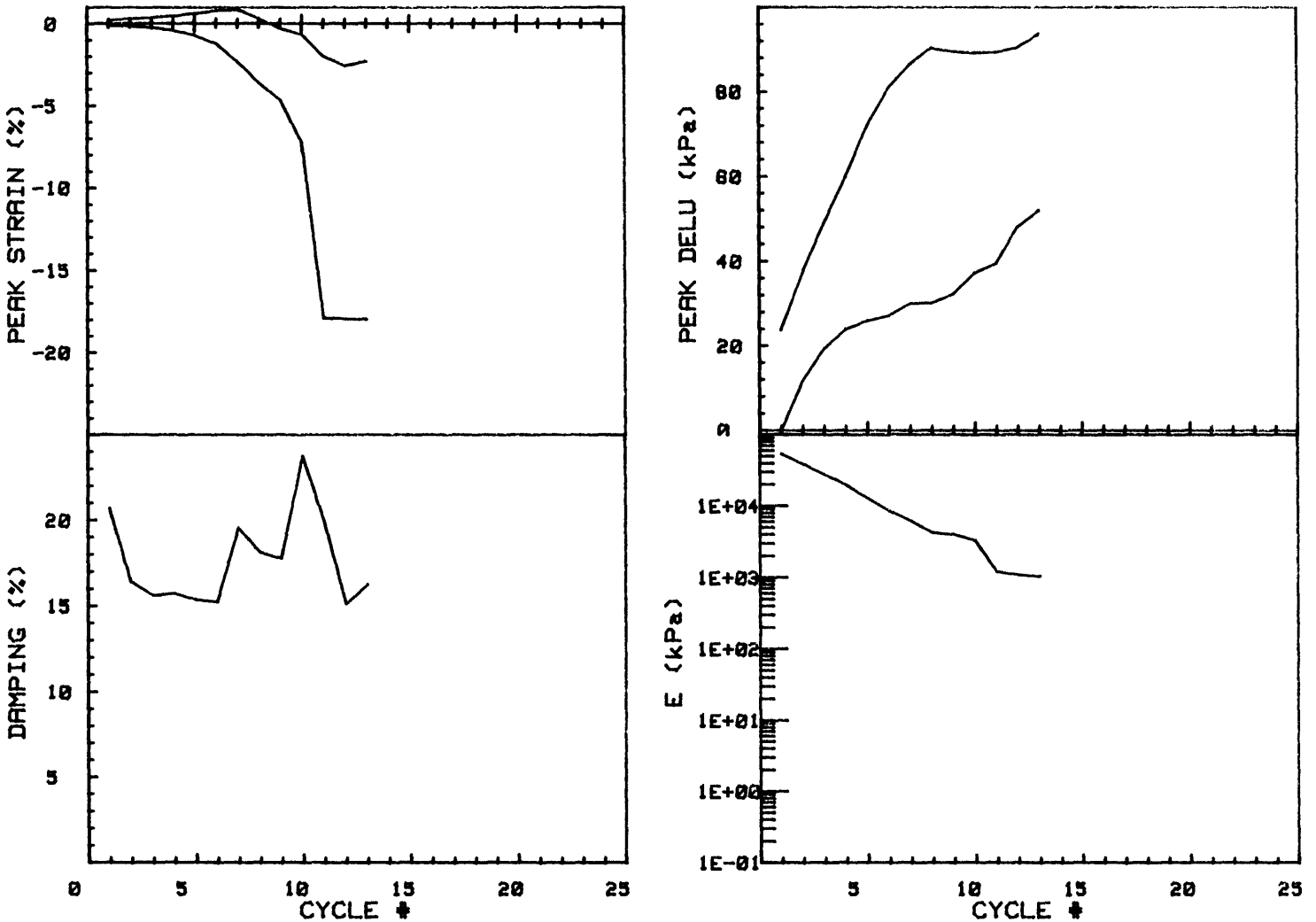

CRUISE ST HELENS		INCREMENT (cm)	REMOLDED-SURF
CORE NO. CC1		TEST NO.	D135
SIG1c'(kPa)	99.5	STATIC qf (kPa)	100.0
SIG3c'(kPa)	99.5	AVG MAX q (kPa)	47.4 (47.4%)
INDUCED OCR	1.0	AVG MIN q (kPa)	-36.4 (36.4%)

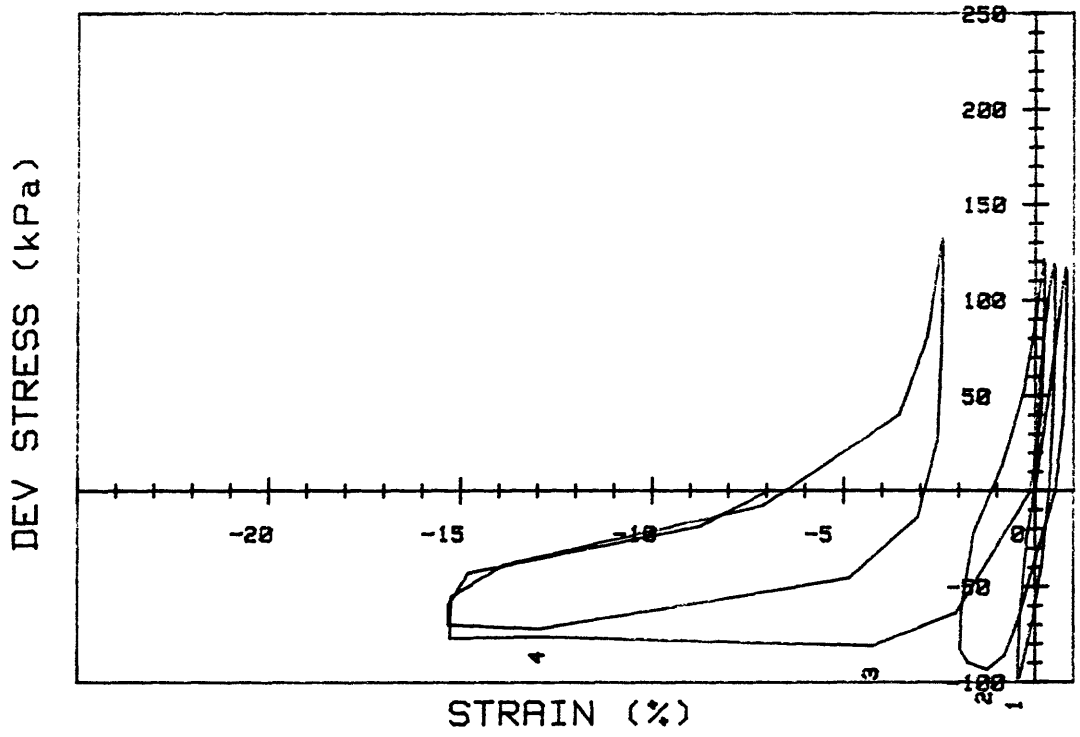

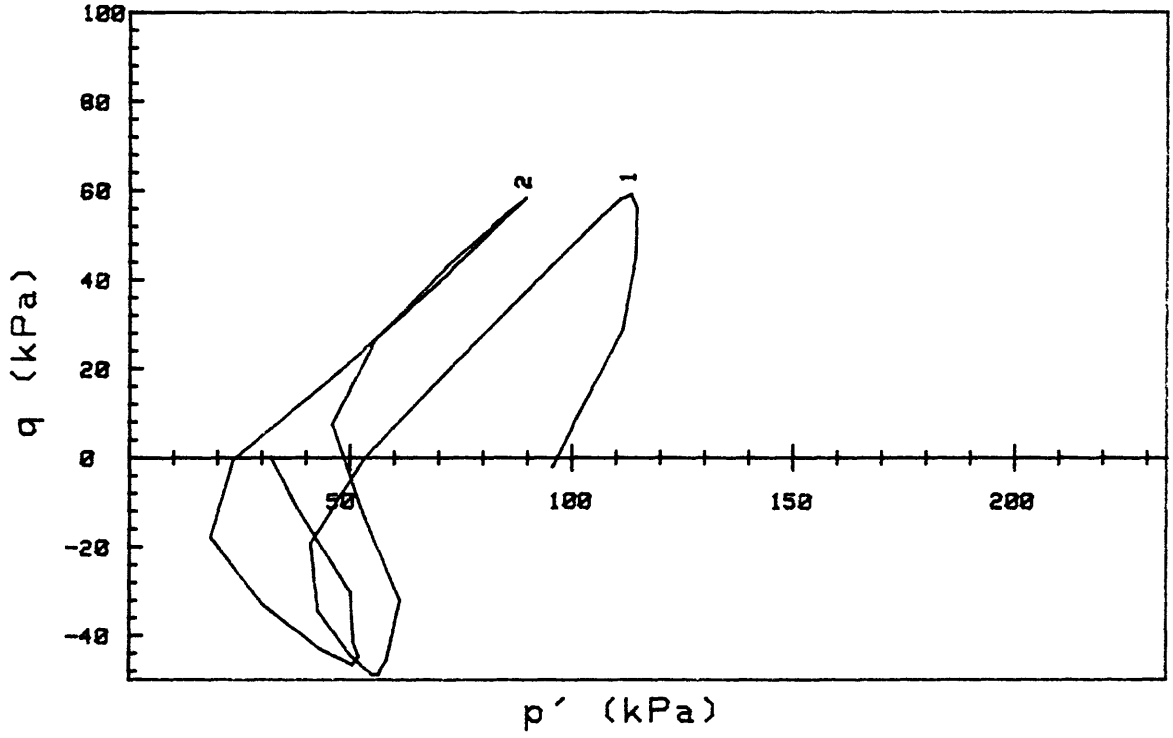

CRUISE ST HELENS		INCREMENT (cm)	REMOLDED-SURF
CORE NO. CC1		TEST NO.	D136
SIG1c'(kPa)	97.8	STATIC qf (kPa)	100.0
SIG3c'(kPa)	97.8	AVG MAX q (kPa)	61.9 (61.9%)
INDUCED OCR	1.0	AVG MIN q (kPa)	-41.5 (41.5%)

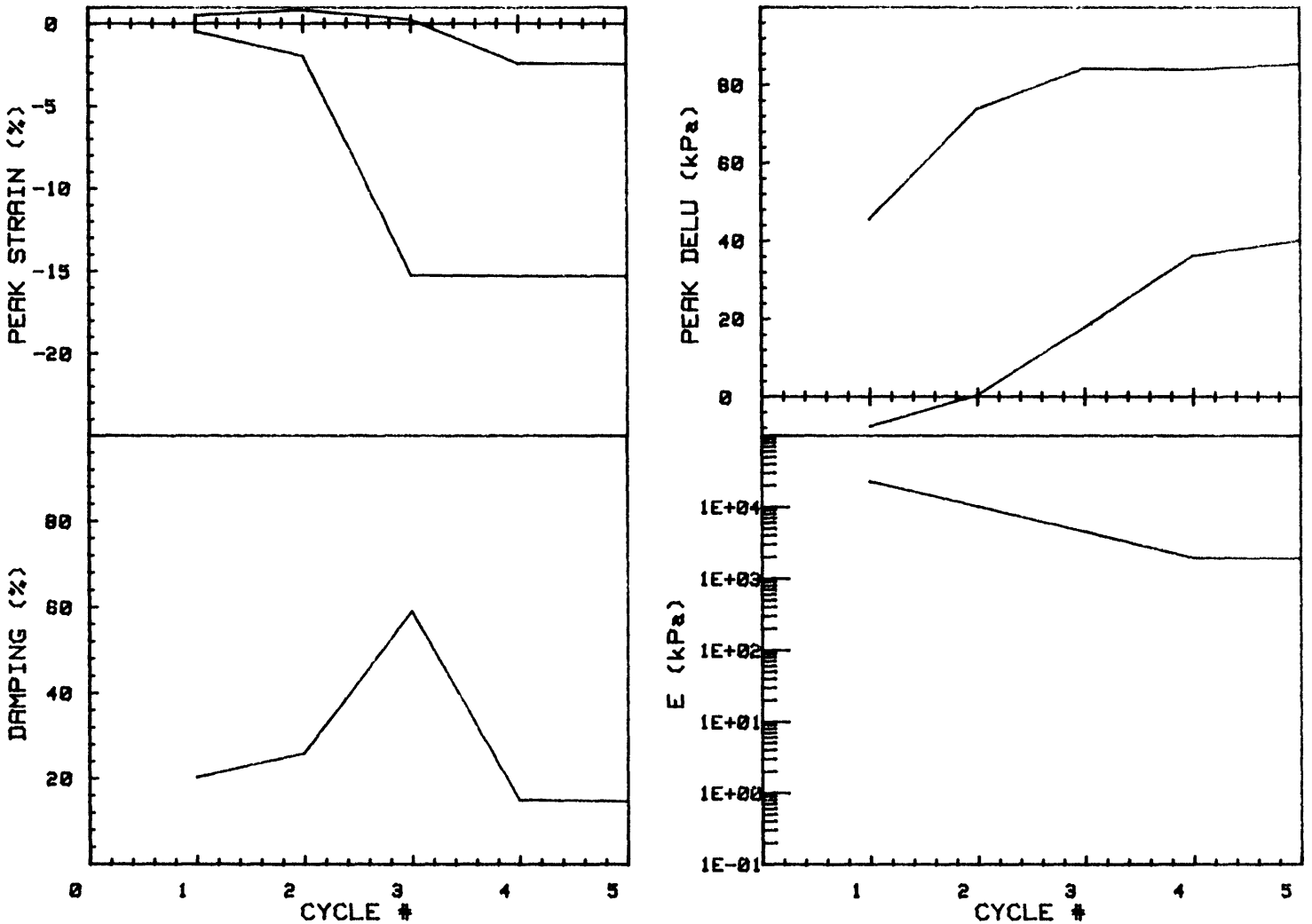

CRUISE ST HELENS		INCREMENT (cm)	REMOLDED-SURF
CORE NO. CC1		TEST NO.	D136
SIG1c'(kPa)	97.8	STATIC qf (kPa)	100.0
SIG3c'(kPa)	97.8	AVG MAX q (kPa)	61.9 (61.9%)
INDUCED OCR	1.0	AVG MIN q (kPa)	-41.5 (41.5%)

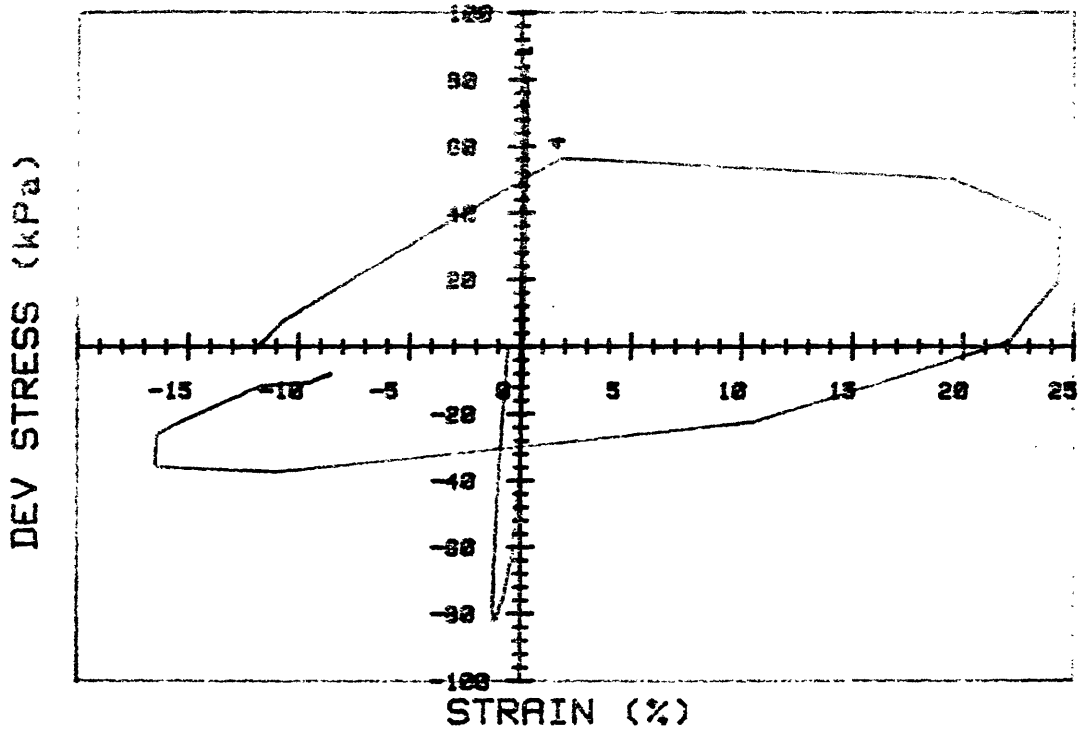

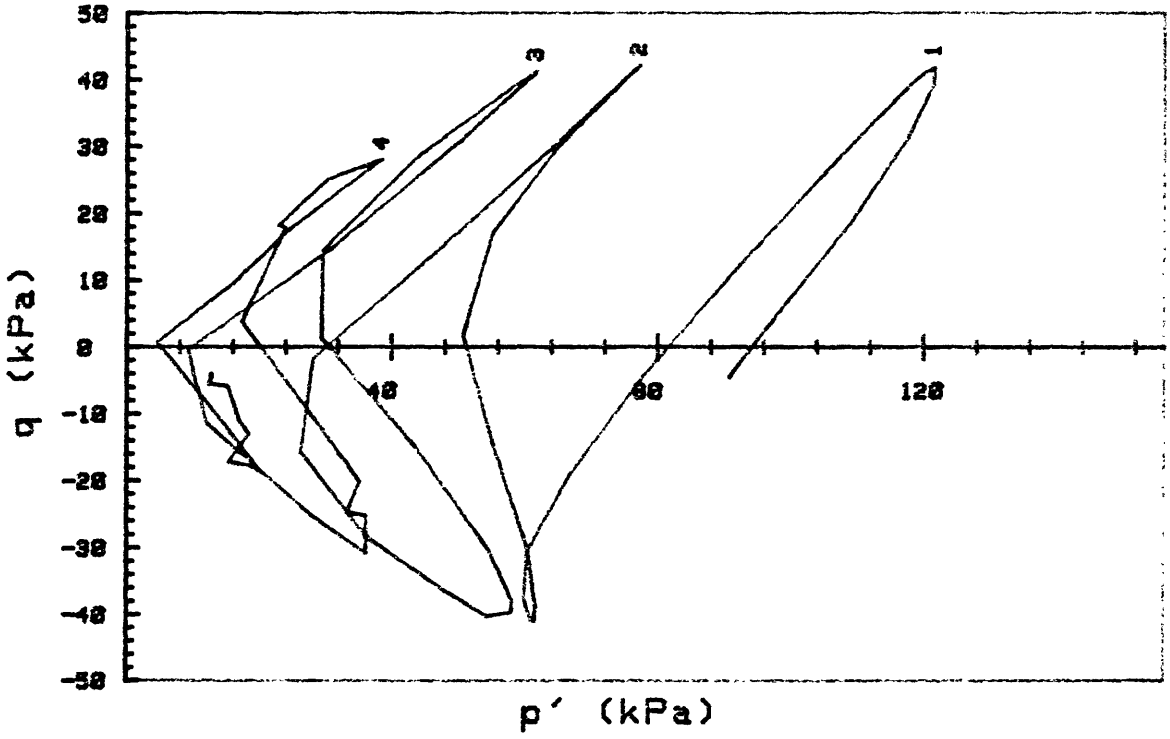

CRUISE ST HELENS		INCREMENT (cm)	REMOLDED SURF
CORE NO.	CC1	TEST NO.	D197
SIG1c'(kPa)	95.3	STATIC qf (kPa)	100.0
SIG3c'(kPa)	95.3	AVG MAX q (kPa)	38.4 (38.4%)
INDUCED OCR	1.0	AVG MIN q (kPa)	-32.8 (32.8%)

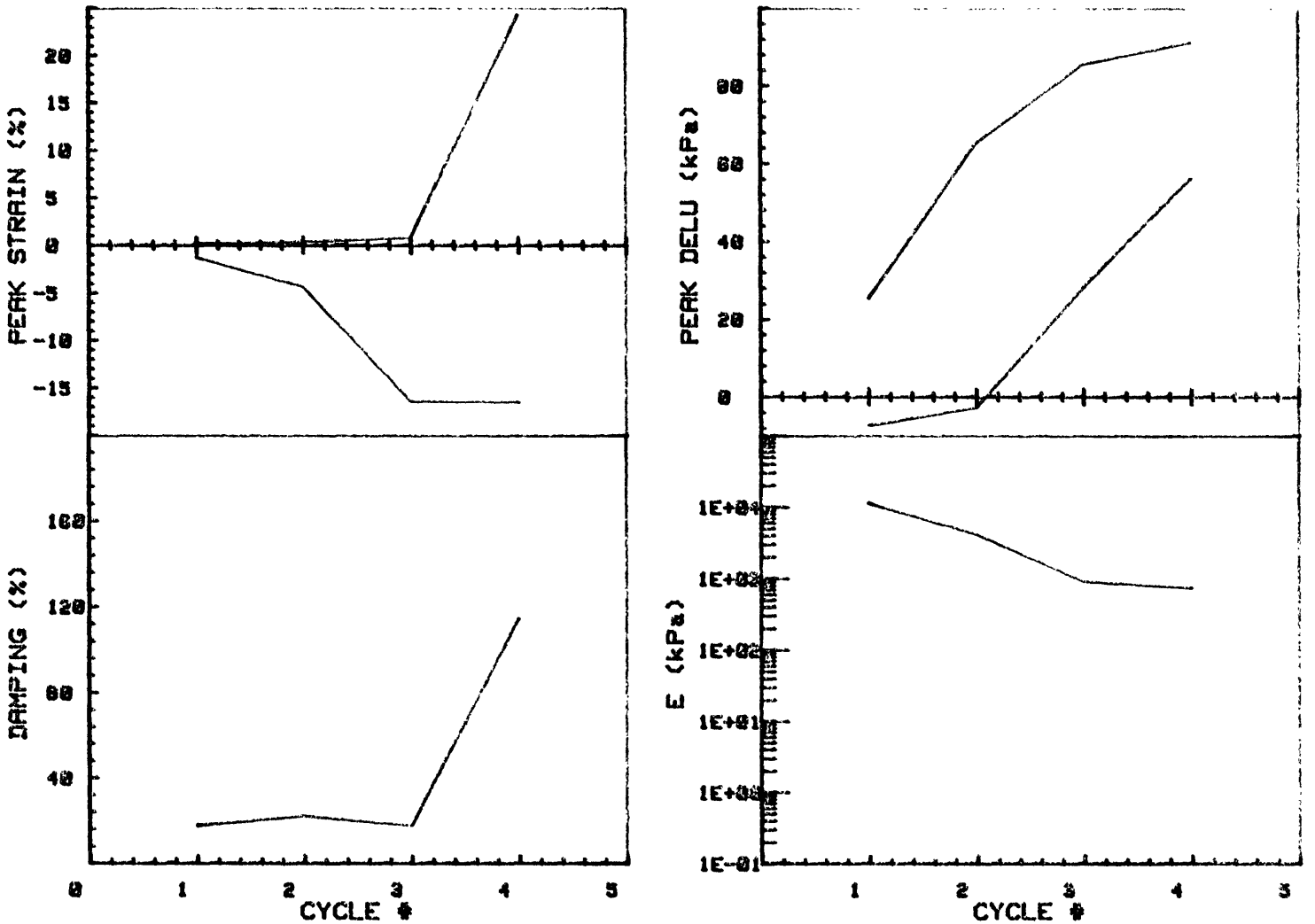

CRUISE ST HELENS		INCREMENT (cm)	REMOLDED SURF
CORE NO.	CC1	TEST NO.	D197
SIG1c'(kPa)	95.3	STATIC qf (kPa)	100.0
SIG3c'(kPa)	95.3	AVG MAX q (kPa)	38.4 (38.4%)
INDUCED OCR	1.0	AVG MIN q (kPa)	-32.8 (32.8%)

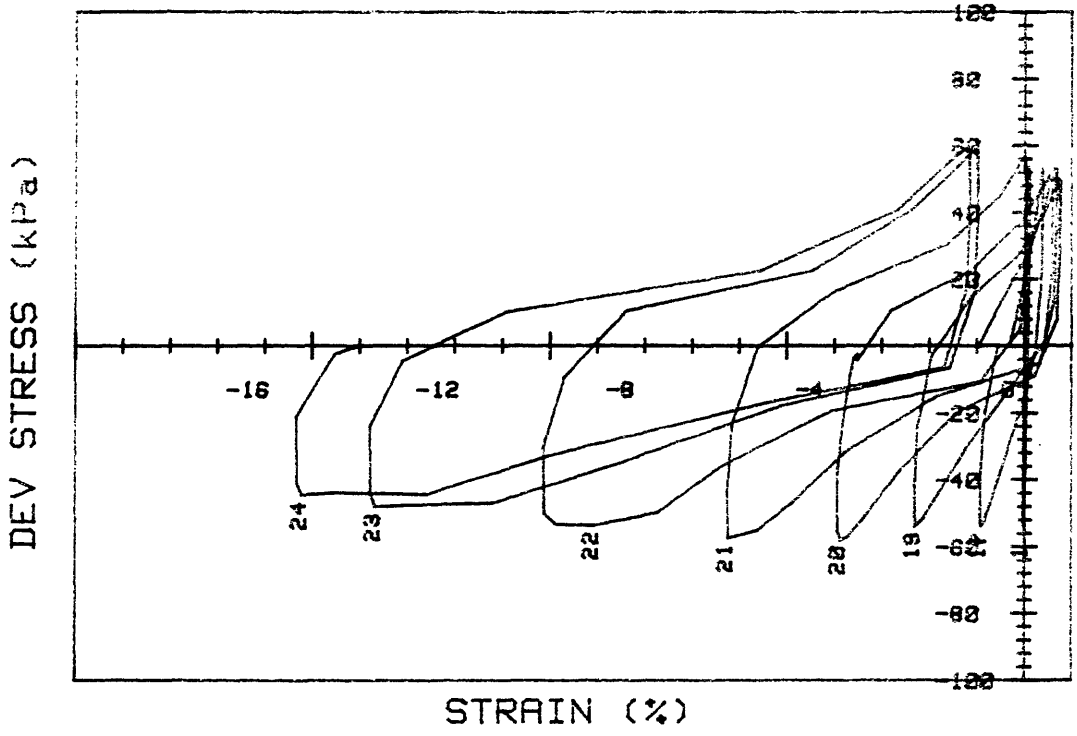

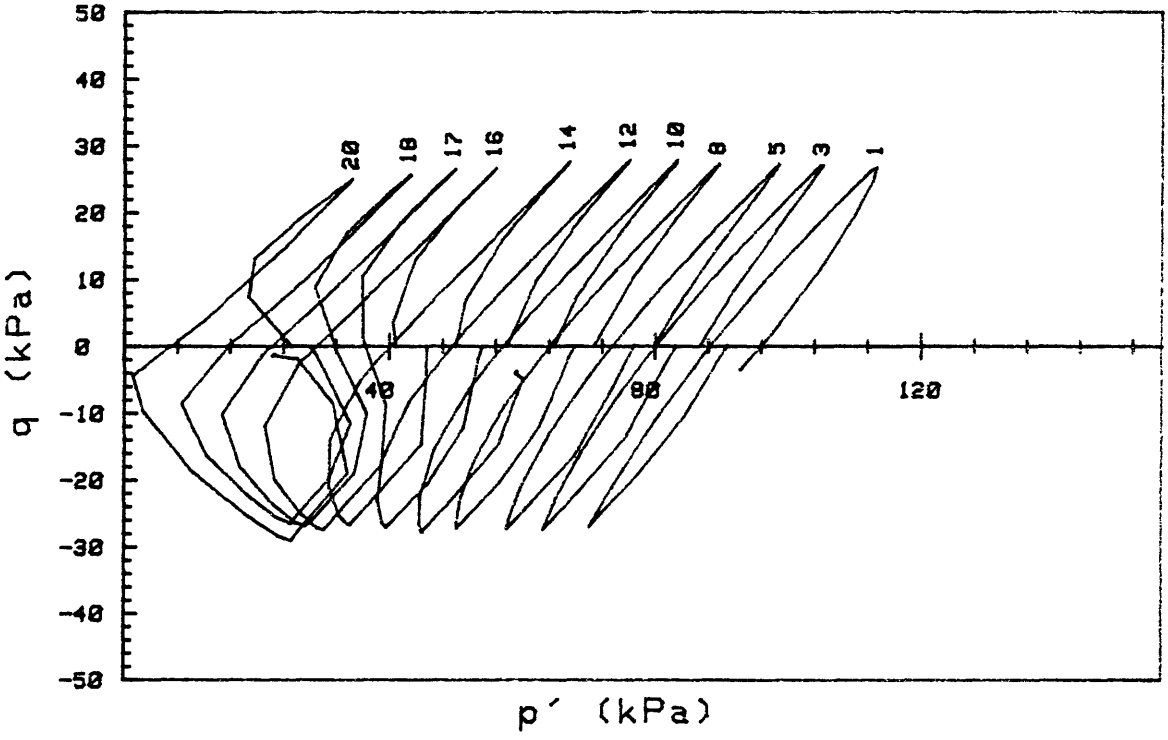

CRUISE ST HELENS		INCREMENT (cm)	REMOLDED SURF
CORE NO.	CC1	TEST NO.	D198
SIG1c´(kPa)	96.3	STATIC qf (kPa)	100.0
SIG3c´(kPa)	96.3	AVG MAX q (kPa)	27.3 (27.3%)
INDUCED OCR	1.0	AVG MIN q (kPa)	-26.7 (26.7%)

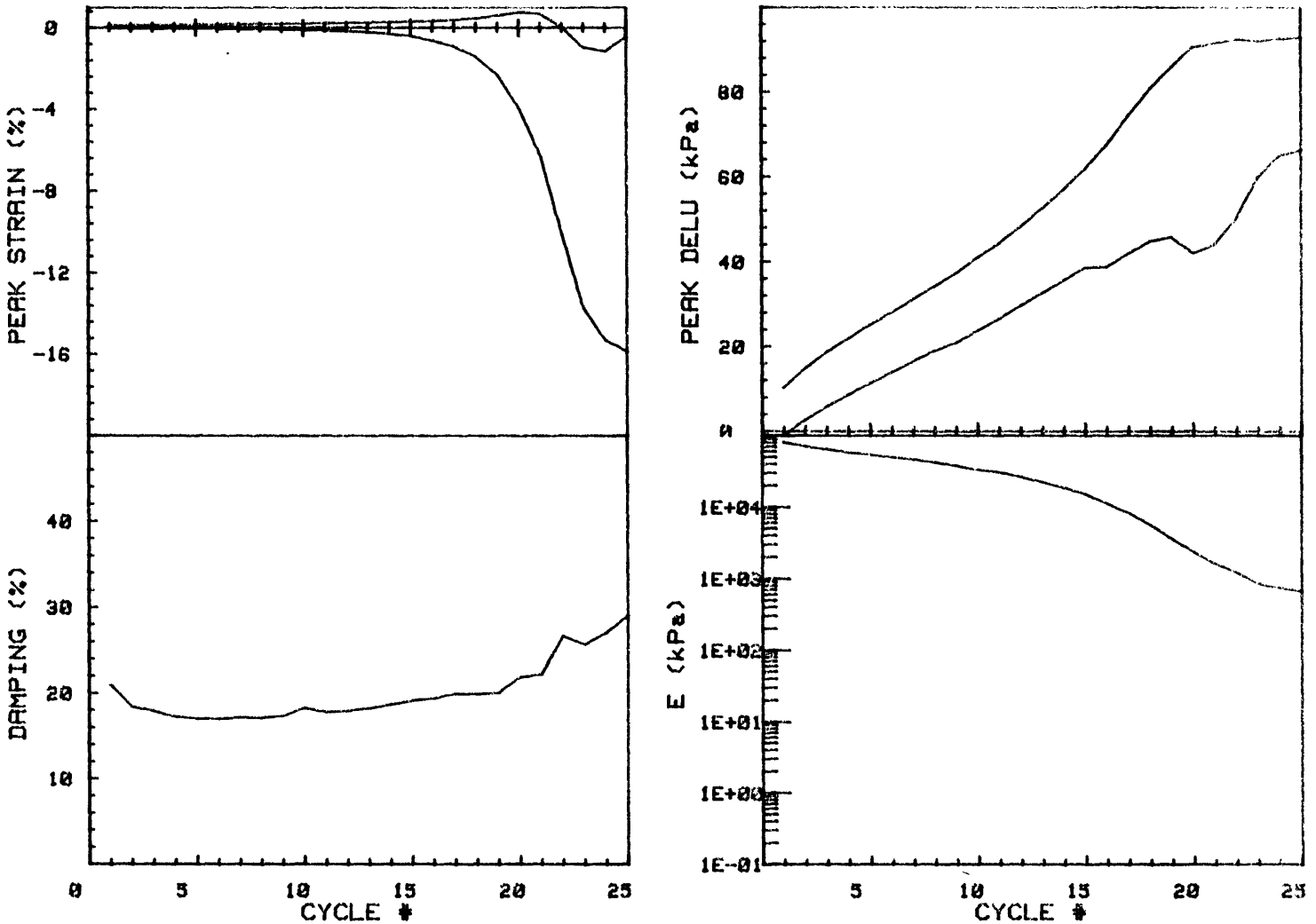

CRUISE ST HELENS		INCREMENT (cm)	REMOLDED SURF
CORE NO.	CC1	TEST NO.	D198
SIG1c'(kPa)	96.3	STATIC qf (kPa)	100.0
SIG3c'(kPa)	96.3	AVG MAX q (kPa)	27.3 (27.3%)
INDUCED OCR	1.0	AVG MIN q (kPa)	-26.7 (26.7%)

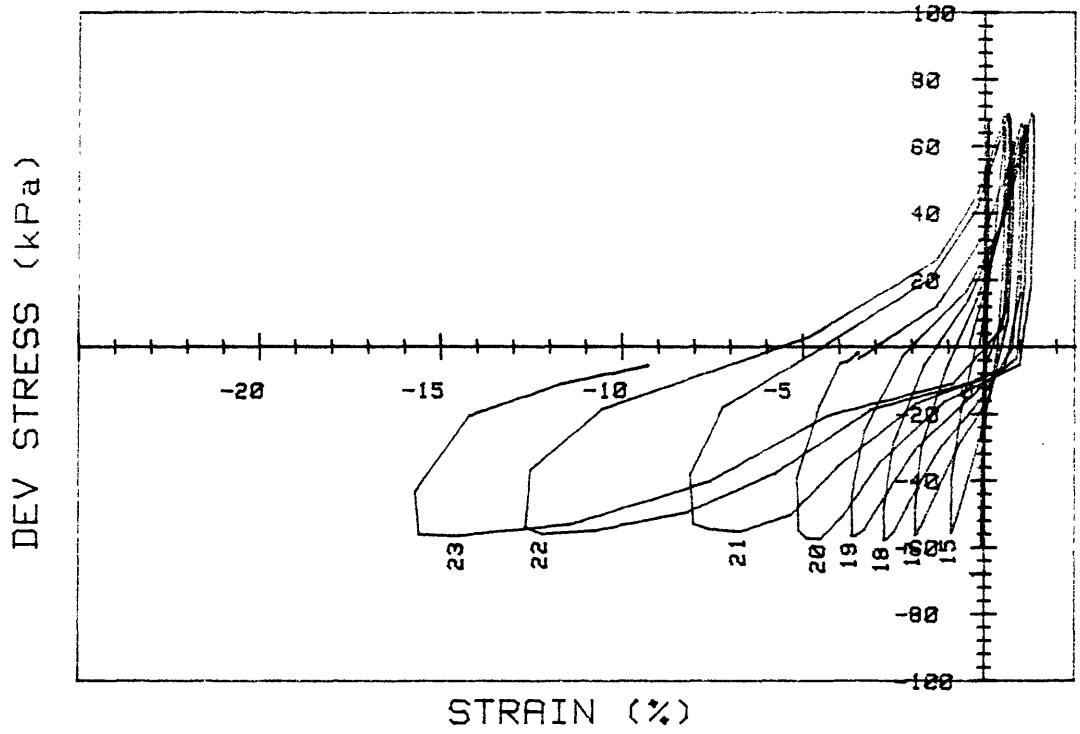

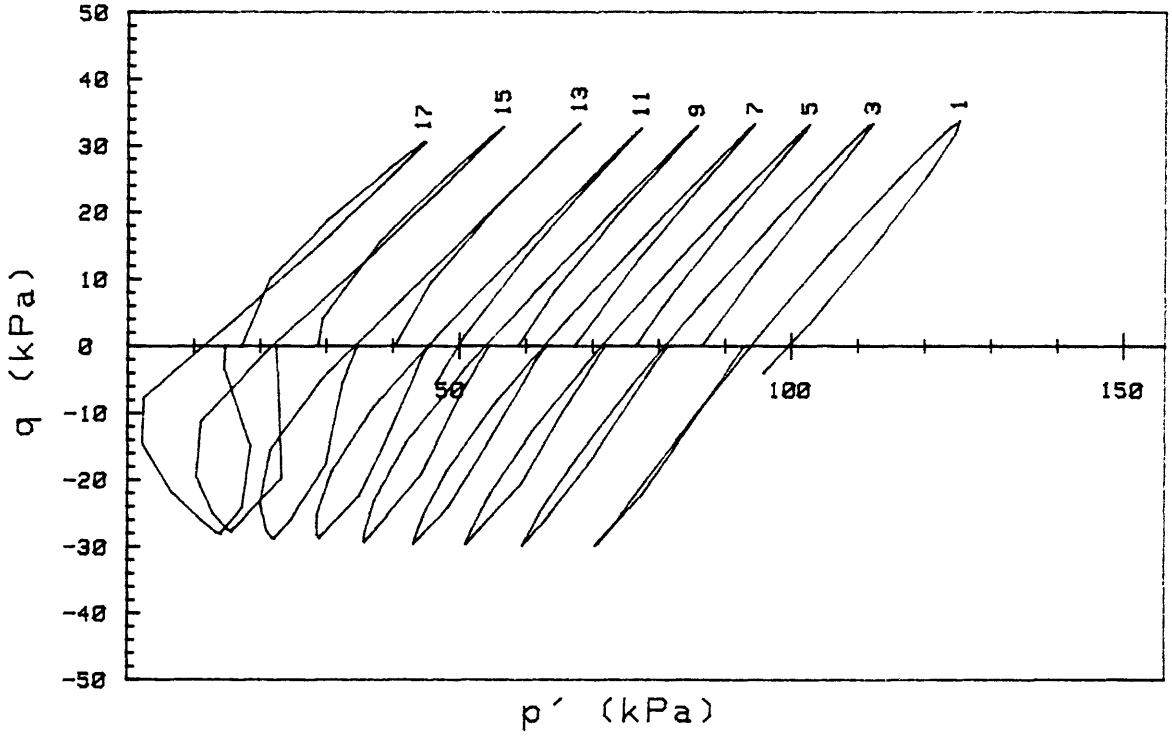

CRUISE ST HELENS		INCREMENT (cm)	REMOLDED-SURF
CORE NO.	CC2	TEST NO.	D137
SIG1c´(kPa)	99.8	STATIC qf (kPa)	100.0
SIG3c´(kPa)	99.8	AVG MAX q (kPa)	33.2 (33.2%)
INDUCED OCR	1.0	AVG MIN q (kPa)	-28.9 (28.9%)

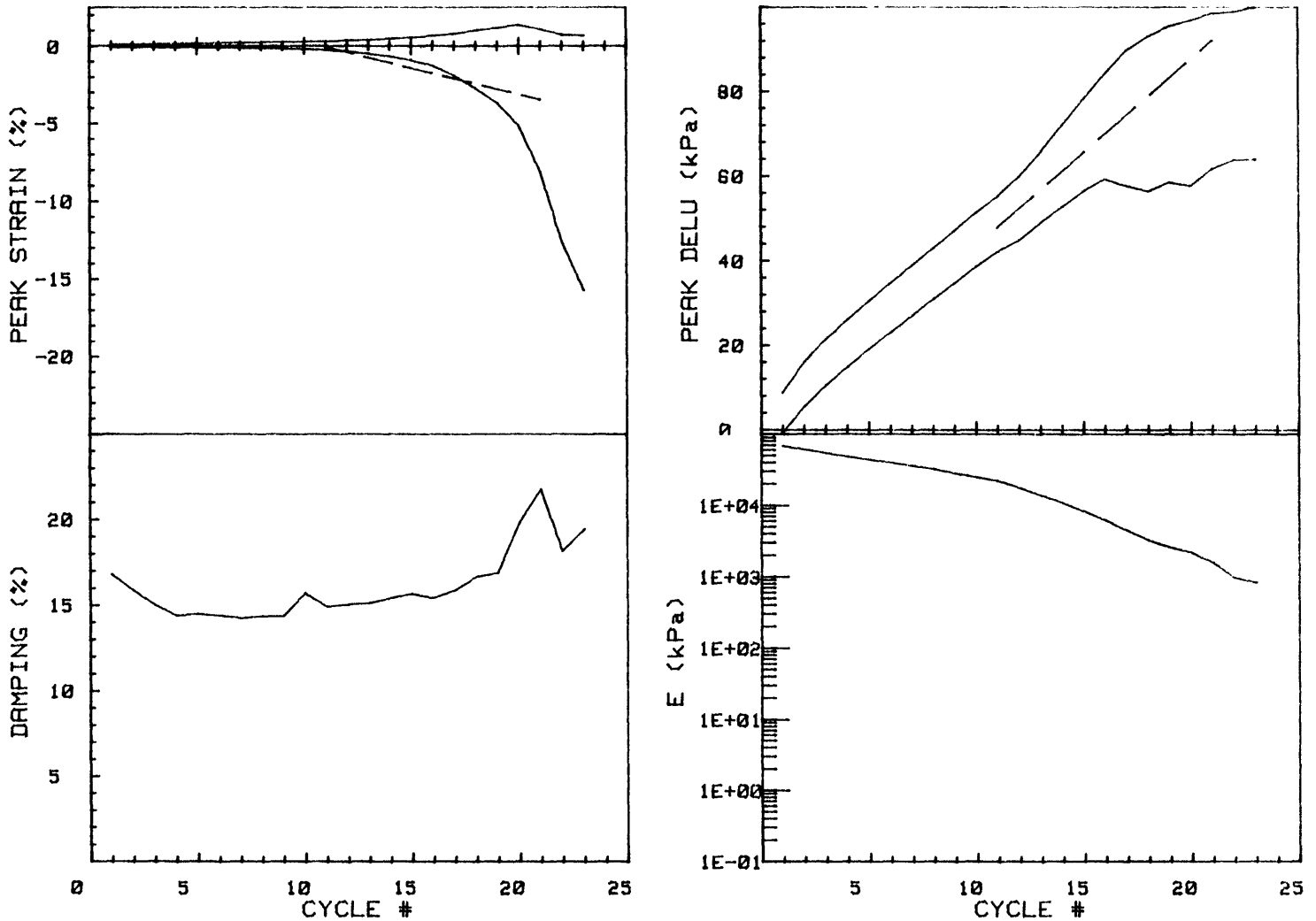

CRUISE ST HELENS		INCREMENT (cm)	REMOLDED-SURF
CORE NO.	CC2	TEST NO.	D137
SIG1c'(kPa)	99.8	STATIC qf (kPa)	100.0
SIG3c'(kPa)	99.8	AVG MAX q (kPa)	33.2 (33.2%)
INDUCED OCR	1.0	AVG MIN q (kPa)	-28.9 (28.9%)

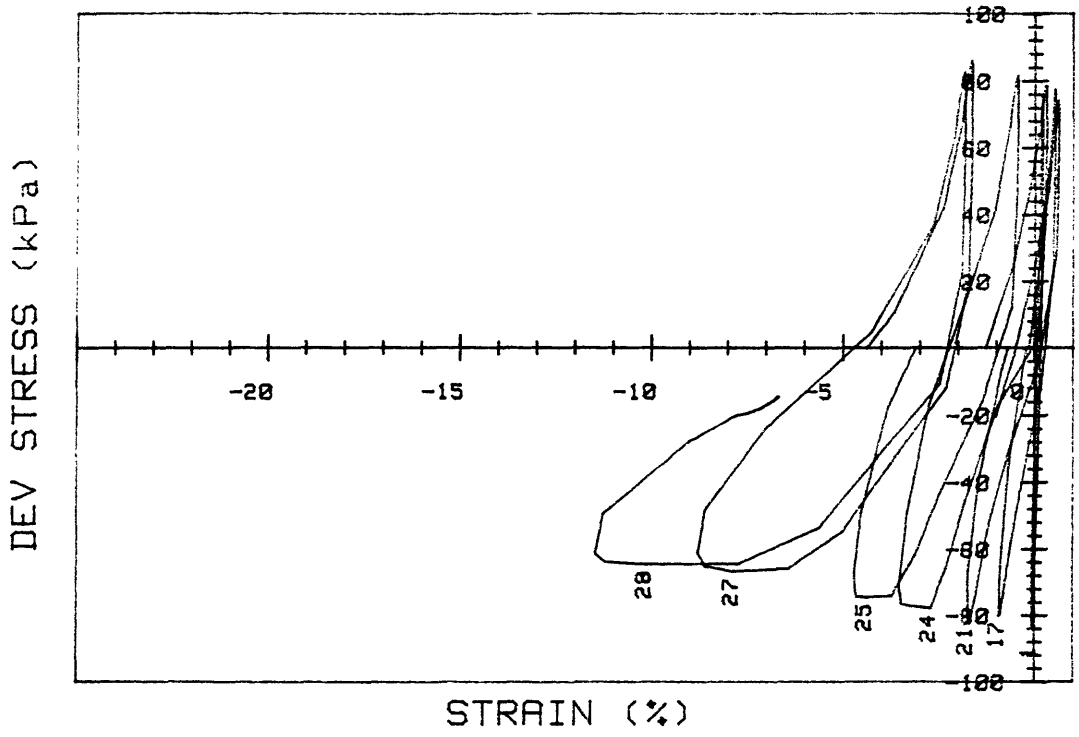

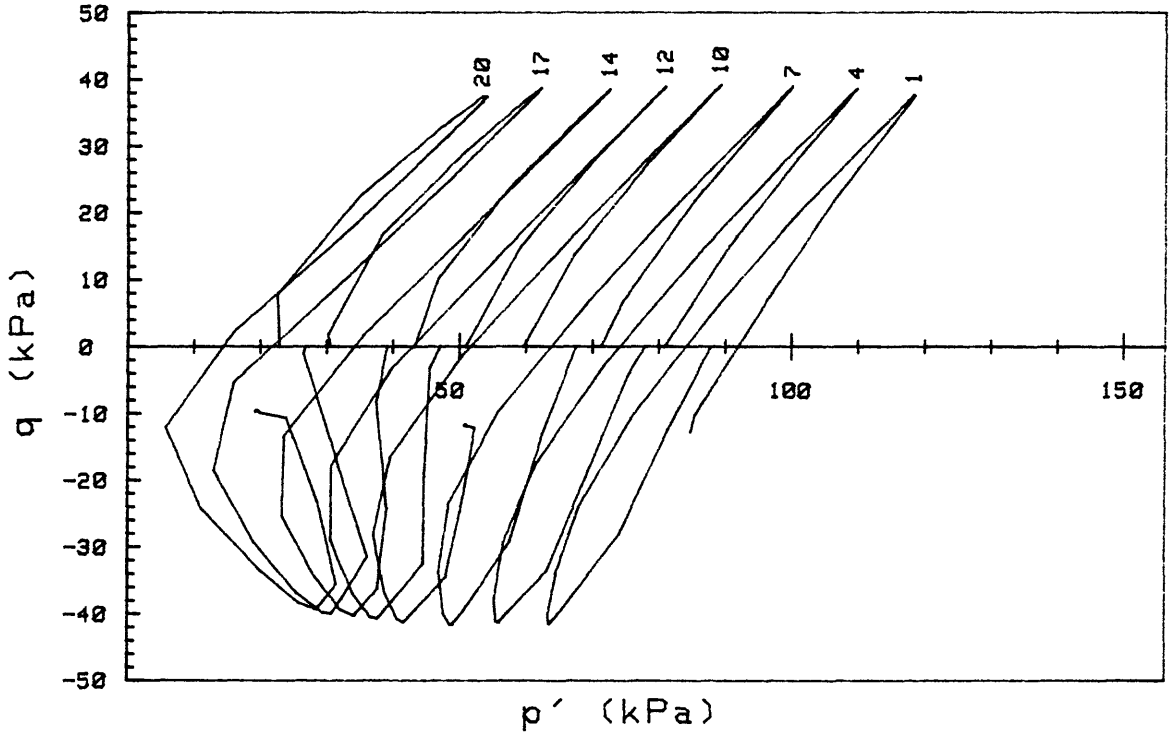

CRUISE ST HELENS		INCREMENT (cm)	REMOLDED-SURF
CORE NO.	CC2	TEST NO.	D138
SIG1c´(kPa)	97.6	STATIC qf (kPa)	100.0
SIG3c´(kPa)	97.6	AVG MAX q (kPa)	39.0 (39.0%)
INDUCED OCR	1.0	AVG MIN q (kPa)	-39.9 (39.9%)

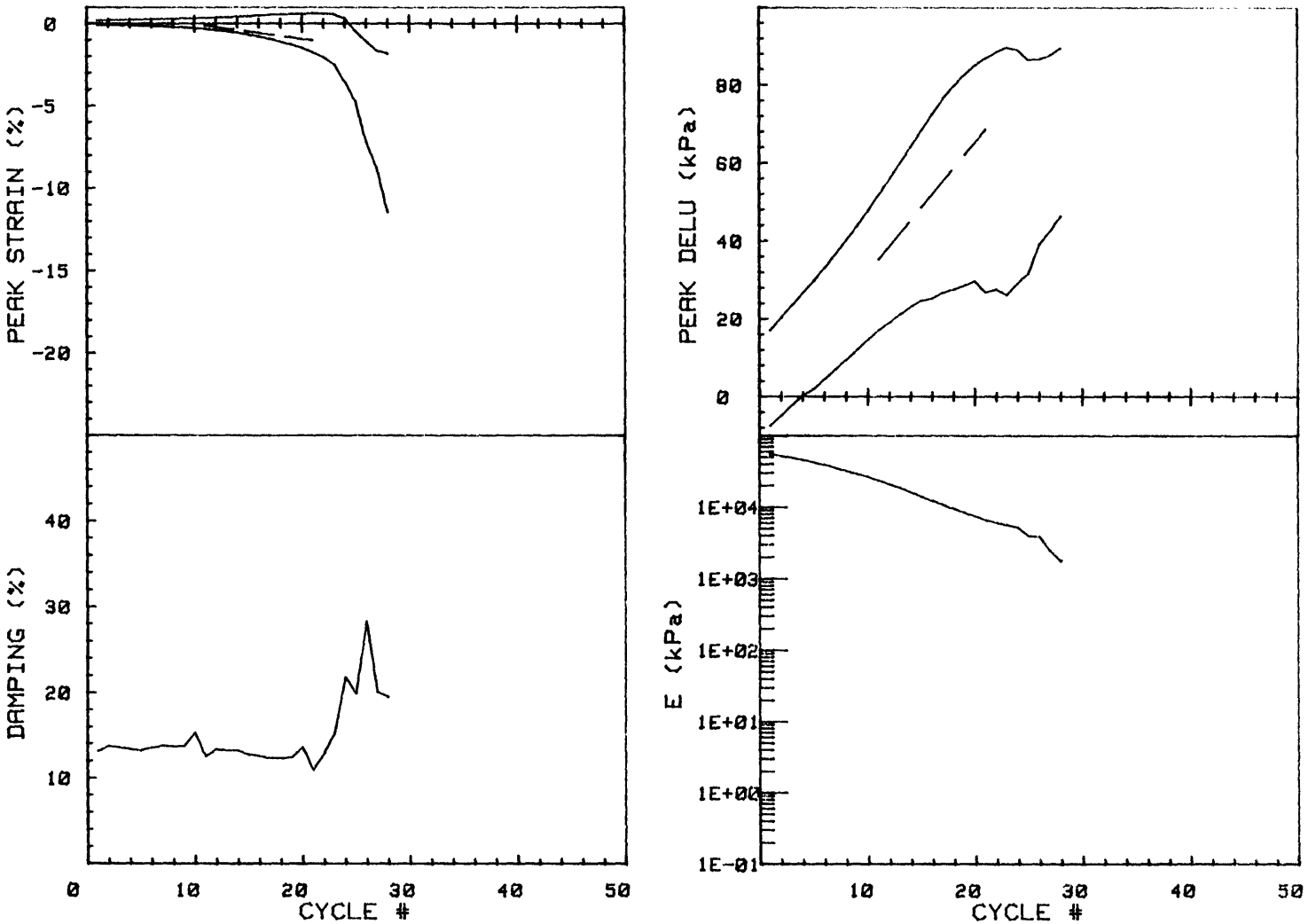

CRUISE ST HELENS		INCREMENT (cm)	REMOLDED-SURF
CORE NO.	CC2	TEST NO.	D138
SIG1c'(kPa)	97.6	STATIC qf (kPa)	100.0
SIG3c'(kPa)	97.6	AVG MAX q (kPa)	39.0 (39.0%)
INDUCED OCR	1.0	AVG MIN q (kPa)	-39.9 (39.9%)

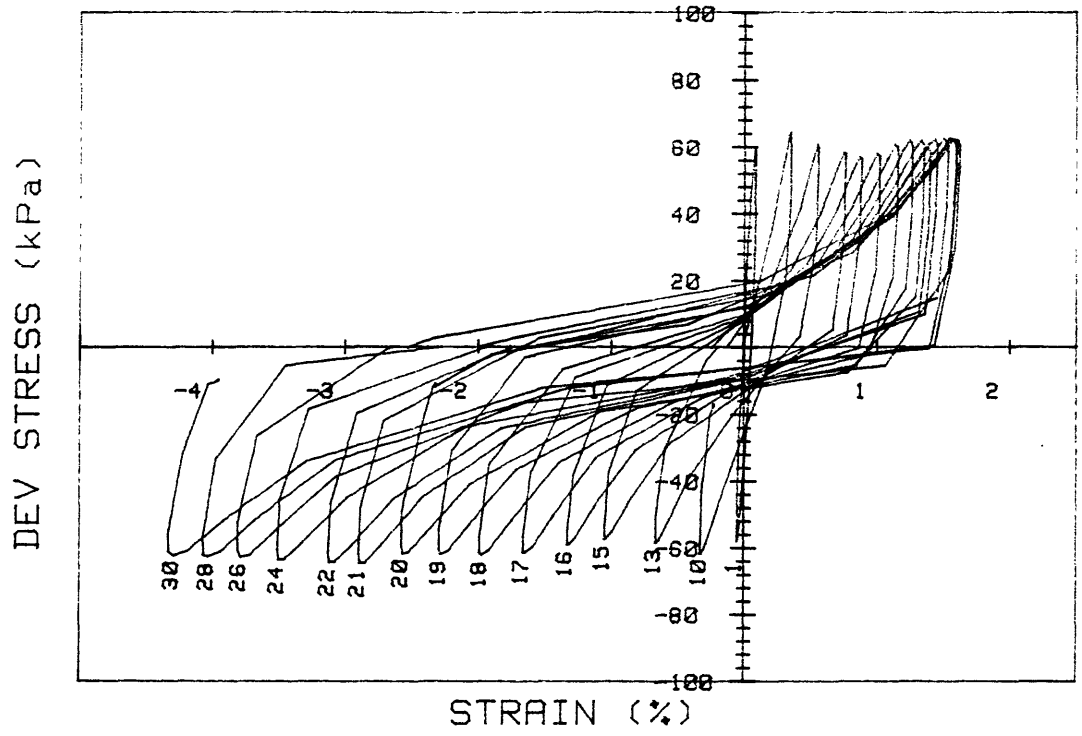

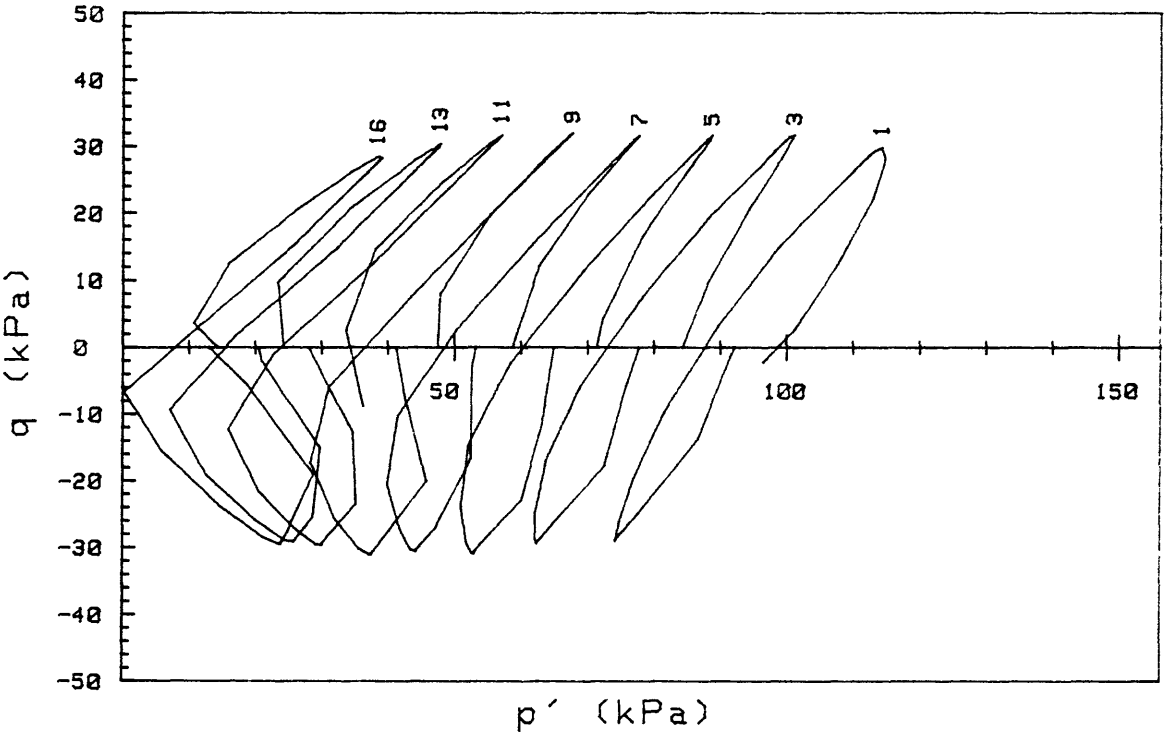

CRUISE ST HELENS		INCREMENT (cm)	REMOLDED-SURF
CORE NO. CC2		TEST NO.	D139
SIG1c'(kPa)	98.6	STATIC qf (kPa)	100.0
SIG3c'(kPa)	98.6	AVG MAX q (kPa)	30.9 (30.9%)
INDUCED OCR	1.0	AVG MIN q (kPa)	-30.6 (30.6%)

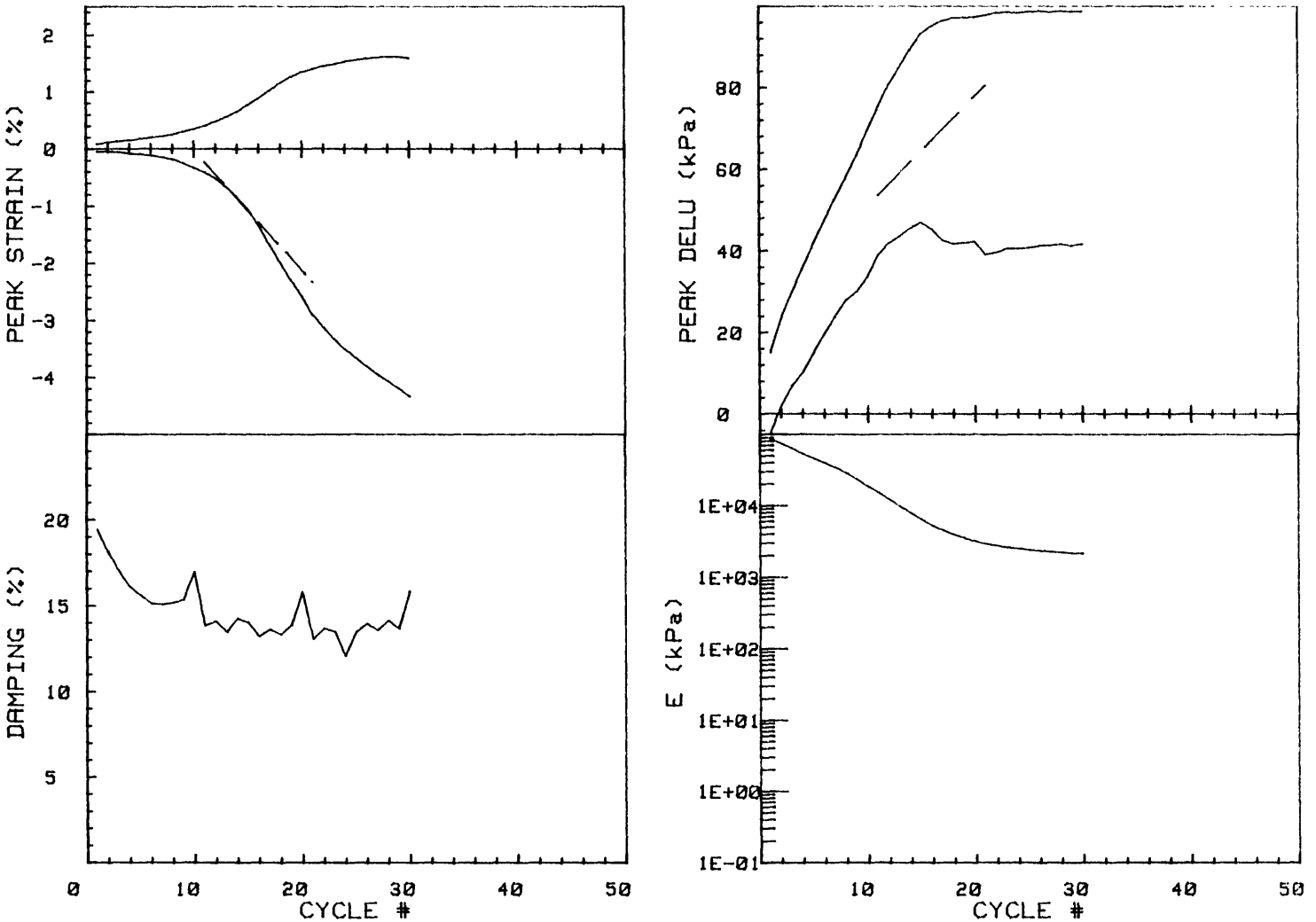

CRUISE ST HELENS		INCREMENT (cm)	REMOLDED-SURF
CORE NO. CC2		TEST NO.	D139
SIG1c'(kPa)	98.6	STATIC qf (kPa)	100.0
SIG3c'(kPa)	98.6	AVG MAX q (kPa)	30.9 (30.9%)
INDUCED OCR	1.0	AVG MIN q (kPa)	-30.6 (30.6%)

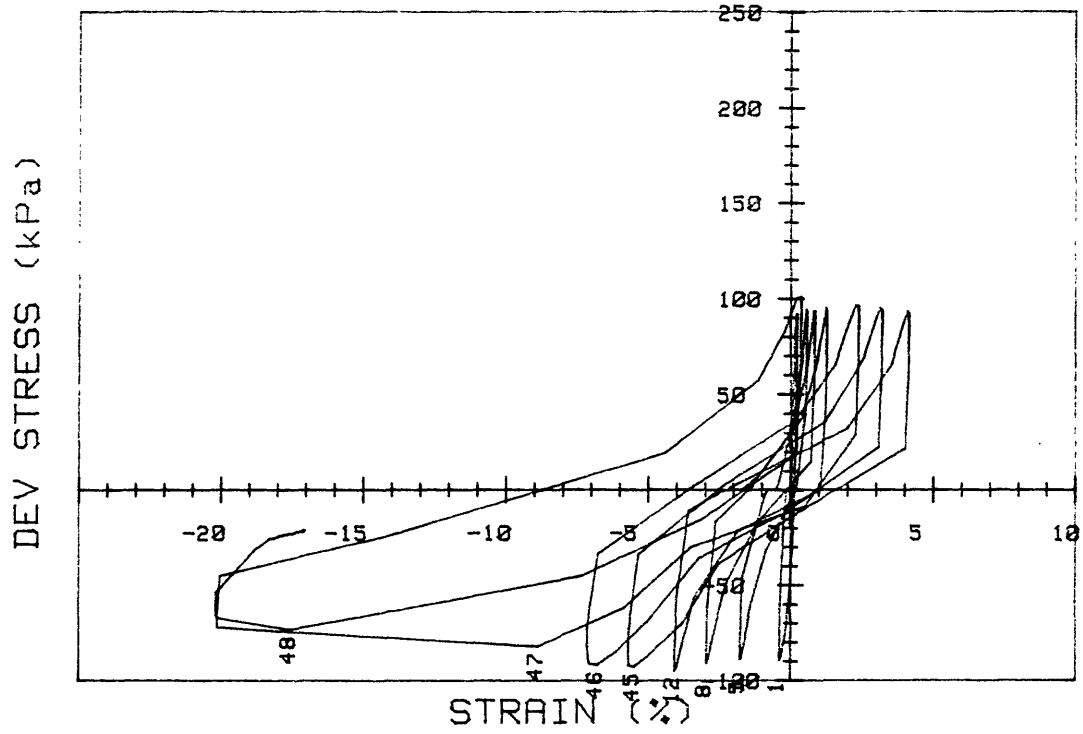

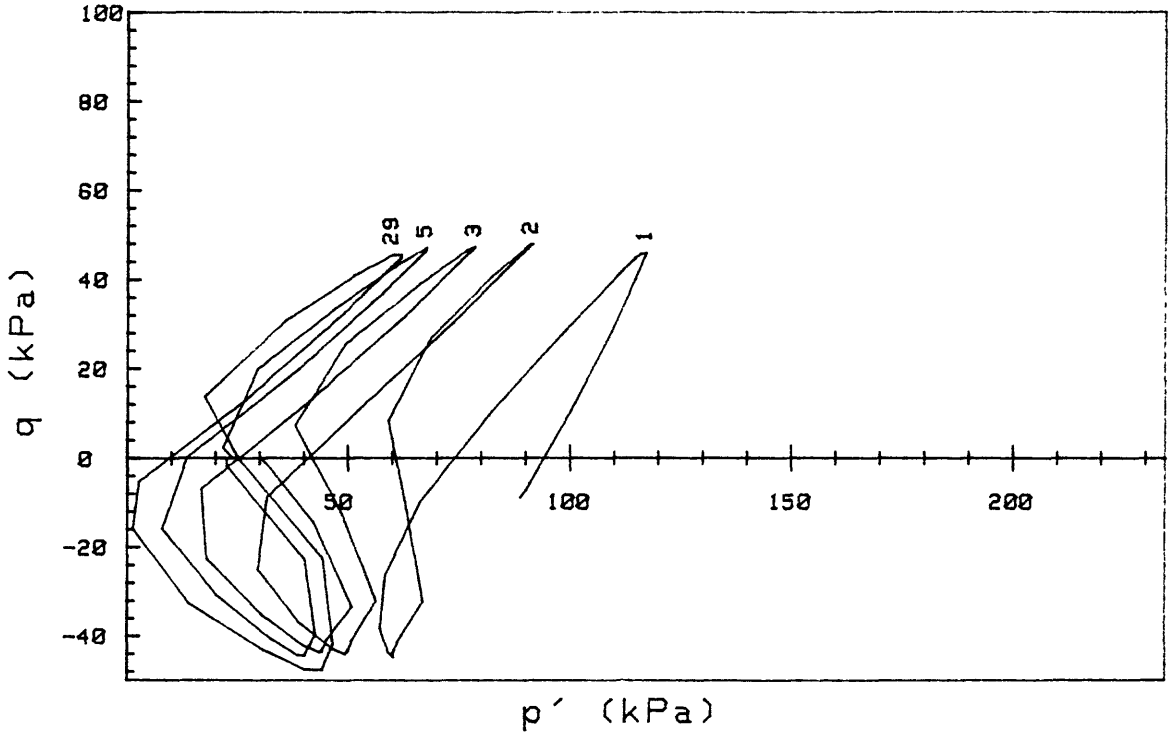

CRUISE ST HELENS		INCREMENT (cm)	REMOLDED-SURF
CORE NO.	CC2	TEST NO.	D140
SIG1c´(kPa)	97.7	STATIC qf (kPa)	100.0
SIG3c´(kPa)	97.7	AVG MAX q (kPa)	46.3 (46.3%)
INDUCED OCR	1.0	AVG MIN q (kPa)	-46.8 (46.8%)

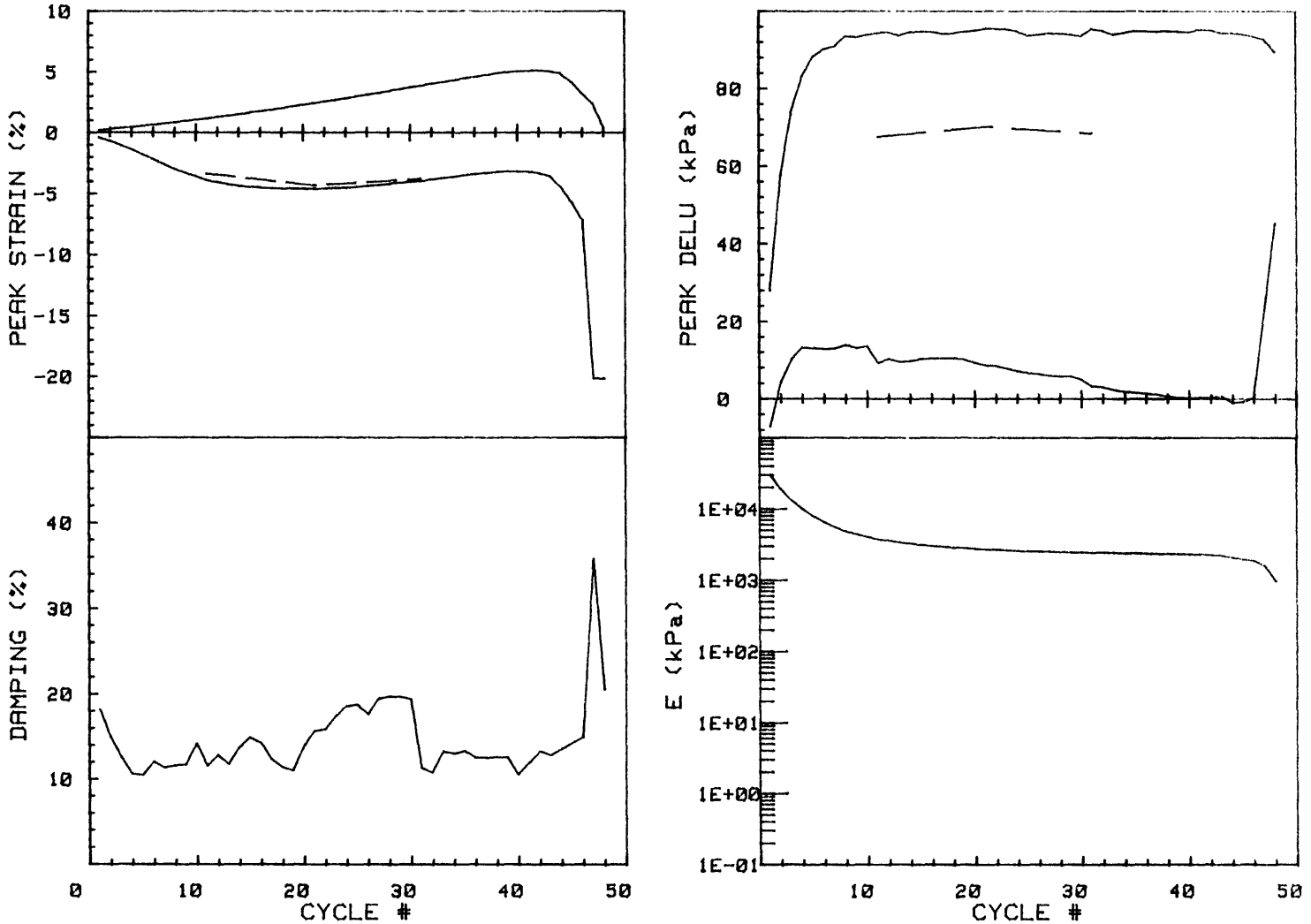

CRUISE ST HELENS		INCREMENT (cm)	REMOLDED-SURF
CORE NO.	CC2	TEST NO.	D140
SIG1c'(kPa)	97.7	STATIC qf (kPa)	100.0
SIG3c'(kPa)	97.7	AVG MAX q (kPa)	46.3 (46.3%)
INDUCED OCR	1.0	AVG MIN q (kPa)	-46.8 (46.8%)

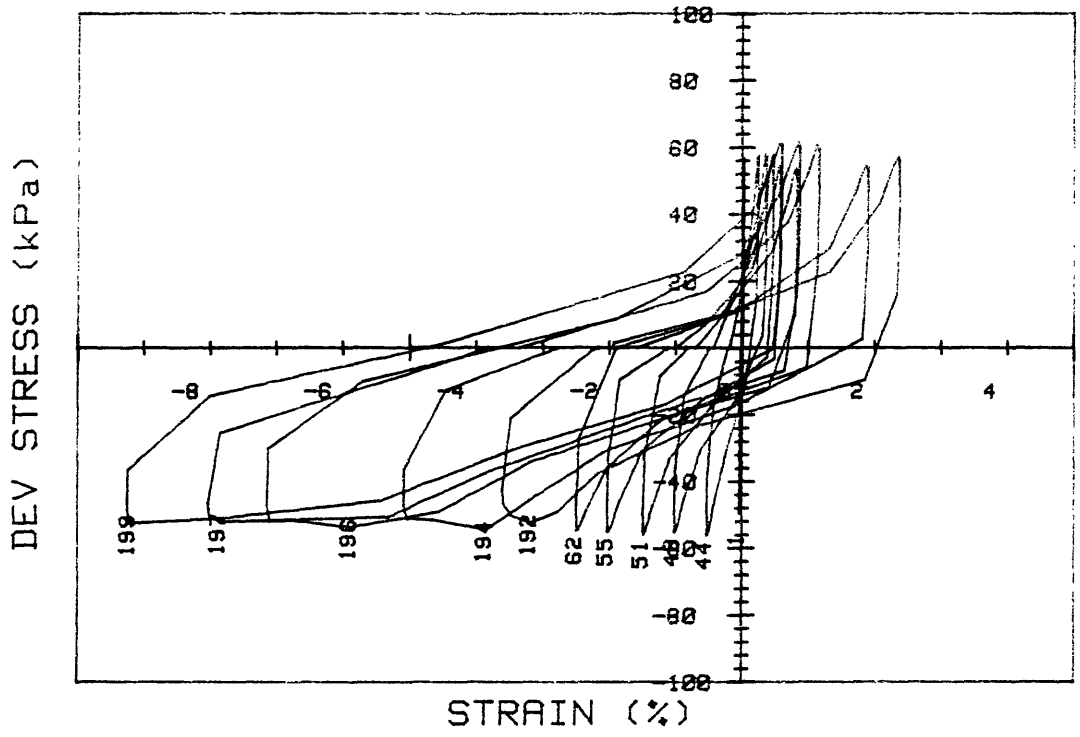

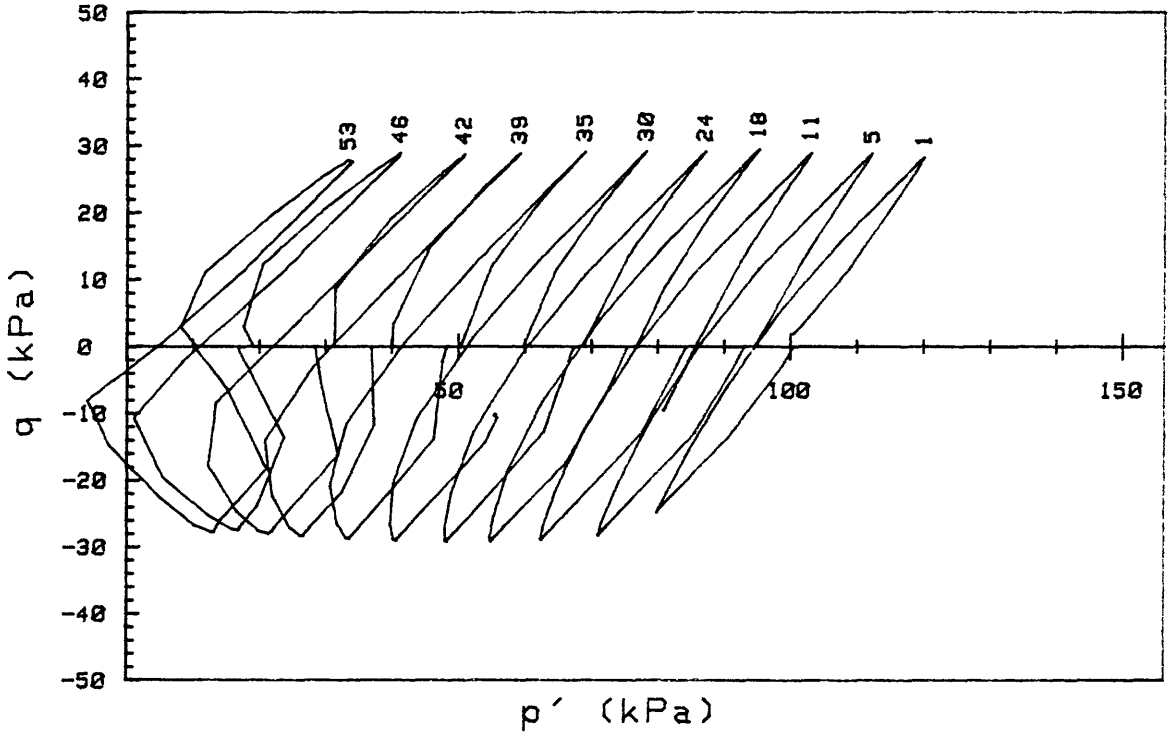

CRUISE ST HELENS		INCREMENT (cm)	REMOLDED-SURF
CORE NO. CC2		TEST NO.	D141
SIG1c´(kPa)	98.5	STATIC qf (kPa)	100.0
SIG3c´(kPa)	98.5	AVG MAX q (kPa)	28.3 (28.3%)
INDUCED OCR	1.0	AVG MIN q (kPa)	-28.9 (28.9%)

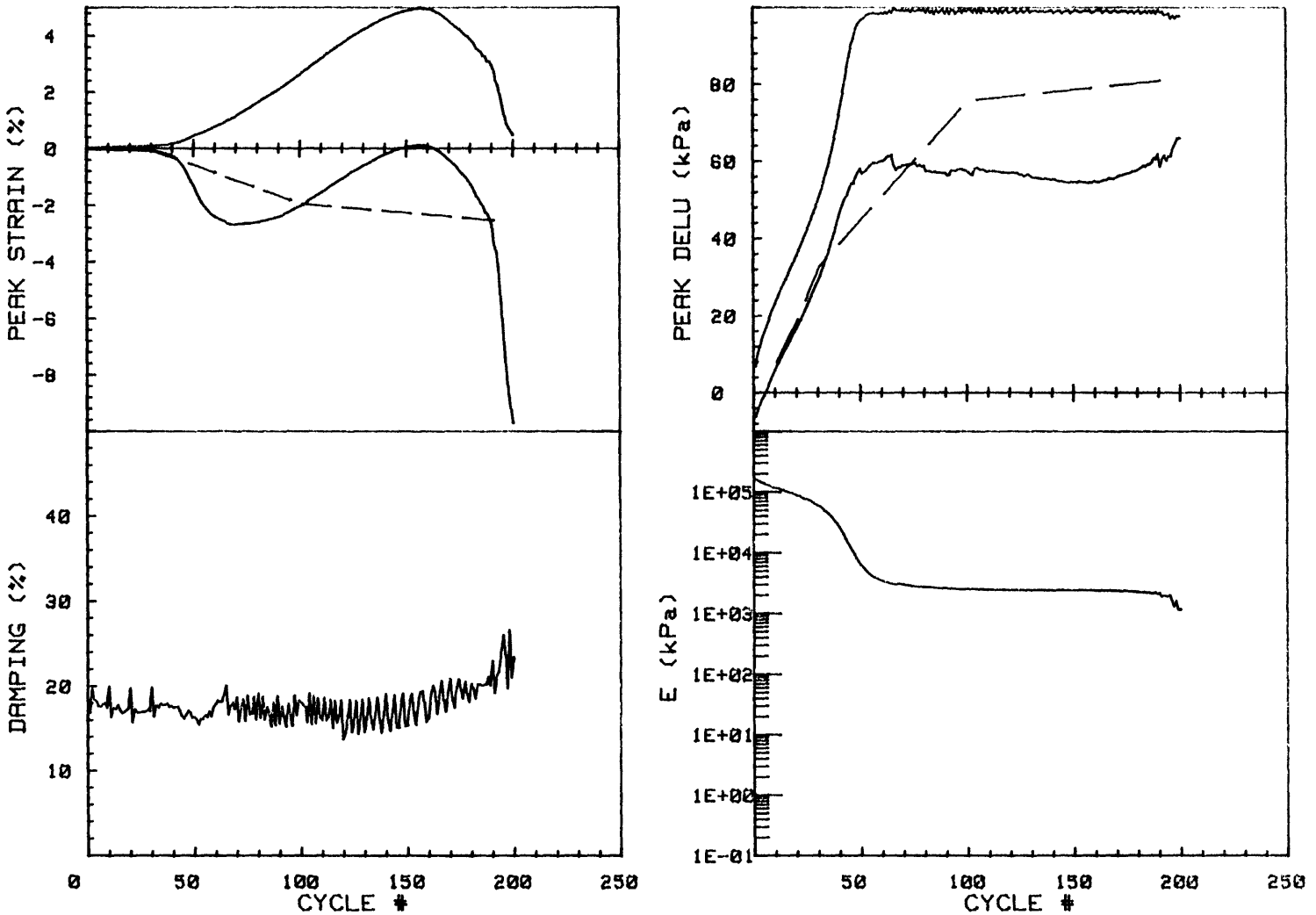

CRUISE ST HELENS		INCREMENT (cm)	REMOLDED-SURF
CORE NO.	CC2	TEST NO.	D141
SIG1c'(kPa)	98.5	STATIC qf (kPa)	100.0
SIG3c'(kPa)	98.5	AVG MAX q (kPa)	28.3 (28.3%)
INDUCED OCR	1.0	AVG MIN q (kPa)	-28.9 (28.9%)

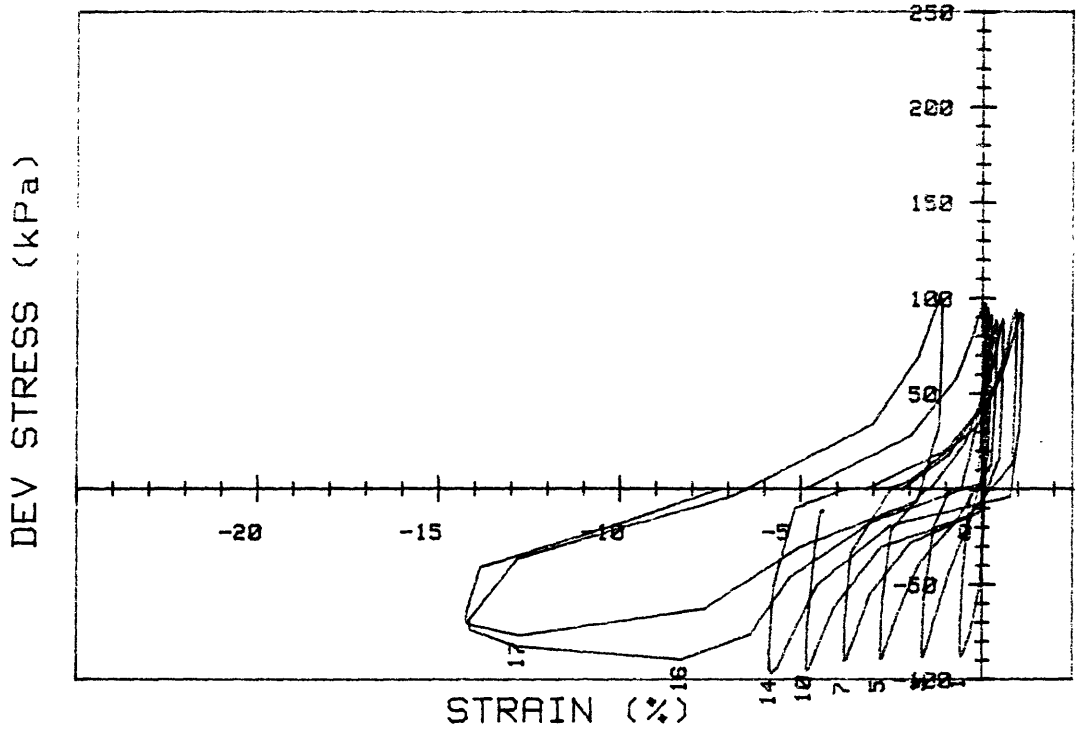

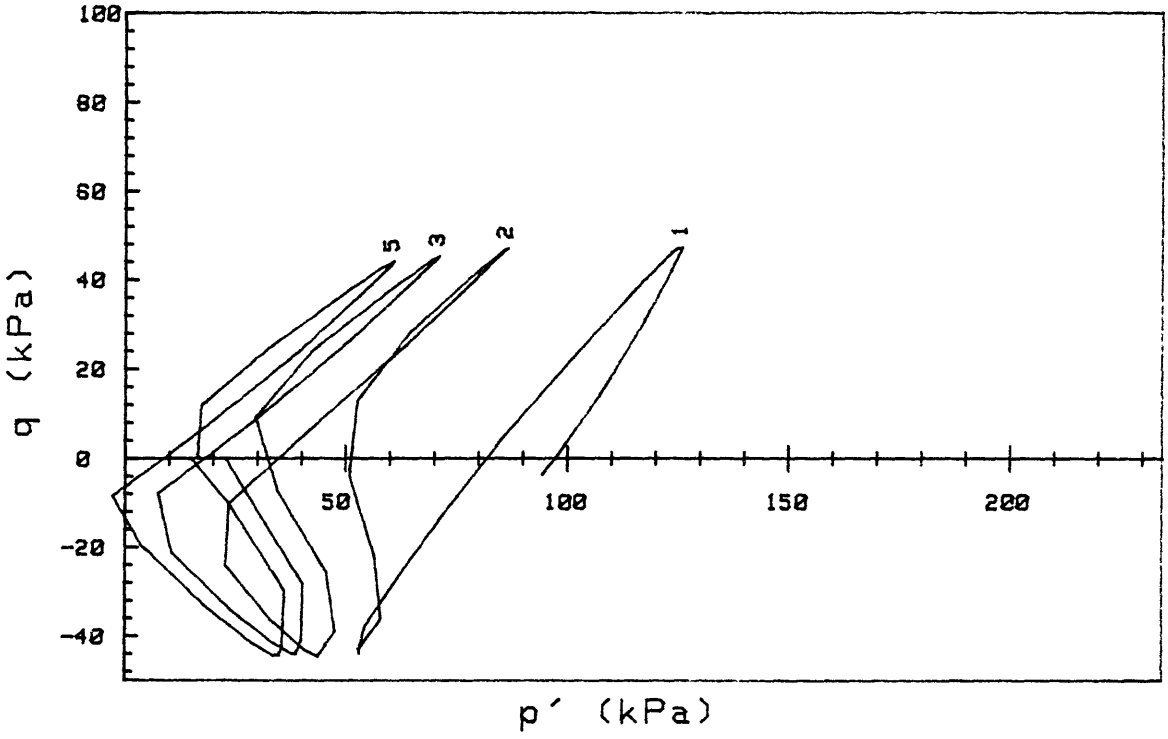

CRUISE ST HELENS		INCREMENT (cm)	REMOLDED-SURF
CORE NO. CC2		TEST NO.	D142
SIG1c´(kPa)	98.0	STATIC qf (kPa)	100.0
SIG3c´(kPa)	98.0	AVG MAX q (kPa)	46.6 (46.6%)
INDUCED OCR	1.0	AVG MIN q (kPa)	-44.5 (44.5%)

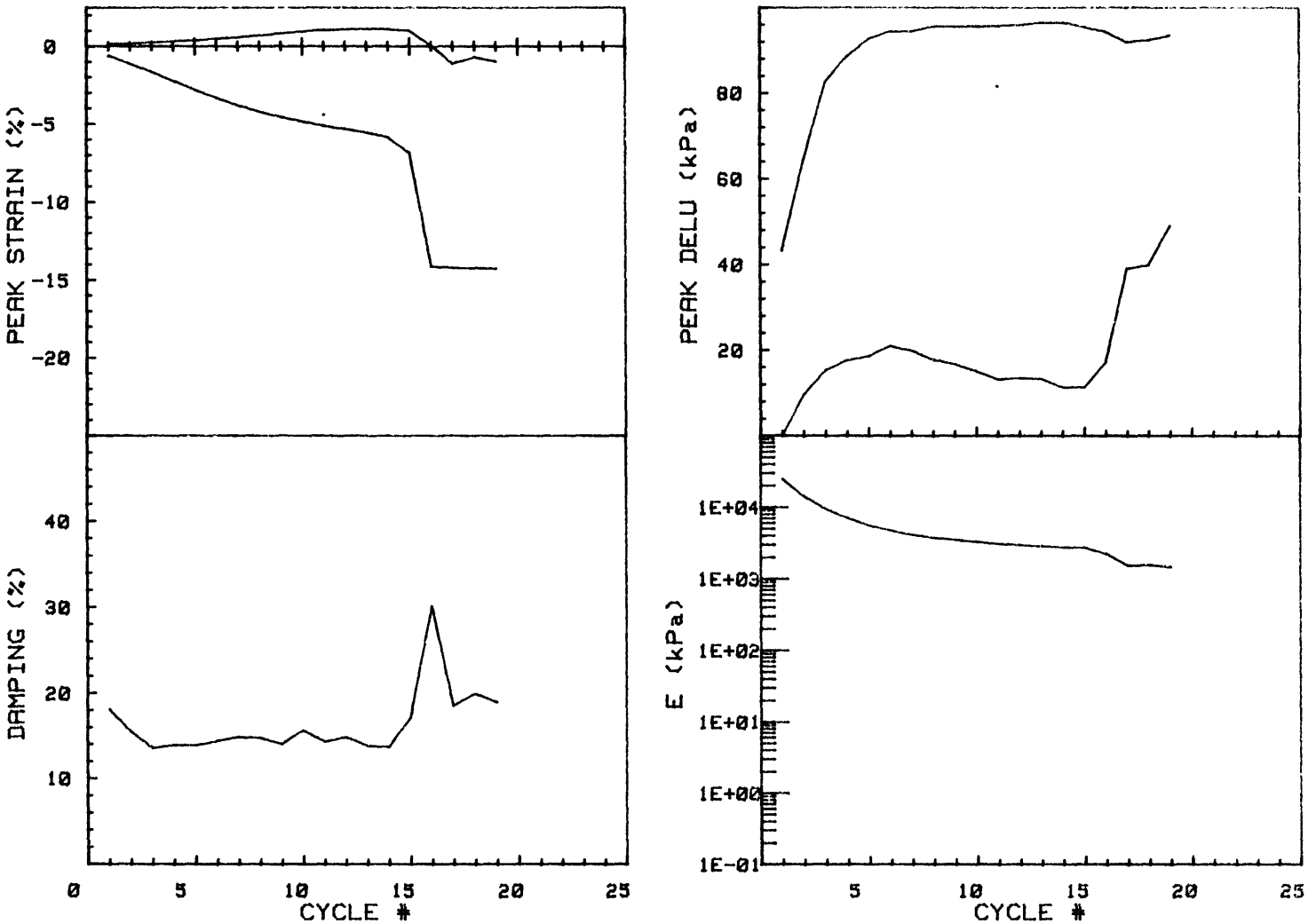

CRUISE ST HELENS		INCREMENT (cm)	REMOLDED-SURF
CORE NO.	CC2	TEST NO.	D142
SIG1c'(kPa)	98.0	STATIC qf (kPa)	100.0
SIG3c'(kPa)	98.0	AVG MAX q (kPa)	46.6 (46.6%)
INDUCED OCR	1.0	AVG MIN q (kPa)	-44.5 (44.5%)

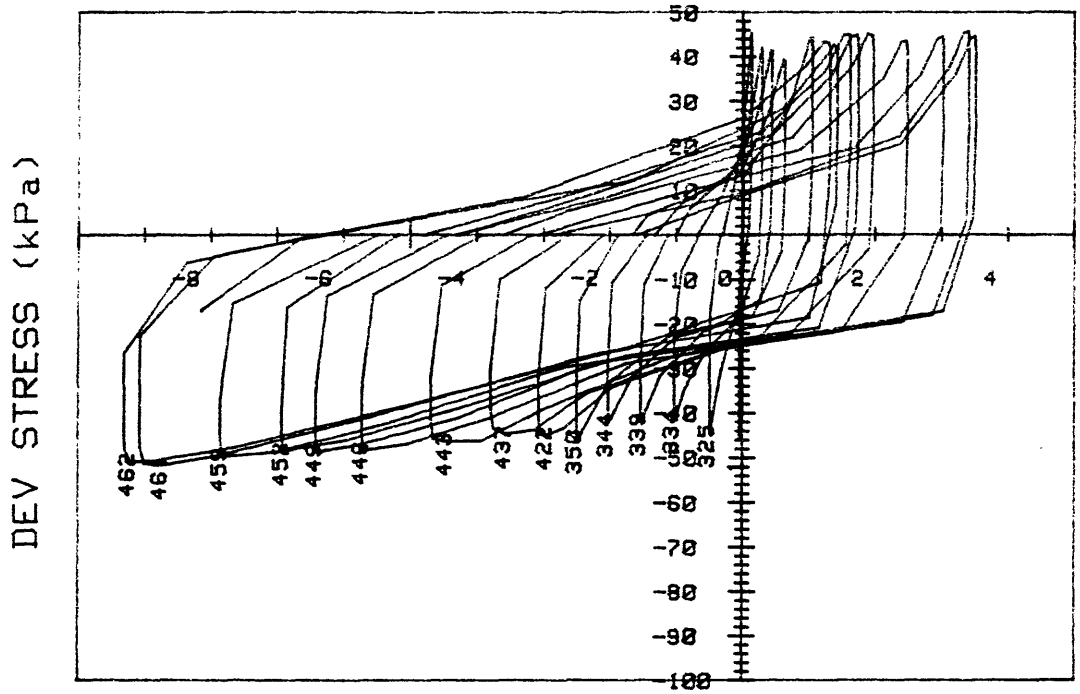

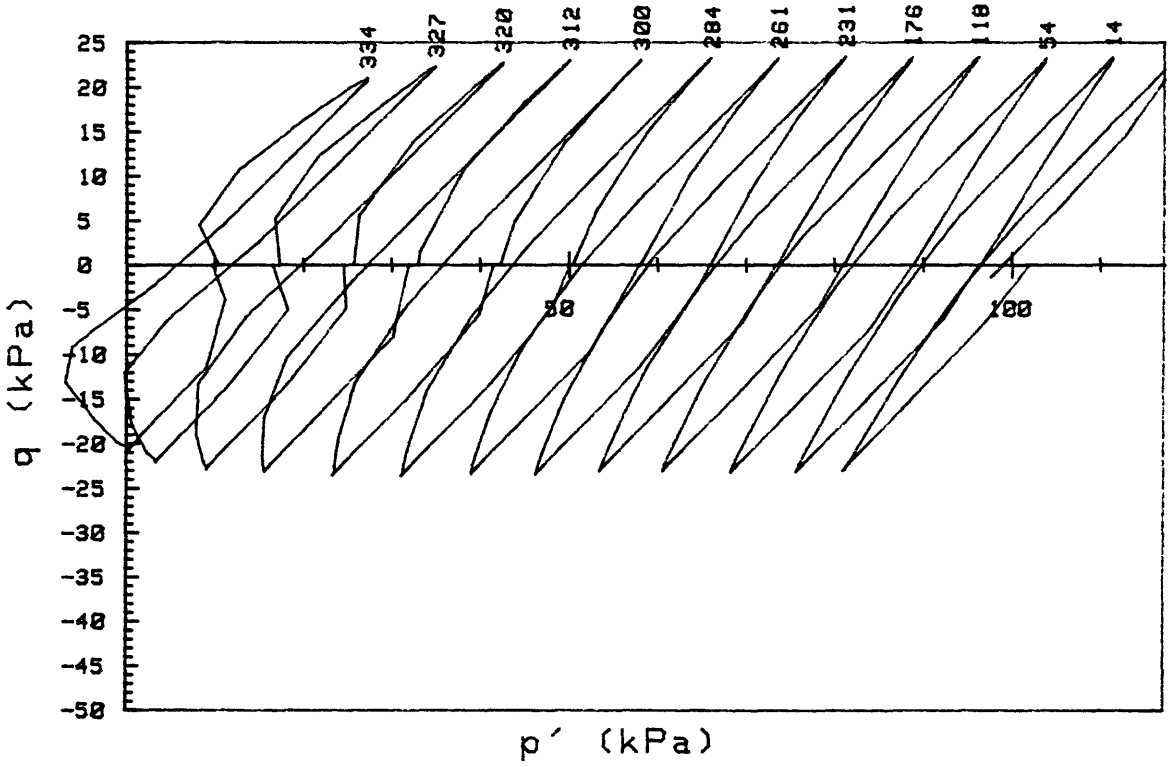

CRUISE ST HELENS		INCREMENT (cm)	REMOLDED-SURF
CORE NO.	CC2	TEST NO.	D143
SIG1c'(kPa)	99.0	STATIC qf (kPa)	100.0
SIG3c'(kPa)	99.0	AVG MAX q (kPa)	22.8 (22.8%)
INDUCED OCR	1.0	AVG MIN q (kPa)	-23.2 (23.2%)

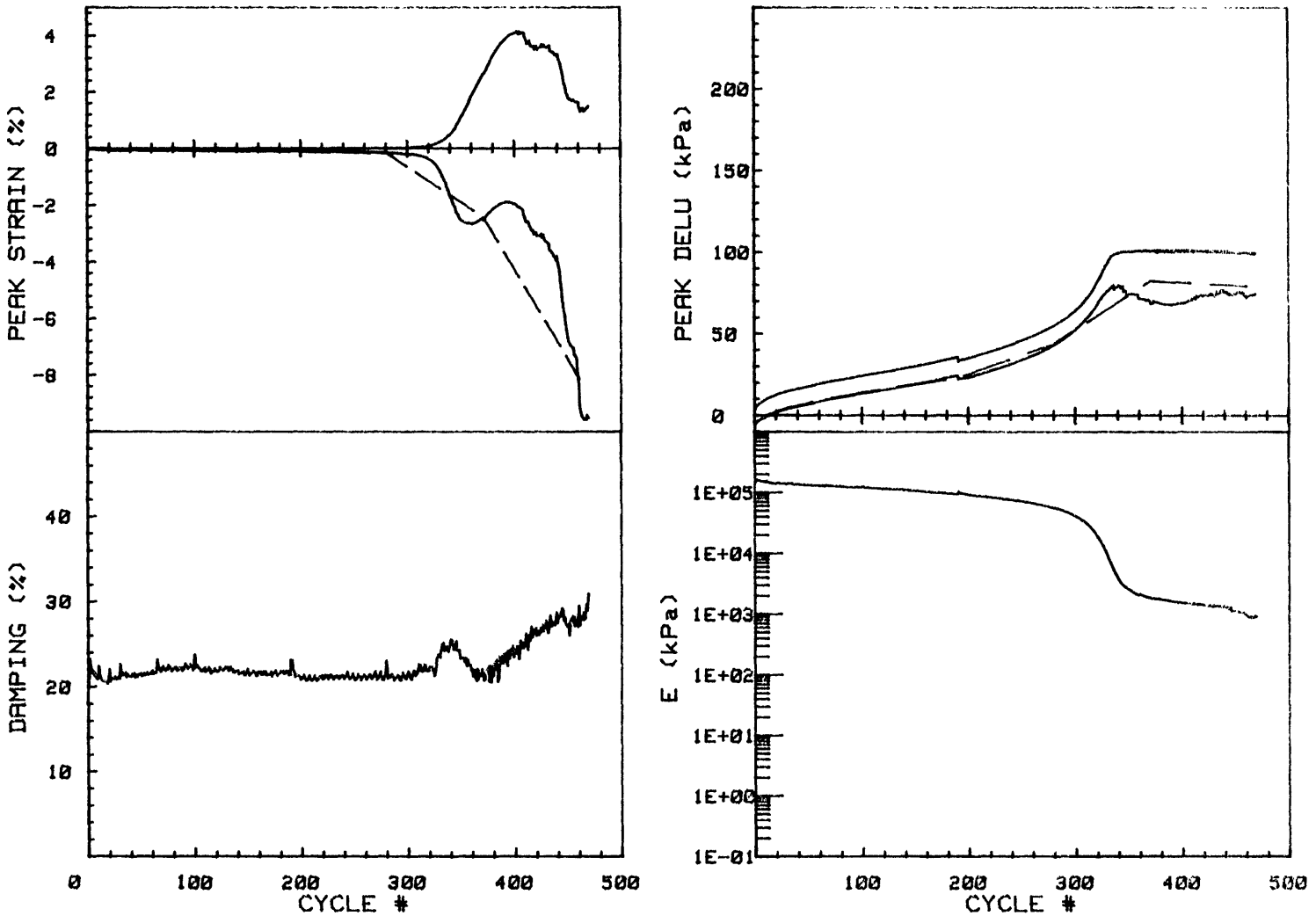

CRUISE ST HELENS		INCREMENT (cm)	REMOLDED-SURF
CORE NO.	CC2	TEST NO.	D143
SIG1c'(kPa)	99.0	STATIC qf (kPa)	100.0
SIG3c'(kPa)	99.0	AVG MAX q (kPa)	22.8 (22.8%)
INDUCED OCR	1.0	AVG MIN q (kPa)	-23.2 (23.2%)

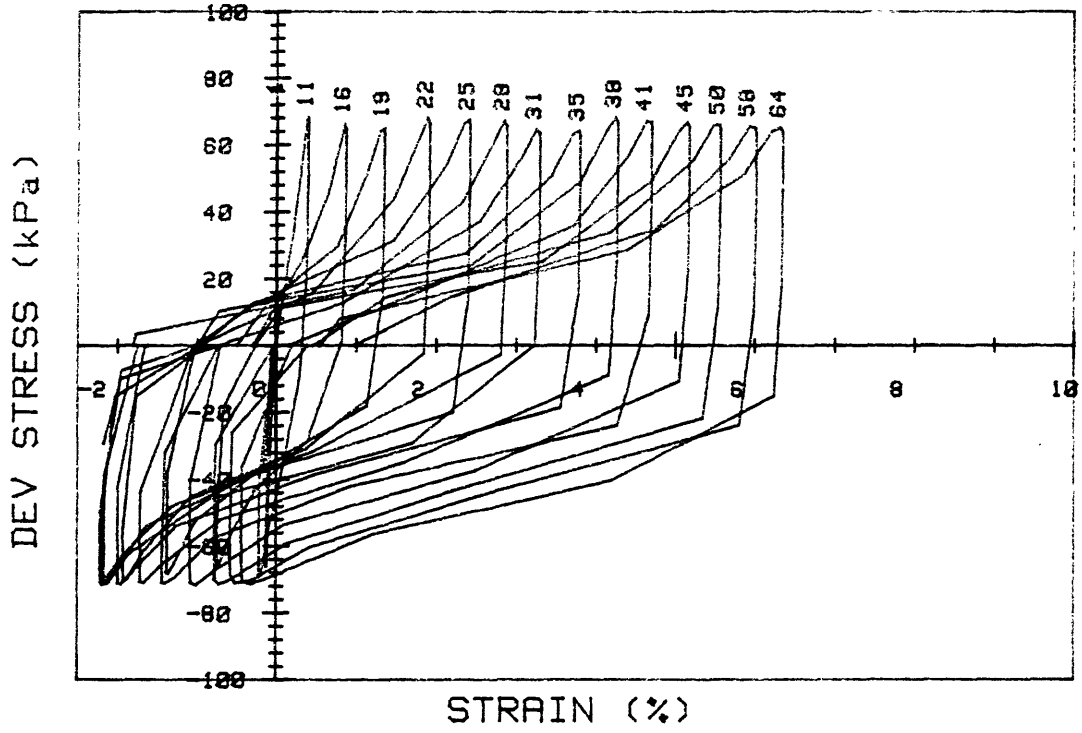

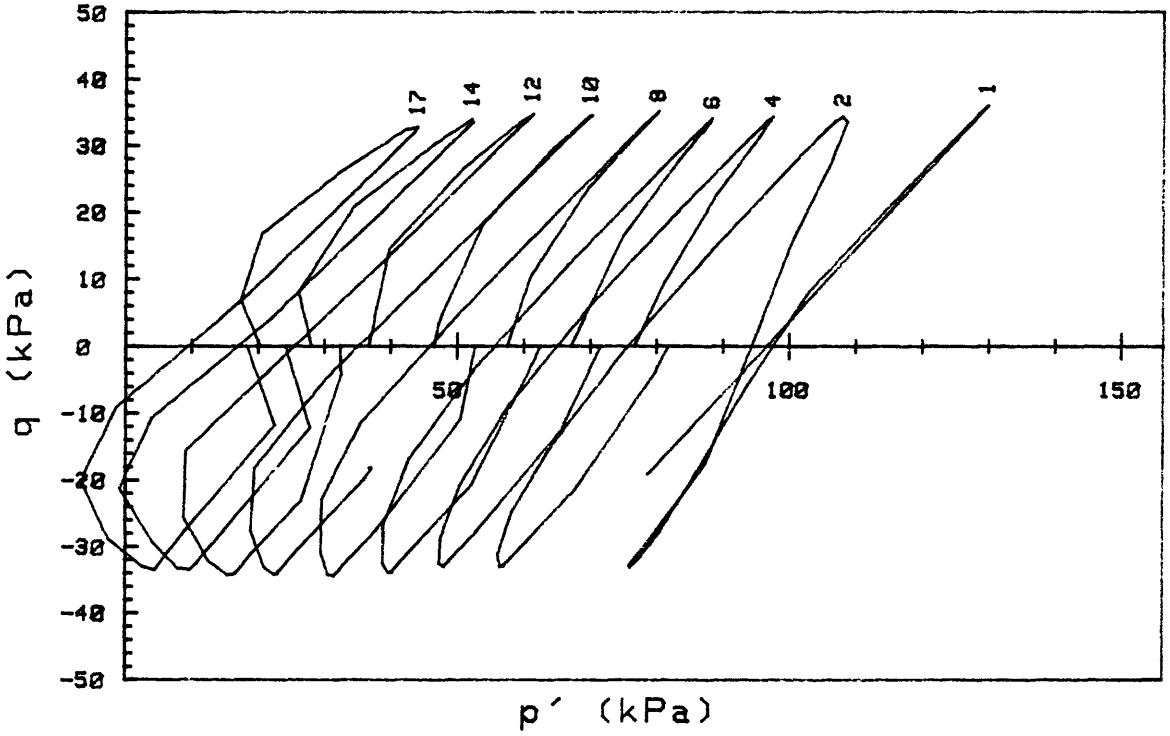

CRUISE ST HELENS		INCREMENT (cm)	REMOLDED-SURF
CORE NO.	CC2	TEST NO.	D144
SIG1c´(kPa)	97.9	STATIC qf (kPa)	100.0
SIG3c´(kPa)	97.9	AVG MAX q (kPa)	32.9 (32.9%)
INDUCED OCR	1.0	AVG MIN q (kPa)	-34.5 (34.5%)

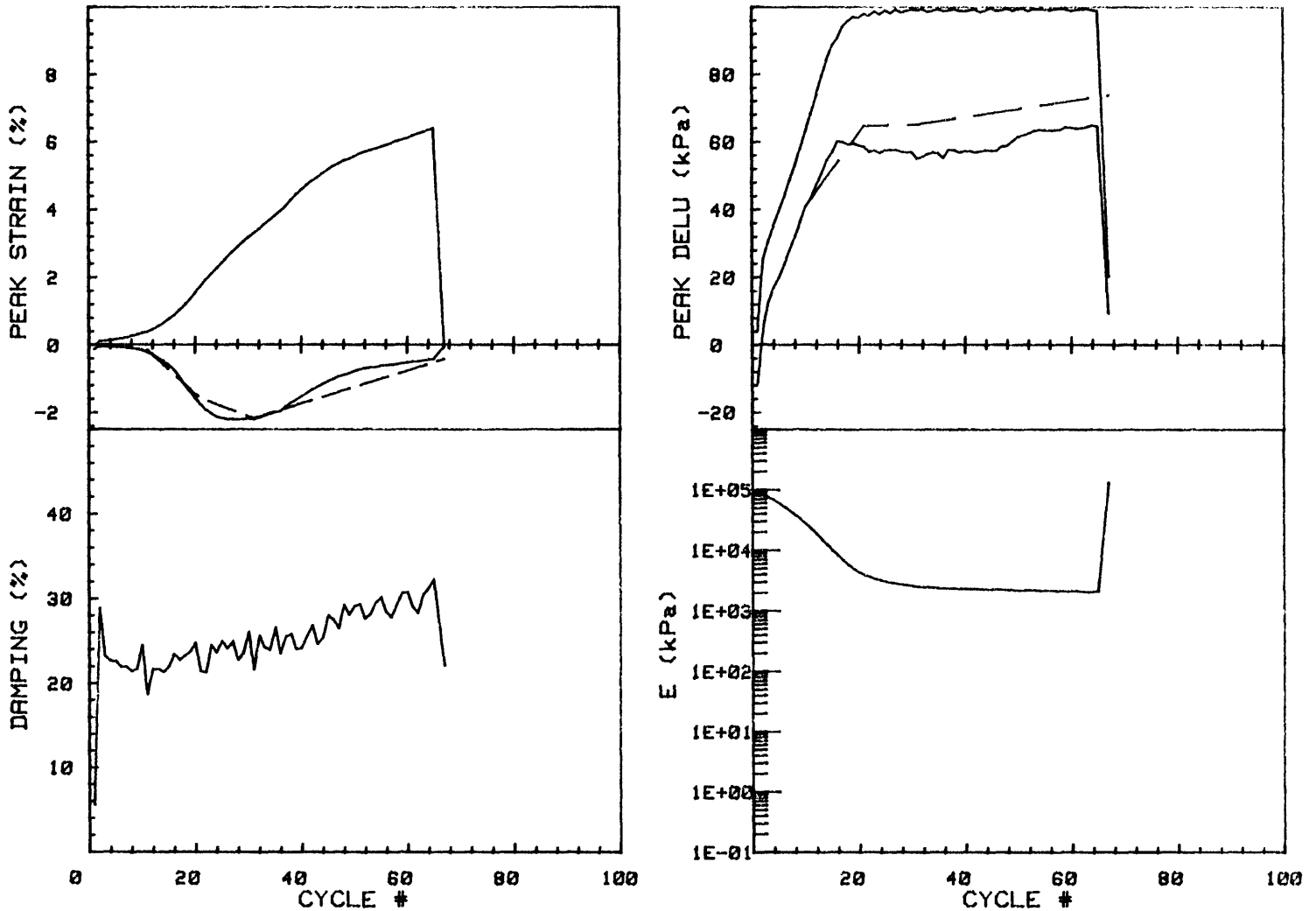

CRUISE ST HELENS		INCREMENT (cm)	REMOLDED-SURF
CORE NO. CC2		TEST NO.	D144
SIG1c'(kPa)	97.9	STATIC qf (kPa)	100.0
SIG3c'(kPa)	97.9	AVG MAX q (kPa)	32.9 (32.9%)
INDUCED OCR	1.0	AVG MIN q (kPa)	-34.5 (34.5%)

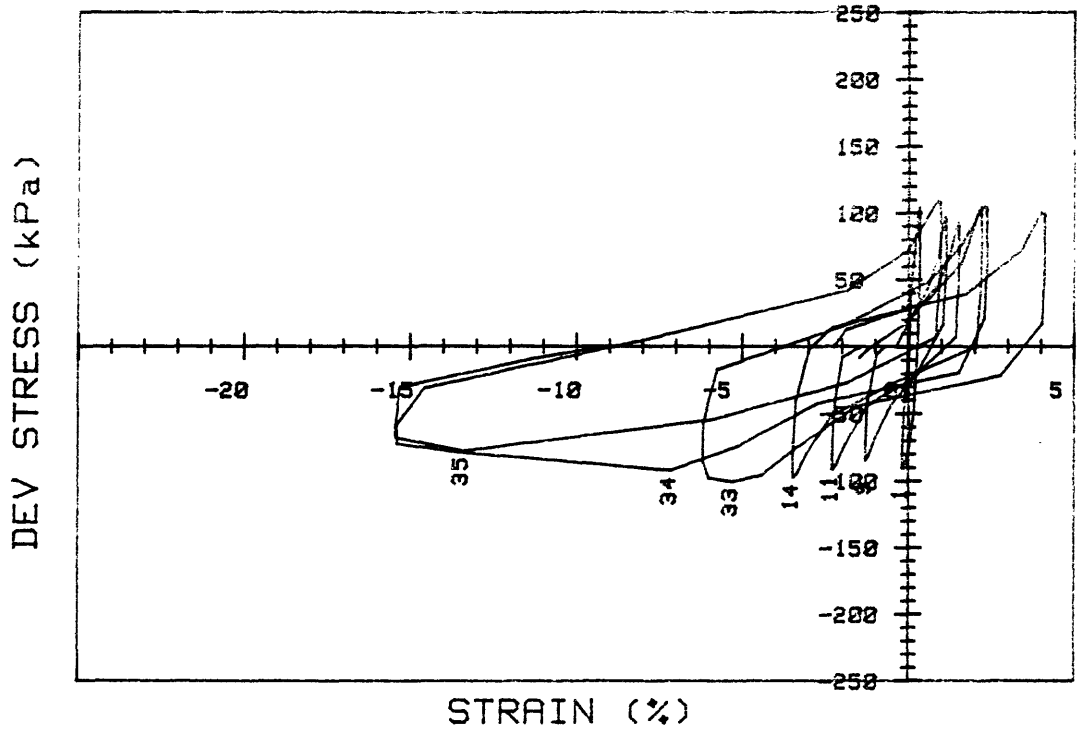

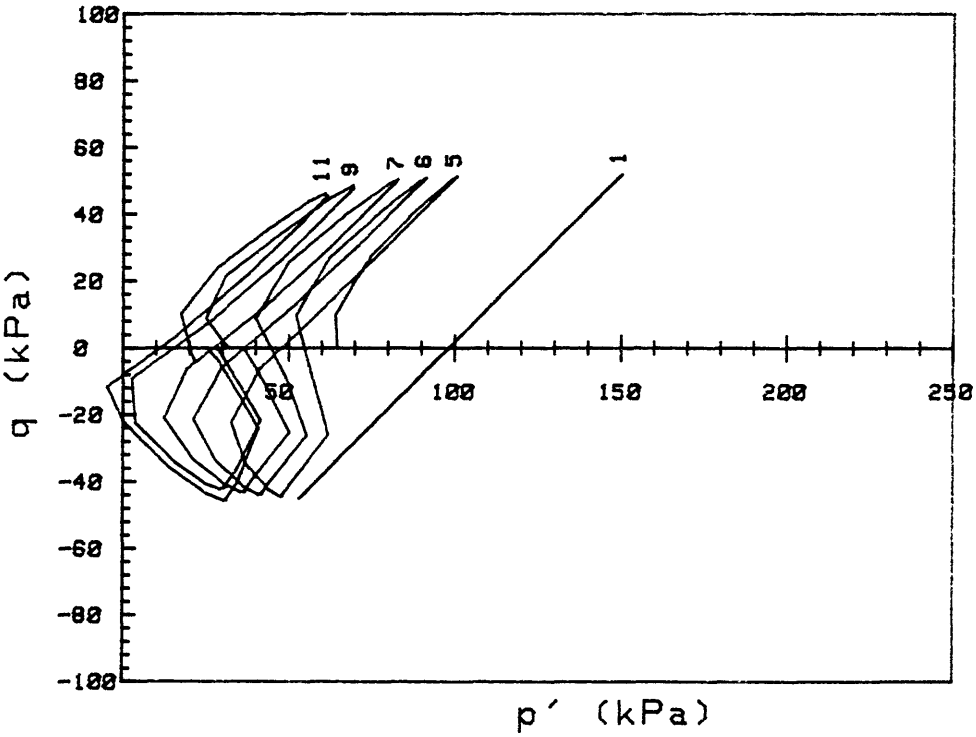

CRUISE ST HELENS		INCREMENT (cm)	REMOLDED-SURF
CORE NO. CC2		TEST NO.	D145
SIG1c'(kPa)	98.1	STATIC qf (kPa)	100.0
SIG3c'(kPa)	98.1	AVG MAX q (kPa)	50.4 (50.4%)
INDUCED OCR	1.0	AVG MIN q (kPa)	-48.3 (48.3%)

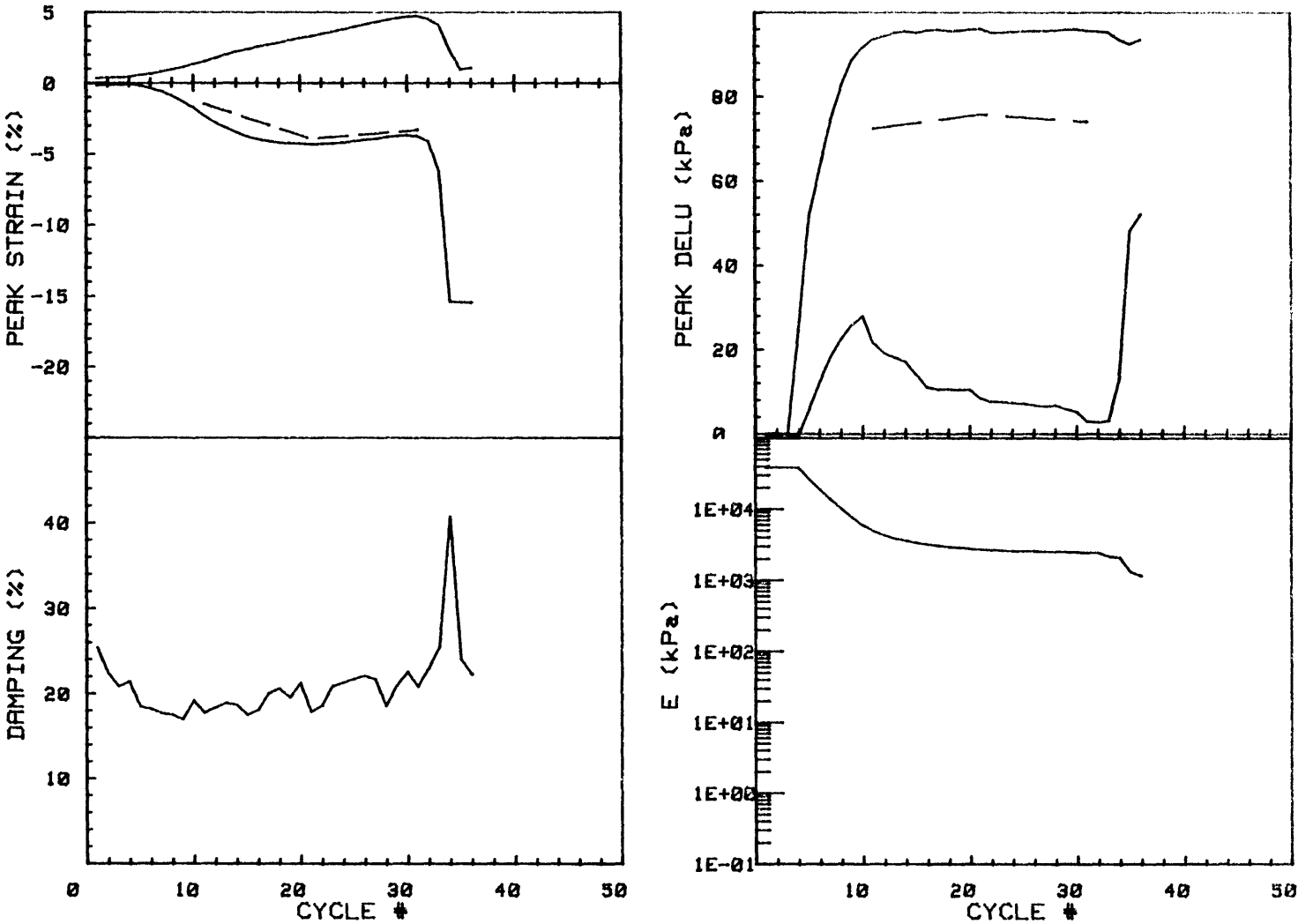

CRUISE ST HELENS		INCREMENT (cm)	REMOLDED-SURF
CORE NO. CC2		TEST NO.	D145
SIG1c'(kPa)	98.1	STATIC qf (kPa)	100.0
SIG3c'(kPa)	98.1	AVG MAX q (kPa)	50.4 (50.4%)
INDUCED OCR	1.0	AVG MIN q (kPa)	-48.3 (48.3%)

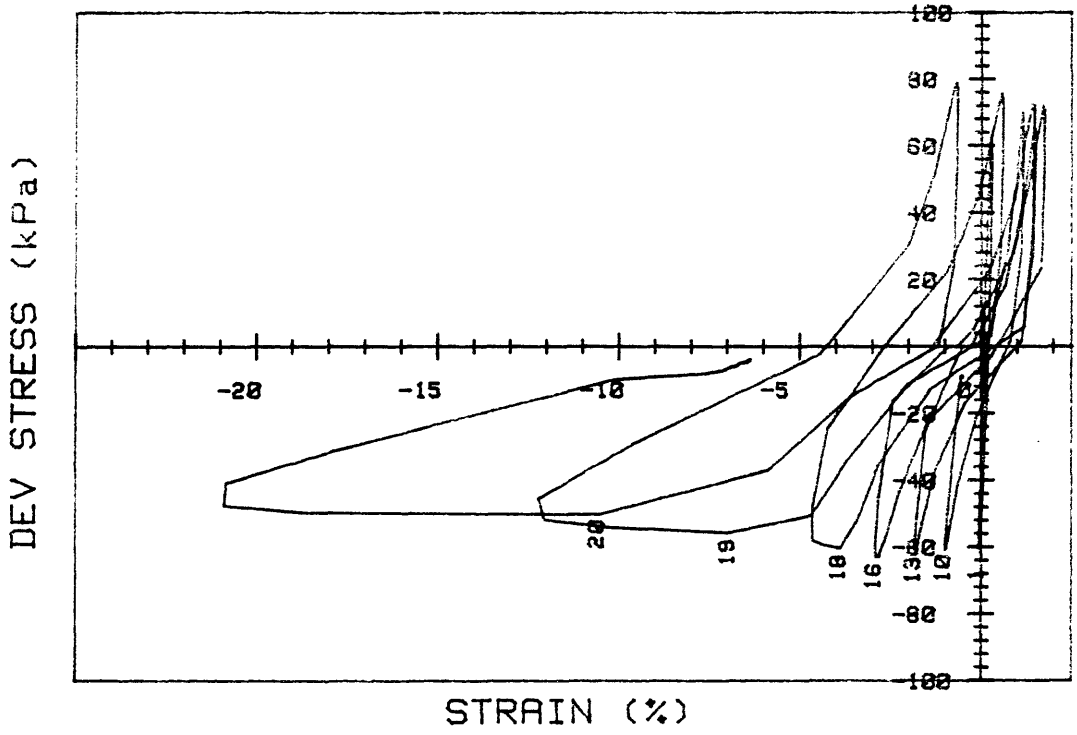

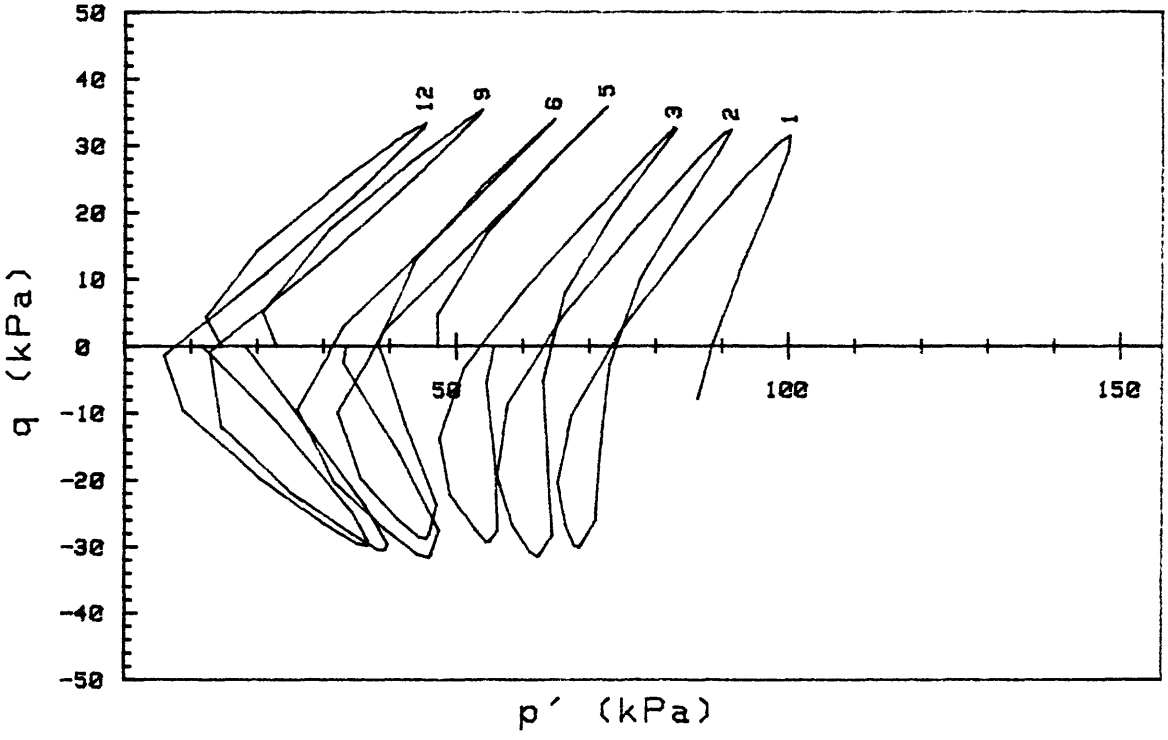

CRUISE ST HELENS		INCREMENT (cm)	REMOLDED-SURF
CORE NO.	CC2	TEST NO.	D161
SIG1c´(kPa)	94.3	STATIC qf (kPa)	100.0
SIG3c´(kPa)	94.3	AVG MAX q (kPa)	34.8 (34.8%)
INDUCED OCR	1.0	AVG MIN q (kPa)	-30.1 (30.1%)

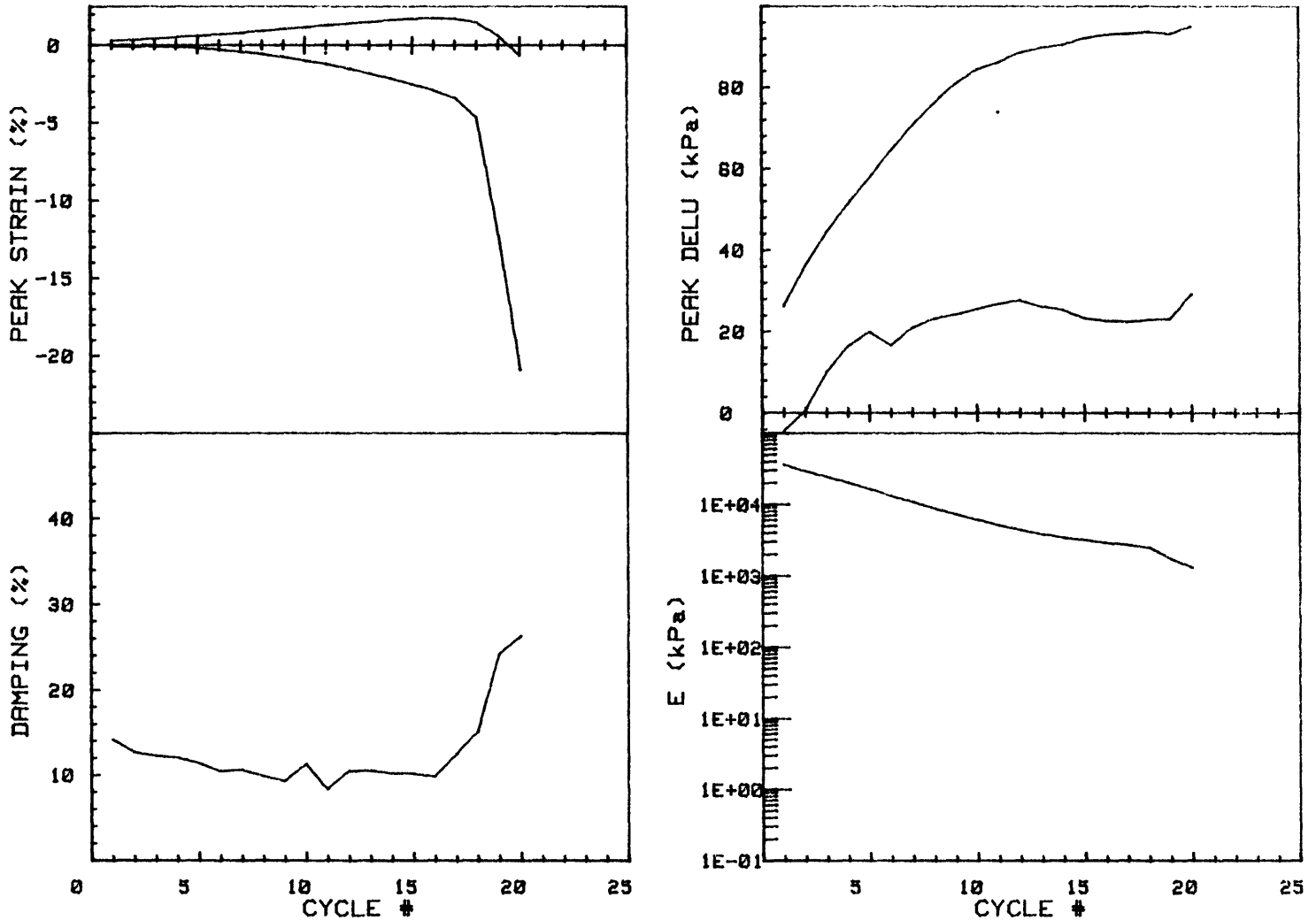

CRUISE ST HELENS		INCREMENT (cm)	REMOLDED-SURF
CORE NO.	CC2	TEST NO.	D161
SIG1c'(kPa)	94.3	STATIC qf (kPa)	100.0
SIG3c'(kPa)	94.3	AVG MAX q (kPa)	34.8 (34.8%)
INDUCED OCR	1.0	AVG MIN q (kPa)	-30.1 (30.1%)

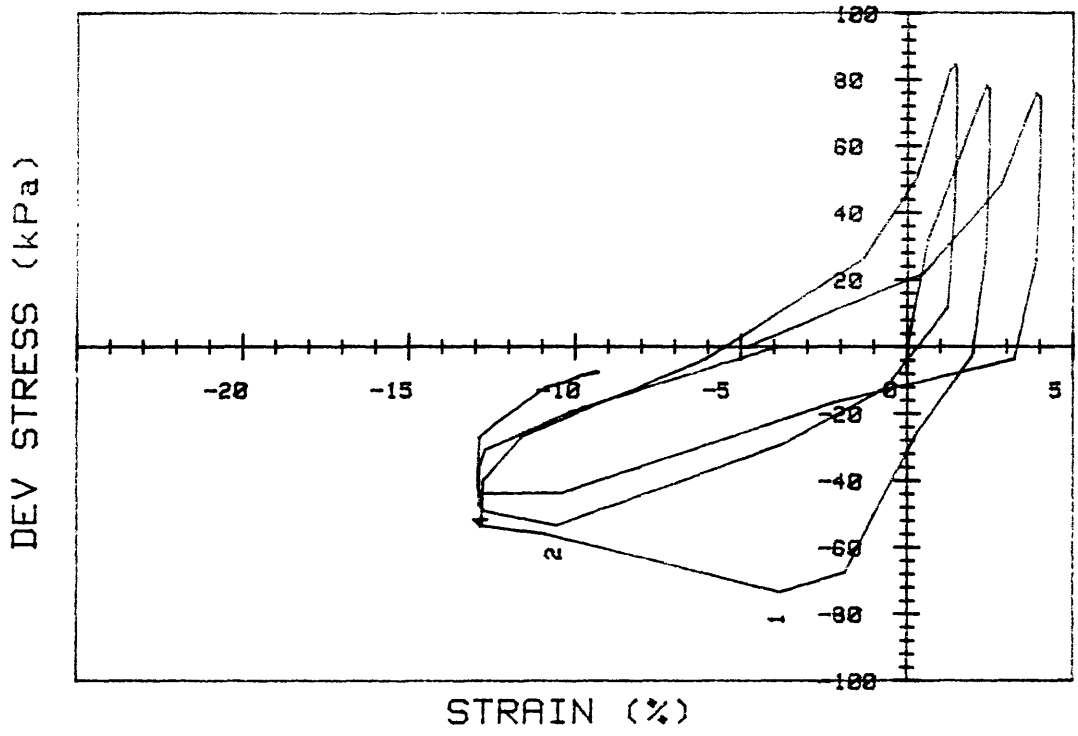

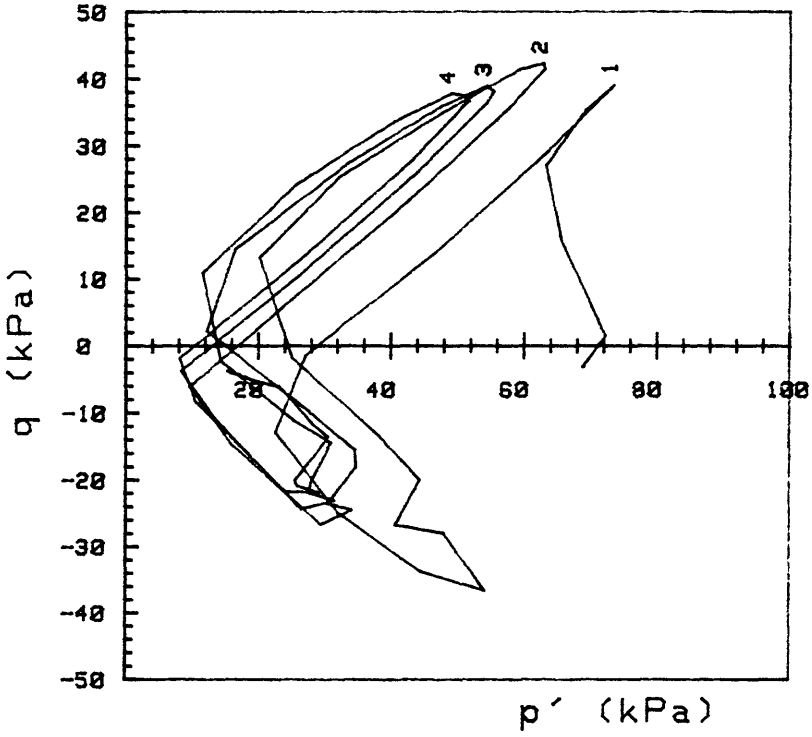

CRUISE ST HELENS		INCREMENT (cm)	REMOLDED-SURF
CORE NO.	CC2	TEST NO.	D162
SIG1c´(kPa)	72.1	STATIC qf (kPa)	100.0
SIG3c´(kPa)	72.1	AVG MAX q (kPa)	39.6 (39.6%)
INDUCED OCR	1.0	AVG MIN q (kPa)	-27.4 (27.4%)

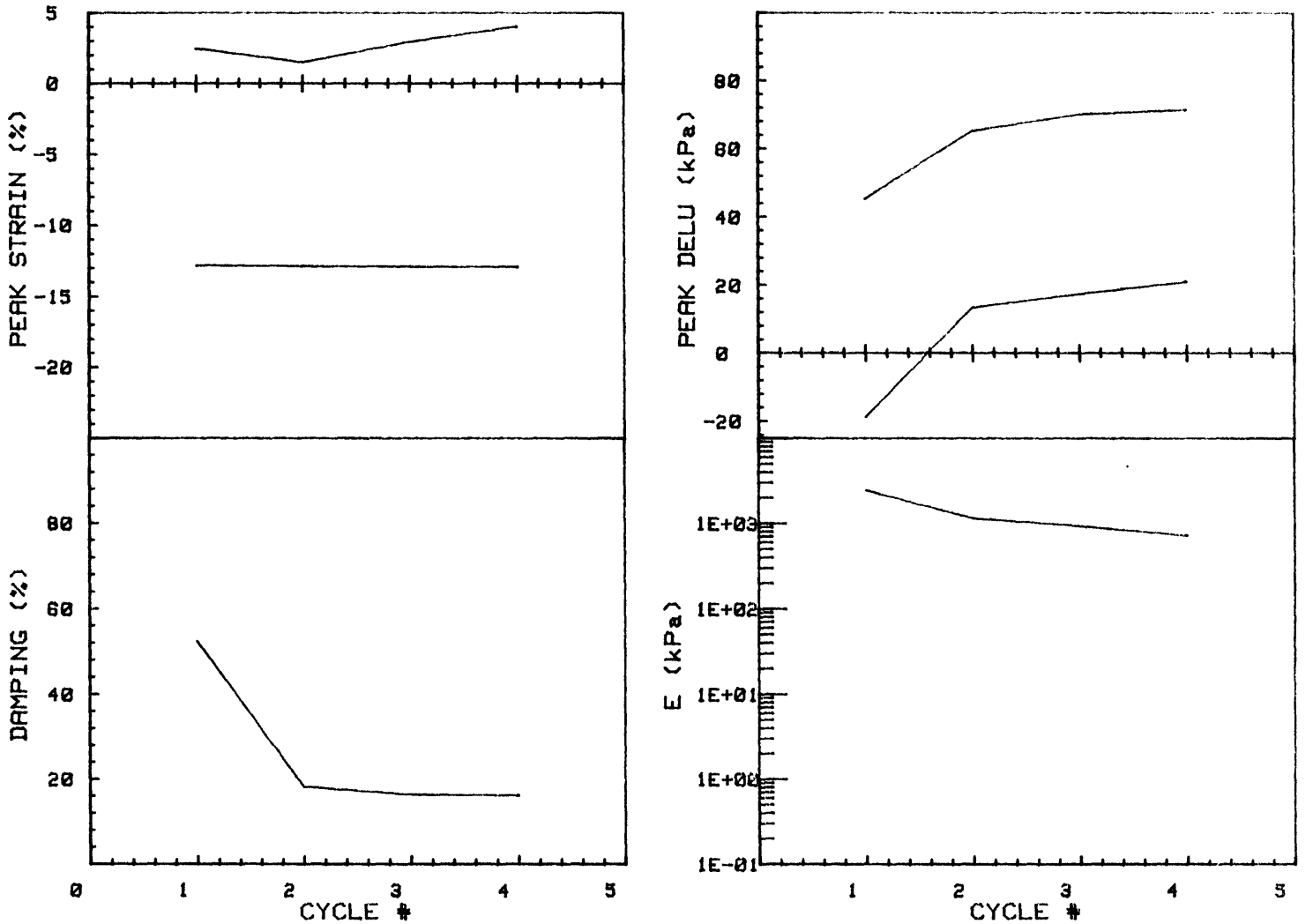

CRUISE ST HELENS		INCREMENT (cm)	REMOLDED-SURF
CORE NO.	CC2	TEST NO.	D162
SIG1c'(kPa)	72.1	STATIC qf (kPa)	100.0
SIG3c'(kPa)	72.1	AVG MAX q (kPa)	39.6 (39.6%)
INDUCED OCR	1.0	AVG MIN q (kPa)	-27.4 (27.4%)

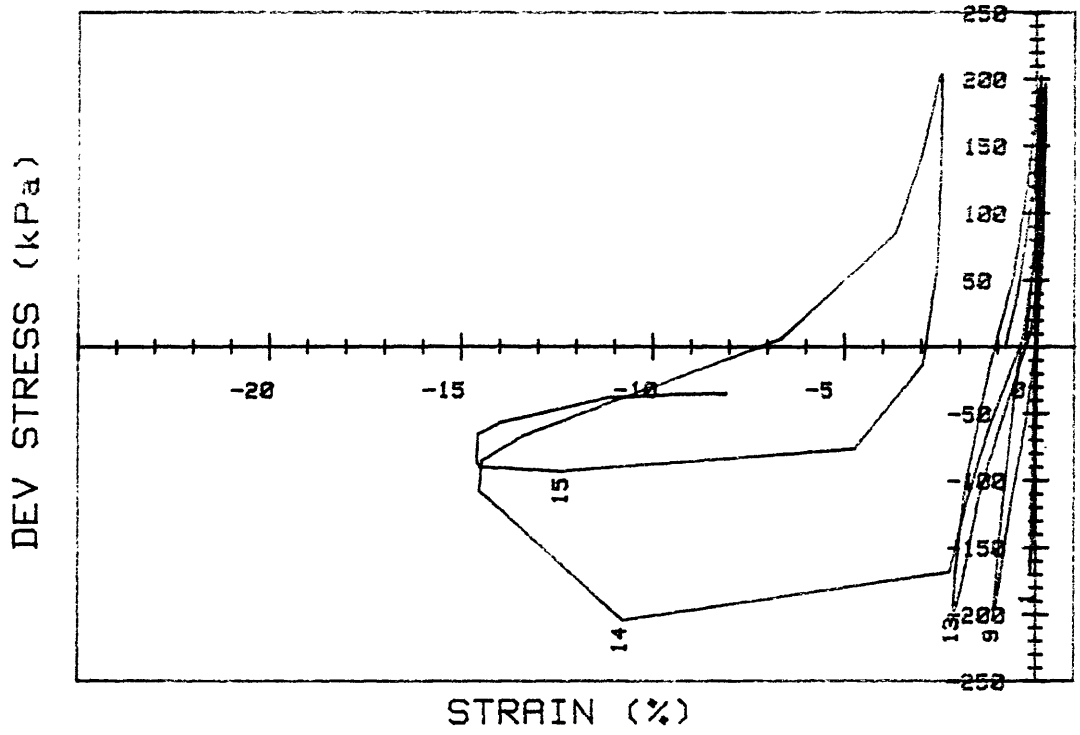

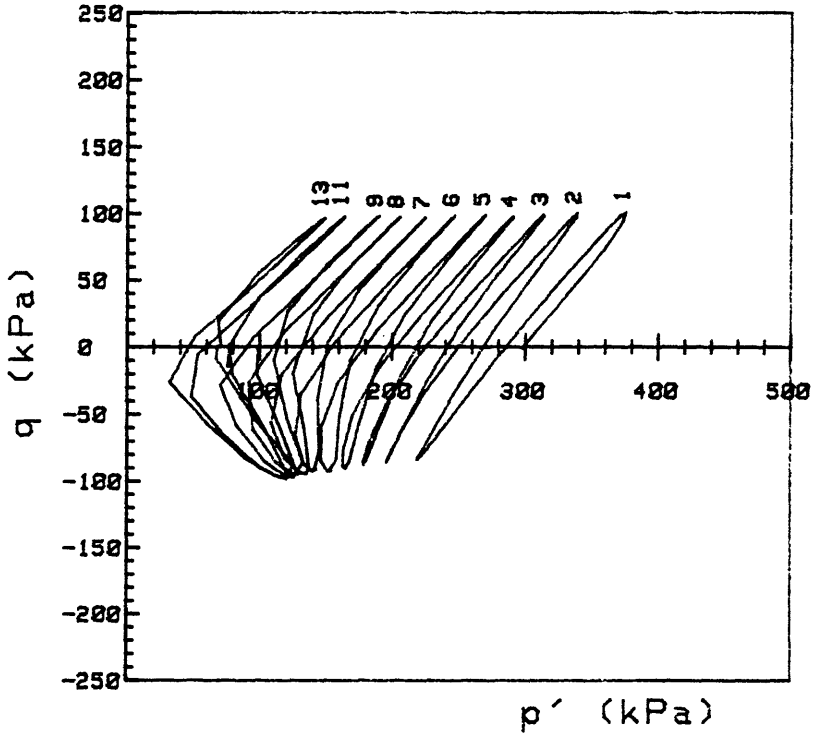

CRUISE ST HELENS		INCREMENT (cm)	REMOLDED-SURF
CORE NO.	CC2	TEST NO.	D146
SIG1c´(kPa)	299.3	STATIC qf (kPa)	300.0
SIG3c´(kPa)	299.3	AVG MAX q (kPa)	98.1 (32.7%)
INDUCED OCR	1.0	AVG MIN q (kPa)	-90.5 (30.2%)

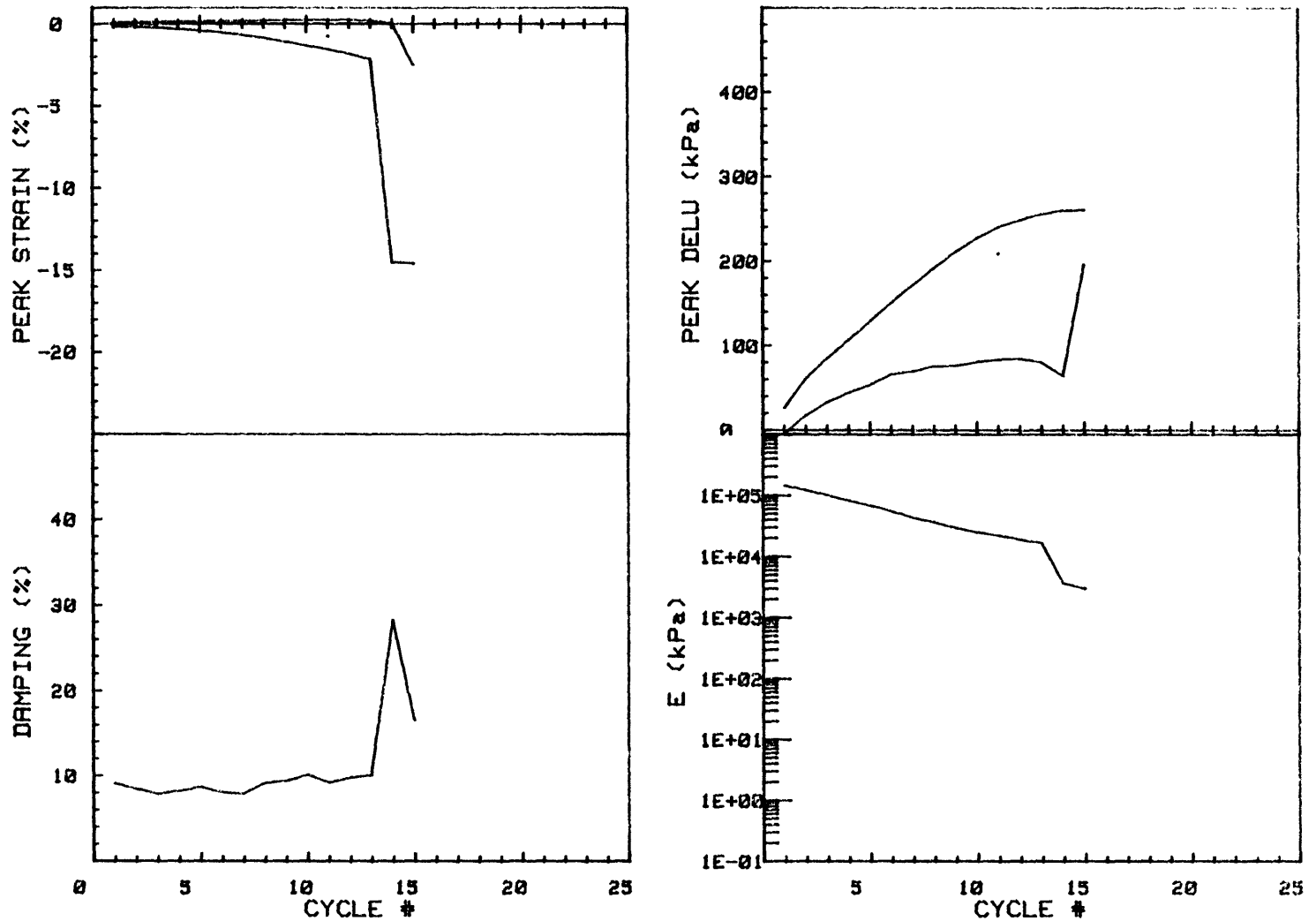

CRUISE ST HELENS		INCREMENT (cm)	REMOLDED-SURF
CORE NO.	CC2	TEST NO.	D146
SIG1c'(kPa)	299.3	STATIC qf (kPa)	300.0
SIG3c'(kPa)	299.3	AVG MAX q (kPa)	98.1 (32.7%)
INDUCED OCR	1.0	AVG MIN q (kPa)	-90.5 (30.2%)

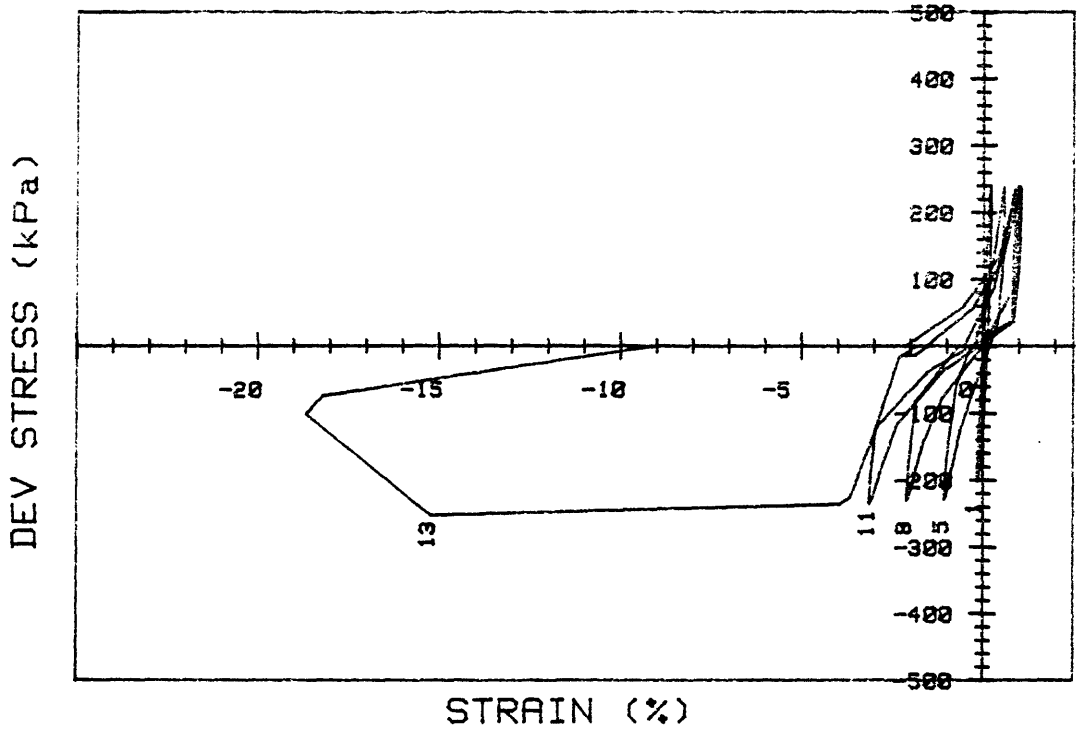

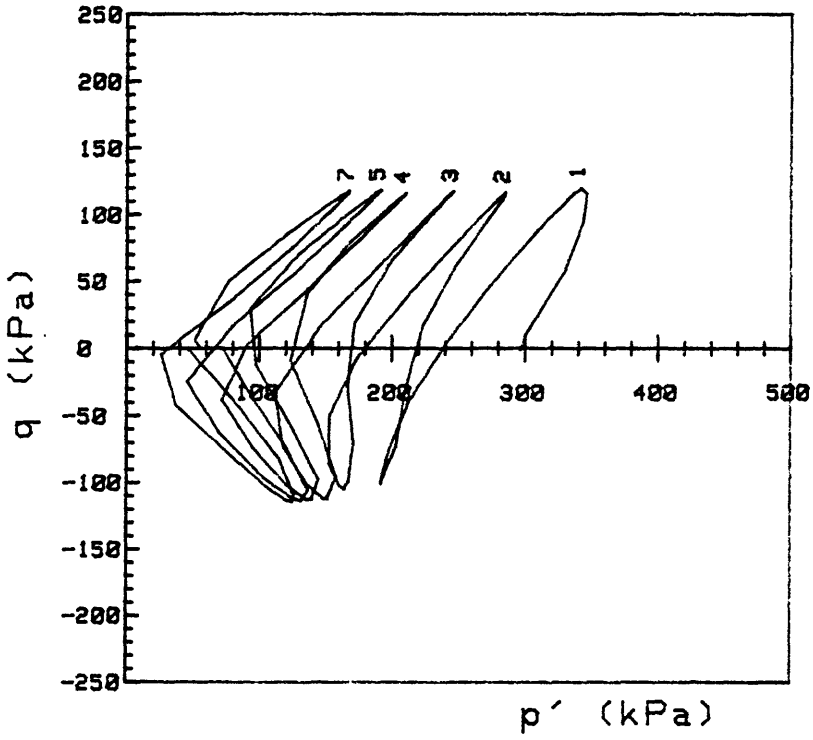

CRUISE ST HELENS		INCREMENT (cm)	REMOLDED-SURF
CORE NO.	CC2	TEST NO.	D147
SIG1c´(kPa)	297.0	STATIC qf (kPa)	300.0
SIG3c´(kPa)	297.0	AVG MAX q (kPa)	118.9 (39.6%)
INDUCED OCR	1.0	AVG MIN q (kPa)	-110.7 (36.9%)

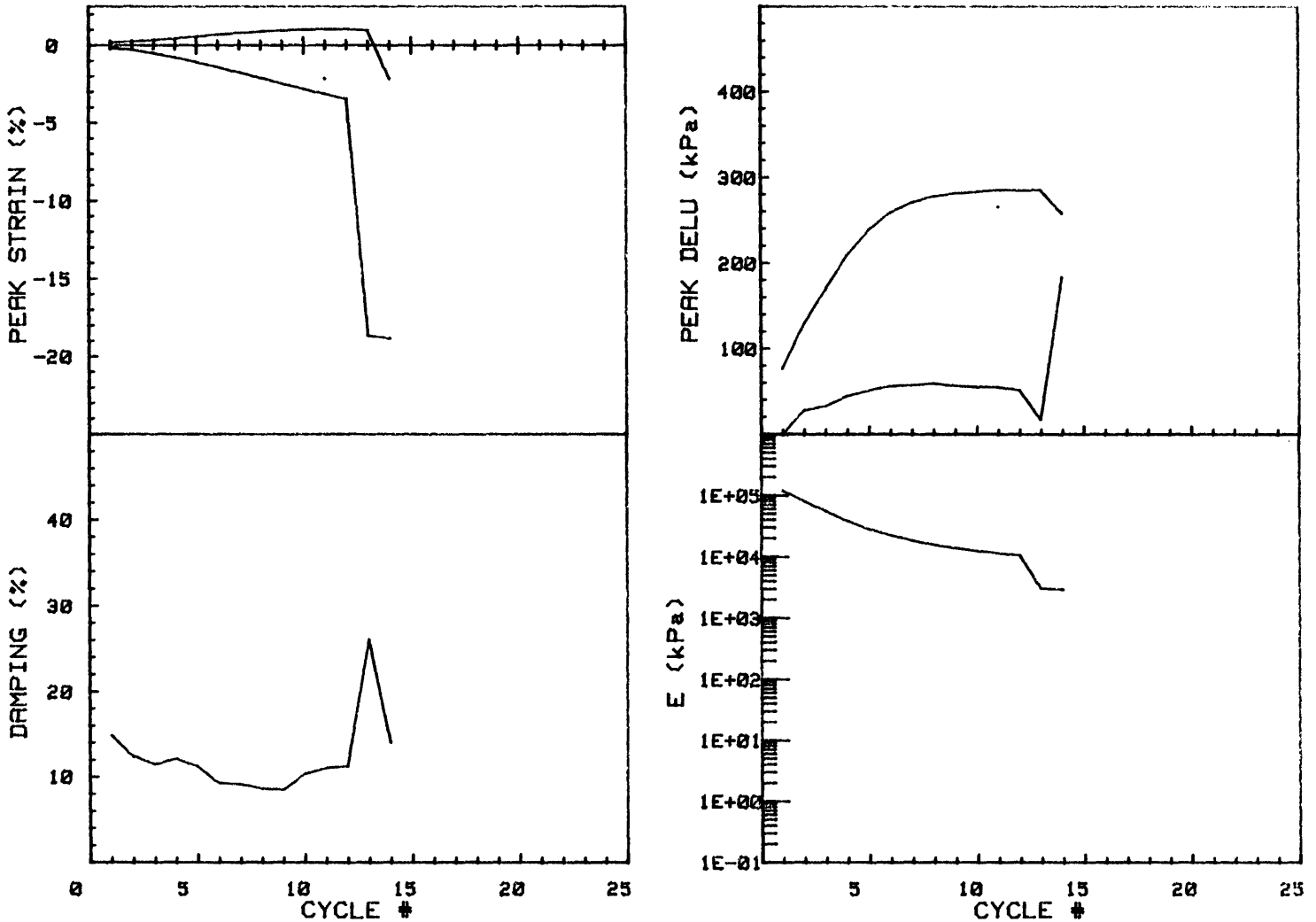

CRUISE ST HELENS		INCREMENT (cm)	REMOLDED-SURF
CORE NO.	CC2	TEST NO.	D147
SIG1c'(kPa)	297.0	STATIC qf (kPa)	300.0
SIG3c'(kPa)	297.0	AVG MAX q (kPa)	118.9 (39.6%)
INDUCED OCR	1.0	AVG MIN q (kPa)	-110.7 (36.9%)

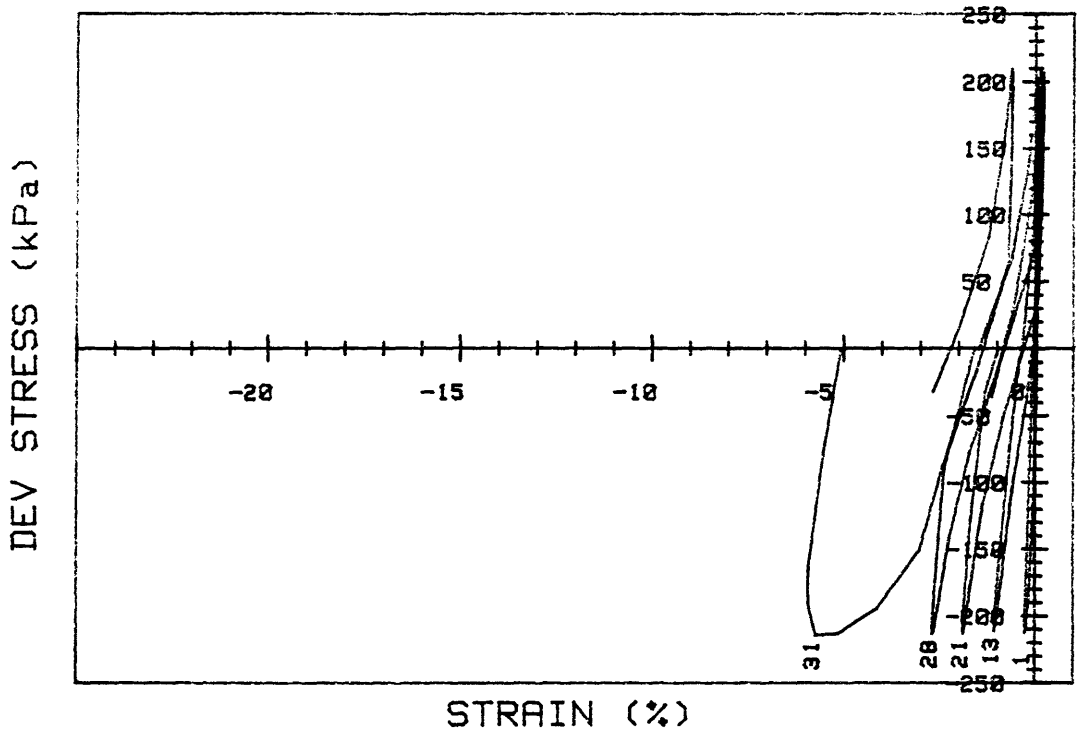

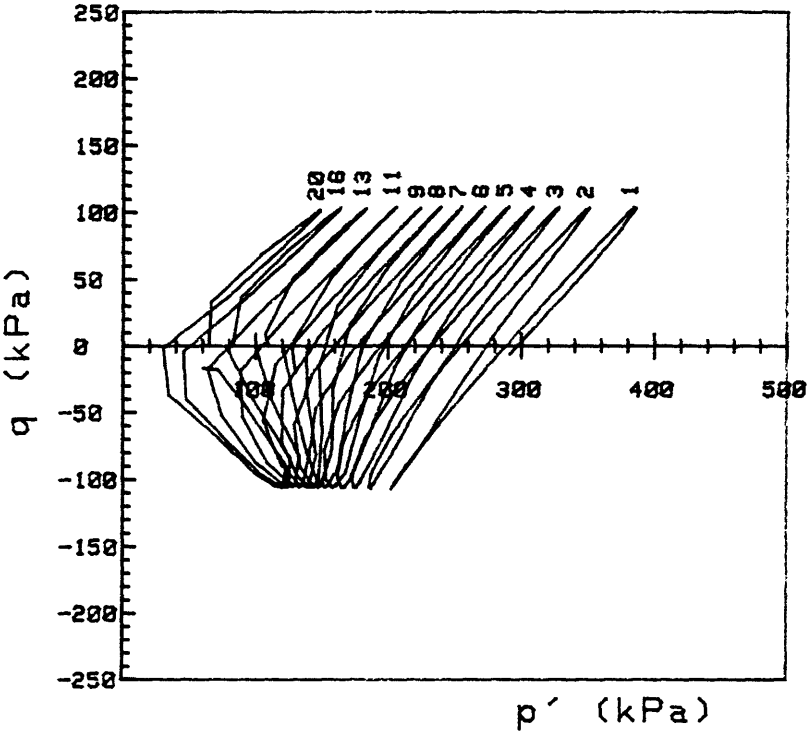

CRUISE ST HELENS		INCREMENT (cm)	REMOLDED-SURF
CORE NO.	CC2	TEST NO.	D148
SIG1c´(kPa)	297.4	STATIC qf (kPa)	300.0
SIG3c´(kPa)	297.4	AVG MAX q (kPa)	103.2 (34.4%)
INDUCED OCR	1.0	AVG MIN q (kPa)	-104.9 (35.0%)

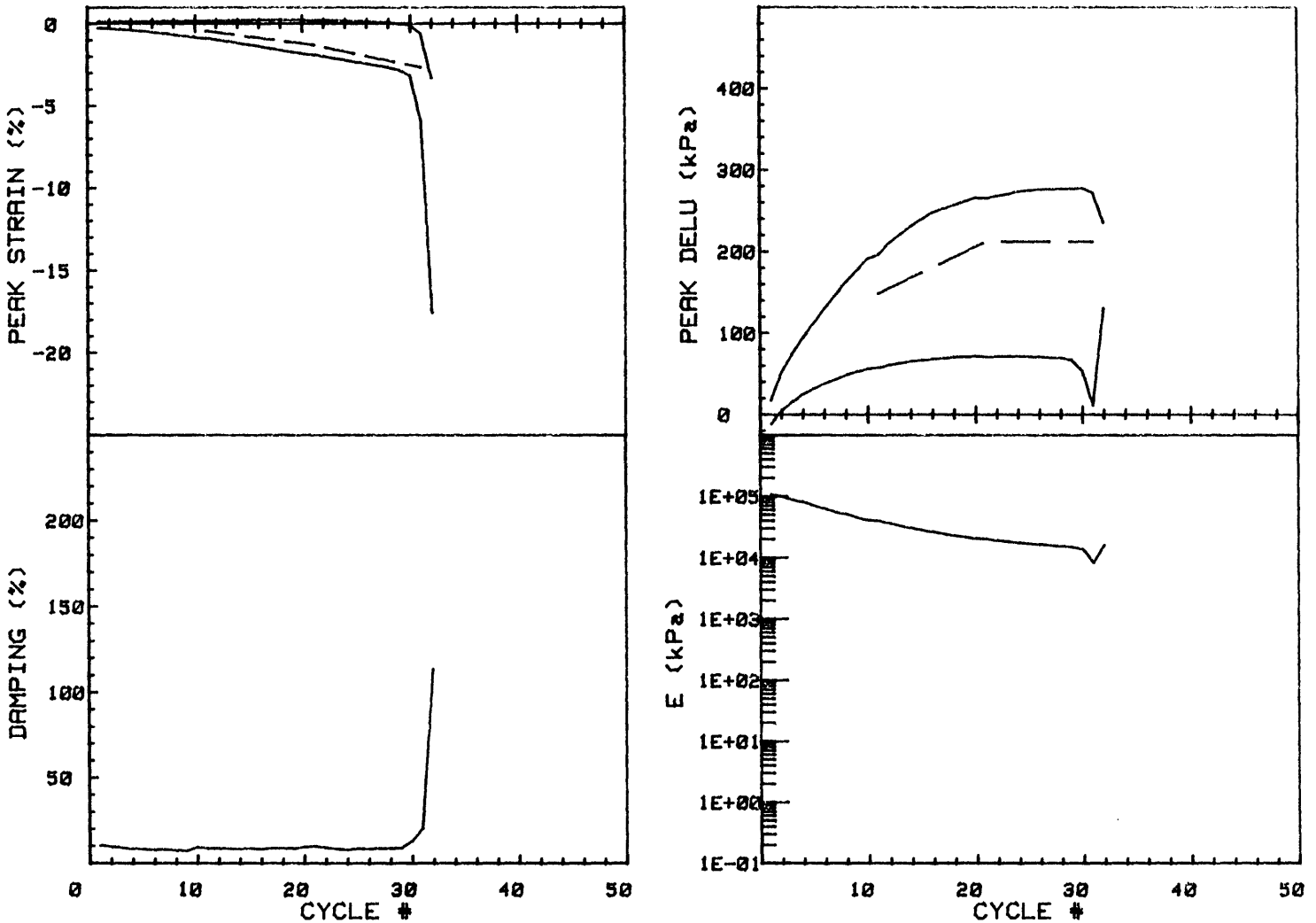

CRUISE ST HELENS		INCREMENT (cm)	REMOLDED-SURF
CORE NO.	CC2	TEST NO.	D148
SIG1c'(kPa)	297.4	STATIC qf (kPa)	300.0
SIG3c'(kPa)	297.4	AVG MAX q (kPa)	103.2 (34.4%)
INDUCED OCR	1.0	AVG MIN q (kPa)	-104.9 (35.0%)

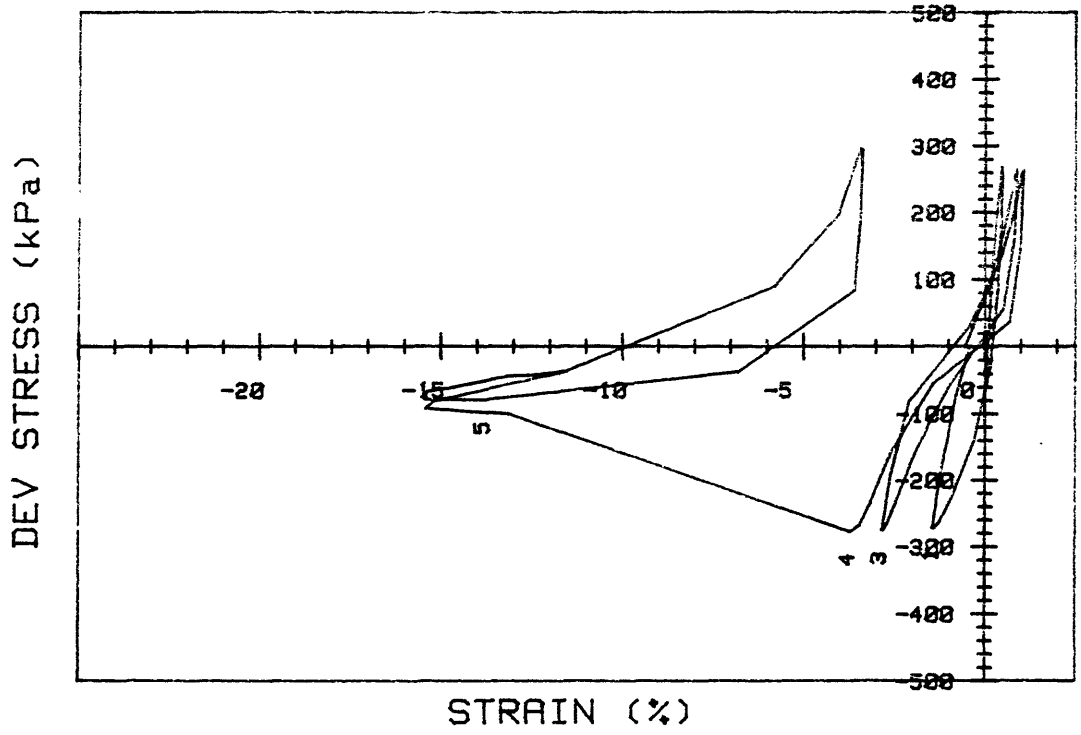

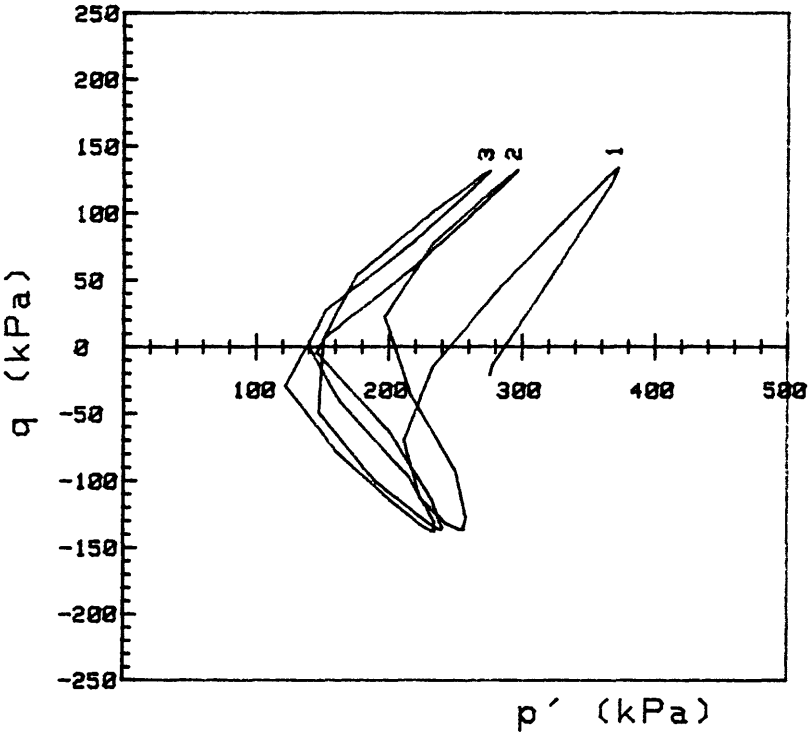

CRUISE ST HELENS		INCREMENT (cm)	REMOLDED-SURF
CORE NO.	CC2	TEST NO.	D149
SIG1c'(kPa)	297.3	STATIC qf (kPa)	300.0
SIG3c'(kPa)	297.3	AVG MAX q (kPa)	135.4 (45.1%)
INDUCED OCR	1.0	AVG MIN q (kPa)	-117.8 (39.3%)

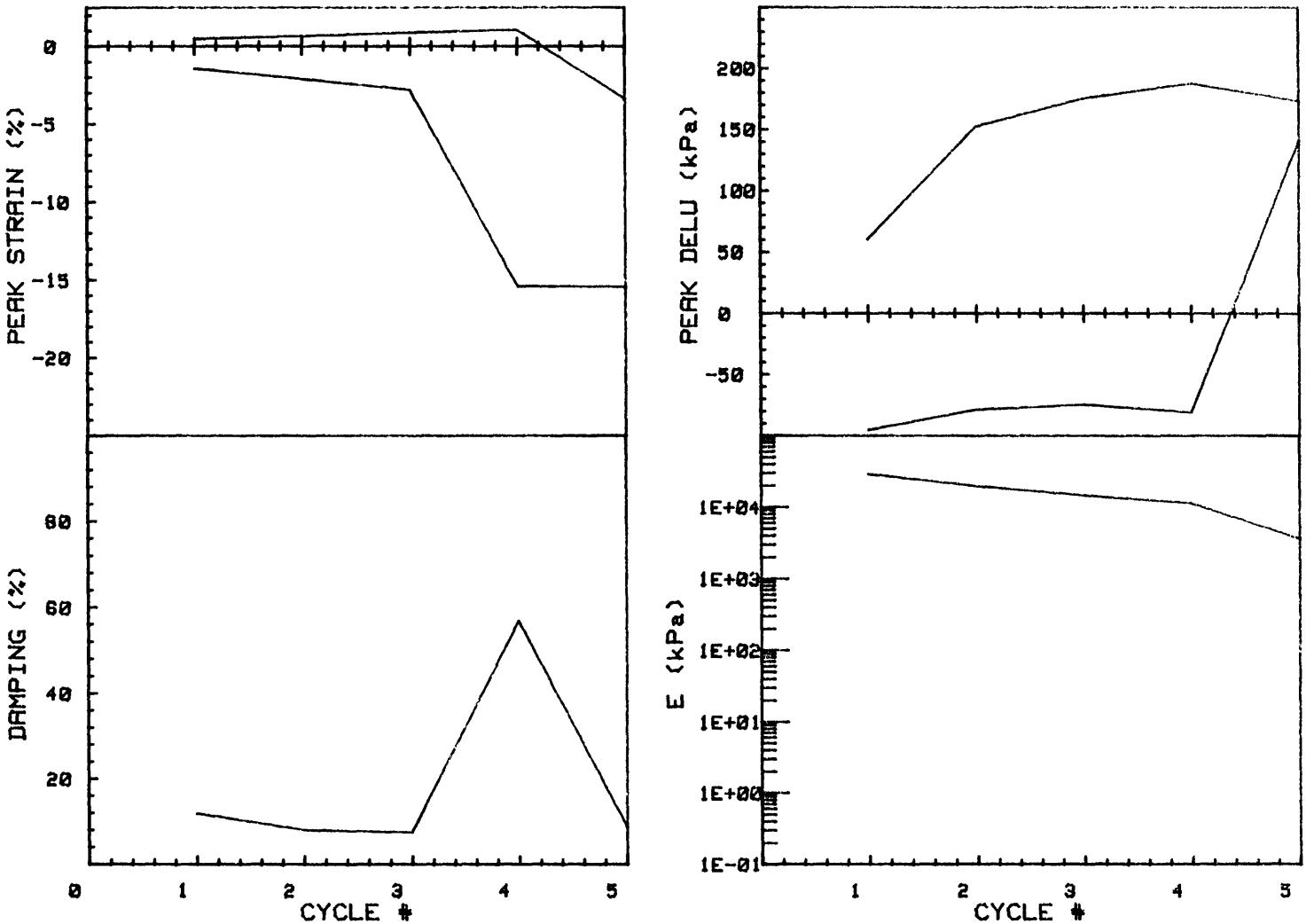

CRUISE ST HELENS		INCREMENT (cm)	REMOLDED-SURF
CORE NO. CC2		TEST NO.	D149
SIG1c'(kPa)	297.3	STATIC qf (kPa)	300.0
SIG3c'(kPa)	297.3	AVG MAX q (kPa)	135.4 (45.1%)
INDUCED OCR	1.0	AVG MIN q (kPa)	-117.8 (39.3%)

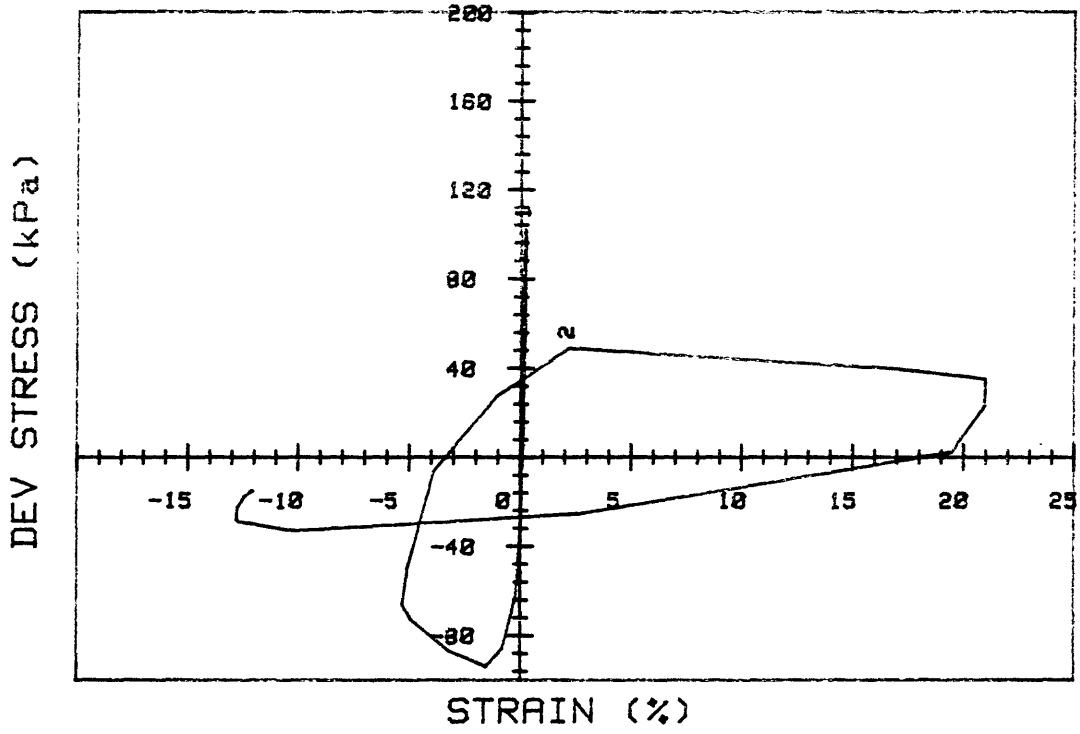

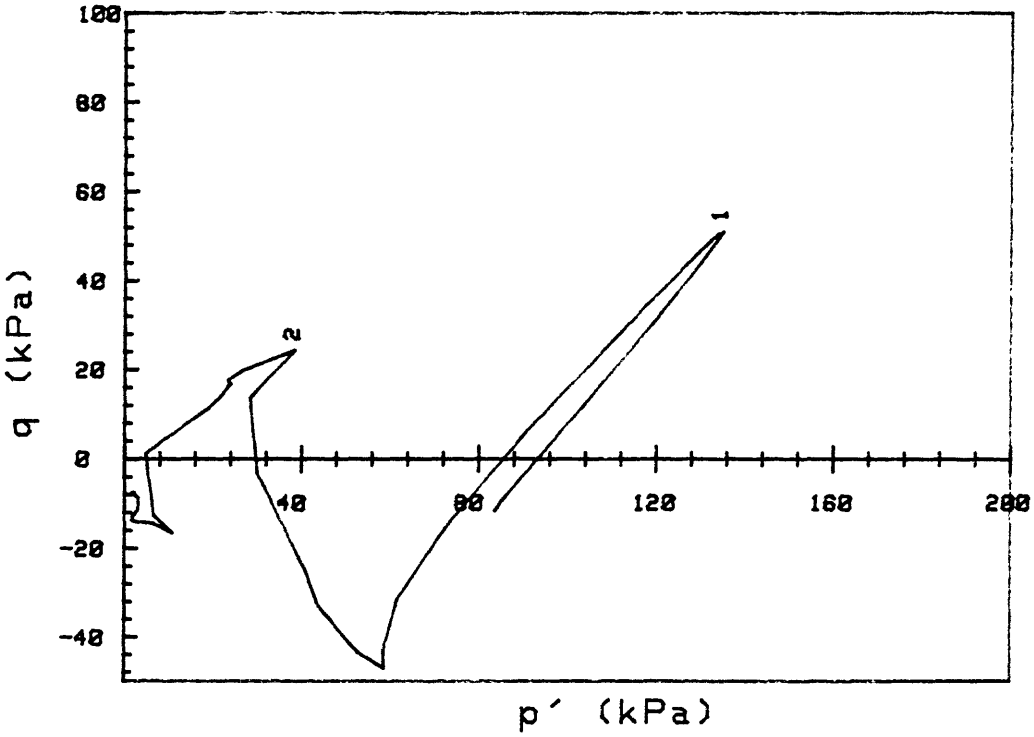

CRUISE ST HELENS		INCREMENT (cm)	REMOLDED-SURF
CORE NO. CC2		TEST NO.	D 179
SIG1c'(kPa)	95.5	STATIC qf (kPa)	100.0
SIG3c'(kPa)	95.5	AVG MAX q (kPa)	37.7 (37.7%)
INDUCED OCR	1.0	AVG MIN q (kPa)	-31.8 (31.8%)

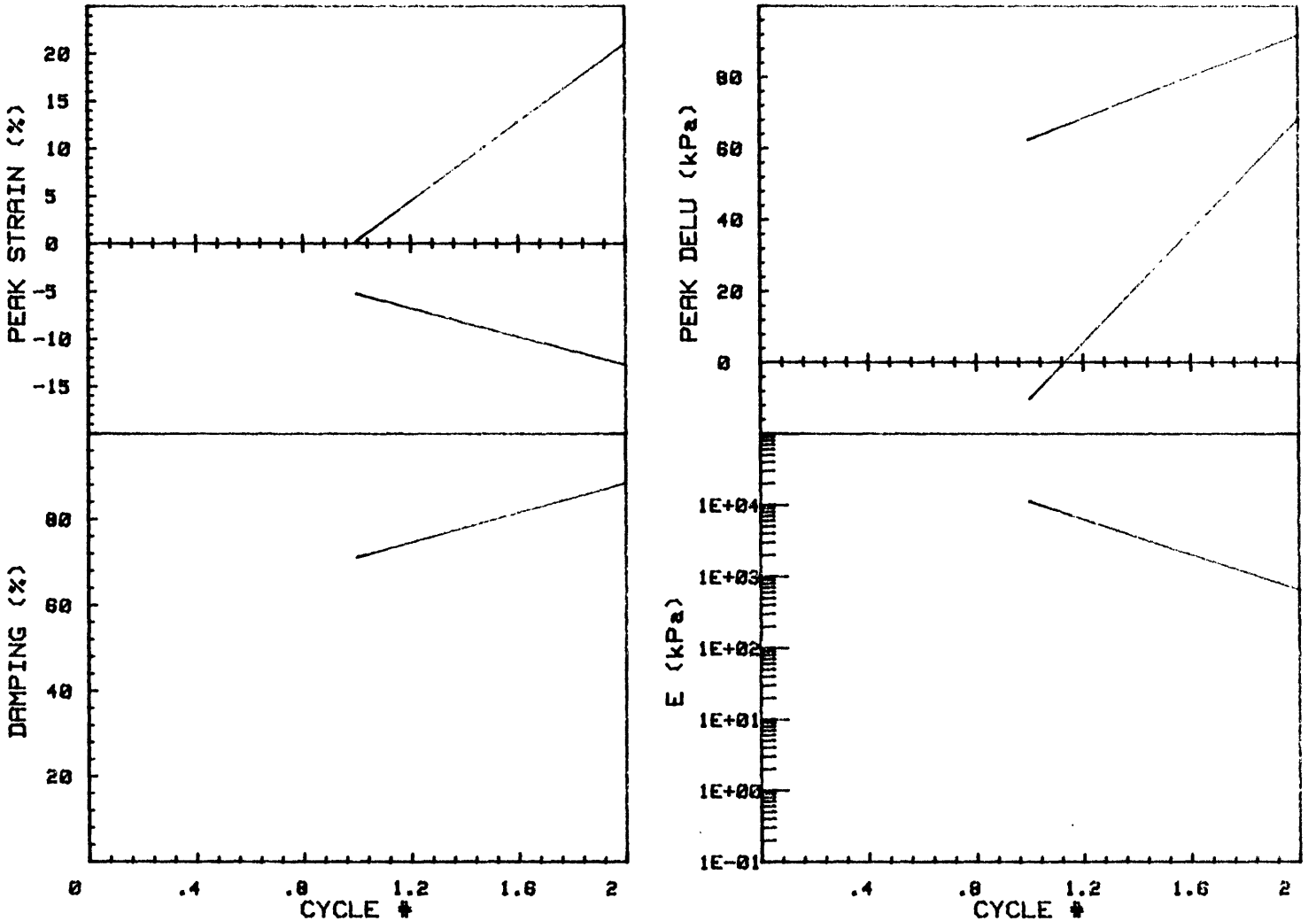

CRUISE ST HELENS		INCREMENT (cm)	REMOLDED-SURF
CORE NO.	CC2	TEST NO.	D 179
SIG1c'(kPa)	95.5	STATIC qf (kPa)	100.0
SIG3c'(kPa)	95.5	AVG MAX q (kPa)	37.7 (37.7%)
INDUCED OCR	1.0	AVG MIN q (kPa)	-31.8 (31.8%)

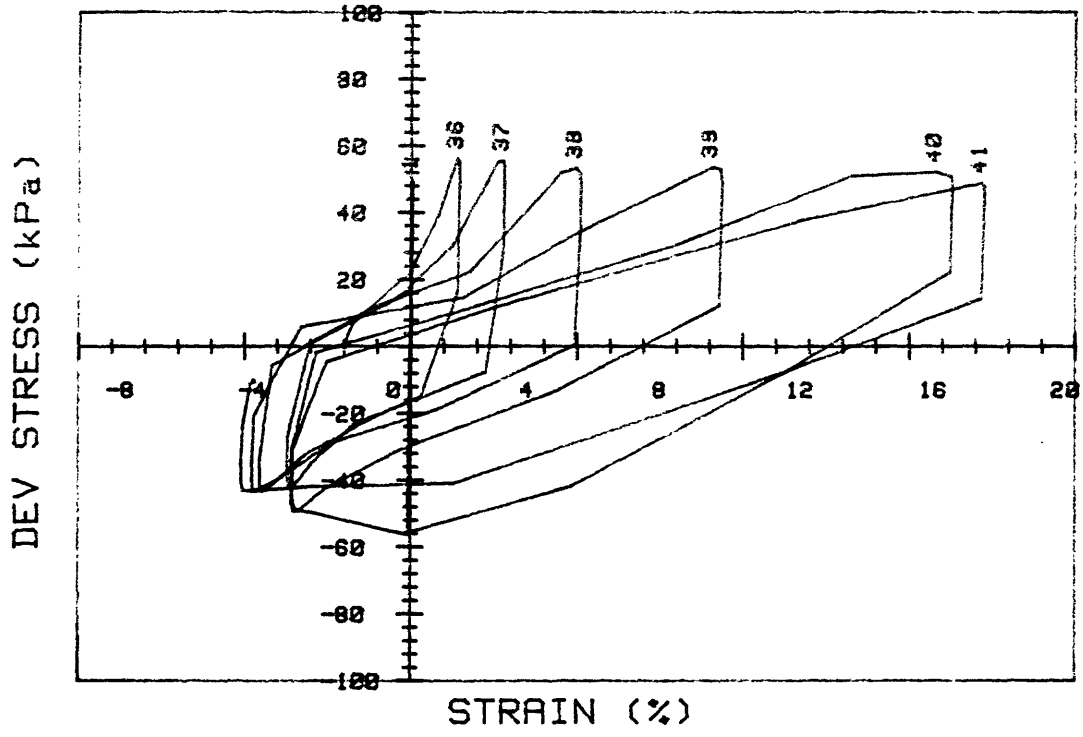

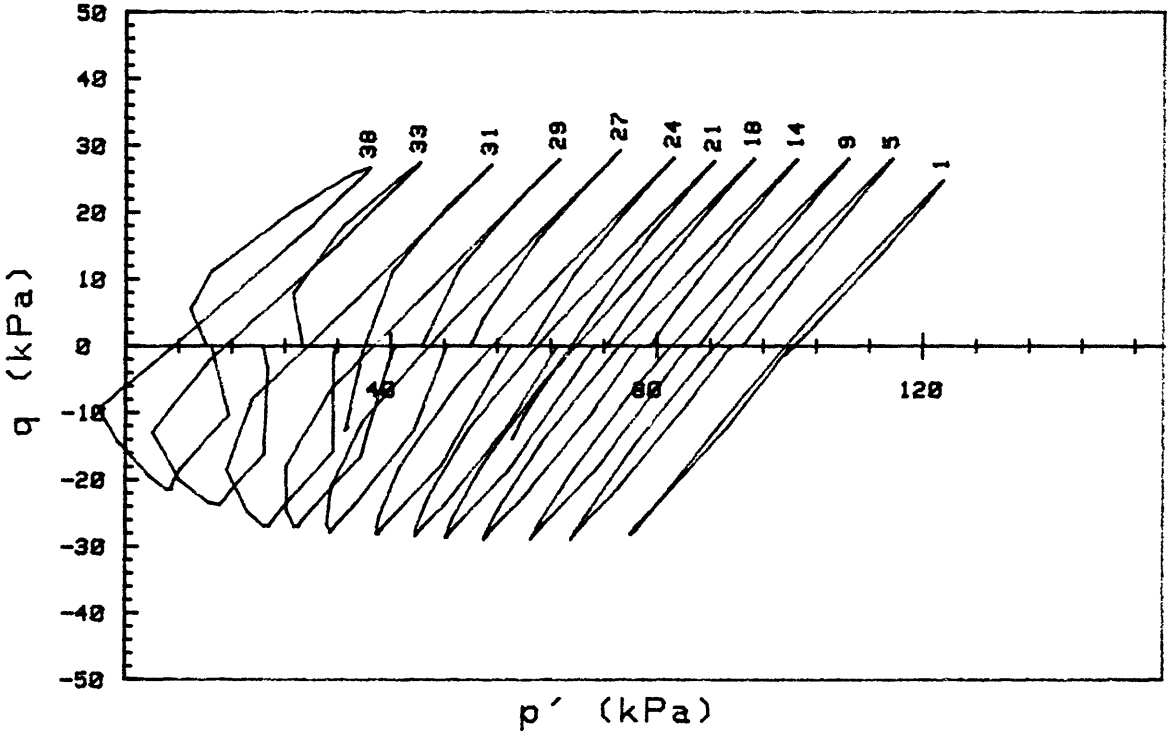

CRUISE ST HELENS		INCREMENT (cm)	REMOLDED-SURF
CORE NO. CC2		TEST NO.	D180
SIG1c´(kPa)	100.7	STATIC qf (kPa)	100.0
SIG3c´(kPa)	100.7	AVG MAX q (kPa)	27.7 (27.7%)
INDUCED OCR	1.0	AVG MIN q (kPa)	-27.3 (27.3%)

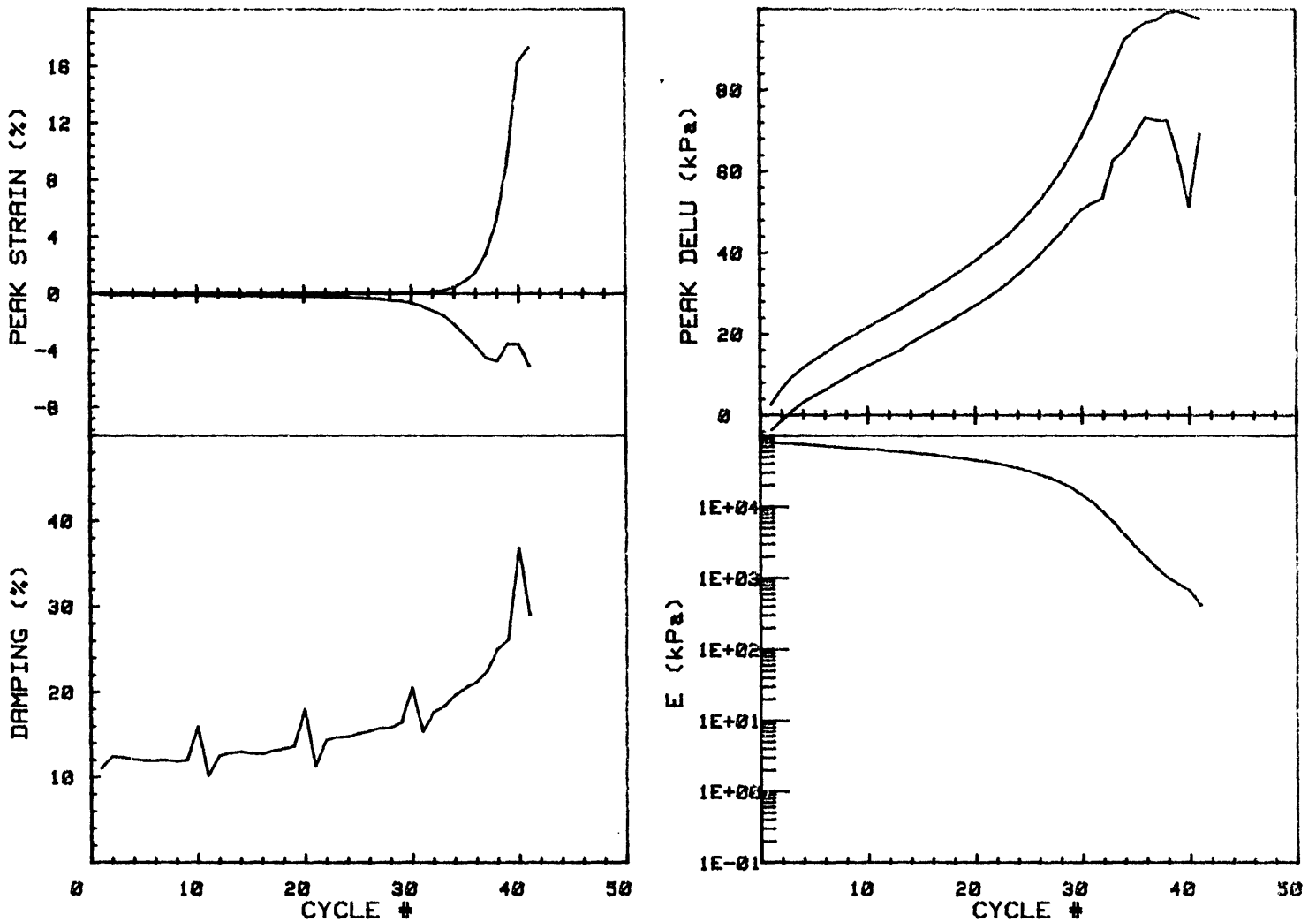

CRUISE ST HELENS		INCREMENT (cm)	REMOLDED-SURF
CORE NO. CC2		TEST NO.	D180
SIG1c'(kPa)	100.7	STATIC qf (kPa)	100.0
SIG3c'(kPa)	100.7	AVG MAX q (kPa)	27.7 (27.7%)
INDUCED OCR	1.0	AVG MIN q (kPa)	-27.3 (27.3%)

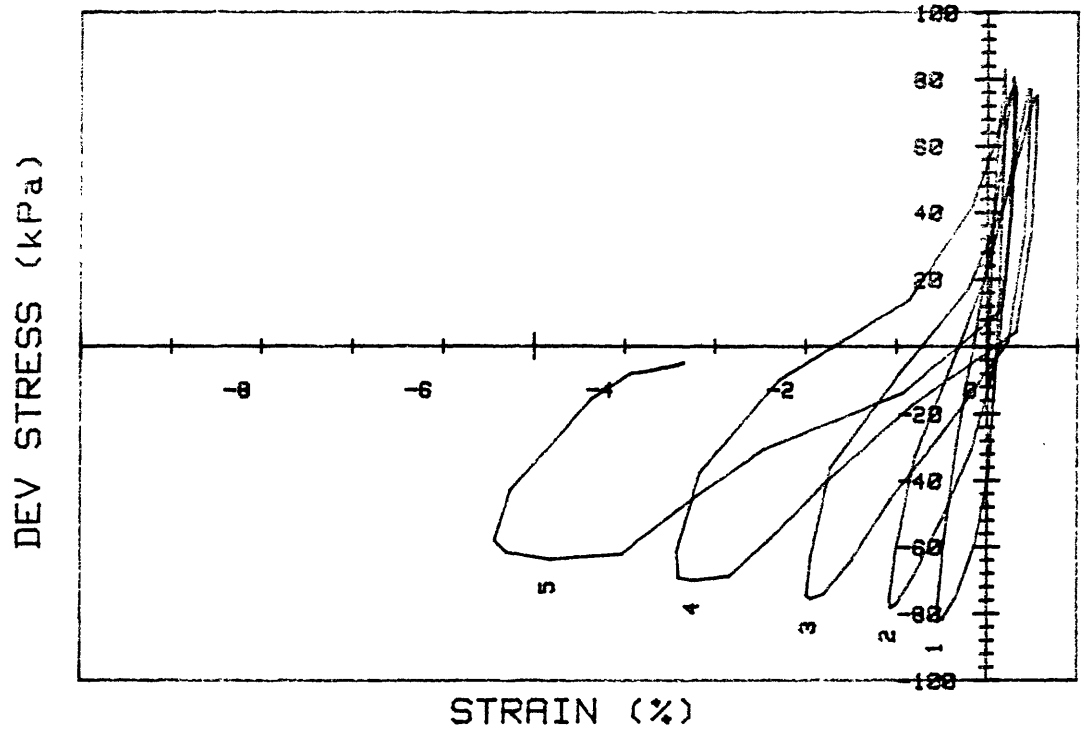

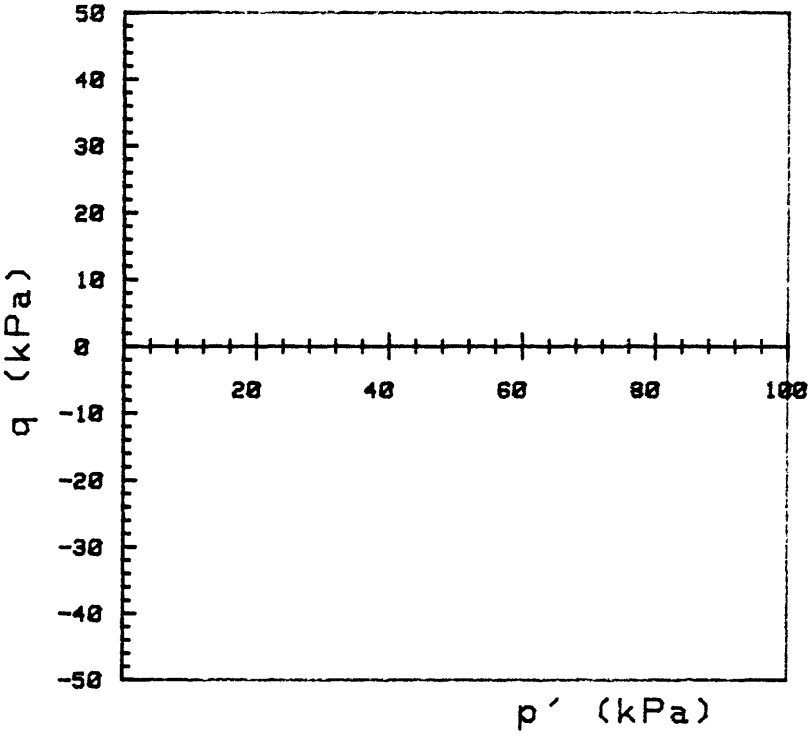

CRUISE ST HELENS		INCREMENT (cm)	REMOLDED-SURF
CORE NO.	CC2	TEST NO.	D181
SIG1c'(kPa)	-108.6	STATIC qf (kPa)	100.0
SIG3c'(kPa)	-108.6	AVG MAX q (kPa)	39.3 (39.3%)
INDUCED OCR	1.0	AVG MIN q (kPa)	-37.0 (37.0%)

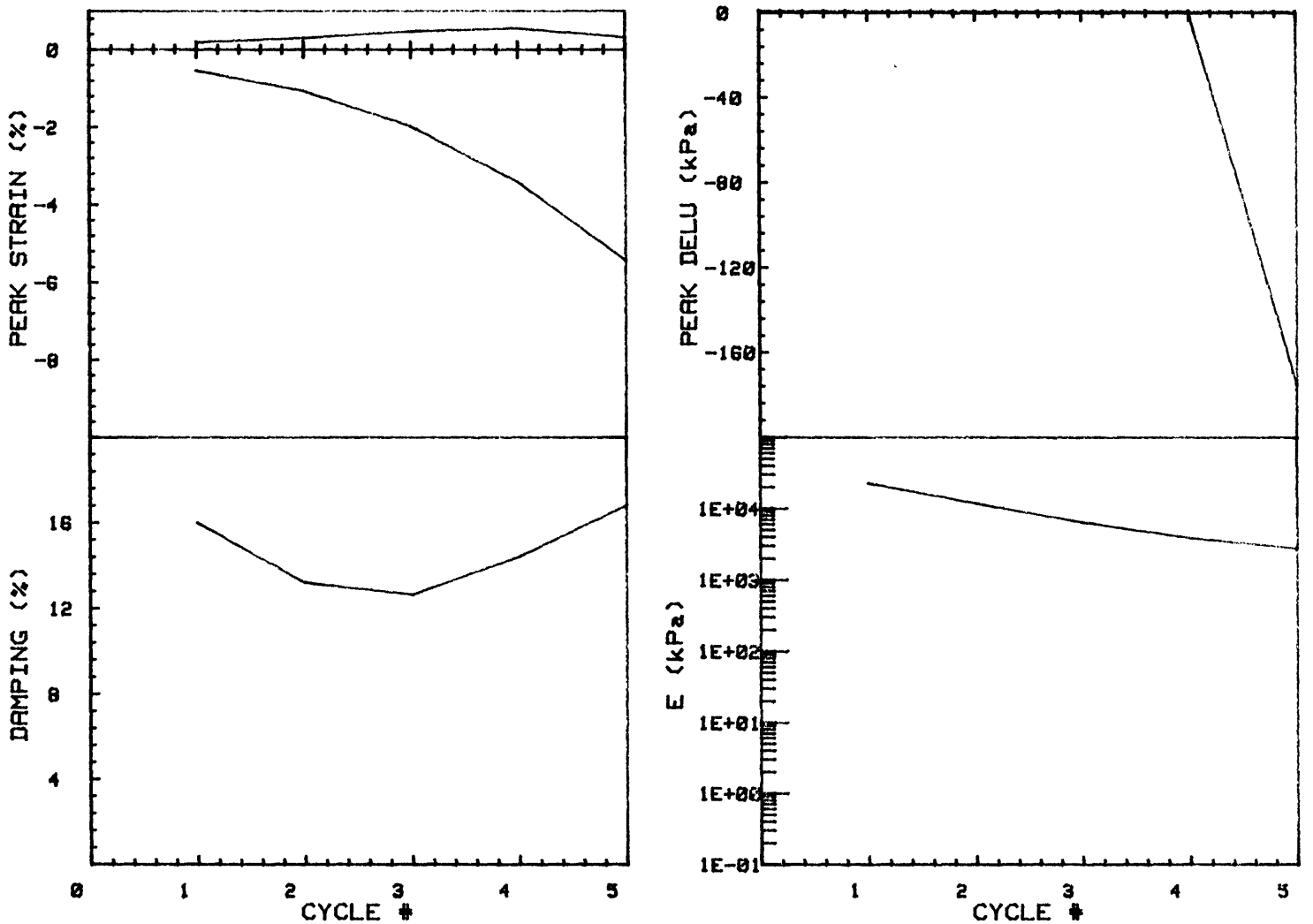

CRUISE ST HELENS		INCREMENT (cm)	REMOLDED-SURF
CORE NO. CC2		TEST NO.	D181
SIG1c'(kPa)	-108.6	STATIC qf (kPa)	100.0
SIG3c'(kPa)	-108.6	AVG MAX q (kPa)	39.3 (39.3%)
INDUCED OCR	1.0	AVG MIN q (kPa)	-37.0 (37.0%)

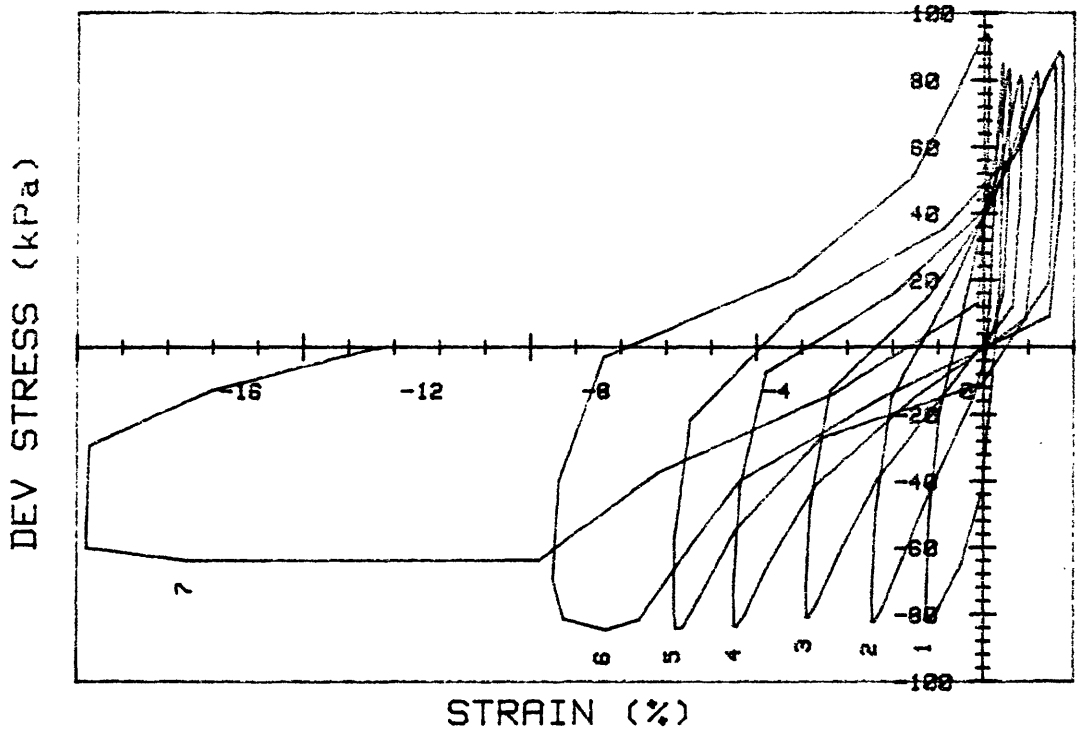

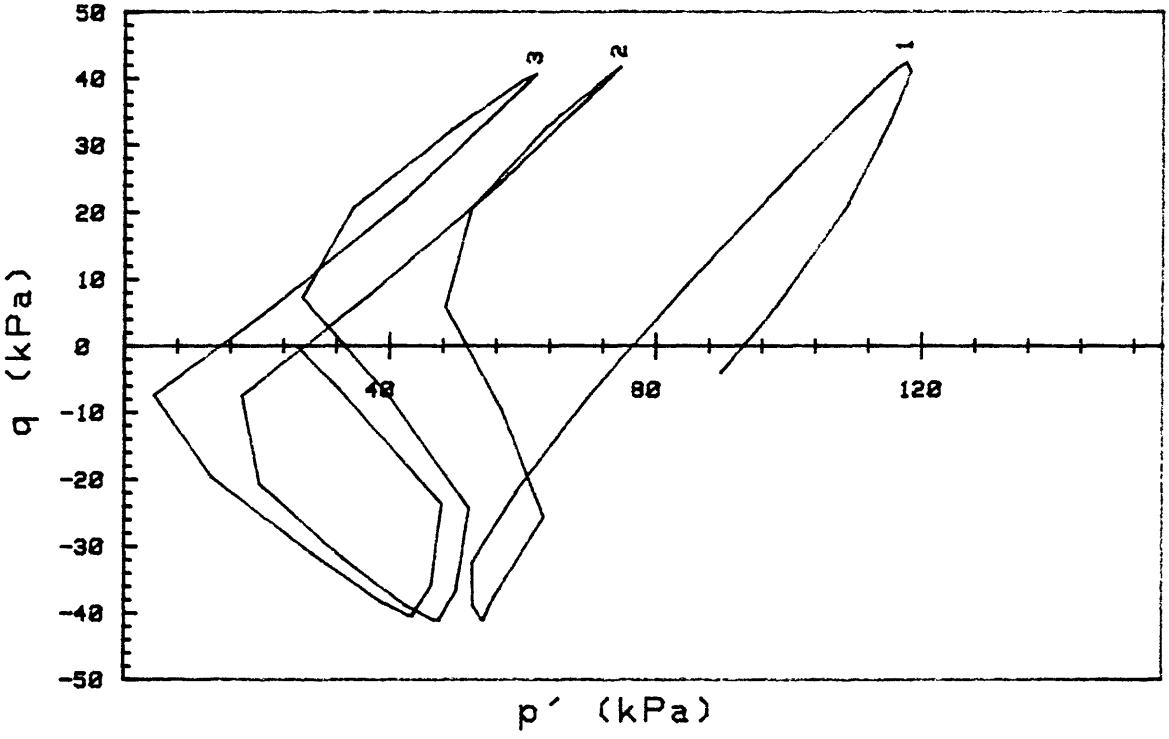

CRUISE ST HELENS		INCREMENT (cm)	REMOLDED-SURF
CORE NO.	CC2	TEST NO.	D182
SIG1c'(kPa)	93.9	STATIC qf (kPa)	100.0
SIG3c'(kPa)	93.9	AVG MAX q (kPa)	43.7 (43.7%)
INDUCED OCR	1.0	AVG MIN q (kPa)	-38.7 (38.7%)

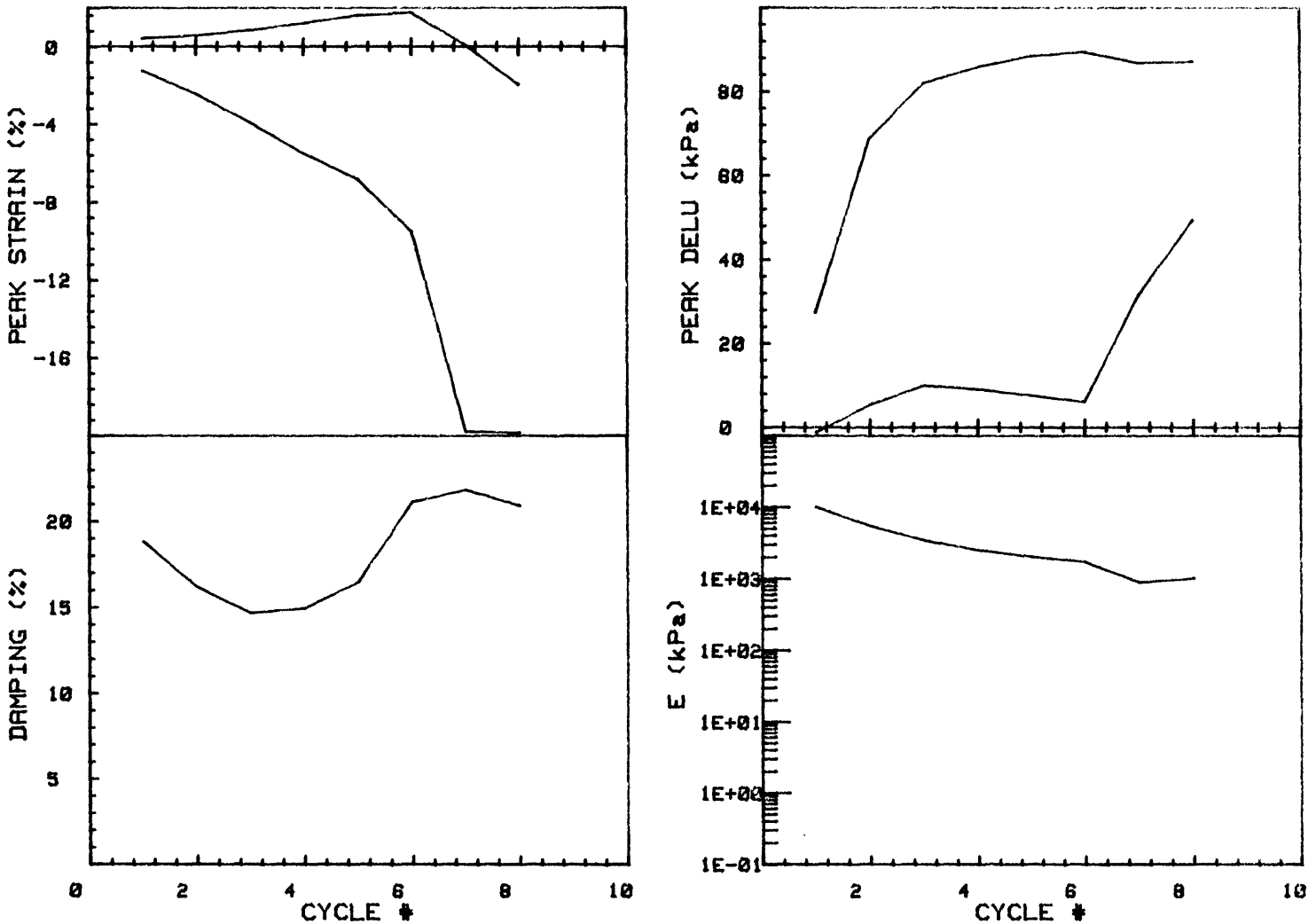

CRUISE ST HELENS		INCREMENT (cm)	REMOLDED-SURF
CORE NO.	CC2	TEST NO.	D182
SIG1c'(kPa)	93.9	STATIC qf (kPa)	100.0
SIG3c'(kPa)	93.9	AVG MAX q (kPa)	43.7 (43.7%)
INDUCED OCR	1.0	AVG MIN q (kPa)	-38.7 (38.7%)

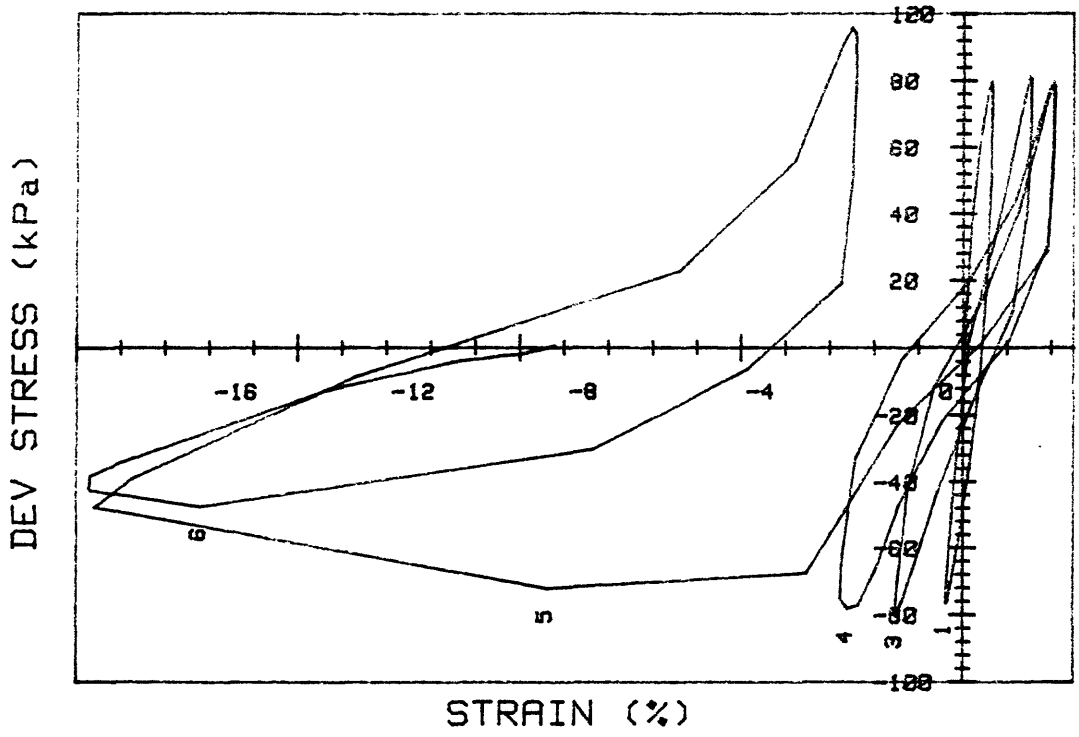

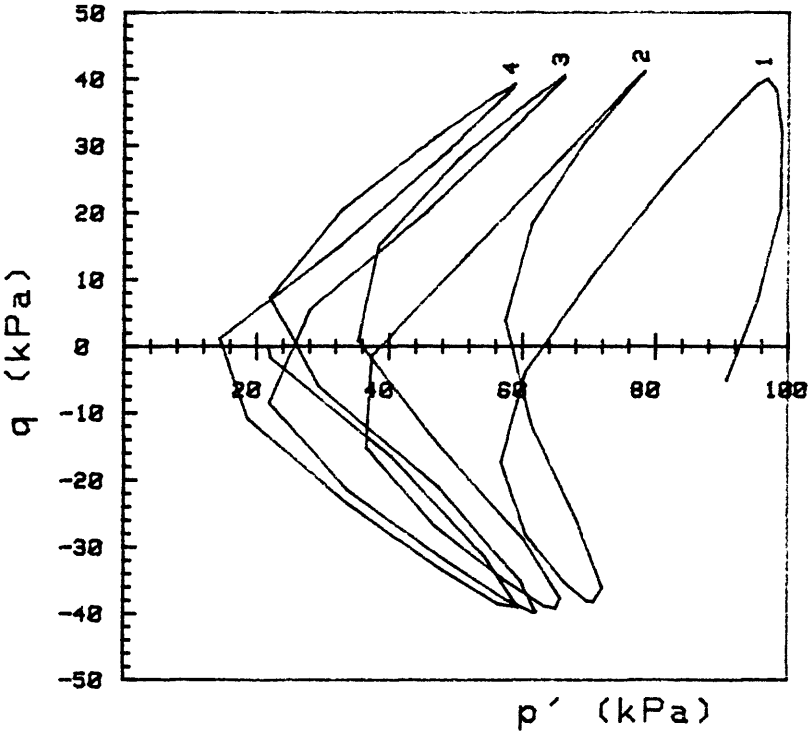

CRUISE ST HELENS		INCREMENT (cm)	REMOLDED-SURF
CORE NO. CC2		TEST NO.	D183
SIG1c´(kPa)	95.8	STATIC qf (kPa)	100.0
SIG3c´(kPa)	95.8	AVG MAX q (kPa)	41.4 (41.4%)
INDUCED OCR	1.0	AVG MIN q (kPa)	-36.1 (36.1%)

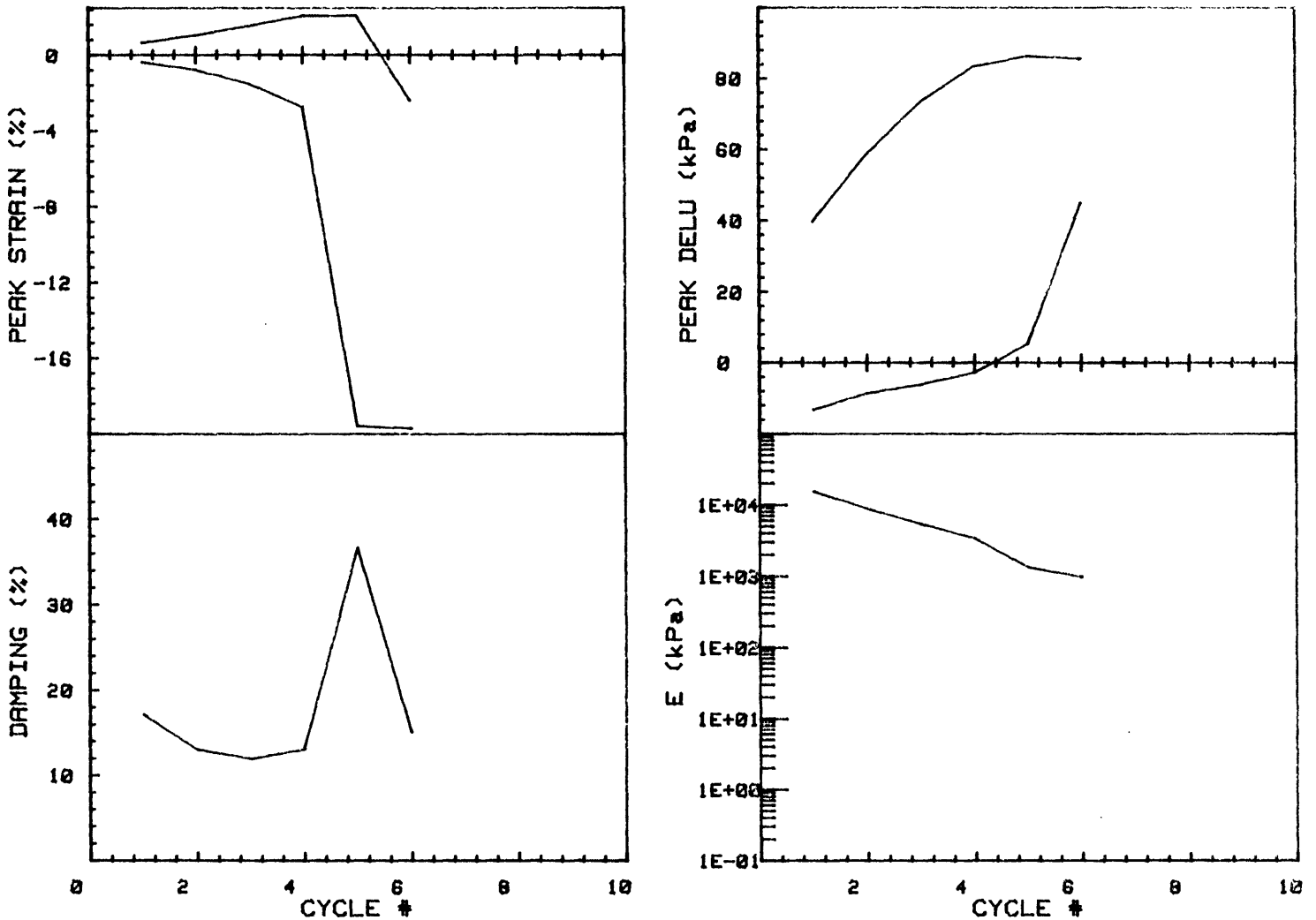

CRUISE ST HELENS		INCREMENT (cm)	REMOLDED-SURF
CORE NO.	CC2	TEST NO.	D183
SIG1c'(kPa)	95.8	STATIC qf (kPa)	100.0
SIG3c'(kPa)	95.8	AVG MAX q (kPa)	41.4 (41.4%)
INDUCED OCR	1.0	AVG MIN q (kPa)	-36.1 (36.1%)

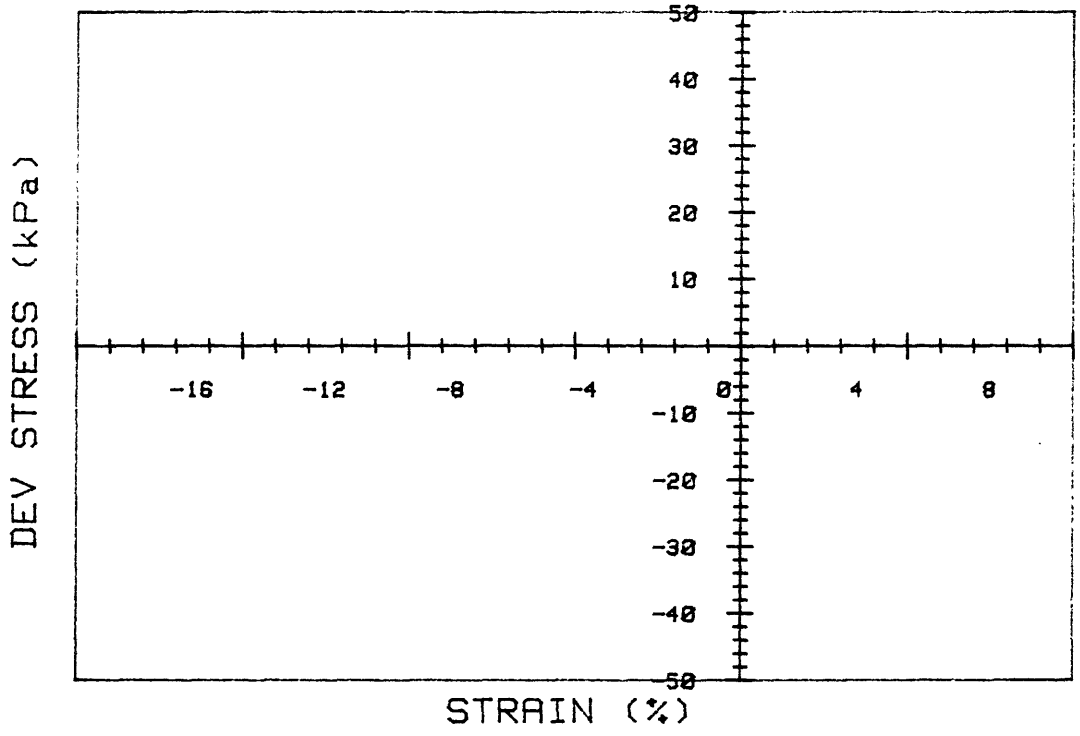

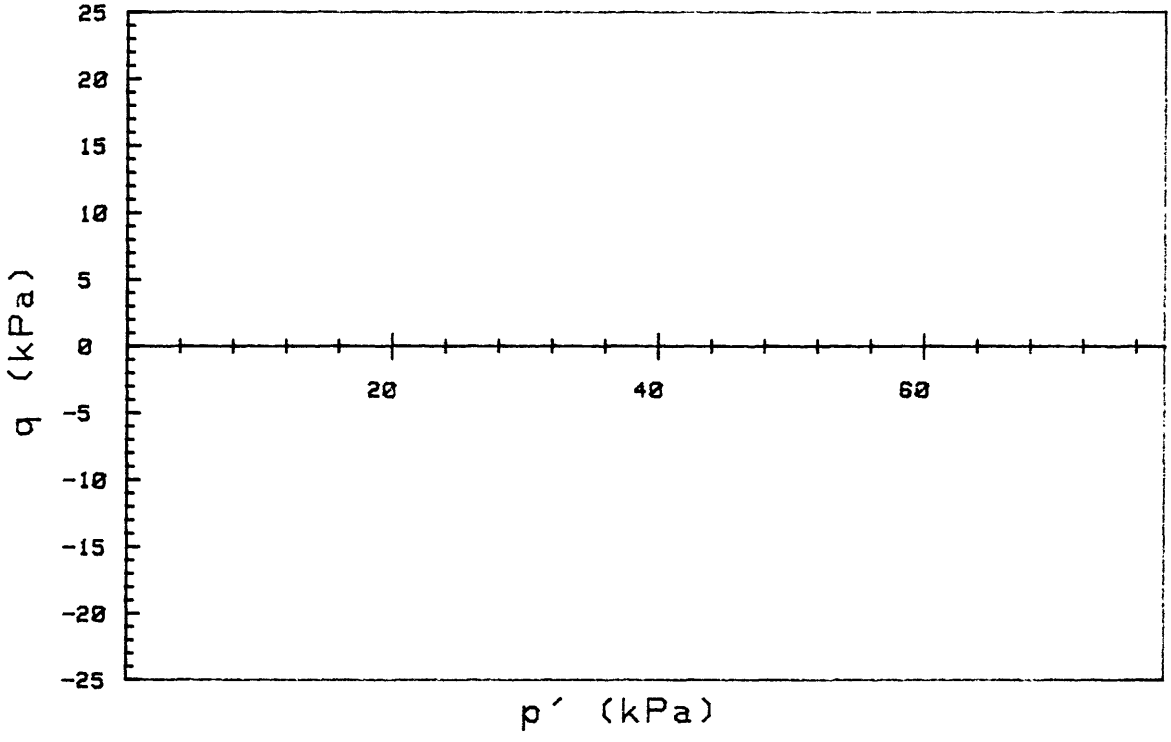

ST HELENS		INCREMENT (cm)	REMOLDED-SURF
CORE NO.	CC2	TEST NO.	D184
SIG1c´(kPa)	100.3	STATIC qf (kPa)	100.0
SIG3c´(kPa)	100.3	AVG MAX q (kPa)	21.9 (21.9%)
INDUCED OCR	N/A	AVG MIN q (kPa)	-21.7 (21.7%)

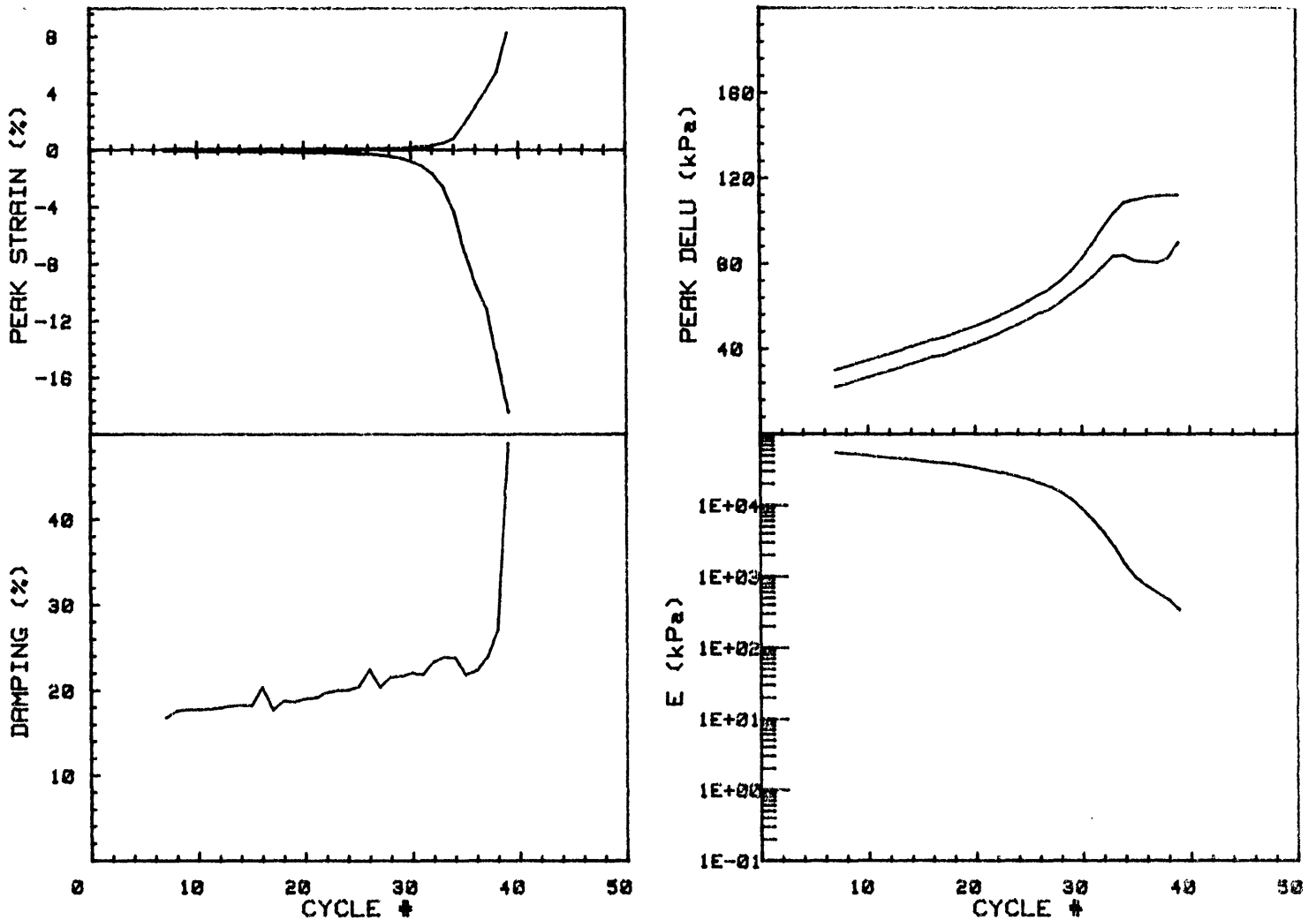

CRUISE ST HELENS		INCREMENT (cm)	REMOLDED-SURF
CORE NO. CC2		TEST NO.	D184
SIG1c'(kPa)	100.3	STATIC qf (kPa)	100.0
SIG3c'(kPa)	100.3	AVG MAX q (kPa)	21.9 (21.9%)
INDUCED OCR	1.0	AVG MIN q (kPa)	-21.7 (21.7%)

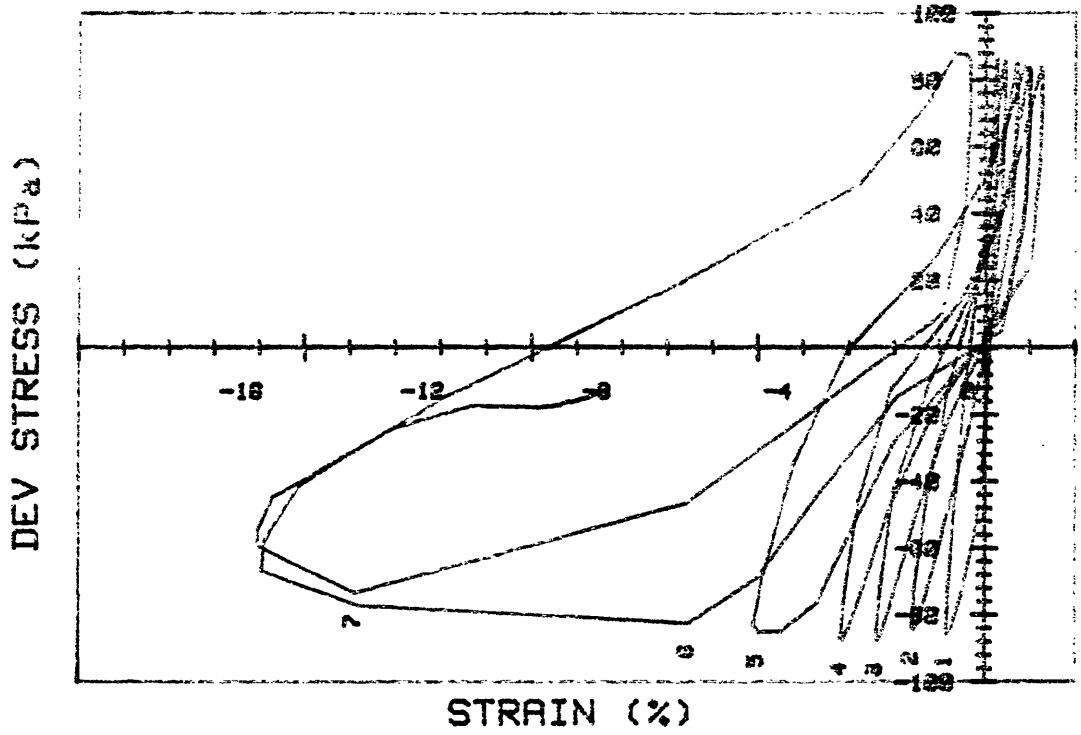

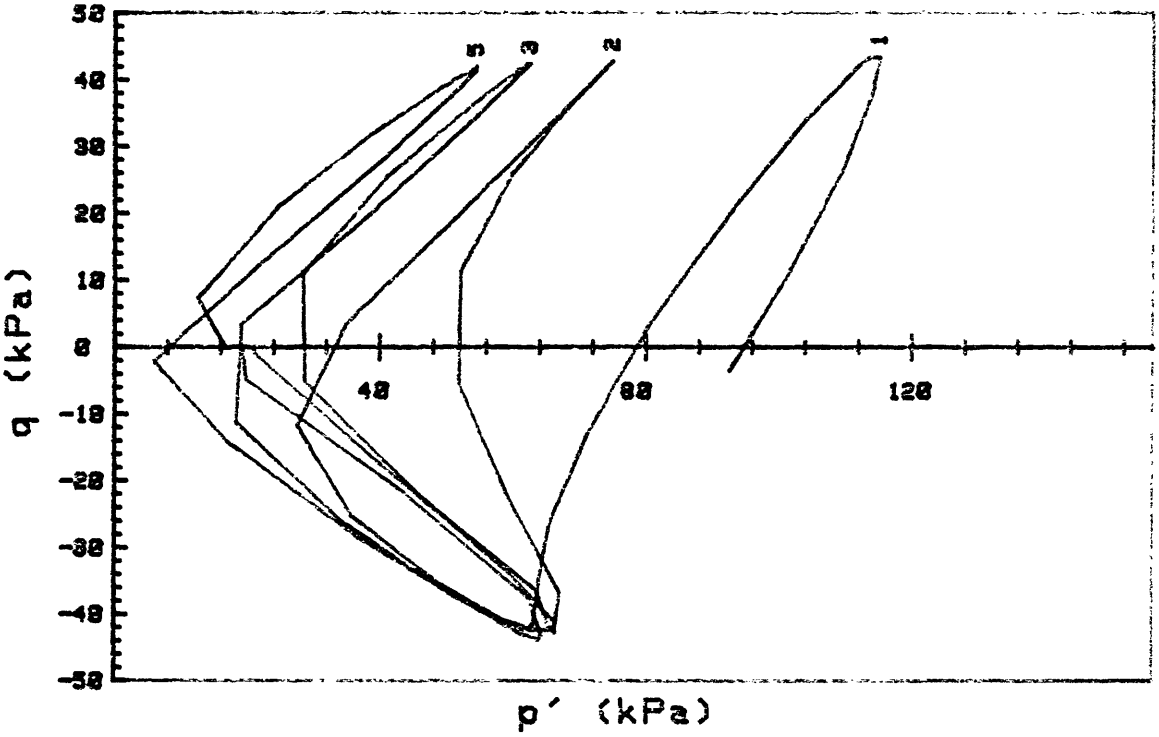

CRUISE ST HELENS		INCREMENT (cm)	REMOLDED SURF
CORE NO.	CC2	TEST NO.	D195
SIG1c'(kPa)	95.9	STATIC qf (kPa)	100.0
SIG3c'(kPa)	95.9	AVG MAX q (kPa)	42.6 (42.6%)
INDUCED OCR	1.0	AVG MIN q (kPa)	-42.0 (42.0%)

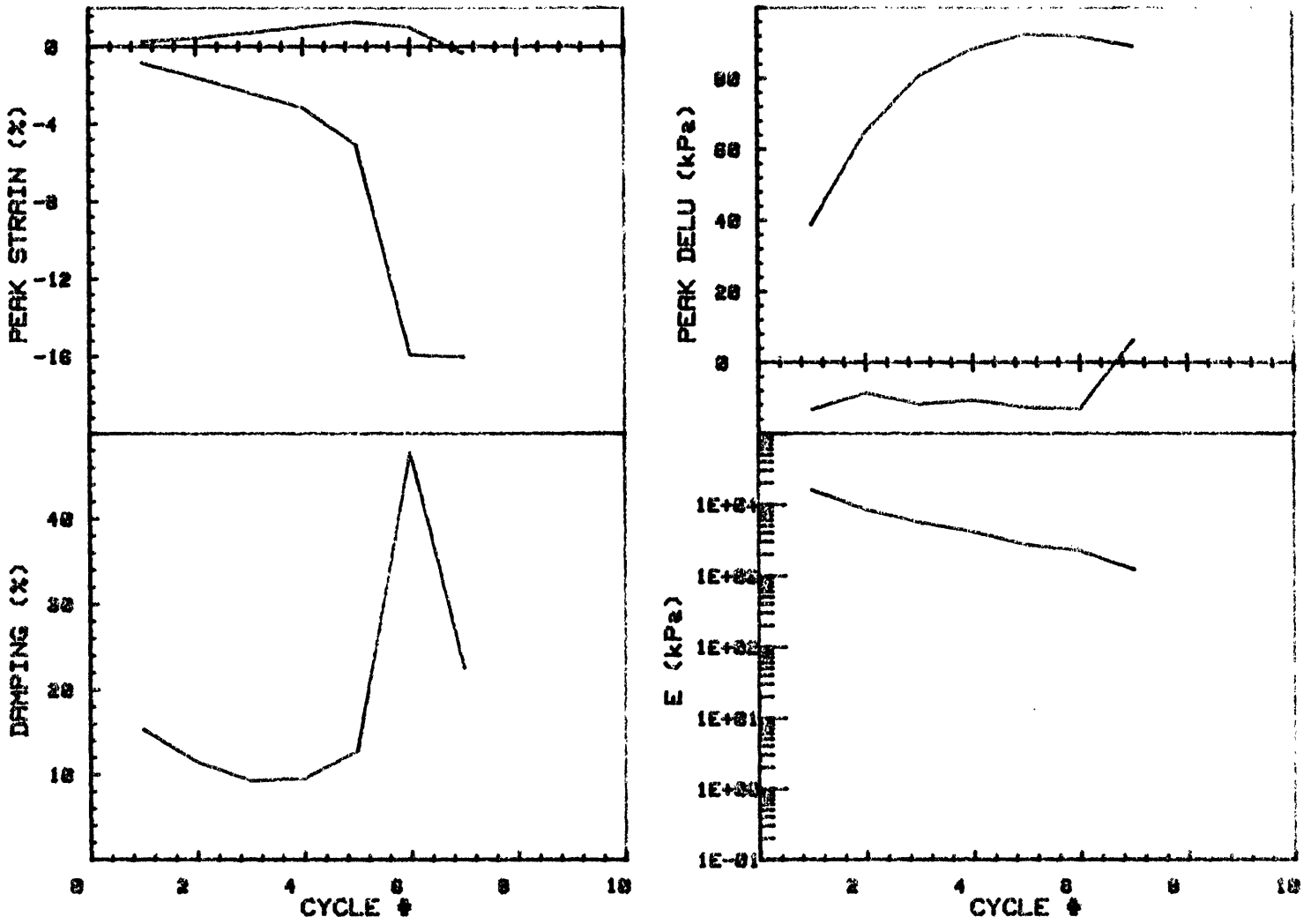

CRUISE ST HELENS		INCREMENT (cm)	REMOLDED SURF
CORE NO.	CC2	TEST NO.	D195
SIG1c'(kPa)	95.9	STATIC qf (kPa)	100.0
SIG3c'(kPa)	95.9	AVG MAX q (kPa)	42.6 (42.6%)
INDUCED OCR	1.0	AVG MIN q (kPa)	-42.0 (42.0%)

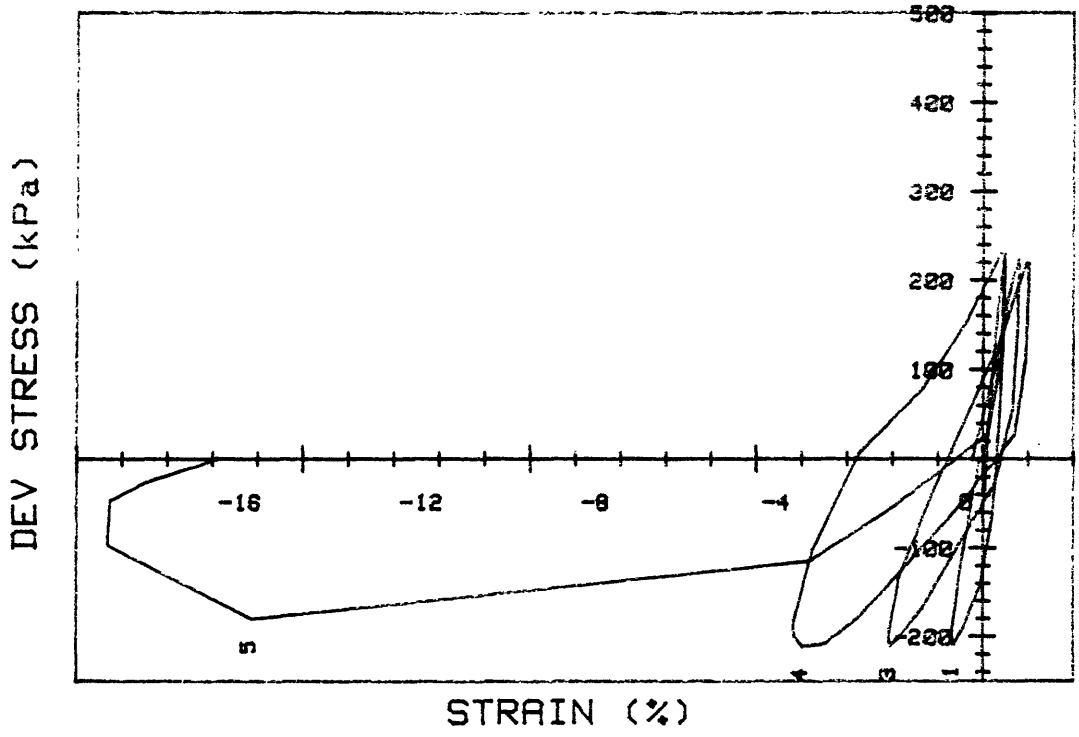

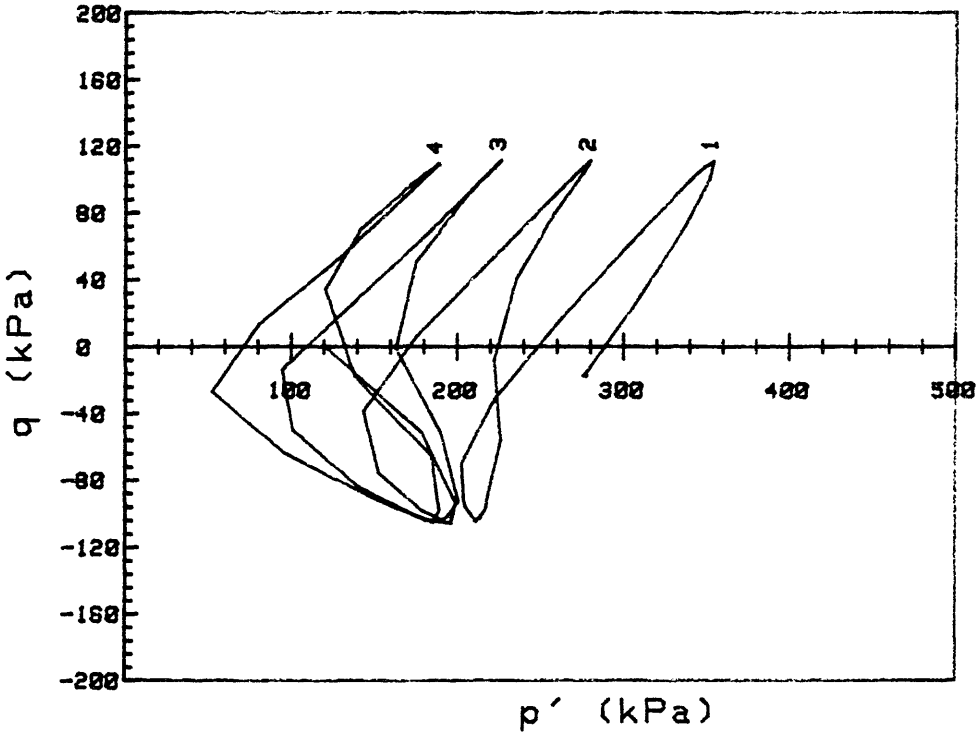

CRUISE SR HELENS		INCREMENT (cm)	REMOLDED SURF
CORE NO. CC2		TEST NO.	D185
SIG1c´(kPa)	294.9	STATIC qf (kPa)	300.0
SIG3c´(kPa)	294.9	AVG MAX q (kPa)	115.2 (38.4%)
INDUCED OCR	1.0	AVG MIN q (kPa)	-91.2 (30.4%)

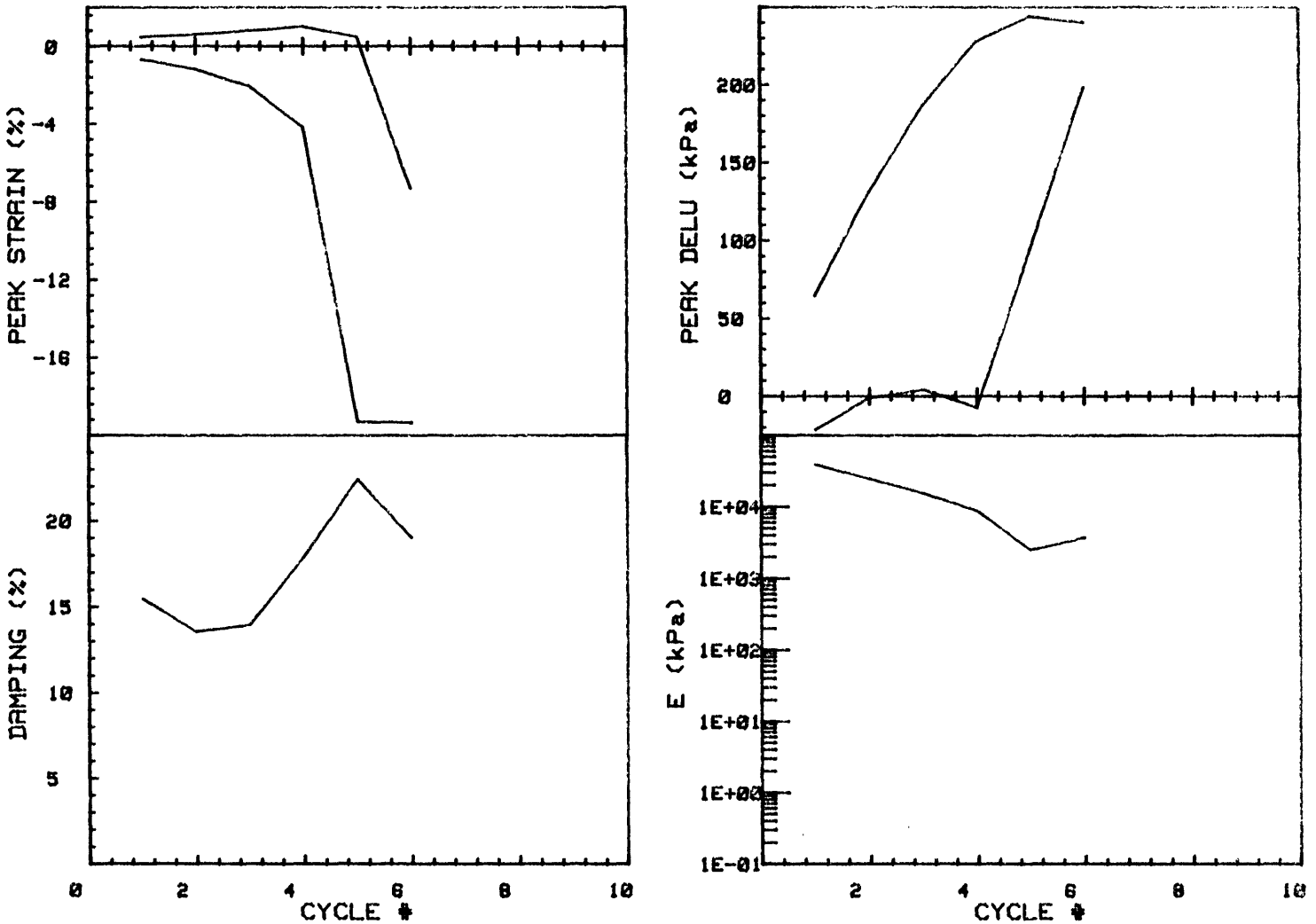

CRUISE SR HELENS		INCREMENT (cm)	REMOLDED SURF
CORE NO.	CC2	TEST NO.	D105
SIG1c'(kPa)	294.9	STATIC qf (kPa)	300.0
SIG3c'(kPa)	294.9	AVG MAX q (kPa)	115.2 (38.4%)
INDUCED OCR	1.0	AVG MIN q (kPa)	-91.2 (30.4%)

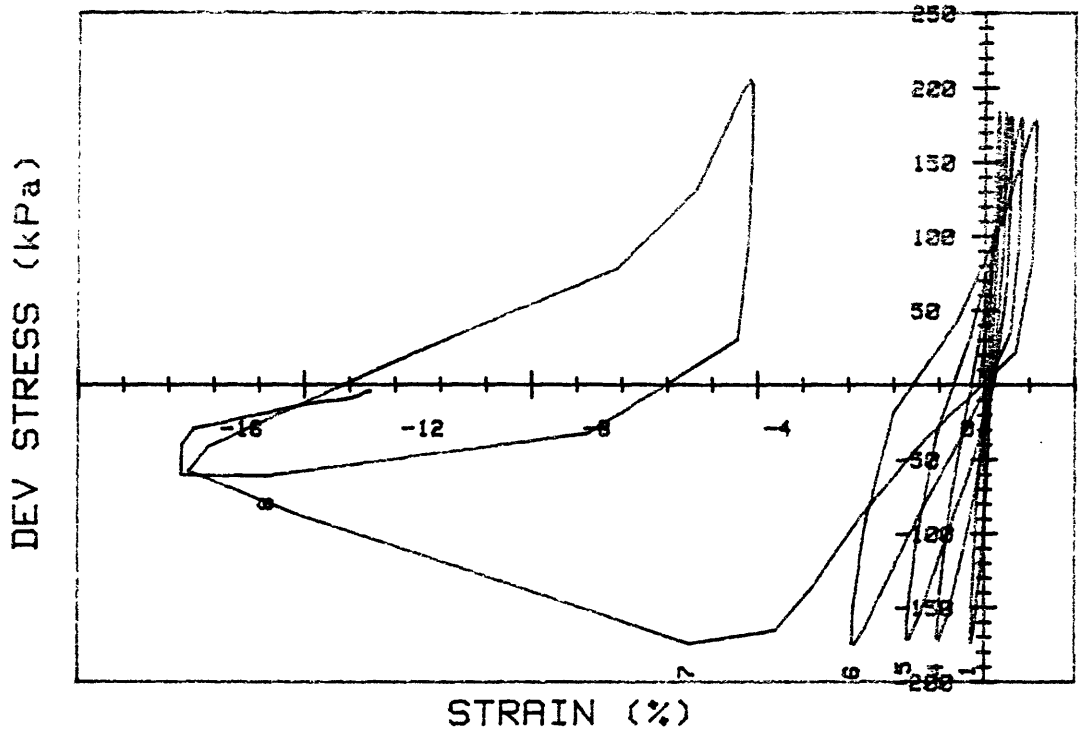

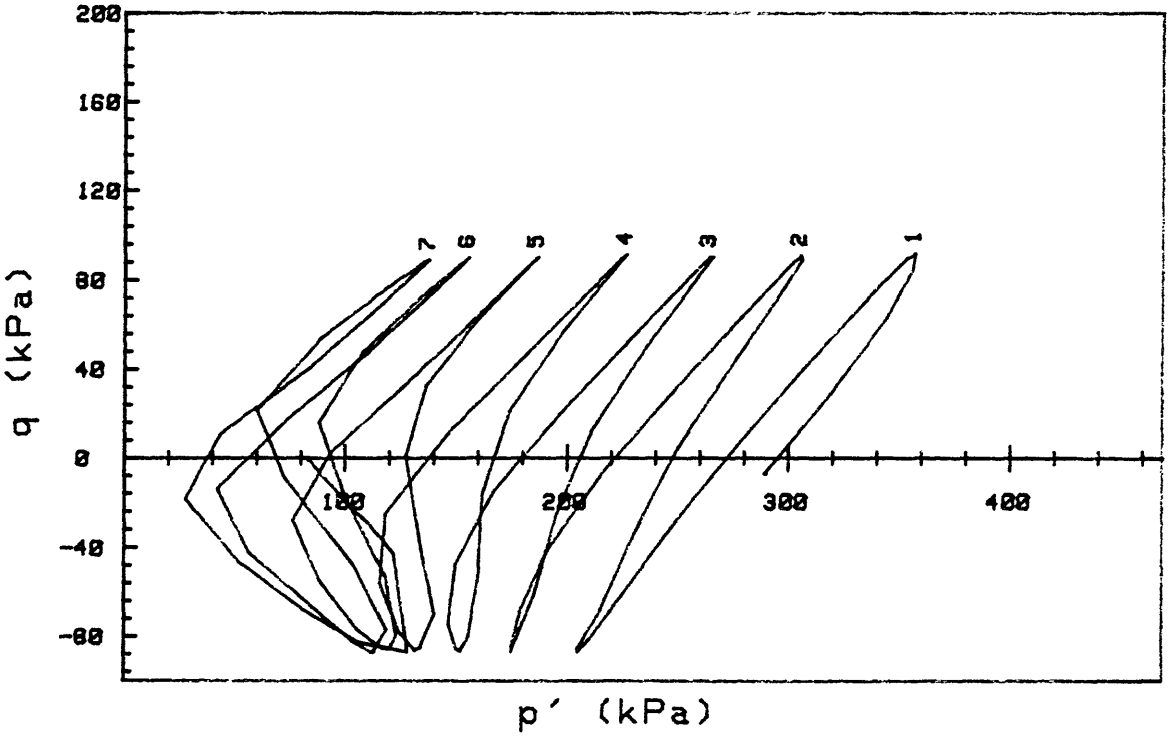

CRUISE ST HELENS		INCREMENT (cm)	REMOLDED SURF
CORE NO.	CC2	TEST NO.	D186
SIG1c'(kPa)	297.3	STATIC qf (kPa)	300.0
SIG3c'(kPa)	297.3	AVG MAX q (kPa)	92.1 (30.7%)
INDUCED OCR	1.0	AVG MIN q (kPa)	-79.7 (26.6%)

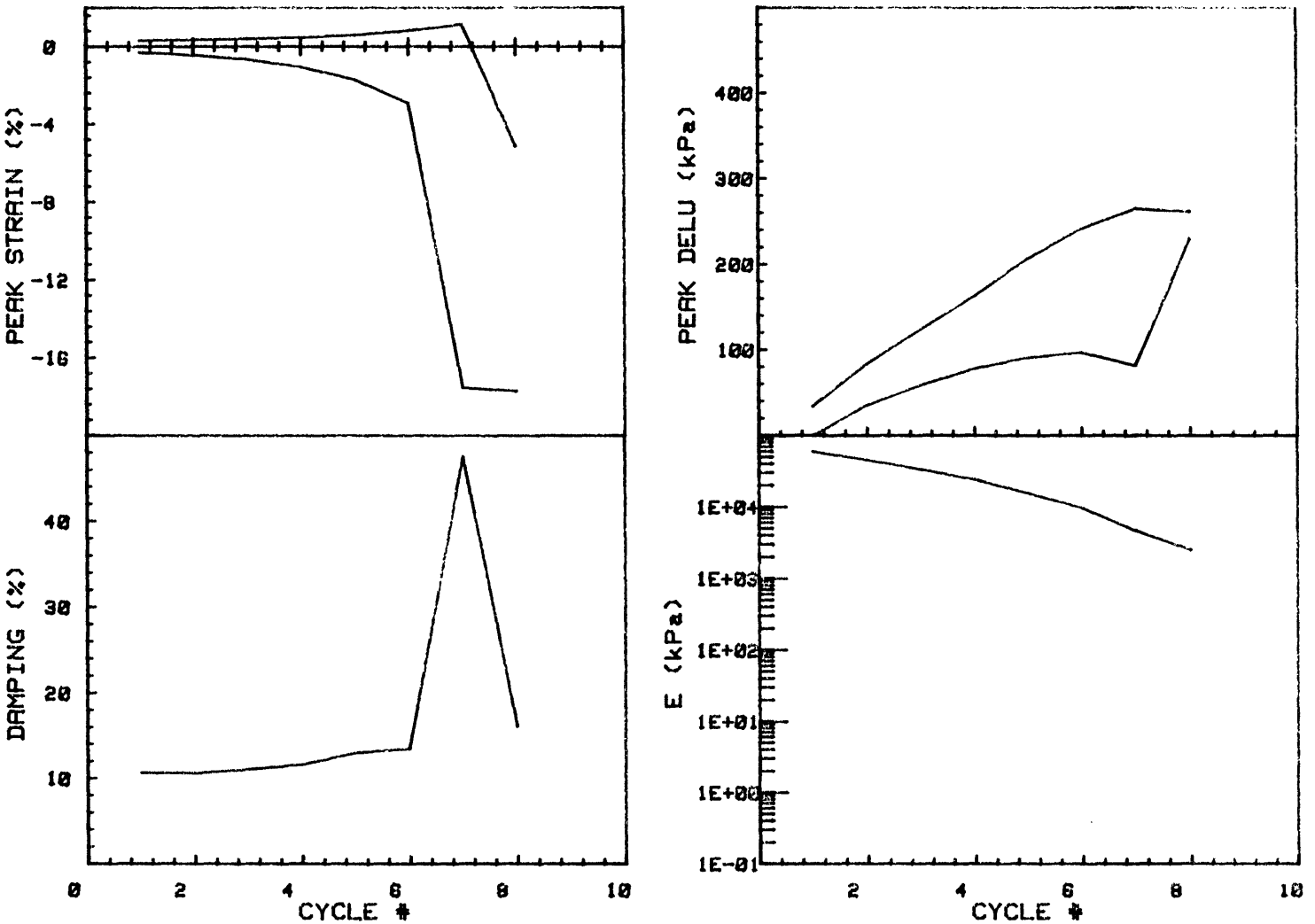

CRUISE ST HELENS		INCREMENT (cm)	REMOLDED SURF
CORE NO. CC2		TEST NO.	D186
SIG1c'(kPa)	297.3	STATIC qf (kPa)	300.0
SIG3c'(kPa)	297.3	AVG MAX q (kPa)	92.1 (30.7%)
INDUCED OCR	1.0	AVG MIN q (kPa)	-79.7 (26.6%)

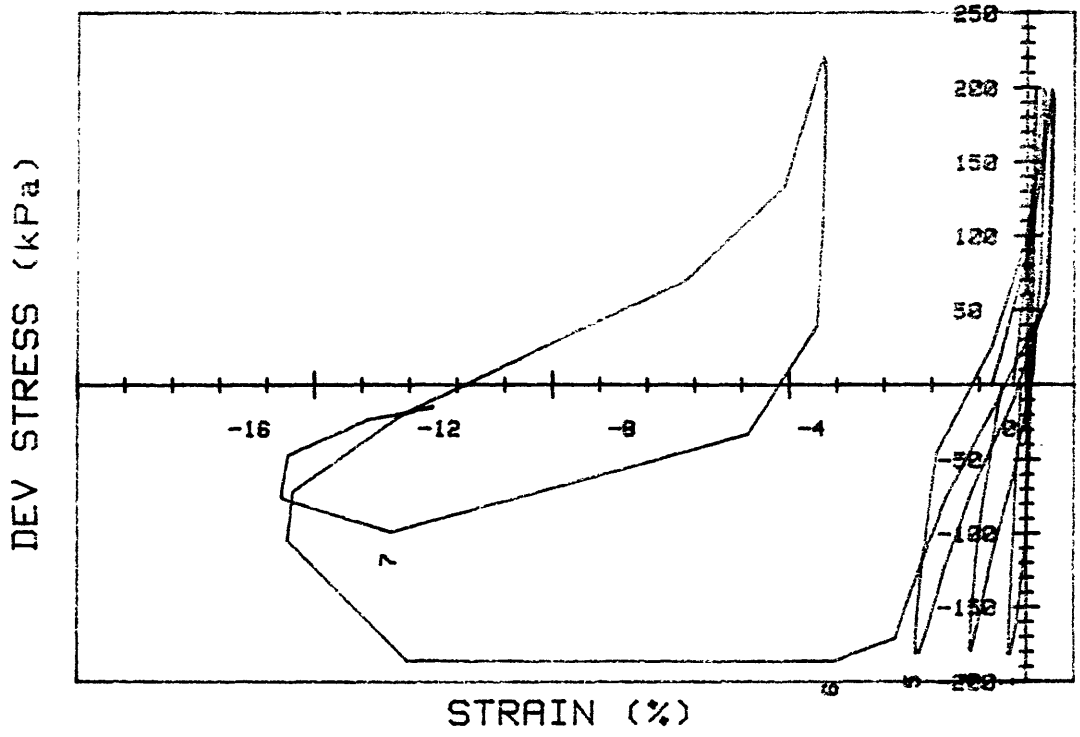

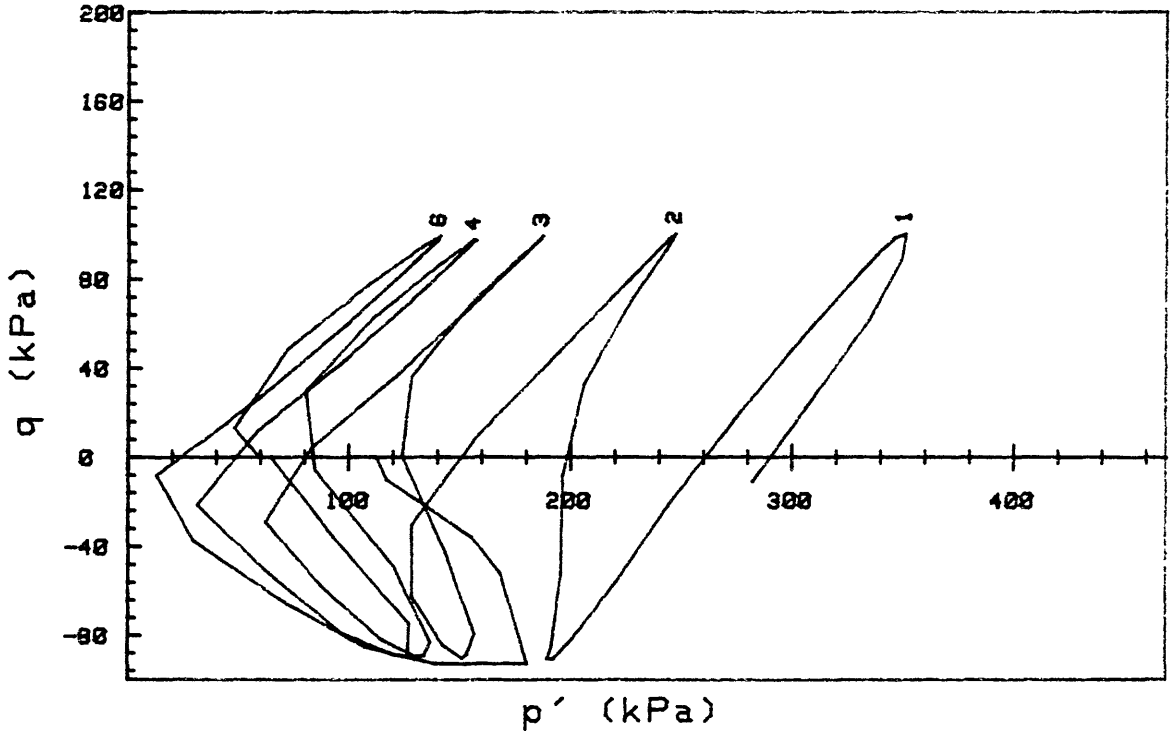

CRUISE ST HELENS		INCREMENT (cm)	REMOLDED SURF
CORE NO. CC2		TEST NO.	D187
SIG1c´(kPa)	293.2	STATIC qf (kPa)	300.0
SIG3c´(kPa)	293.2	AVG MAX q (kPa)	100.7 (33.6%)
INDUCED OCR	1.0	AVG MIN q (kPa)	-84.9 (28.3%)

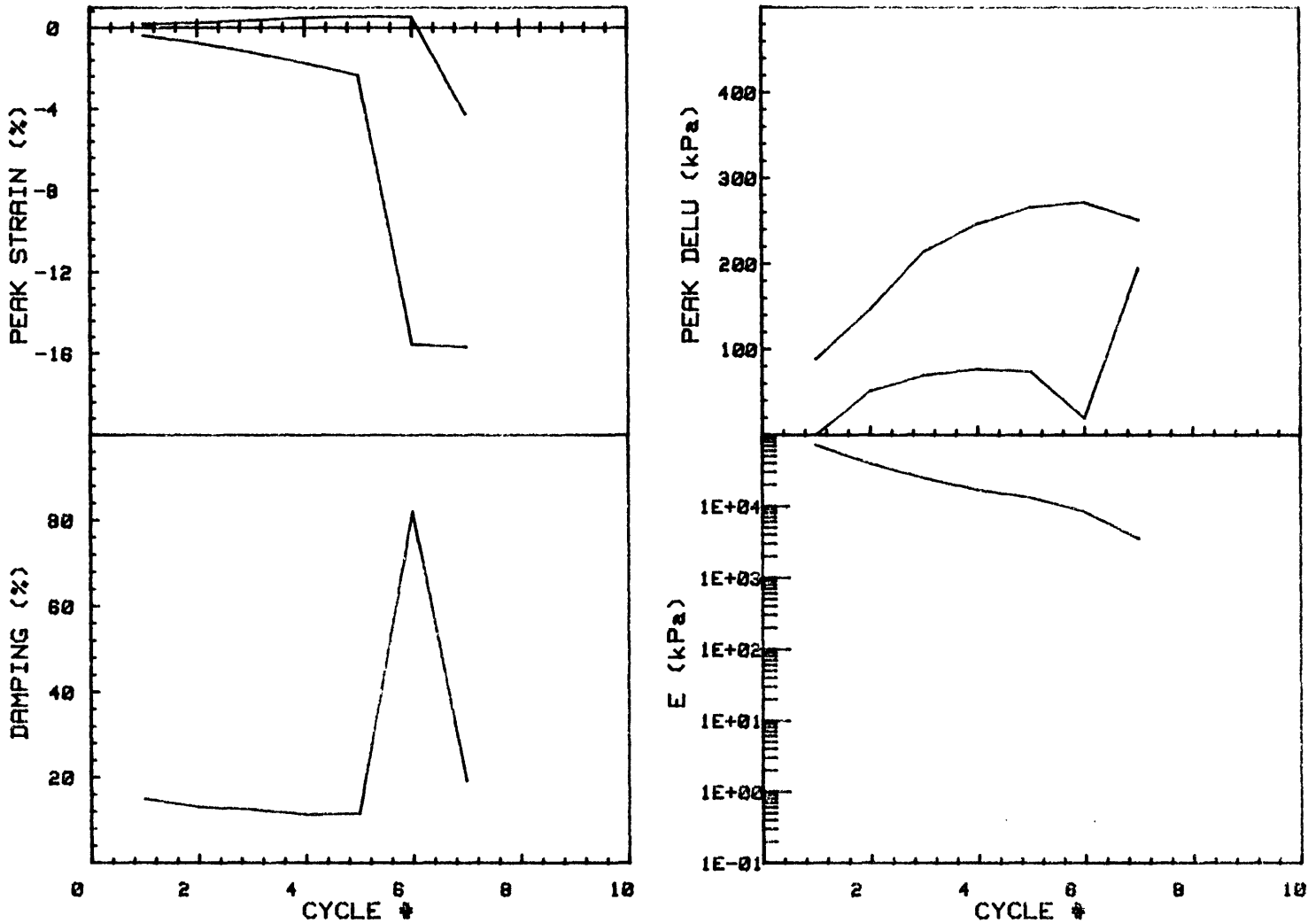

CRUISE ST HELENS		INCREMENT (cm)	REMOLDED SURF
CORE NO.	CC2	TEST NO.	D187
SIG1c'(kPa)	293.2	STATIC qf (kPa)	300.0
SIG3c'(kPa)	293.2	AVG MAX q (kPa)	100.7 (33.6%)
INDUCED OCR	1.0	AVG MIN q (kPa)	-84.9 (28.3%)

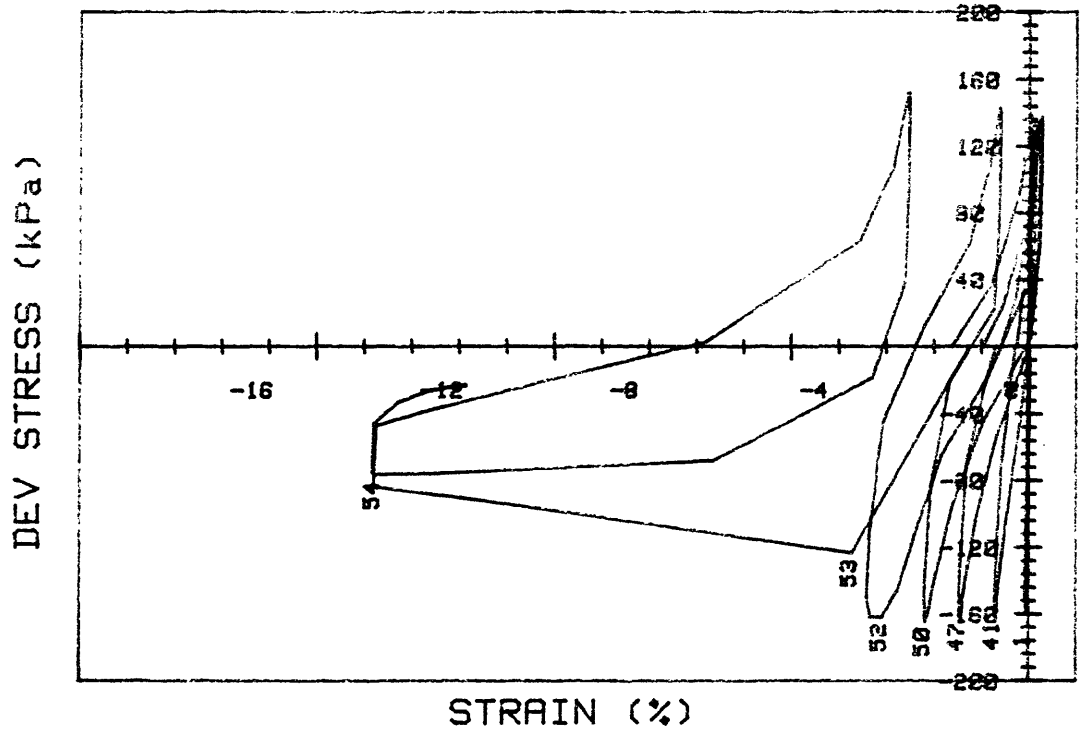

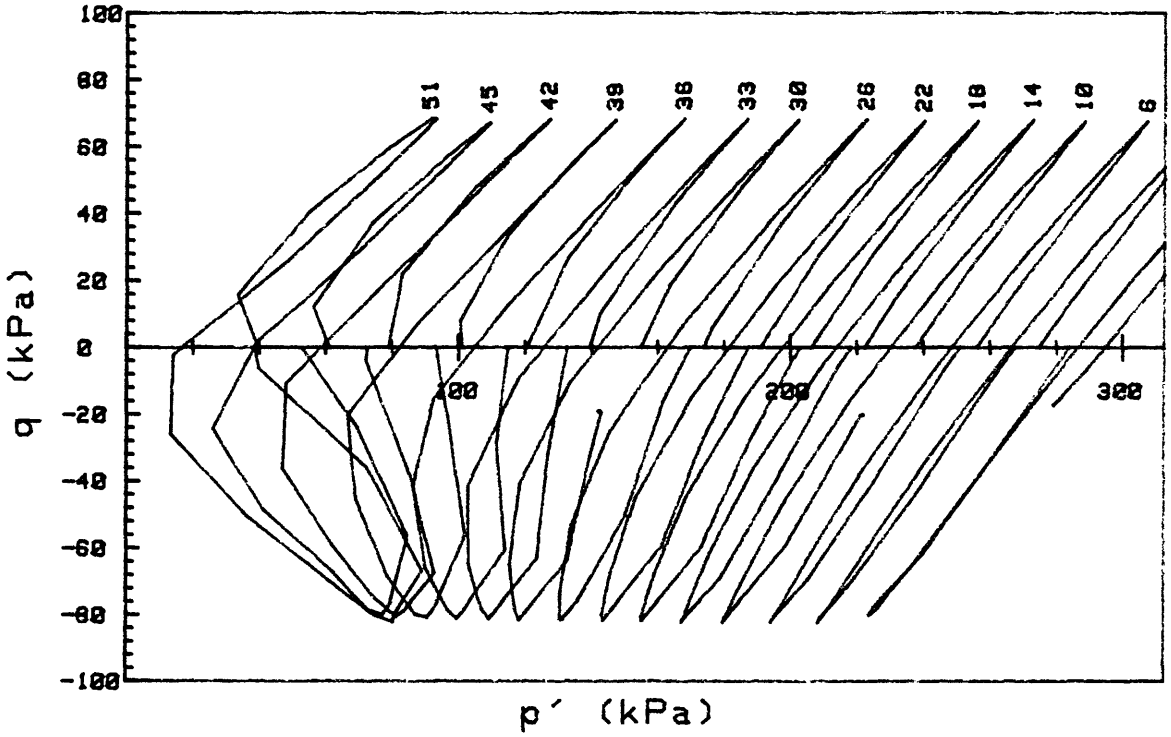

CRUISE ST HELENS		INCREMENT (cm)	REMOLDED SURF
CORE NO. CC2		TEST NO.	D188
SIG1c´(kPa)	296.5	STATIC qf (kPa)	300.0
SIG3c´(kPa)	296.5	AVG MAX q (kPa)	68.0 (22.7%)
INDUCED OCR	1.0	AVG MIN q (kPa)	-80.4 (26.8%)

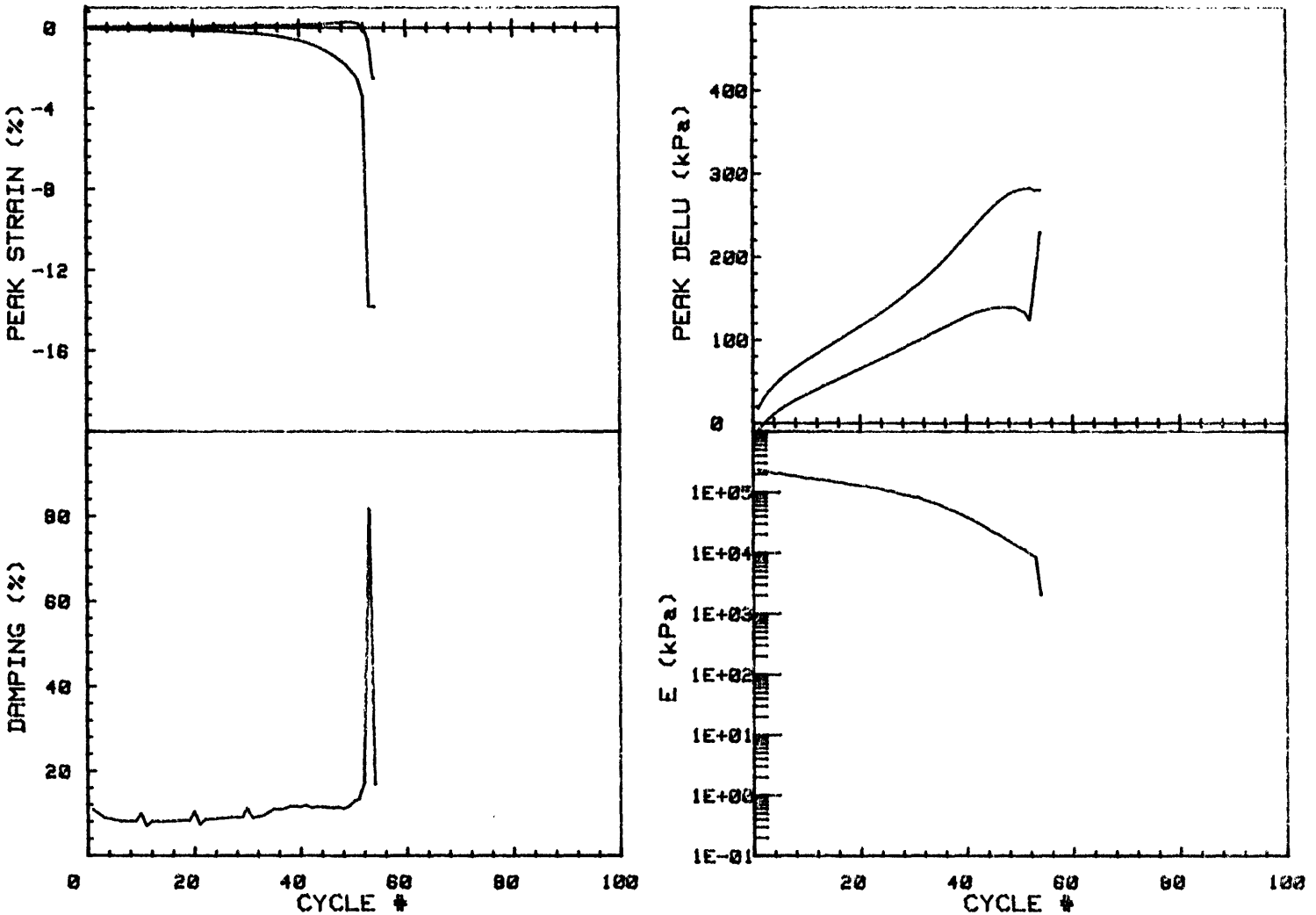

CRUISE ST HELENS		INCREMENT (cm)	REMOLDED SURF
CORE NO.	CC2	TEST NO.	D100
SIG1c'(kPa)	296.5	STATIC qf (kPa)	300.0
SIG3c'(kPa)	296.5	AVG MAX q (kPa)	68.0 (22.7%)
INDUCED OCR	1.0	AVG MIN q (kPa)	-80.4 (26.8%)

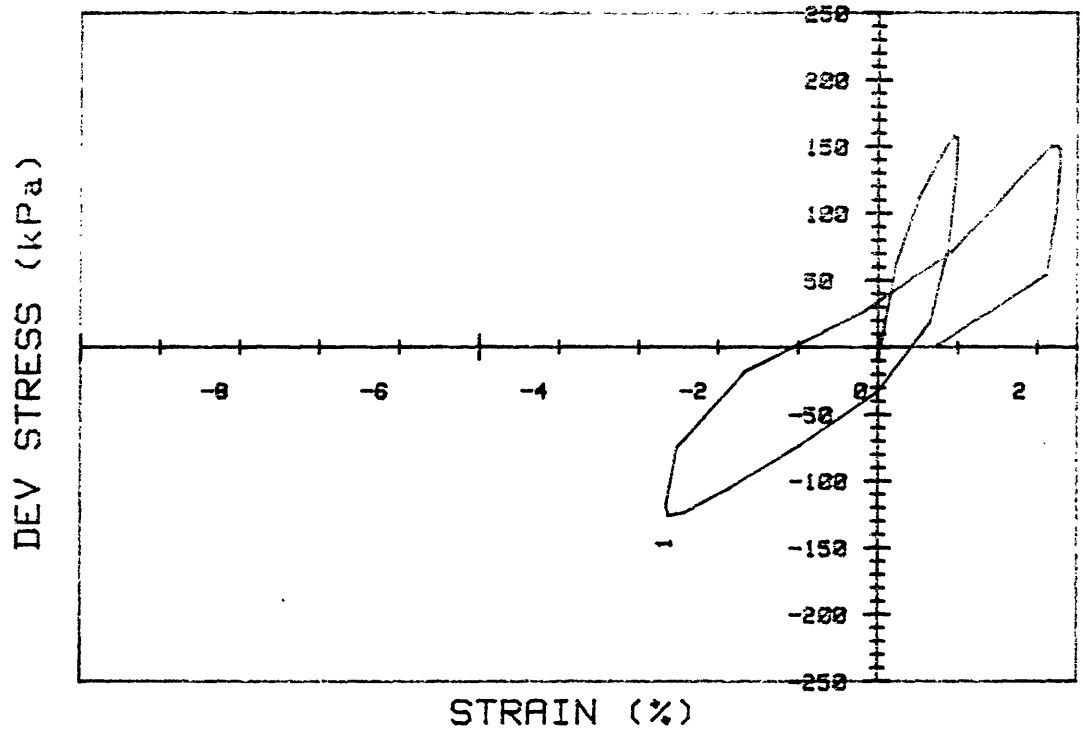

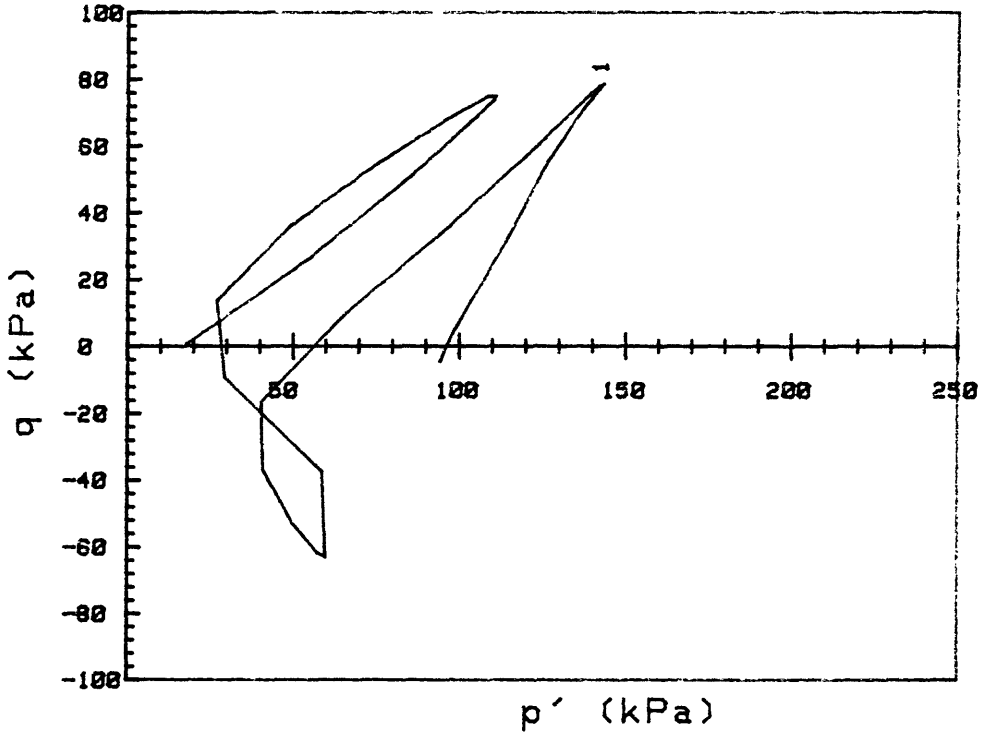

CRUISE ST HELENS		INCREMENT (cm)	ASH (TUBE)
CORE NO.	SL1	TEST NO.	D155
SIG1c'(kPa)	98.7	STATIC qf (kPa)	96.4
SIG3c'(kPa)	98.7	AVG MAX q (kPa)	78.6 (81.5%)
INDUCED OCR	1.0	AVG MIN q (kPa)	-63.2 (65.6%)

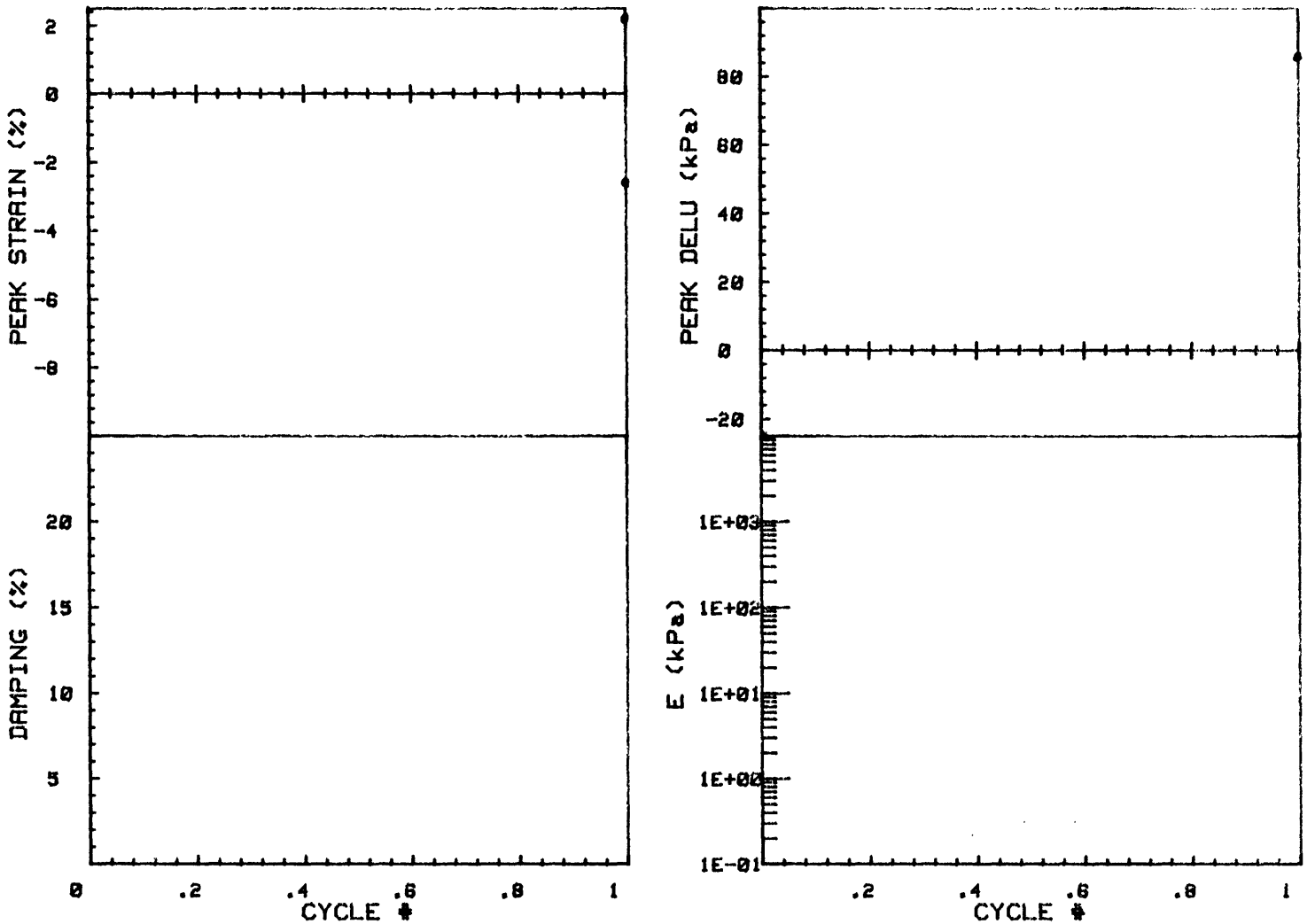

CRUISE ST HELENS		INCREMENT (cm)	ASH (TUBE)
CORE NO.	SL1	TEST NO.	D155
SIG1c'(kPa)	98.7	STATIC qf (kPa)	96.4
SIG3c'(kPa)	98.7	AVG MAX q (kPa)	78.6 (81.5%)
INDUCED OCR	1.0	AVG MIN q (kPa)	-63.2 (65.6%)

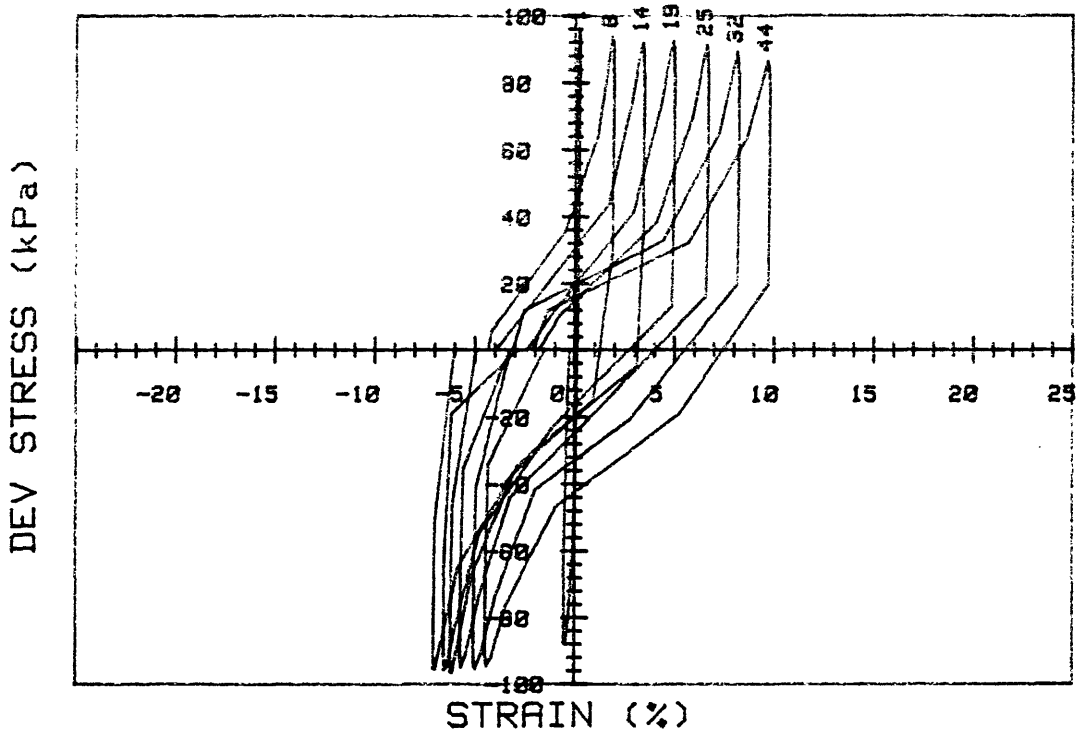

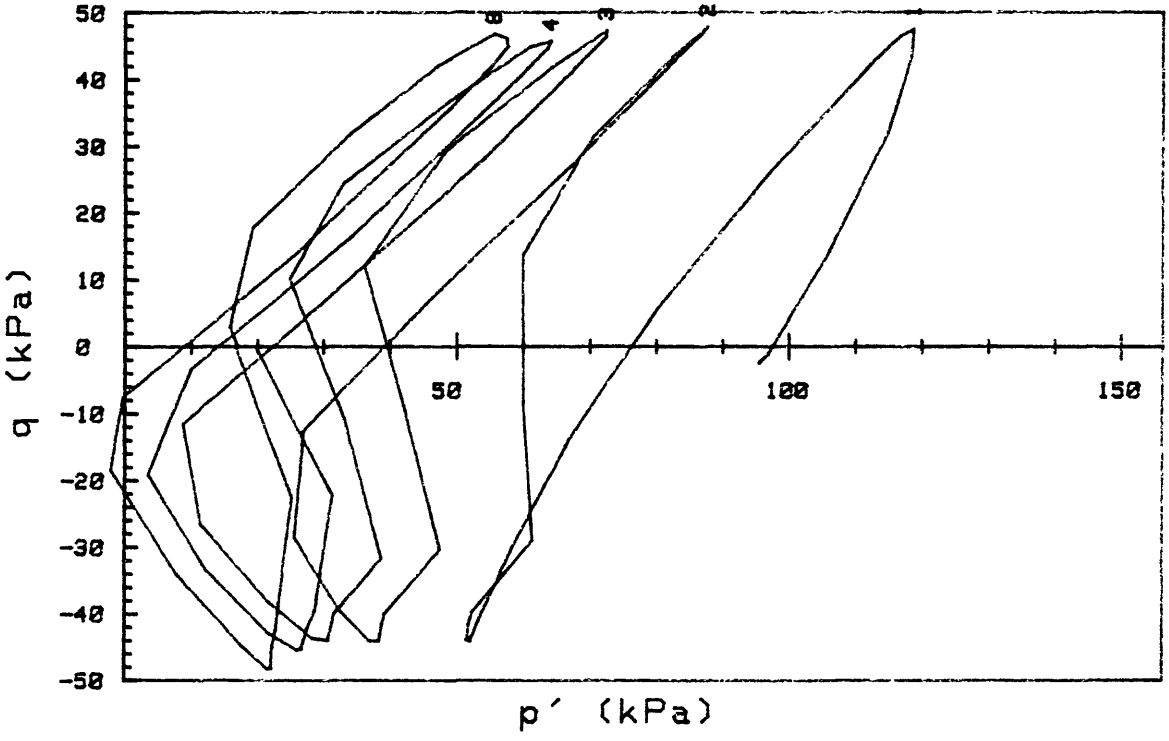

CRUISE ST HELENS		INCREMENT (cm)	ASH (TUBE)
CORE NO.	SL1	TEST NO.	D156
SIG1c´(kPa)	98.0	STATIC qf (kPa)	96.4
SIG3c´(kPa)	98.0	AVG MAX q (kPa)	45.0 (46.7%)
INDUCED OCR	1.0	AVG MIN q (kPa)	-46.9 (48.7%)

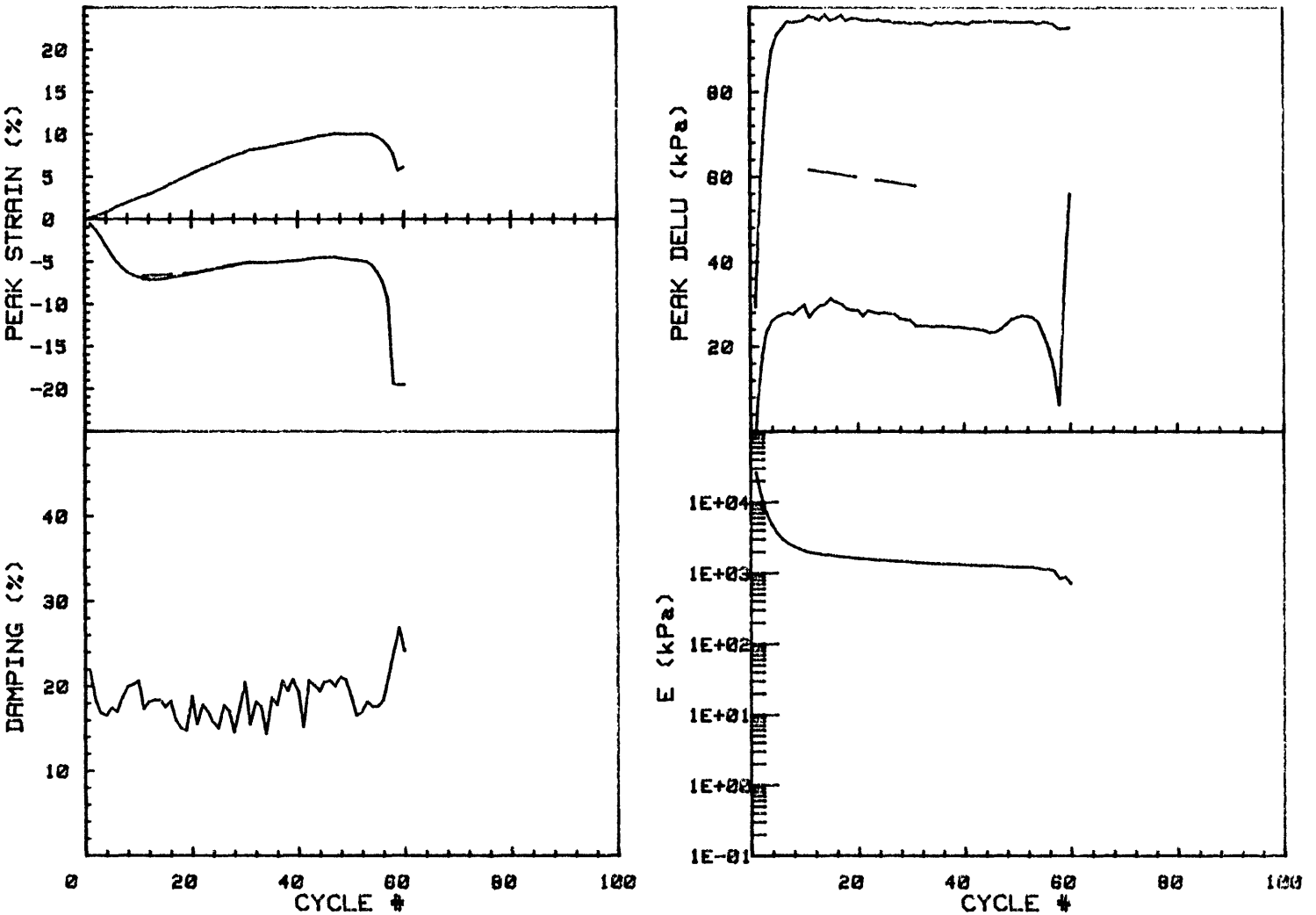

CRUISE ST HELENS		INCREMENT (cm)	ASH (TUBE)
CORE NO.	SL1	TEST NO.	D156
SIG1c'(kPa)	98.0	STATIC qf (kPa)	96.4
SIG3c'(kPa)	98.0	AVG MAX q (kPa)	45.0 (46.7%)
INDUCED OCR	1.0	AVG MIN q (kPa)	-46.9 (48.7%)

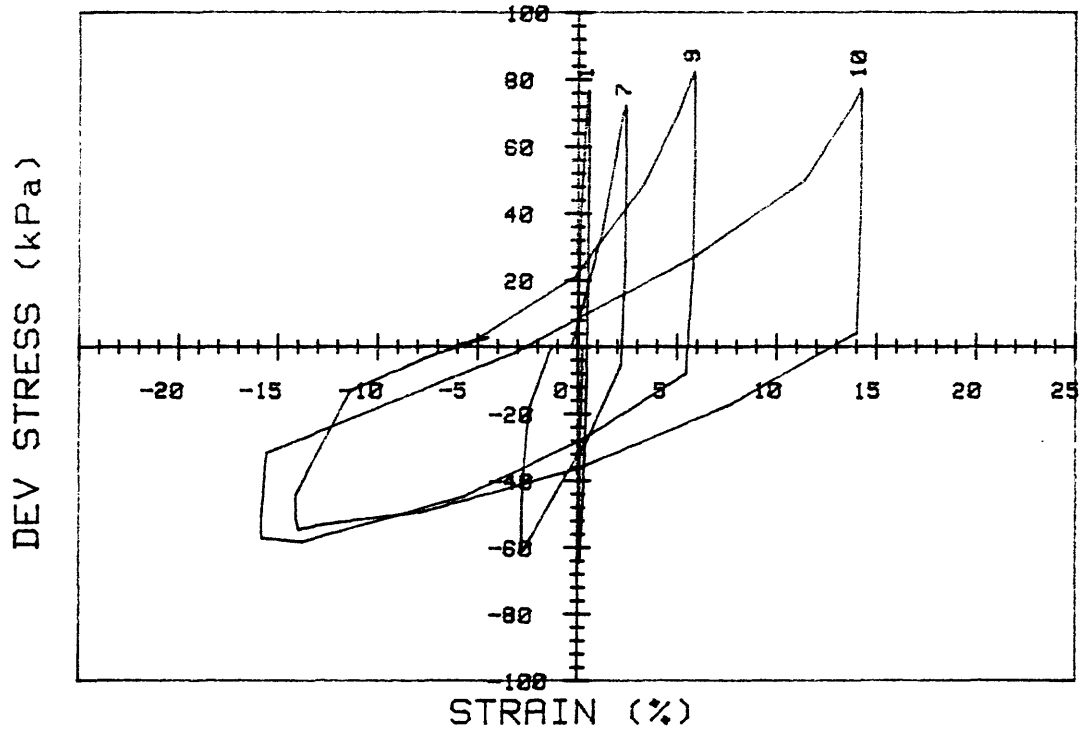

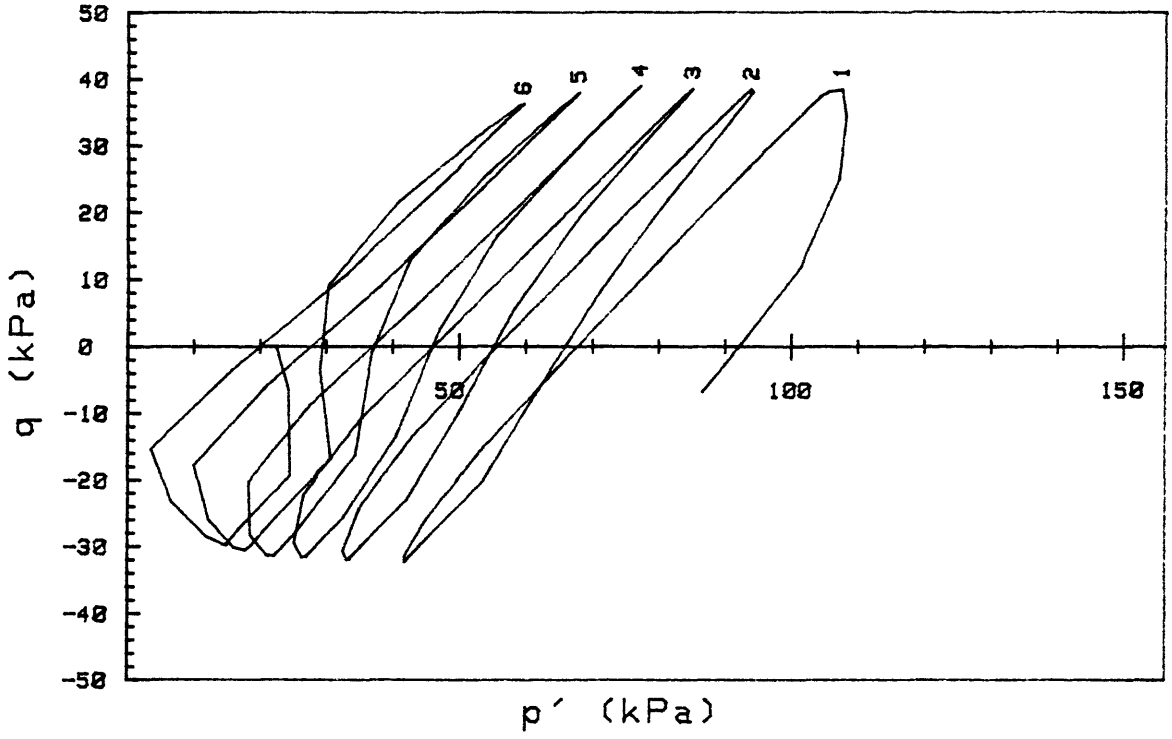

CRUISE ST HELENS		INCREMENT (cm)	REMOLDED-SURF
CORE NO.	SL4	TEST NO.	D163
SIG1c'(kPa)	93.3	STATIC qf (kPa)	100.0
SIG3c'(kPa)	93.3	AVG MAX q (kPa)	38.2 (38.2%)
INDUCED OCR	1.0	AVG MIN q (kPa)	-30.5 (30.5%)

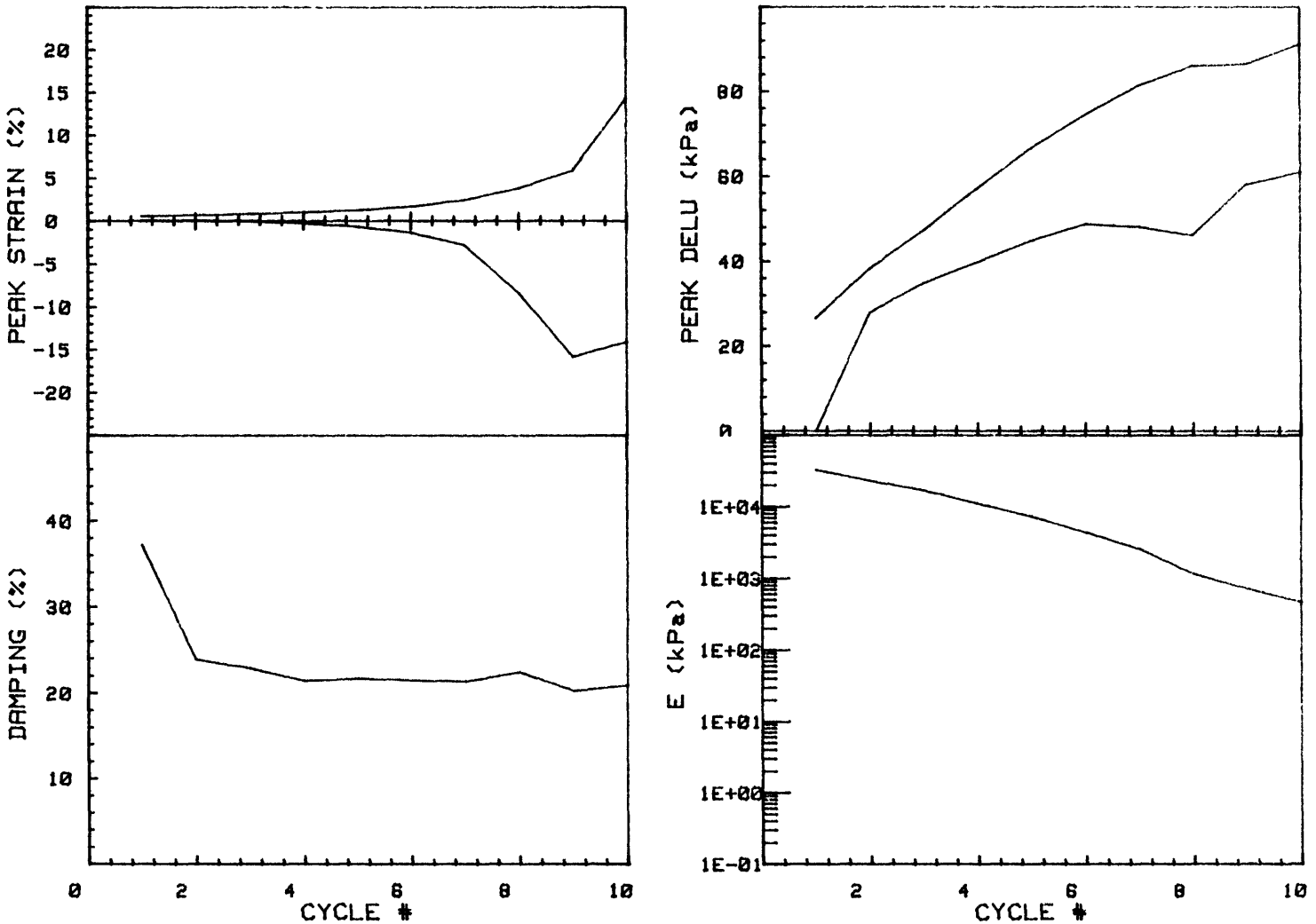

CRUISE ST HELENS		INCREMENT (cm)	REMOLDED-SURF
CORE NO.	SL4	TEST NO.	D163
SIG1c'(kPa)	93.3	STATIC qf (kPa)	100.0
SIG3c'(kPa)	93.3	AVG MAX q (kPa)	38.2 (38.2%)
INDUCED OCR	1.0	AVG MIN q (kPa)	-30.5 (30.5%)

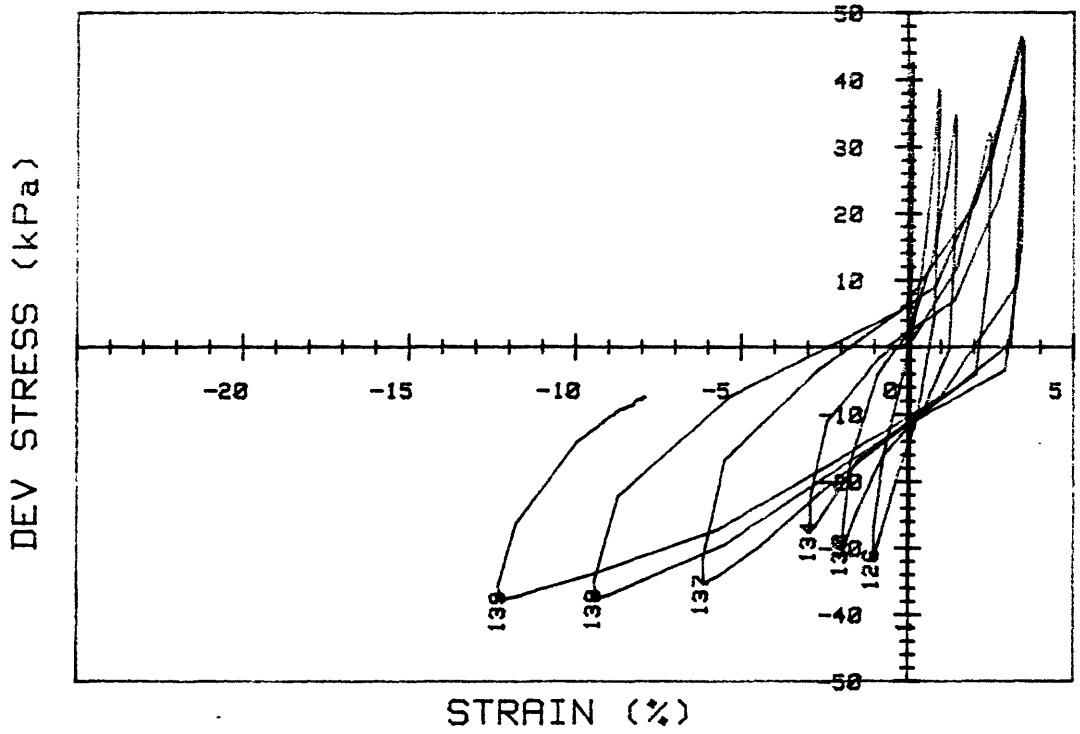

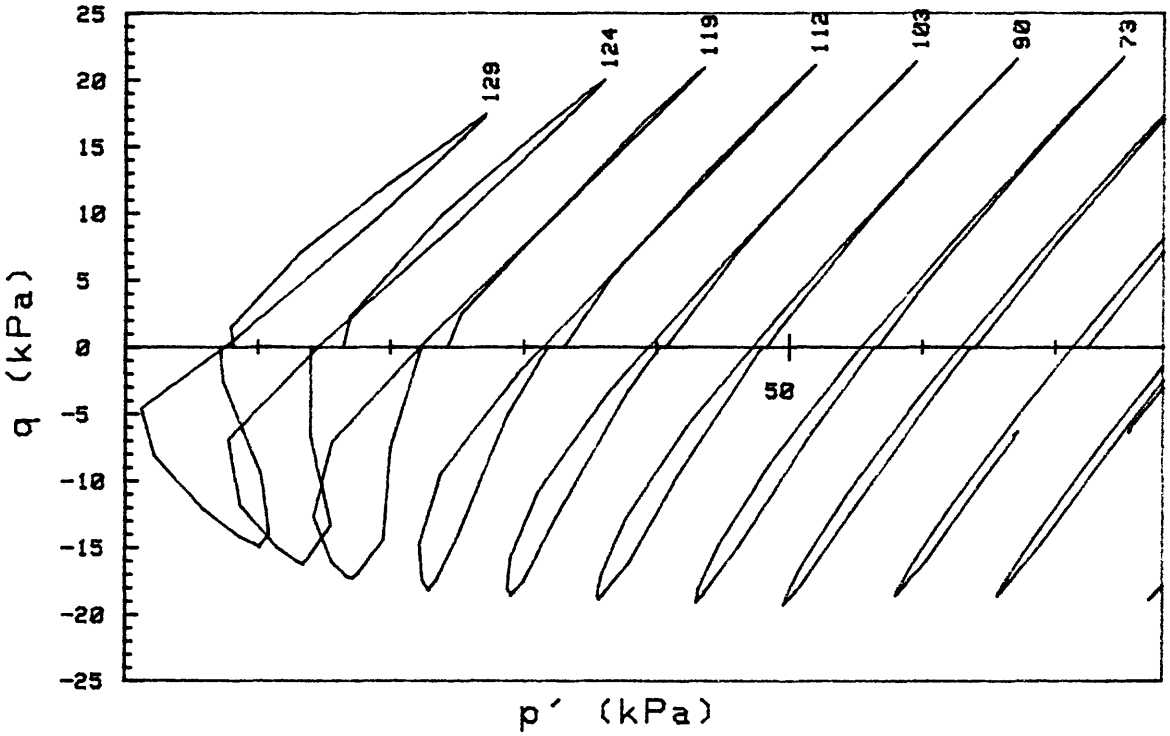

CRUISE ST HELENS		INCREMENT (cm)	REMOLDED-SURF
CORE NO.	SL4	TEST NO.	D164
SIG1c'(kPa)	96.0	STATIC qf (kPa)	100.0
SIG3c'(kPa)	96.0	AVG MAX q (kPa)	21.1 (21.1%)
INDUCED OCR	1.0	AVG MIN q (kPa)	-18.3 (18.3%)

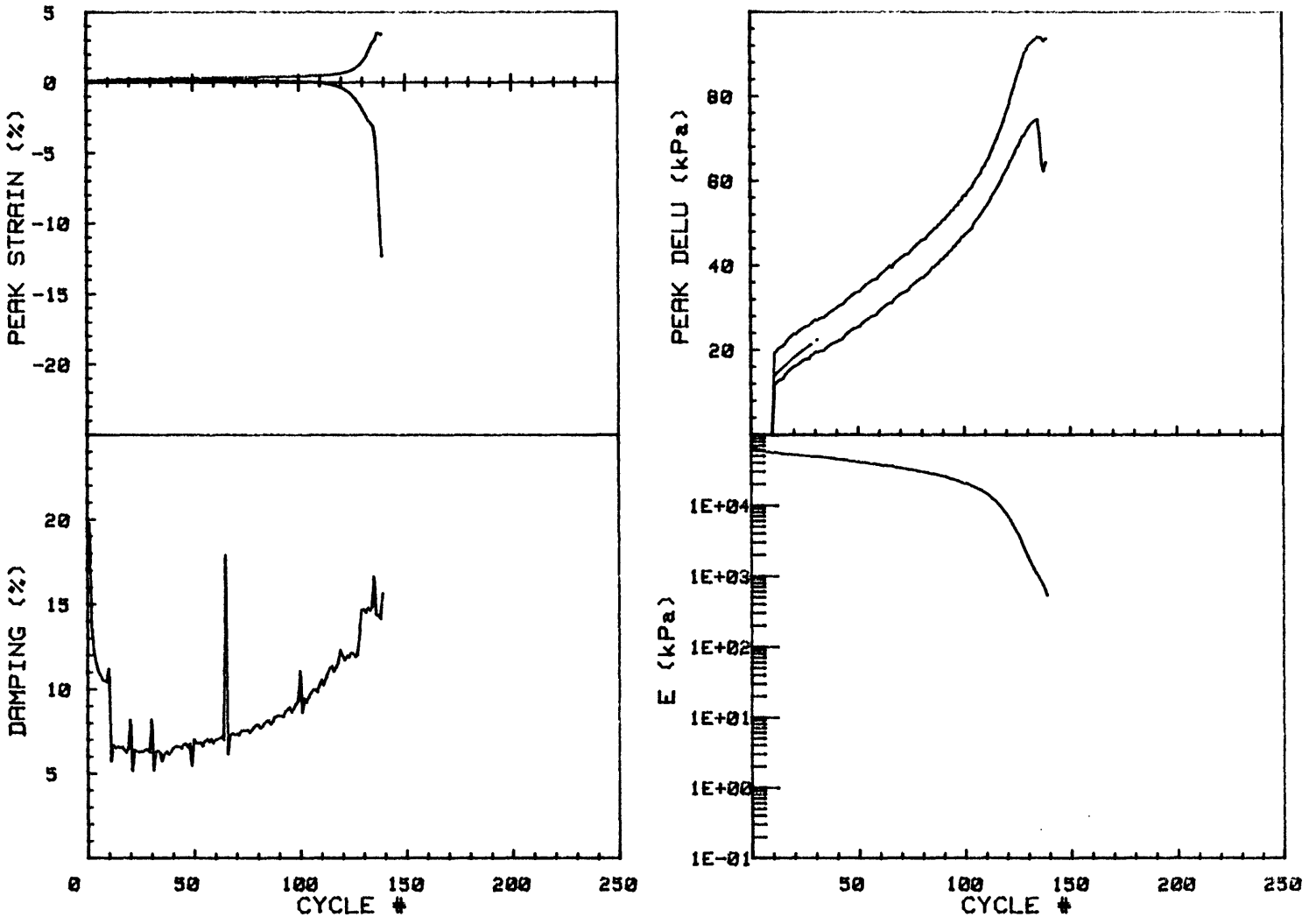

CRUISE ST HELENS		INCREMENT (cm)	REMOLDED-SURF
CORE NO.	SL4	TEST NO.	D164
SIG1c'(kPa)	96.0	STATIC qf (kPa)	100.0
SIG3c'(kPa)	96.0	AVG MAX q (kPa)	21.1 (21.1%)
INDUCED OCR	1.0	AVG MIN q (kPa)	-18.3 (18.3%)

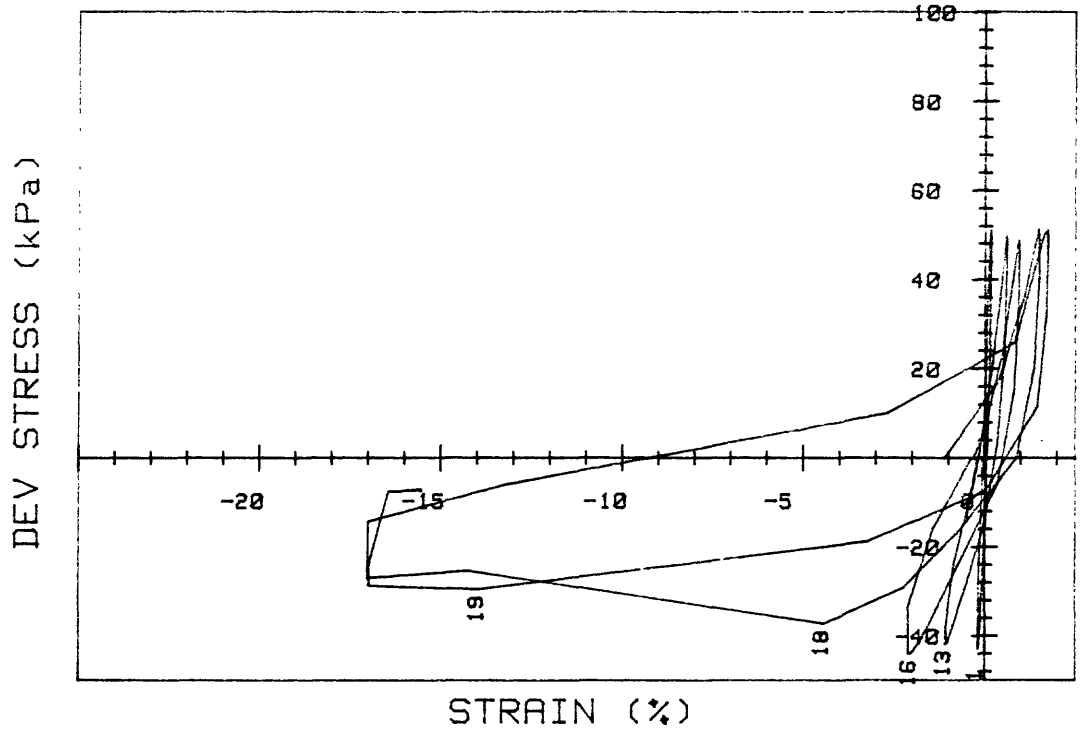

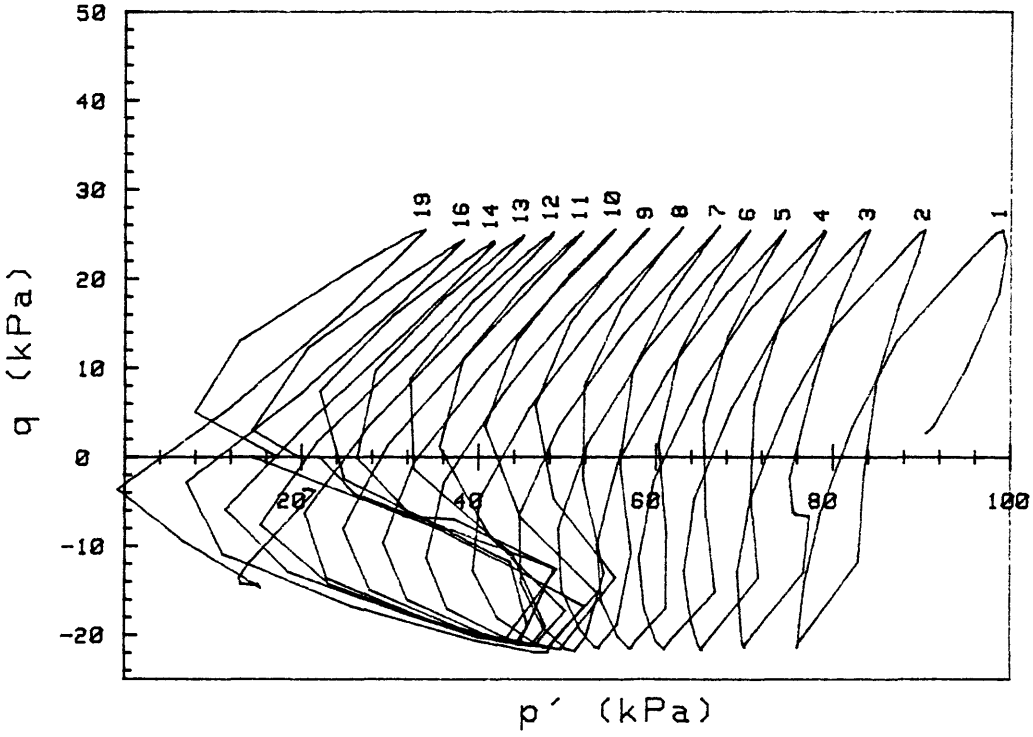

CRUISE ST HELENS		INCREMENT (cm)	REMOLDED-SURF
CORE NO.	SL4	TEST NO.	D165
SIG1c´(kPa)	87.8	STATIC qf (kPa)	100.0
SIG3c´(kPa)	87.8	AVG MAX q (kPa)	25.2 (25.2%)
INDUCED OCR	1.0	AVG MIN q (kPa)	-20.9 (20.9%)

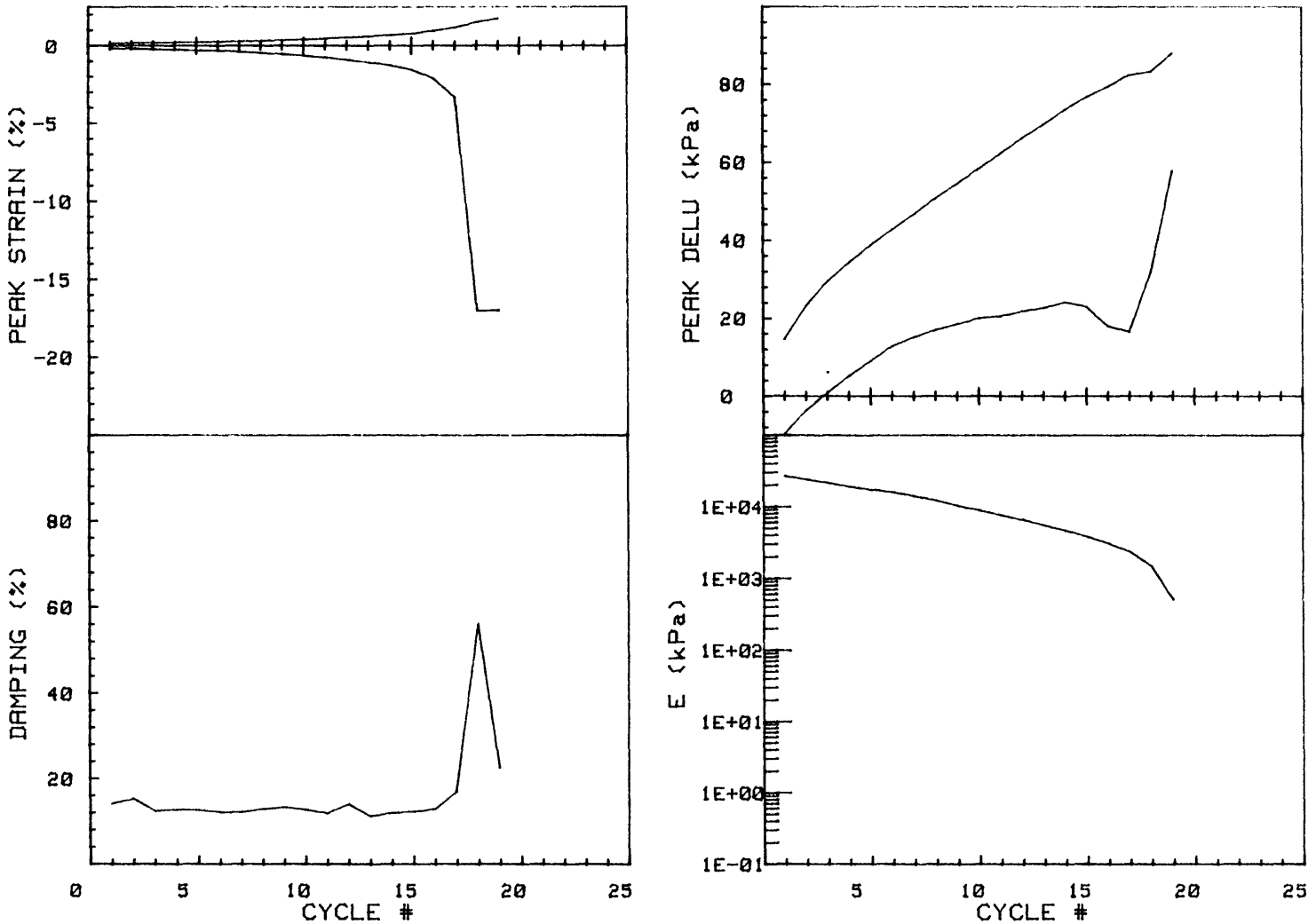

CRUISE ST HELENS		INCREMENT (cm)	REMOLDED-SURF
CORE NO.	SL4	TEST NO.	D165
SIG1c'(kPa)	87.8	STATIC qf (kPa)	100.0
SIG3c'(kPa)	87.8	AVG MAX q (kPa)	25.2 (25.2%)
INDUCED OCR	1.0	AVG MIN q (kPa)	-20.9 (20.9%)

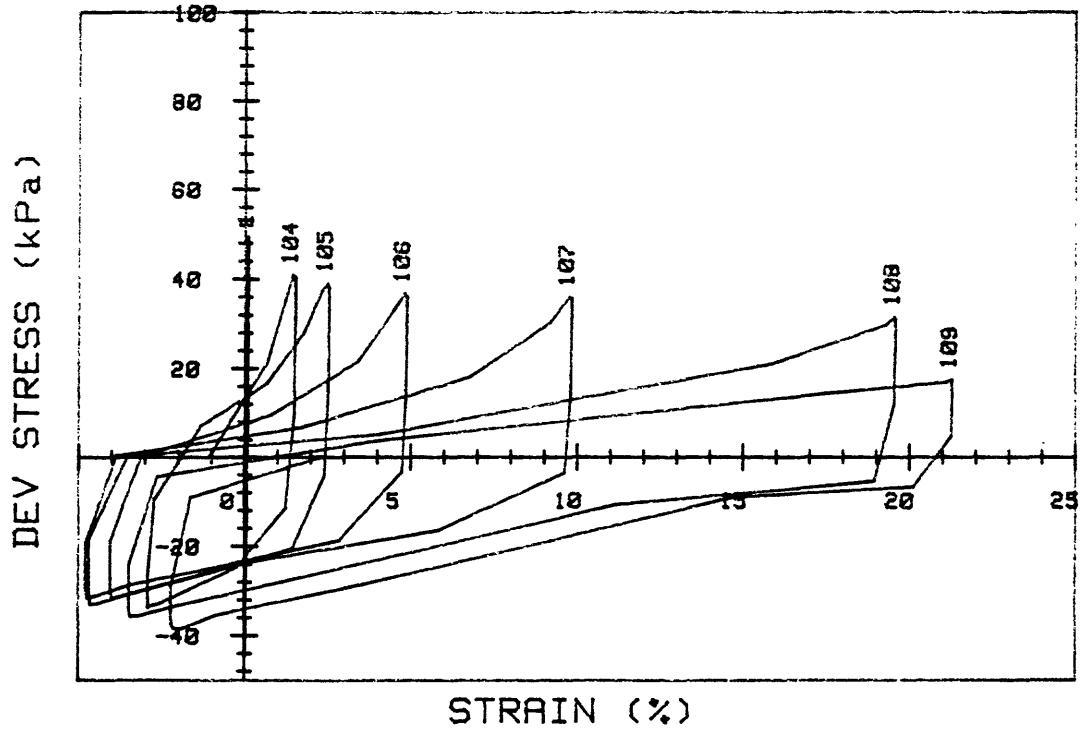

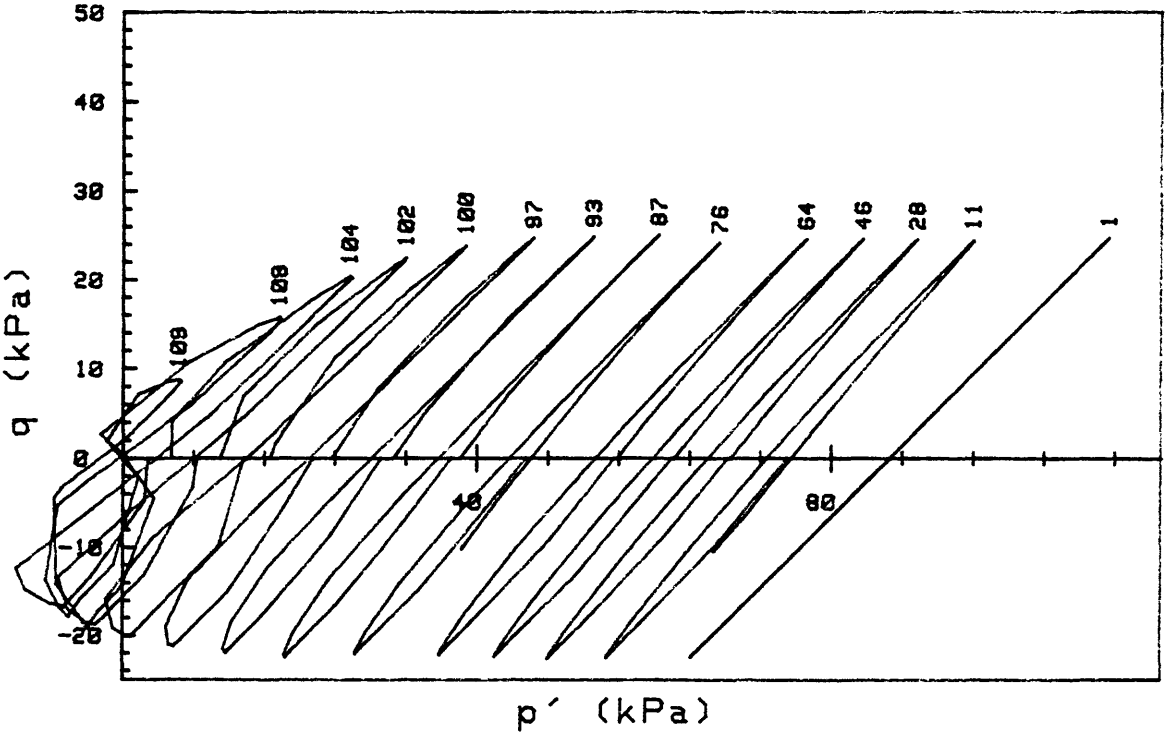

CRUISE ST HELENS		INCREMENT (cm)	REMOLDED-SURF
CORE NO.	SL4	TEST NO.	D166
SIG1c´(kPa)	86.6	STATIC qf (kPa)	100.0
SIG3c´(kPa)	86.6	AVG MAX q (kPa)	23.9 (23.9%)
INDUCED OCR	1.0	AVG MIN q (kPa)	-21.9 (21.9%)

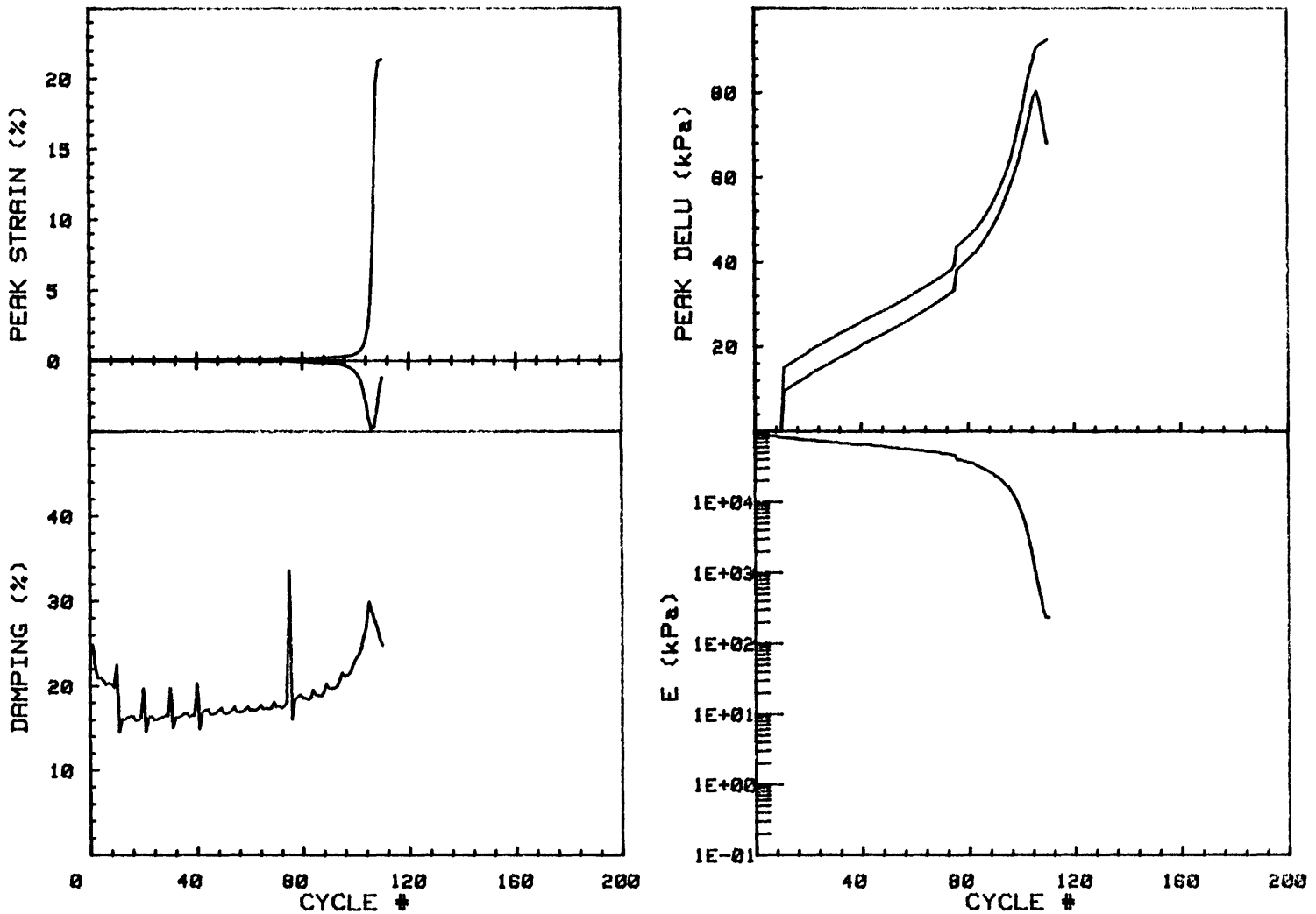

CRUISE ST HELENS		INCREMENT (cm)	REMOLDED-SURF
CORE NO.	SL4	TEST NO.	D166
SIG1c'(kPa)	86.6	STATIC qf (kPa)	100.0
SIG3c'(kPa)	86.6	AVG MAX q (kPa)	23.9 (23.9%)
INDUCED OCR	1.0	AVG MIN q (kPa)	-21.9 (21.9%)

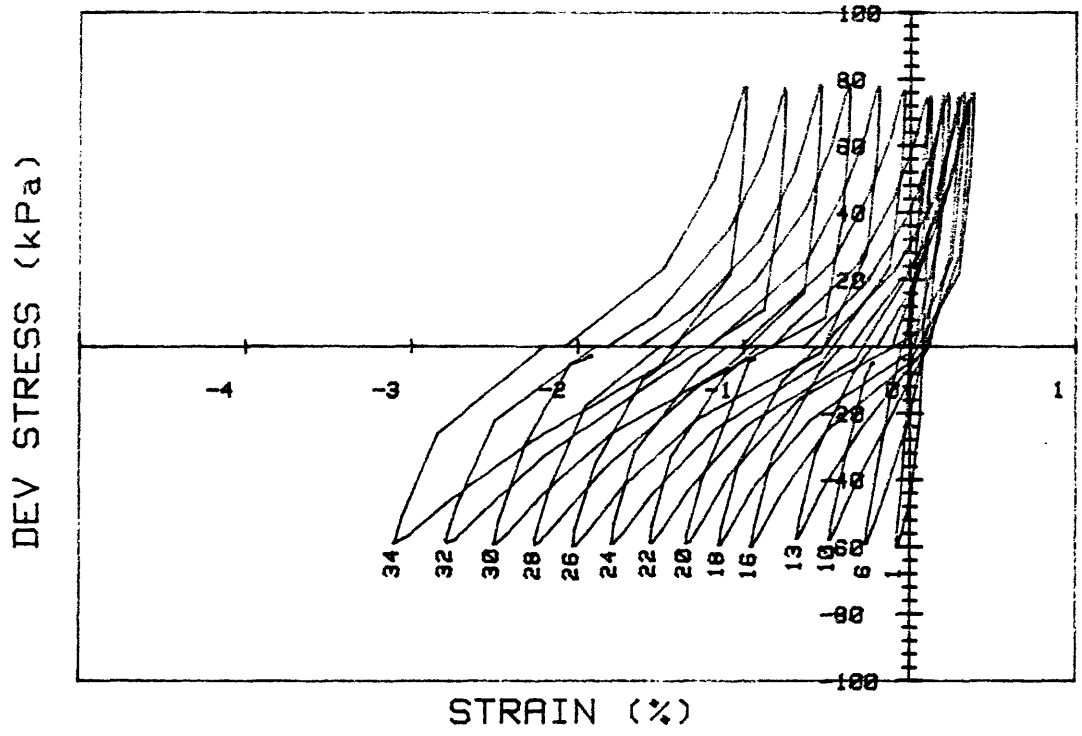

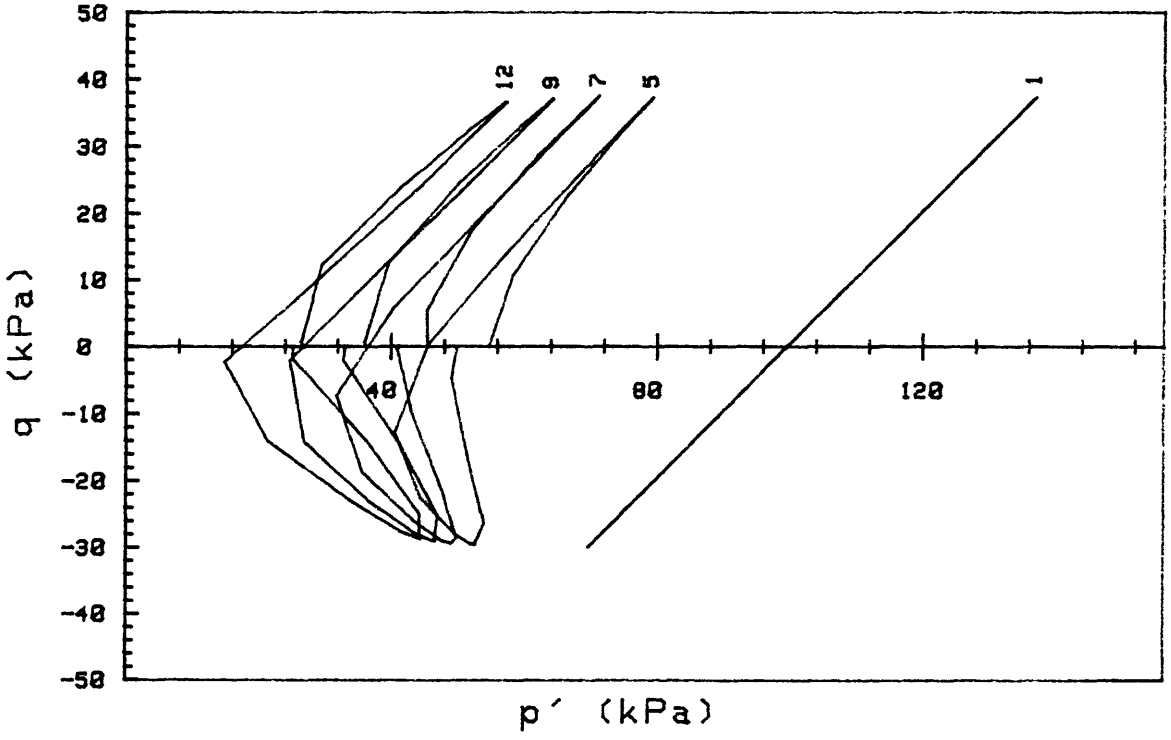

CRUISE ST HELENS		INCREMENT (cm)	REMOLDED SURF
CORE NO.	SL4	TEST NO.	D169
SIG1c´(kPa)	99.5	STATIC qf (kPa)	100.0
SIG3c´(kPa)	99.5	AVG MAX q (kPa)	37.9 (37.9%)
INDUCED OCR	1.0	AVG MIN q (kPa)	-29.4 (29.4%)

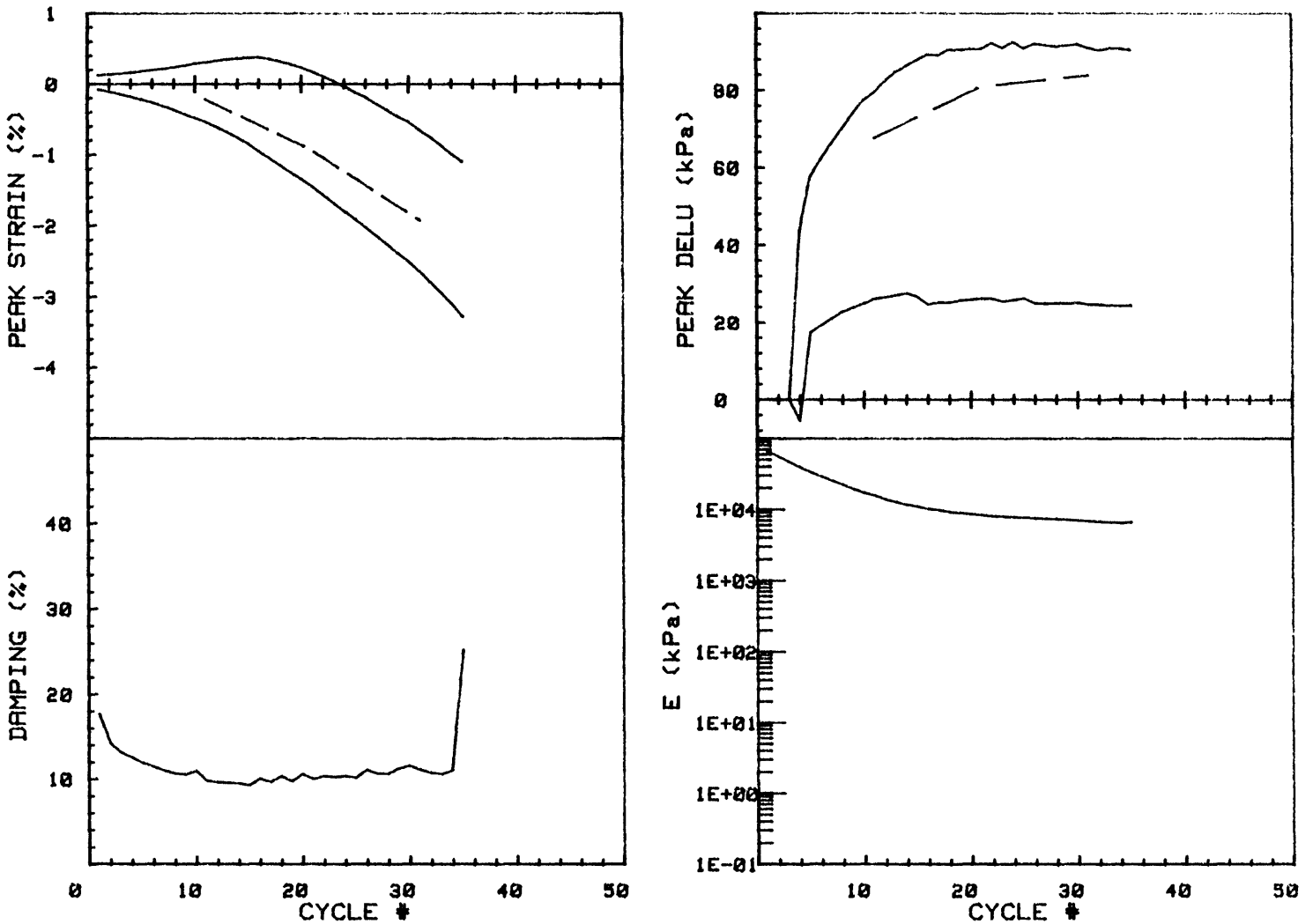

CRUISE ST HELENS		INCREMENT (cm)	REMOLDED SURF
CORE NO.	SL4	TEST NO.	D169
SIG1c'(kPa)	99.5	STATIC qf (kPa)	100.0
SIG3c'(kPa)	99.5	AVG MAX q (kPa)	37.9 (37.9%)
INDUCED OCR	1.0	AVG MIN q (kPa)	-29.4 (29.4%)

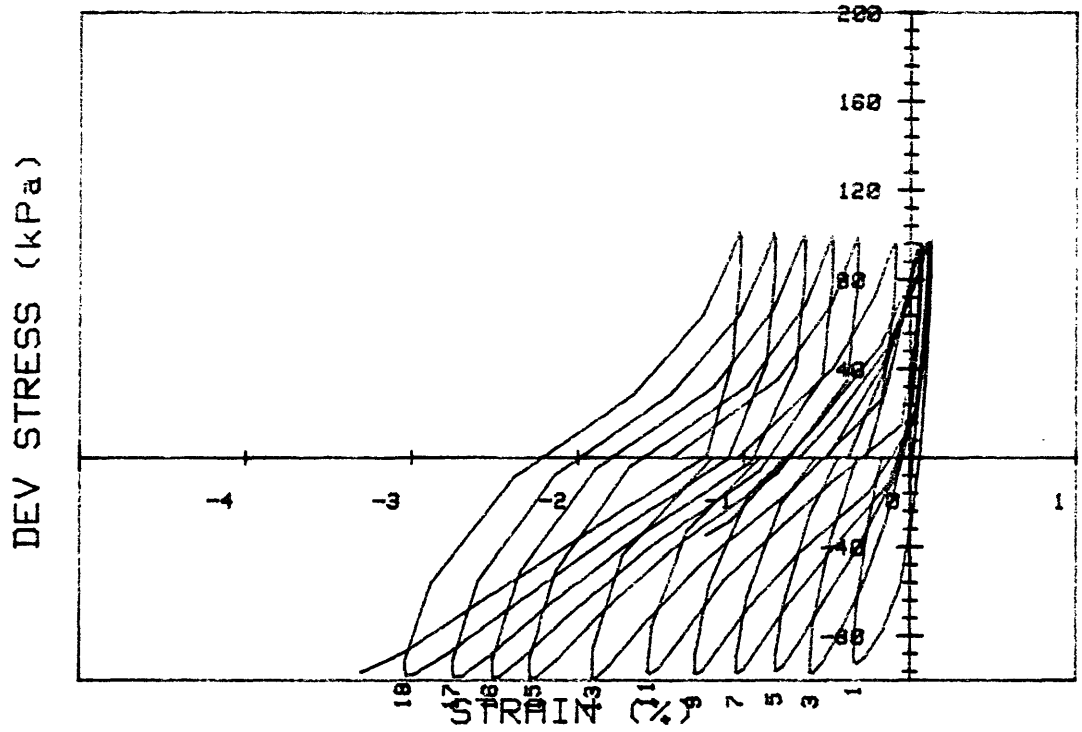

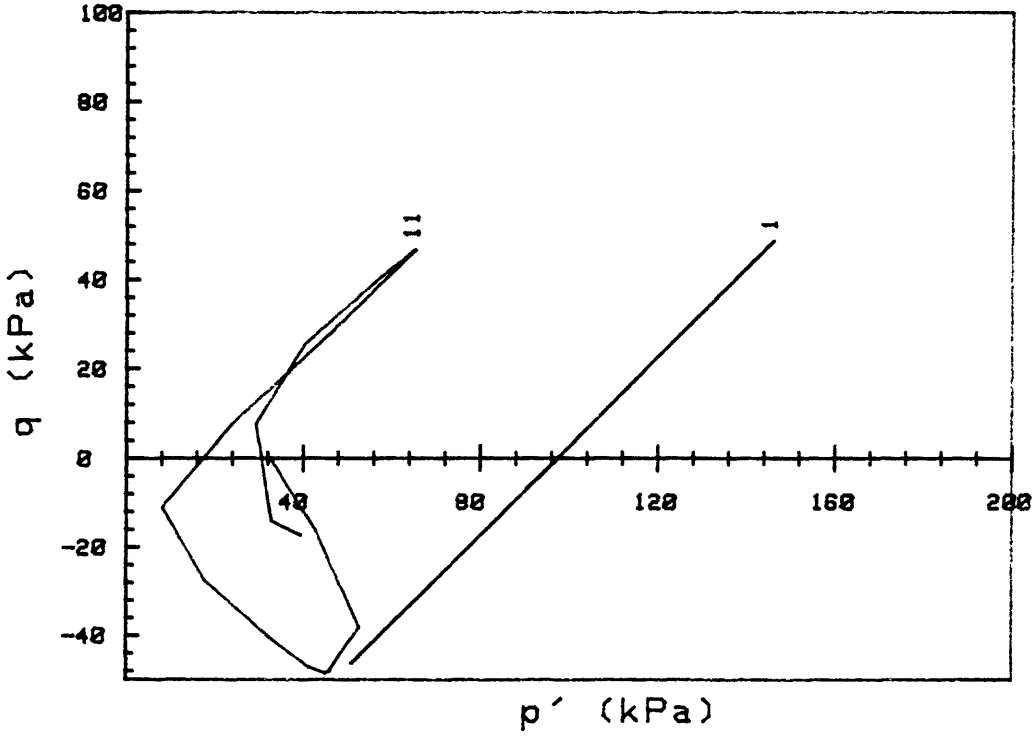

CRUISE ST HELENS		INCREMENT (cm)	SURF
CORE NO.	SL4	TEST NO.	D170
SIG1c´(kPa)	97.4	STATIC qf (kPa)	100.0
SIG3c´(kPa)	97.4	AVG MAX q (kPa)	48.3 (48.3%)
INDUCED OCR	1.0	AVG MIN q (kPa)	-48.6 (48.6%)

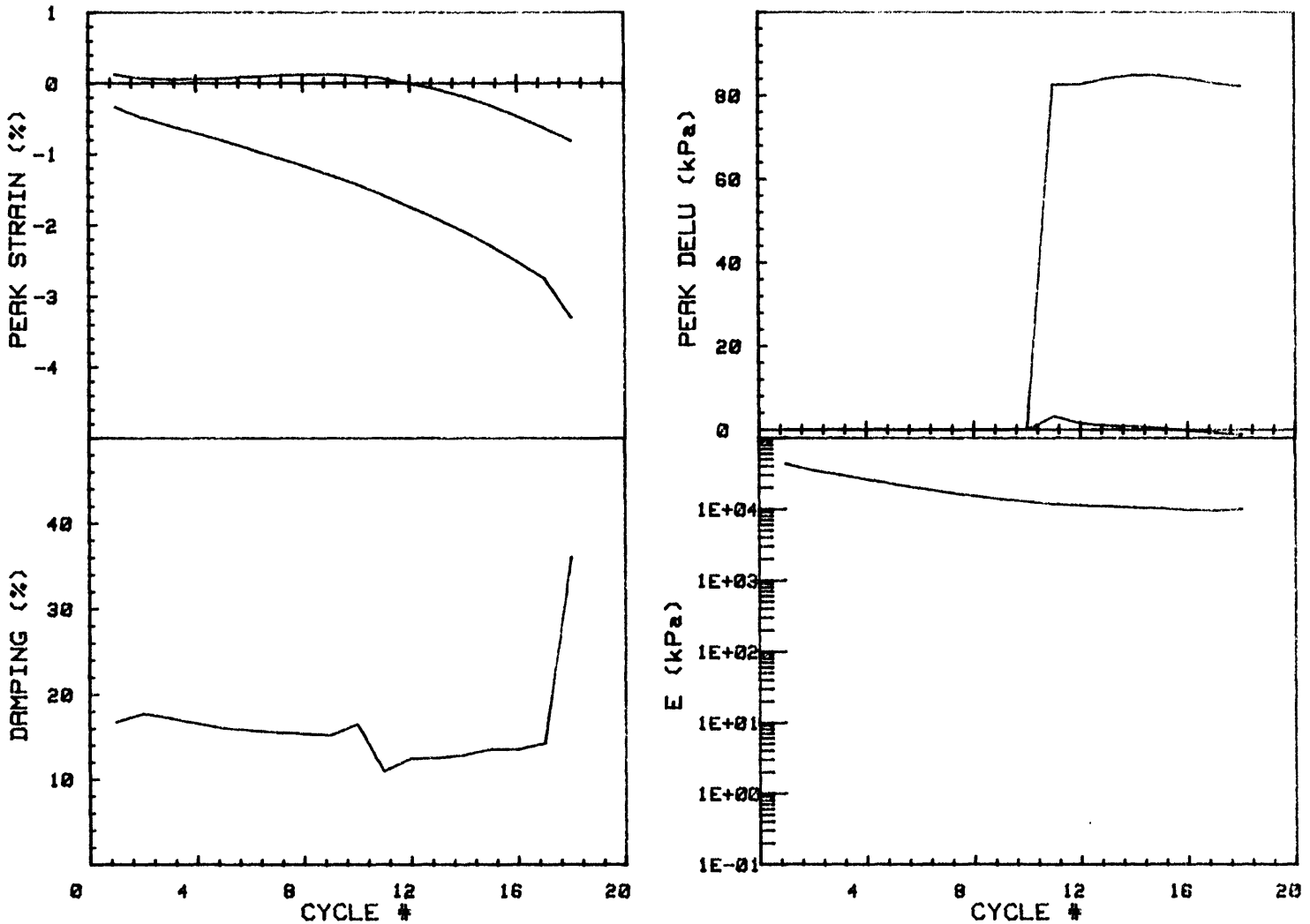

CRUISE ST HELENS		INCREMENT (cm)	SURF
CORE NO.	SL4	TEST NO.	D170
SIG1c'(kPa)	97.4	STATIC qf (kPa)	100.0
SIG3c'(kPa)	97.4	AVG MAX q (kPa)	48.3 (48.3%)
INDUCED OCR	1.0	AVG MIN q (kPa)	-48.6 (48.6%)

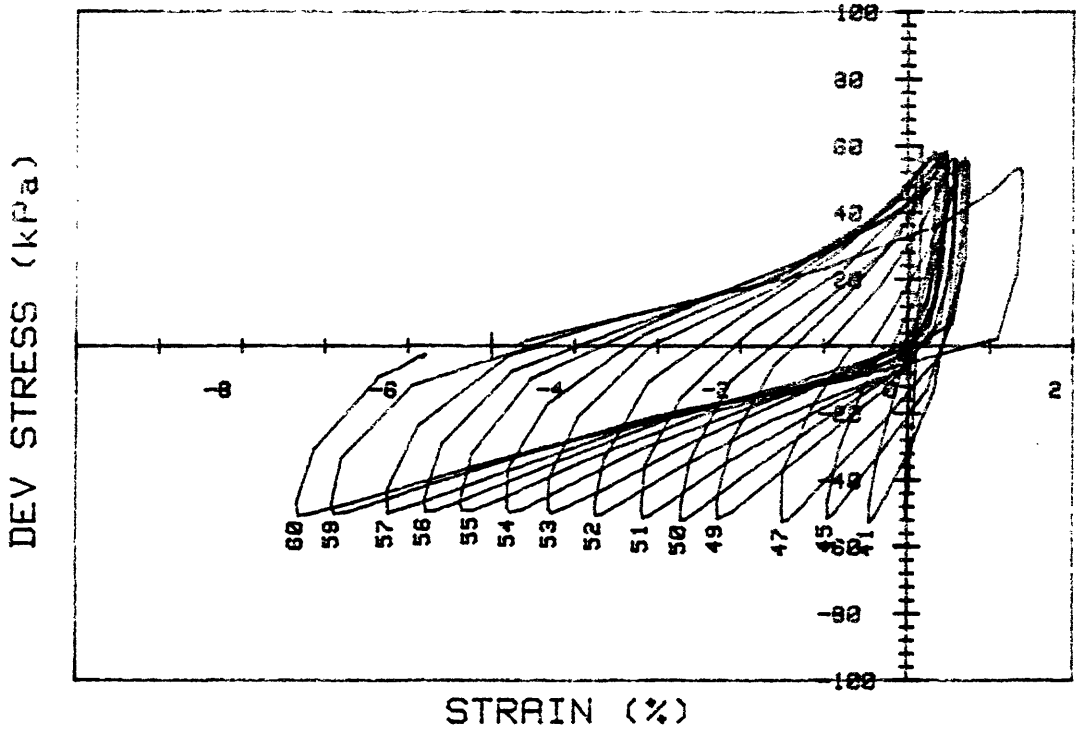

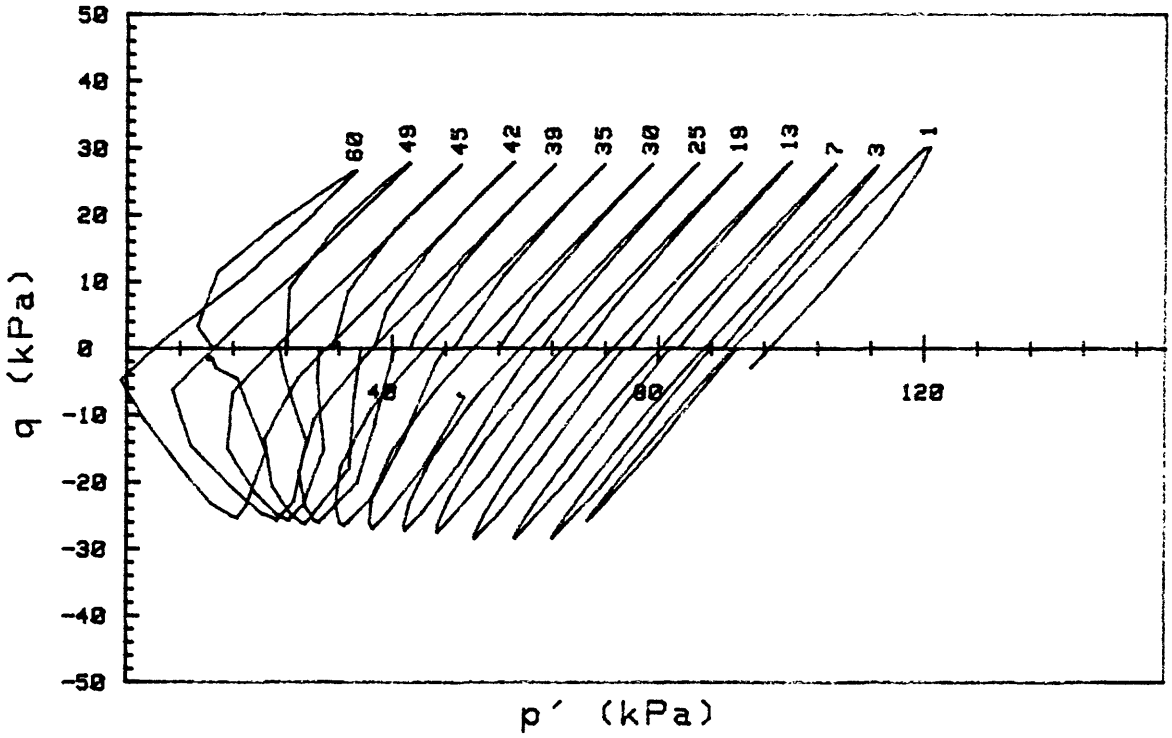

CRUISE ST HELENS		INCREMENT (cm)	REMOLDED SURF
CORE NO.	SL4	TEST NO.	D189
SIG1c´(kPa)	96.8	STATIC qf (kPa)	100.0
SIG3c´(kPa)	96.8	AVG MAX q (kPa)	27.9 (27.9%)
INDUCED OCR	1.0	AVG MIN q (kPa)	-26.8 (26.8%)

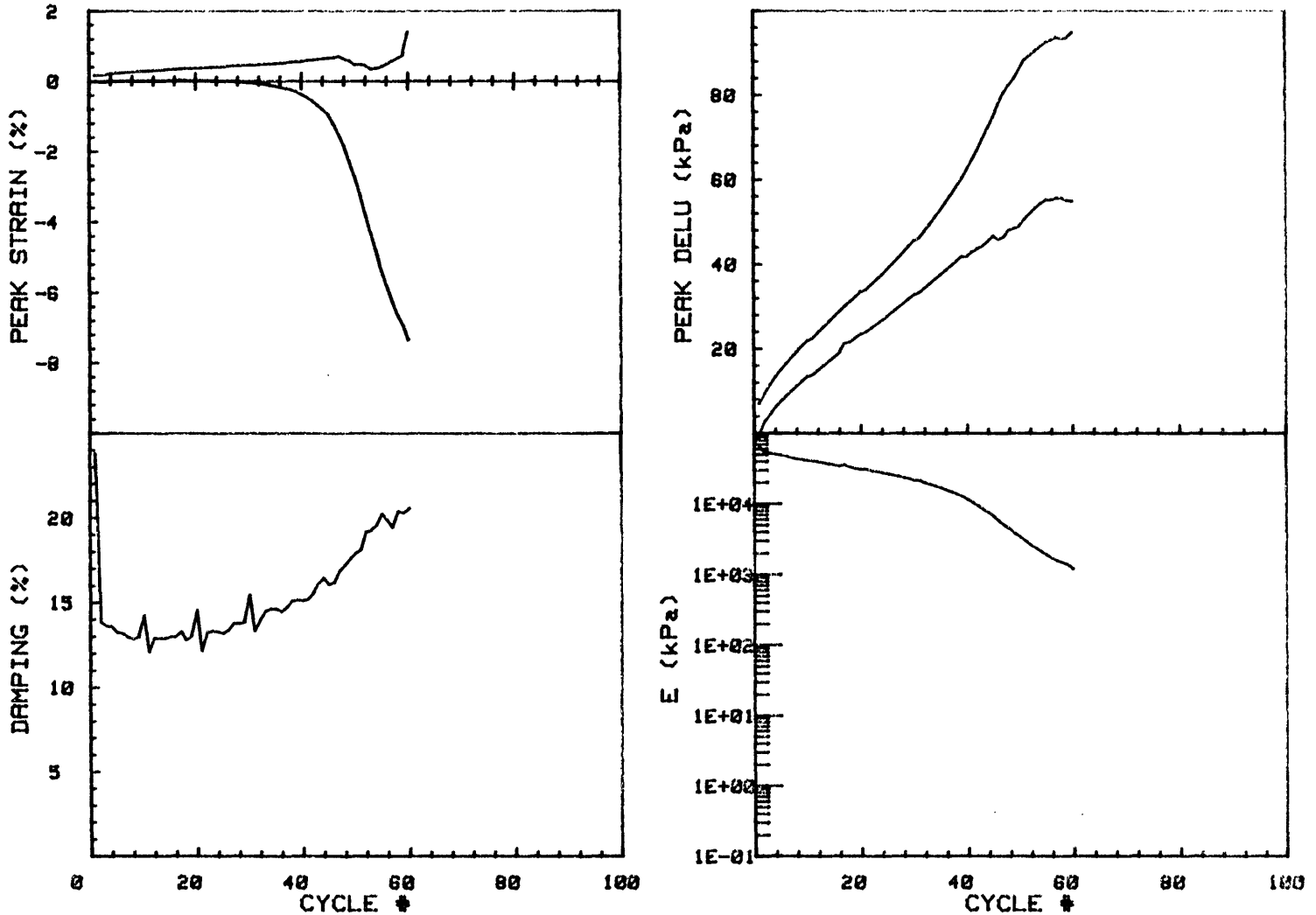

CRUISE ST HELENS		INCREMENT (cm)	REMOLDED SURF
CORE NO.	SL4	TEST NO.	D109
SIG1c'(kPa)	96.8	STATIC qf (kPa)	100.0
SIG3c'(kPa)	96.8	AVG MAX q (kPa)	27.9 (27.9%)
INDUCED OCR	1.0	AVG MIN q (kPa)	-26.8 (26.8%)

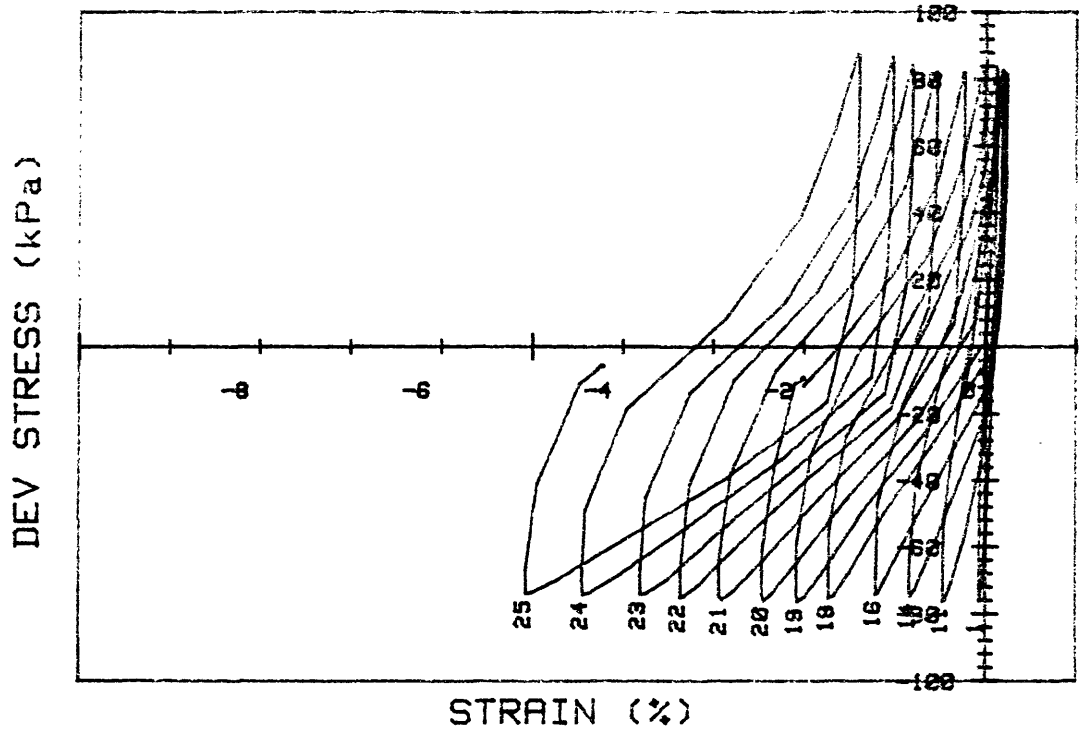

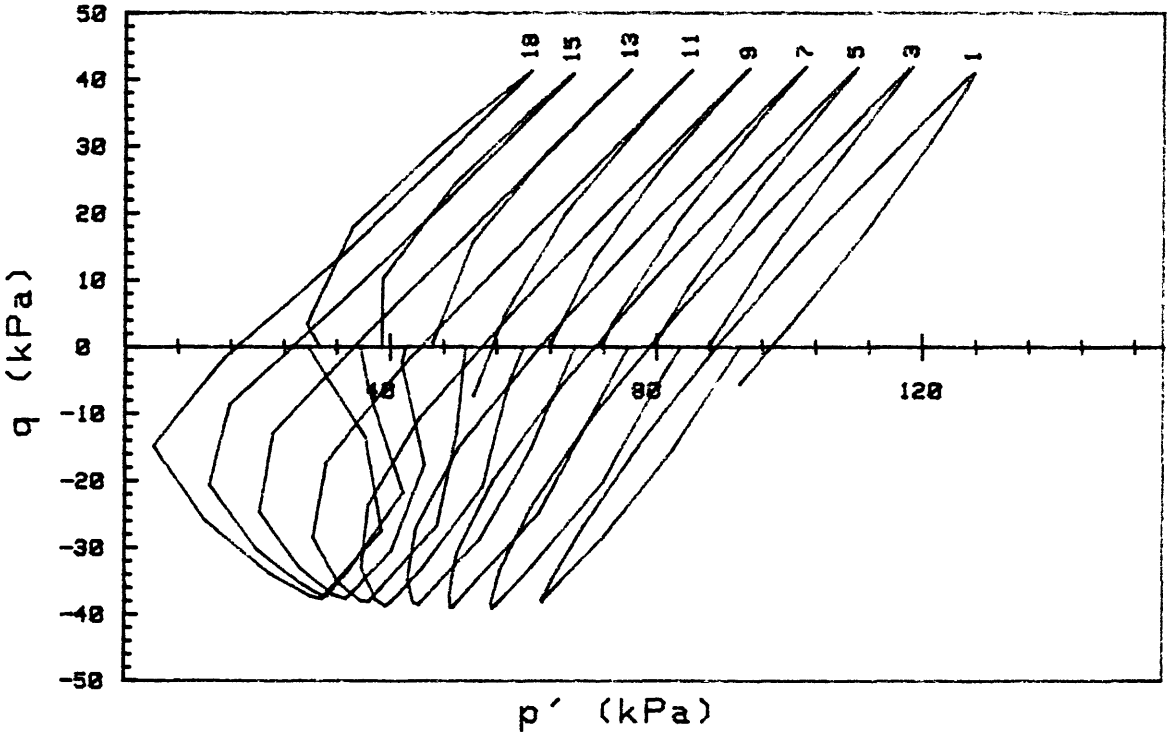

CRUISE ST HELENS		INCREMENT (cm)	REMOLDED SURF
CORE NO.	SL4	TEST NO.	D190
SIG1c'(kPa)	98.1	STATIC qf (kPa)	100.0
SIG3c'(kPa)	98.1	AVG MAX q (kPa)	41.6 (41.6%)
INDUCED OCR	1.0	AVG MIN q (kPa)	-38.1 (38.1%)

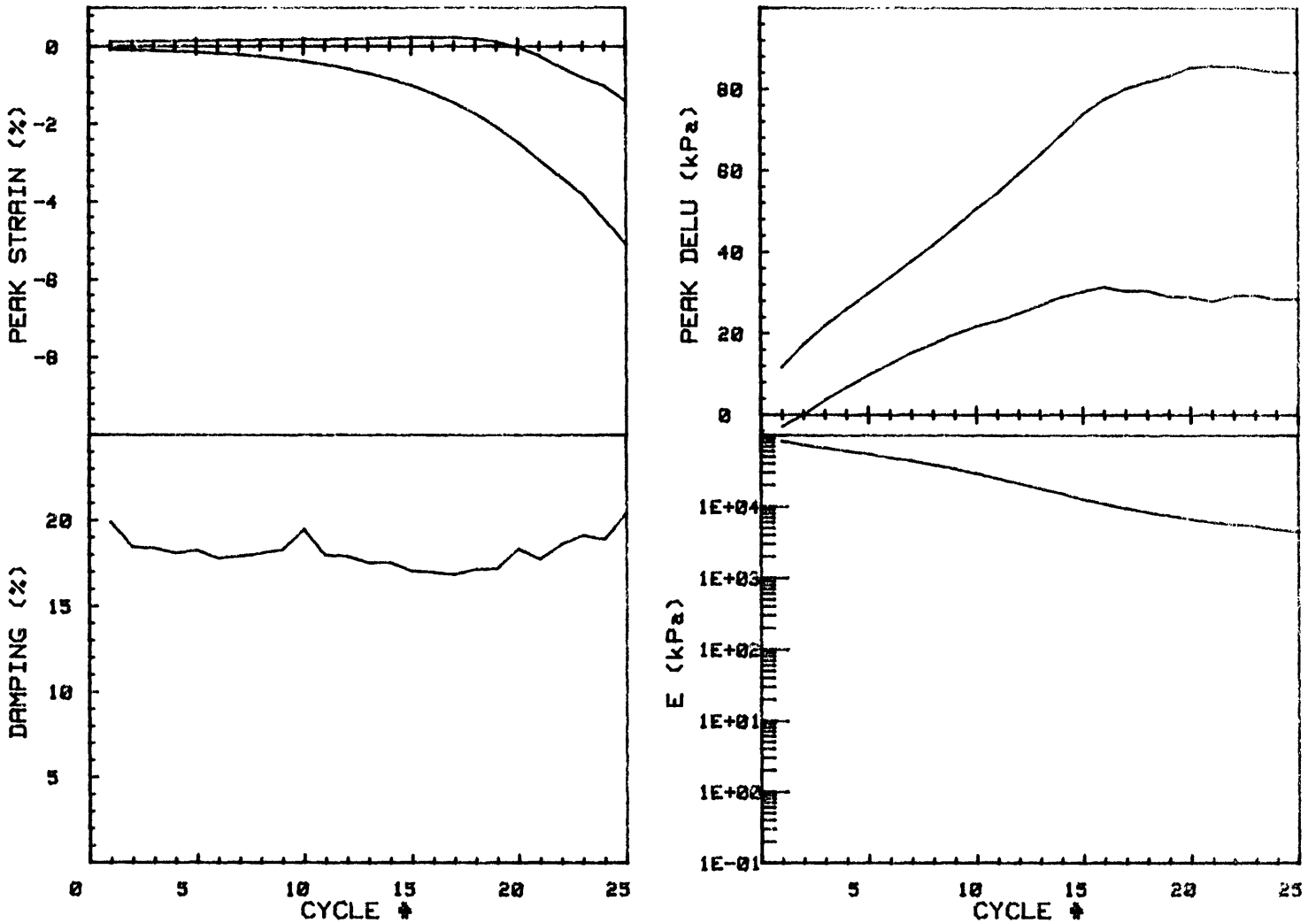

CRUISE ST HELENS		INCREMENT (cm)	REMOLDED SURF
CORE NO.	SL4	TEST NO.	D190
SIG1c'(kPa)	98.1	STATIC qf (kPa)	100.0
SIG3c'(kPa)	98.1	AVG MAX q (kPa)	41.6 (41.6%)
INDUCED OCR	1.0	AVG MIN q (kPa)	-38.1 (38.1%)

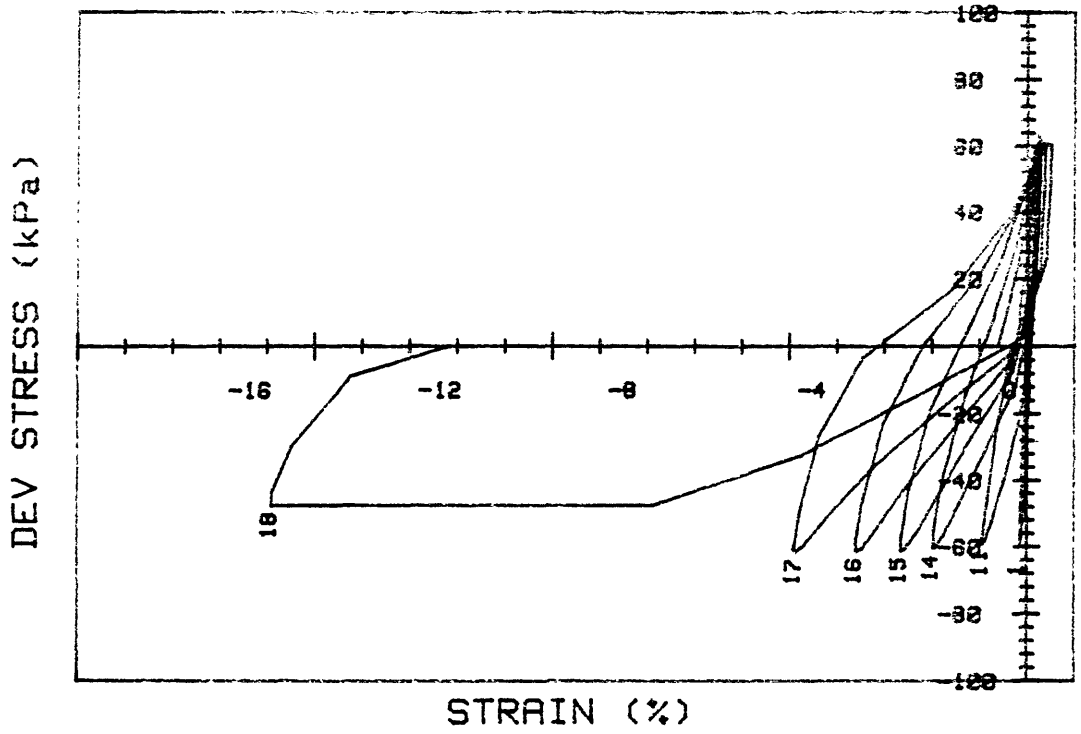

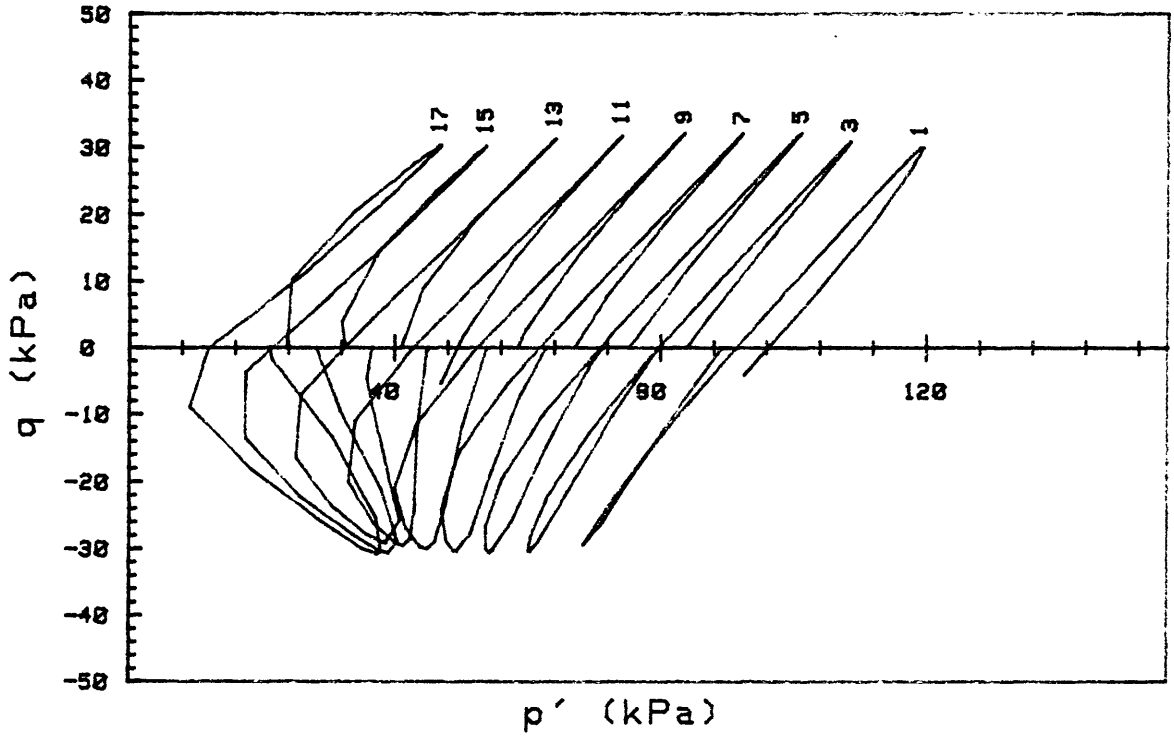

CRUISE ST HELENS		INCREMENT (cm)	REMOLDED SURF
CORE NO.	SL4	TEST NO.	D191
SIG1c′(kPa)	96.6	STATIC qf (kPa)	100.0
SIG3c′(kPa)	96.6	AVG MAX q (kPa)	31.3 (31.3%)
INDUCED OCR	1.0	AVG MIN q (kPa)	-28.6 (28.6%)

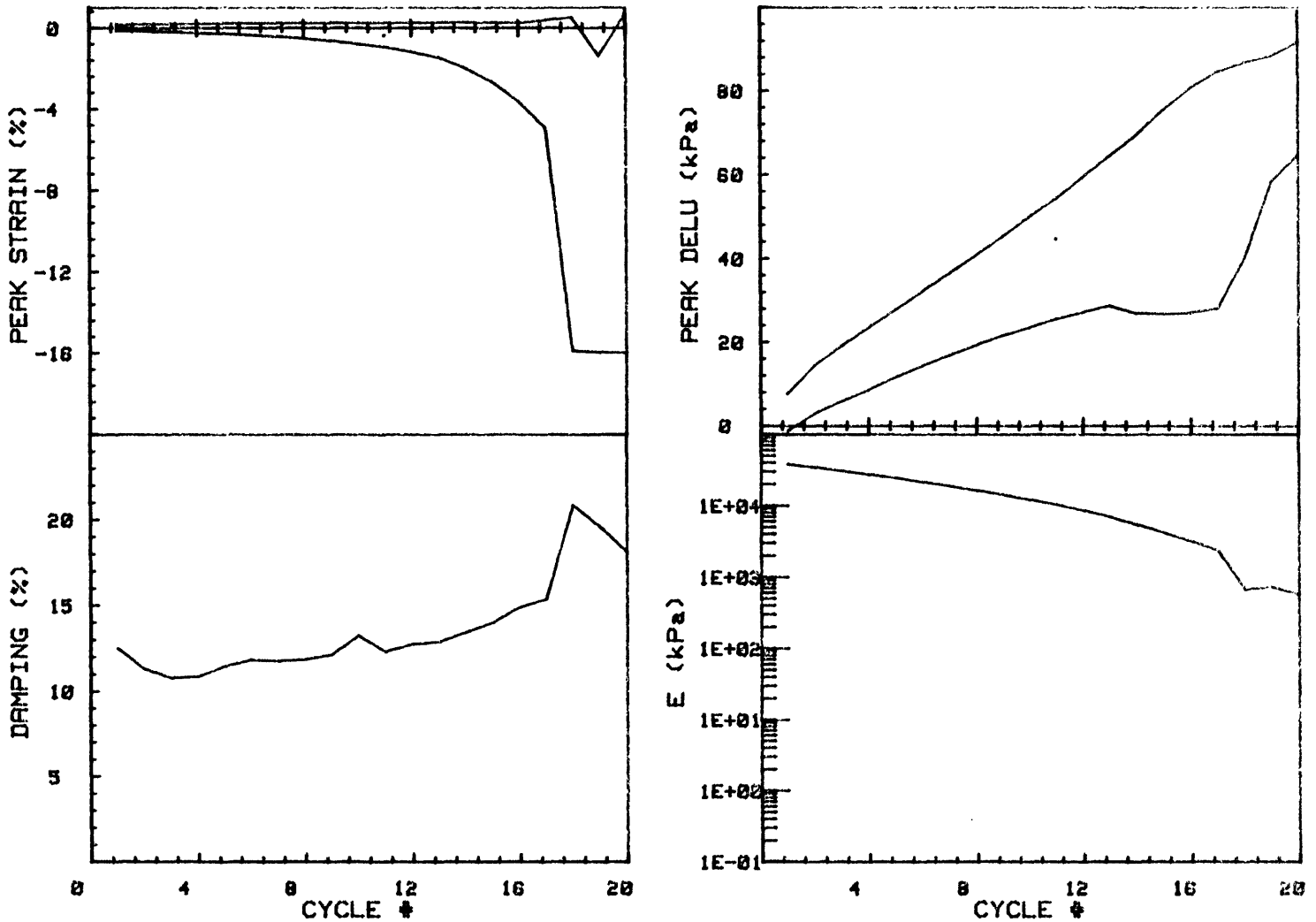

CRUISE ST HELENS		INCREMENT (cm)	REMOLDED SURF
CORE NO.	SL4	TEST NO.	D191
SIG1c'(kPa)	96.6	STATIC qf (kPa)	100.0
SIG3c'(kPa)	96.6	AVG MAX q (kPa)	31.3 (31.3%)
INDUCED OCR	1.0	AVG MIN q (kPa)	-28.6 (28.6%)

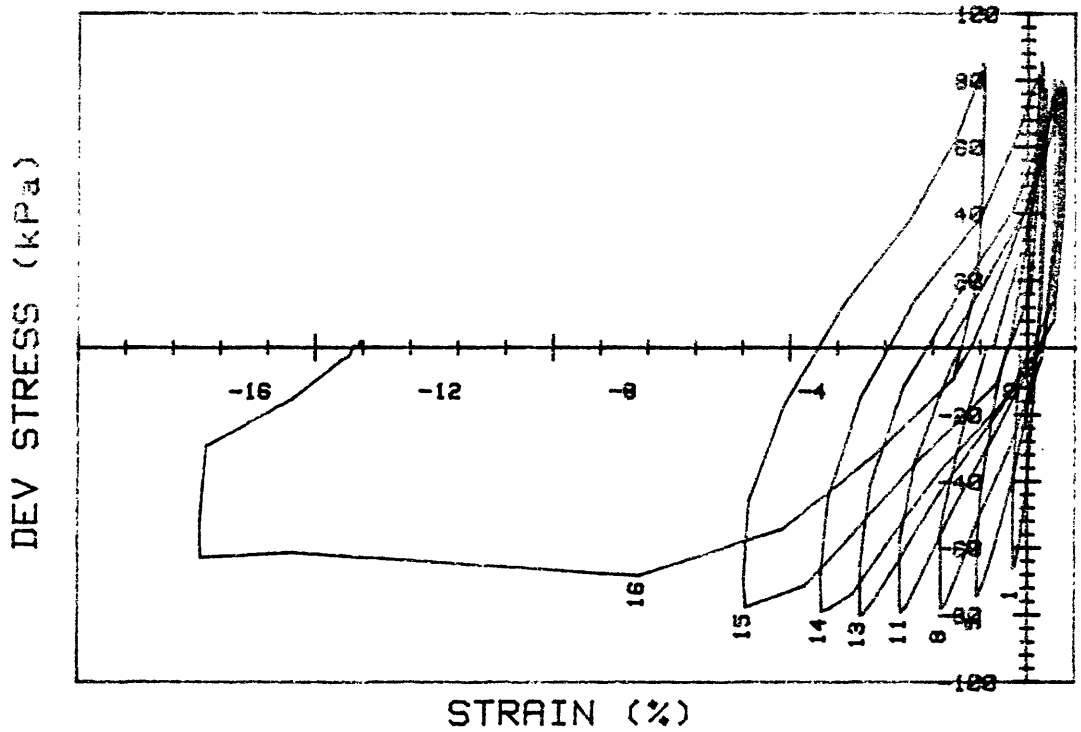

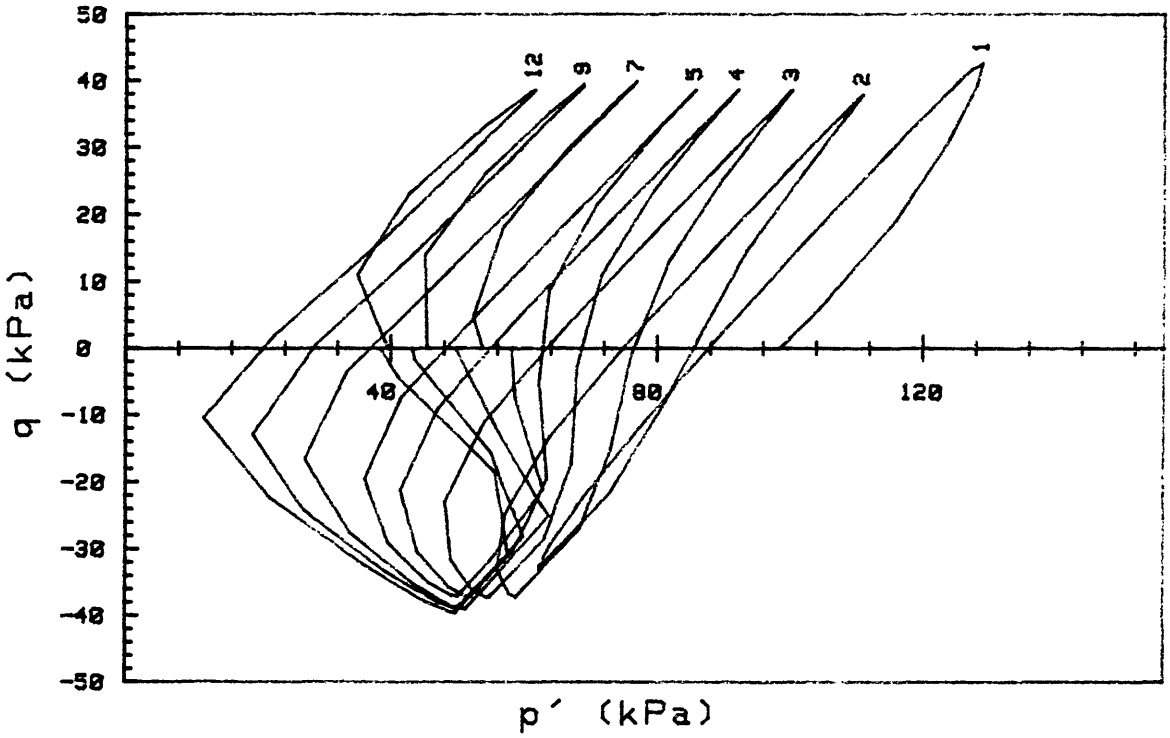

CRUISE ST HELENS		INCREMENT (cm)	REMOLDED SURF
CORE NO.	SL4	TEST NO.	D192
SIG1c´(kPa)	98.5	STATIC qf (kPa)	100.0
SIG3c´(kPa)	98.5	AVG MAX q (kPa)	39.6 (39.6%)
INDUCED OCR	1.0	AVG MIN q (kPa)	-38.0 (38.0%)

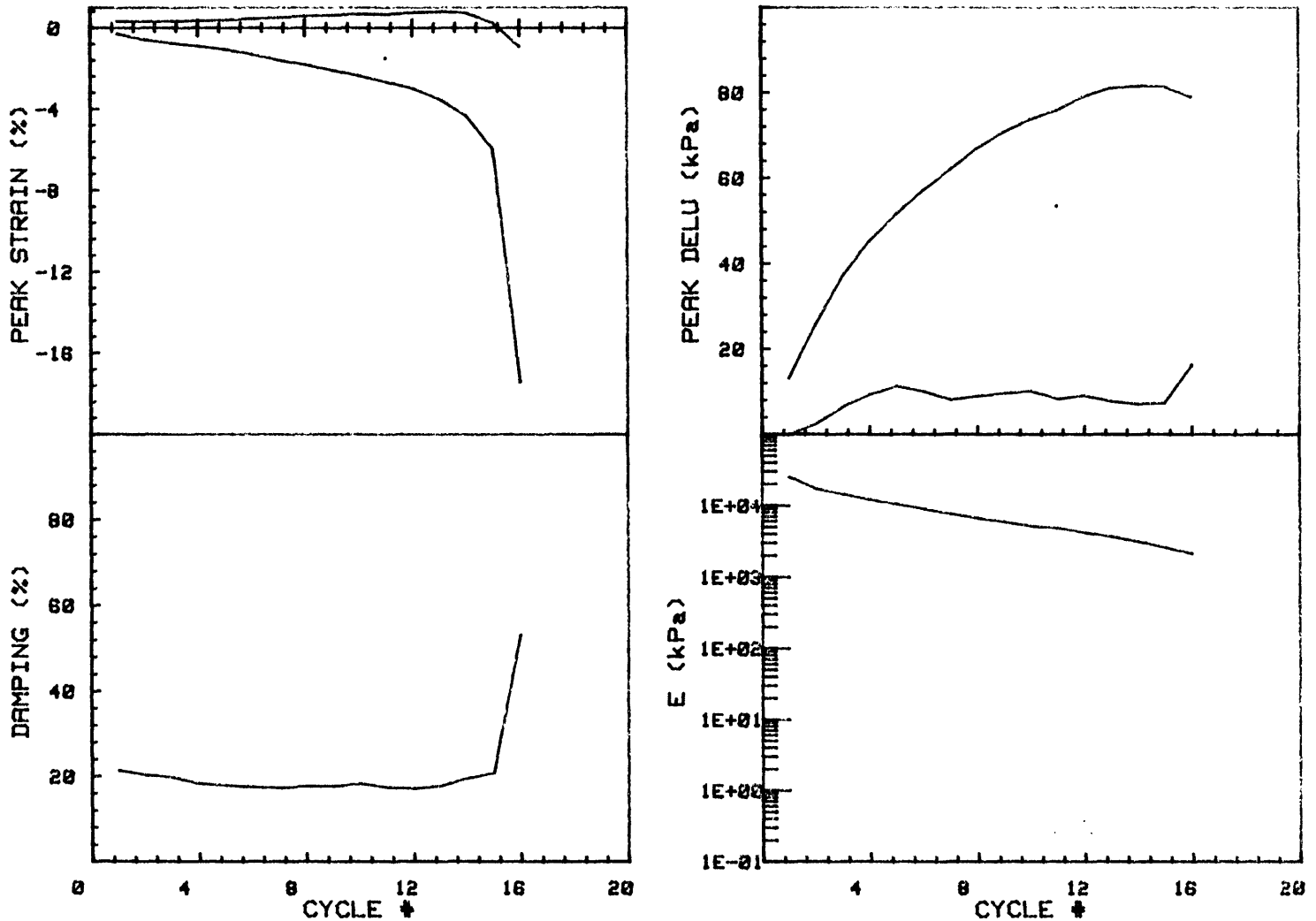

CRUISE ST HELENS		INCREMENT (cm)	REMOLDED SURF
CORE NO. SL4		TEST NO.	D192
SIG1c'(kPa)	98.5	STATIC qf (kPa)	100.0
SIG3c'(kPa)	98.5	AVG MAX q (kPa)	39.6 (39.6%)
INDUCED OCR	1.0	AVG MIN q (kPa)	-38.0 (38.0%)

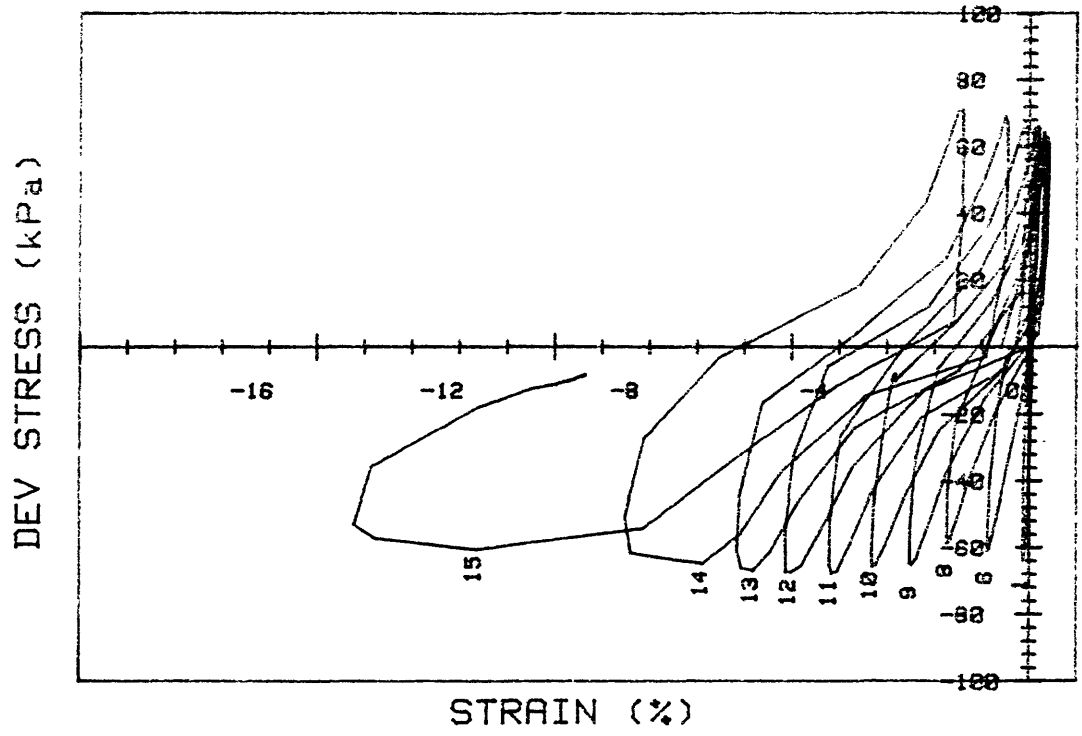

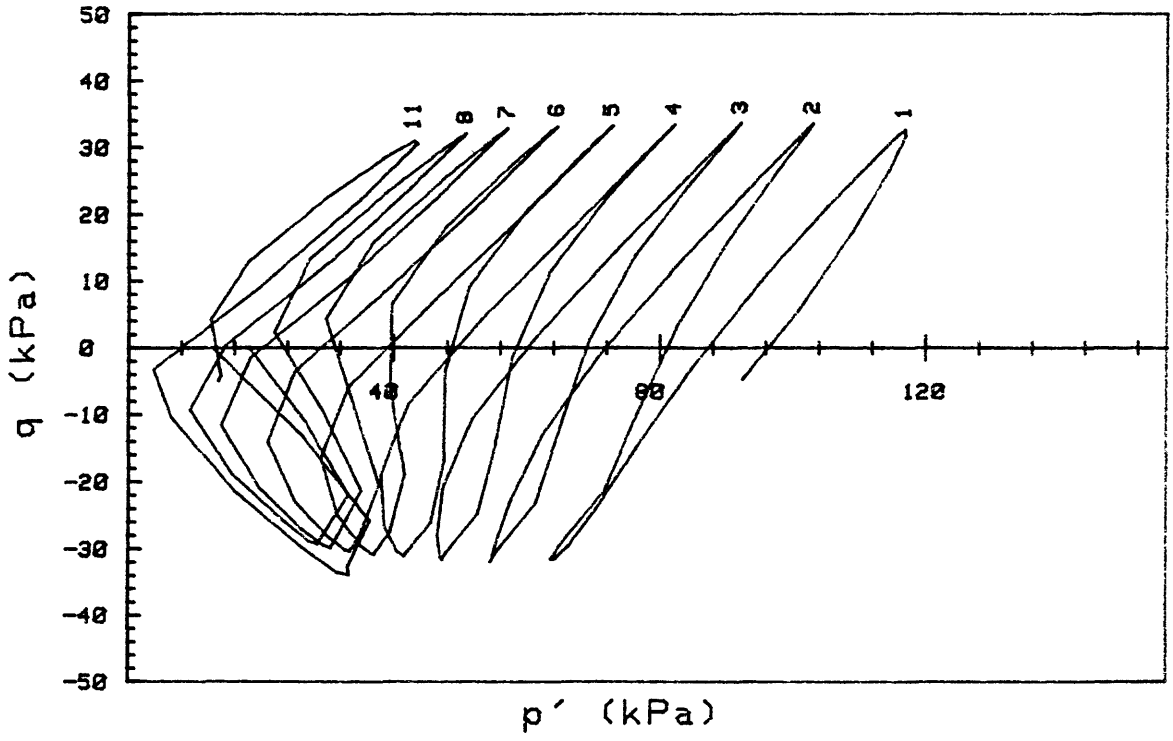

CRUISE ST HELENS		INCREMENT (cm)	REMOLDED SURF
CORE NO.	SL4	TEST NO.	D196
SIG1c'(kPa)	97.3	STATIC qf (kPa)	100.0
SIG3c'(kPa)	97.3	AVG MAX q (kPa)	32.9 (32.9%)
INDUCED OCR	1.0	AVG MIN q (kPa)	-31.8 (31.8%)

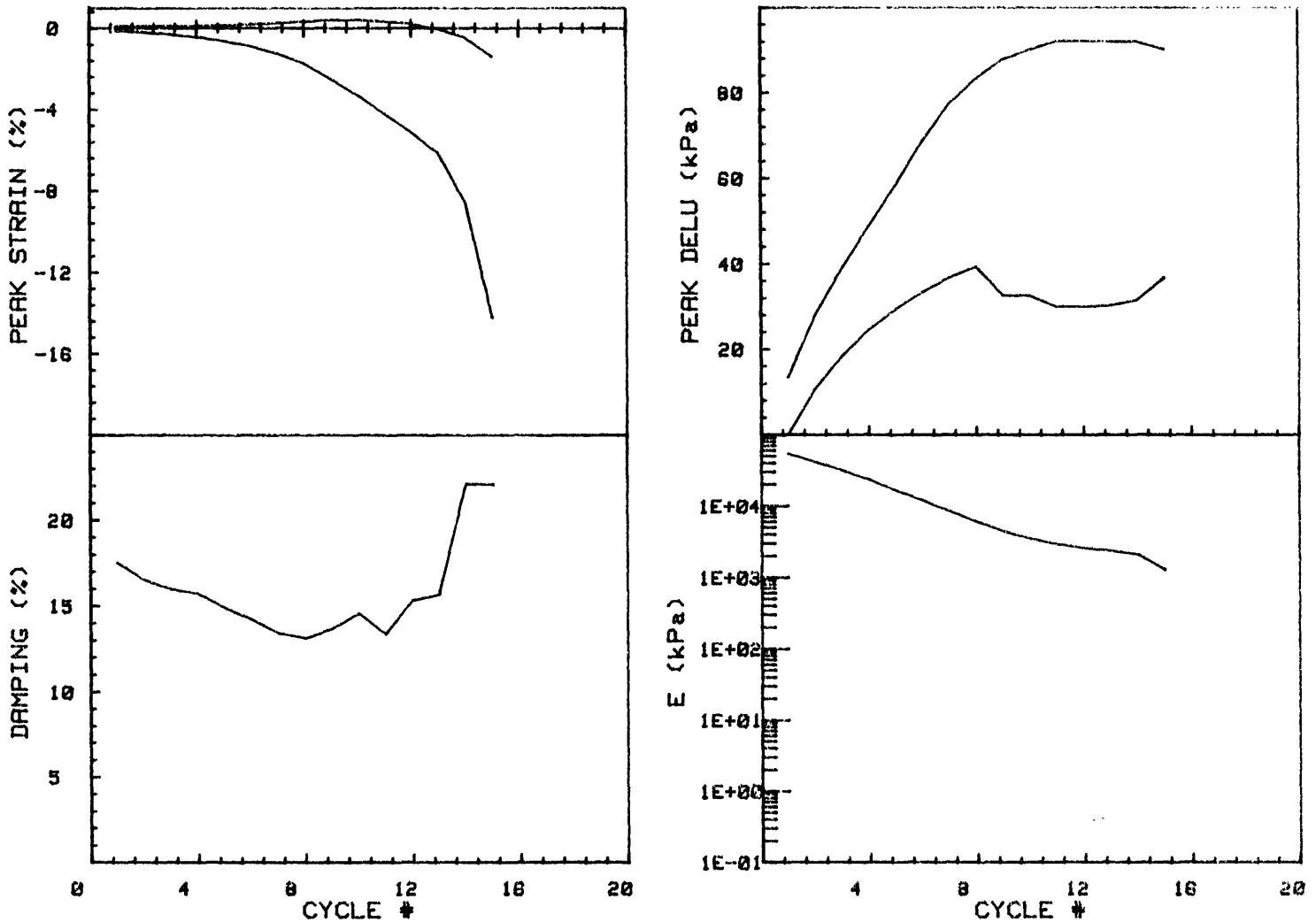

CRUISE ST HELENS		INCREMENT (cm)	REMOLDED SURF
CORE NO.	SL4	TEST NO.	D196
SIG1c'(kPa)	97.3	STATIC qf (kPa)	100.0
SIG3c'(kPa)	97.3	AVG MAX q (kPa)	32.9 (32.9%)
INDUCED OCR	1.0	AVG MIN q (kPa)	-31.8 (31.8%)

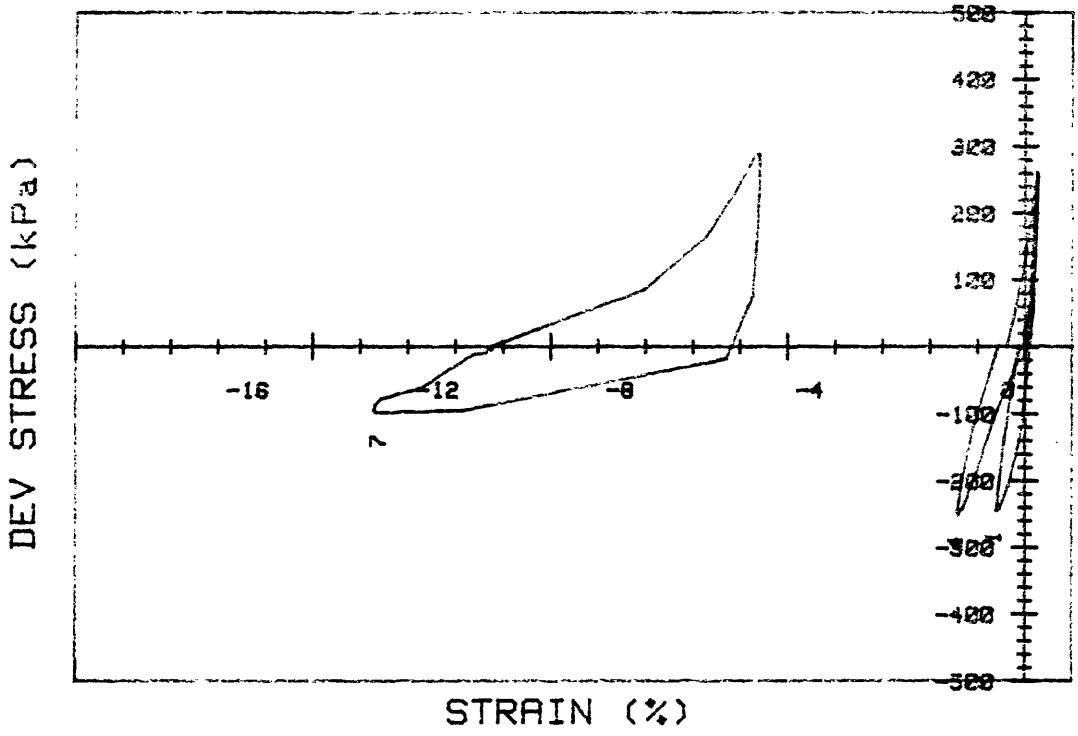

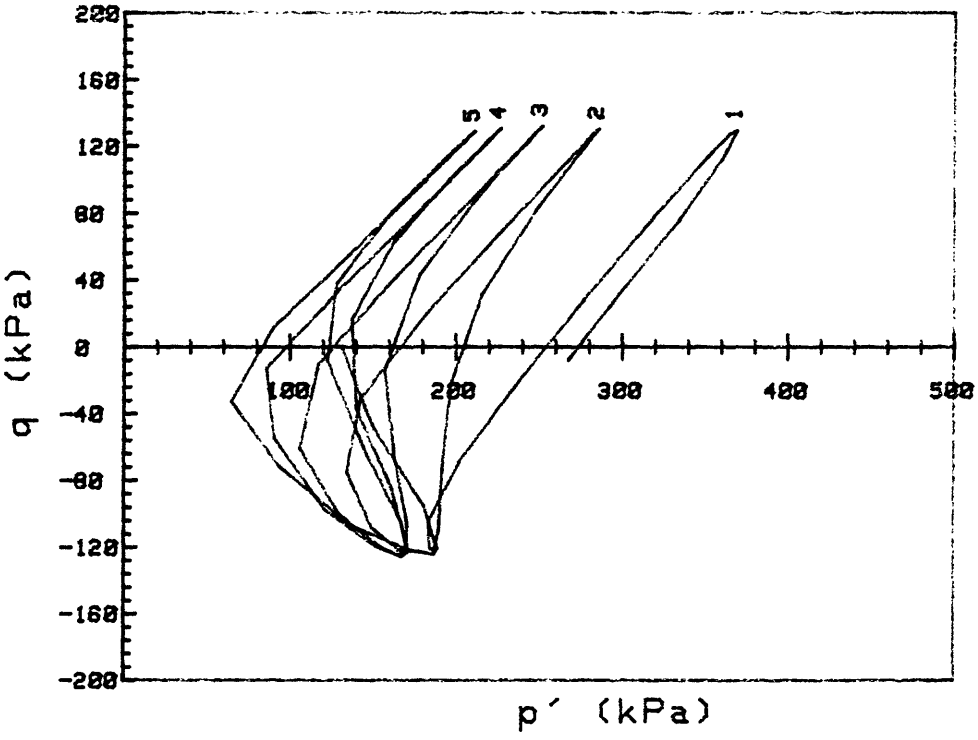

CRUISE ST HELENS		INCREMENT (cm)	REMOLDED SURF
CORE NO.	SL4	TEST NO.	D193
SIG1c´(kPa)	275.4	STATIC qf (kPa)	280.0
SIG3c´(kPa)	275.4	AVG MAX q (kPa)	132.6 (47.4%)
INDUCED OCR	1.0	AVG MIN q (kPa)	-107.6 (38.4%)

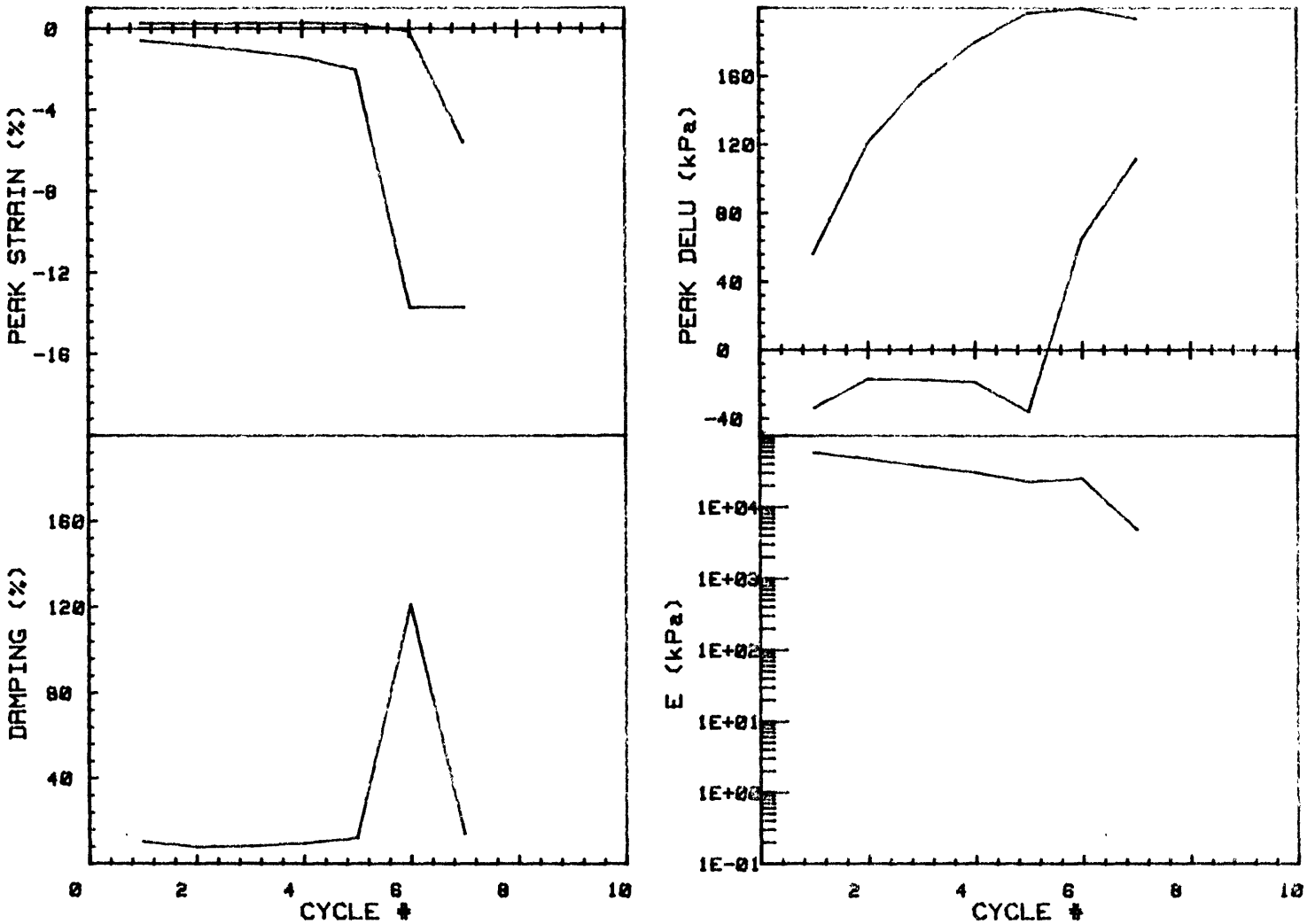

CRUISE ST HELENS		INCREMENT (cm)	REMOLDED SURF
CORE NO.	SL4	TEST NO.	D193
SIG1c'(kPa)	275.4	STATIC qf (kPa)	280.0
SIG3c'(kPa)	275.4	AVG MAX q (kPa)	132.6 (47.4%)
INDUCED OCR	1.0	AVG MIN q (kPa)	-107.6 (38.4%)

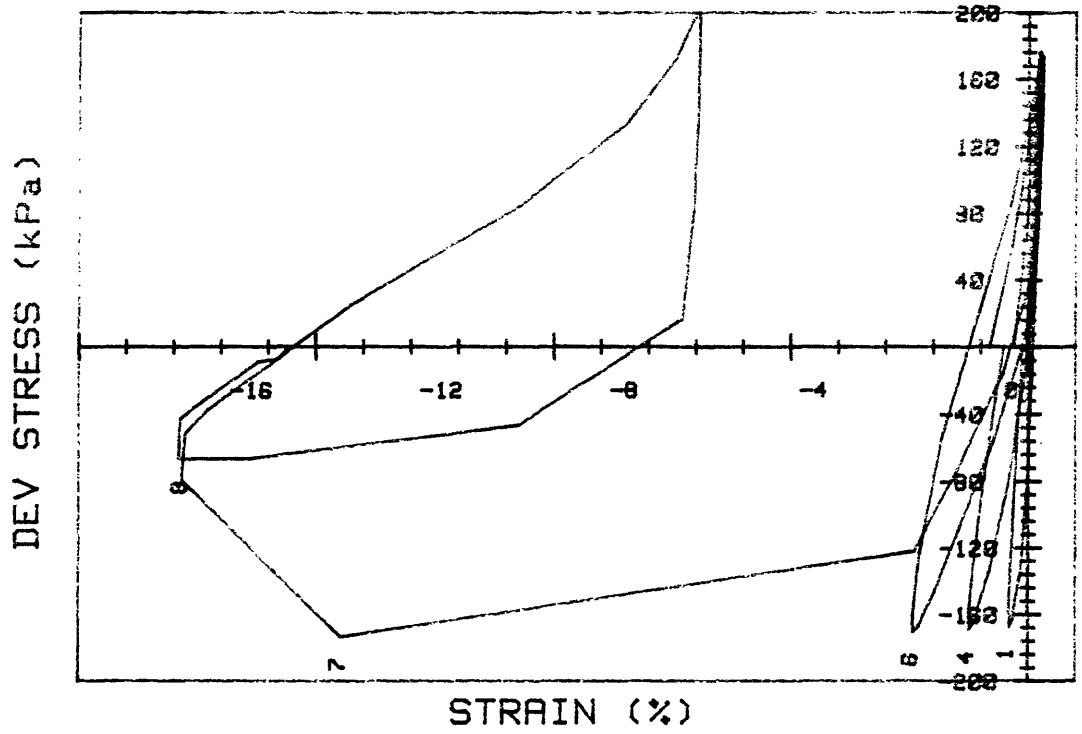

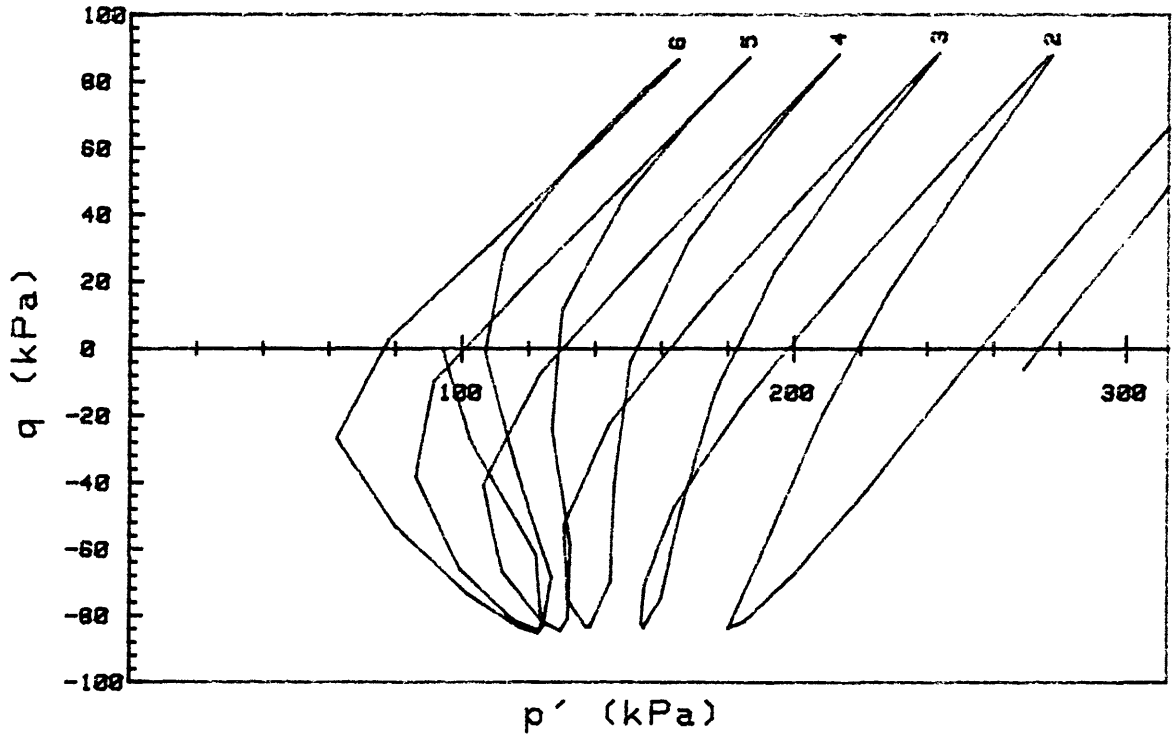

CRUISE ST HELENS		INCREMENT (cm)	REMOLDED SURF
CORE NO.	SL4	TEST NO.	D194
SIG1c'(kPa)	275.2	STATIC qf (kPa)	280.0
SIG3c'(kPa)	275.2	AVG MAX q (kPa)	89.2 (31.9%)
INDUCED OCR	1.0	AVG MIN q (kPa)	-78.1 (27.9%)